Spring 5-23-2021

Beyond the Standard Models of Particle Physics and Cosmology

Gabriele Rigo
Syracuse University

Abstract

Despite their numerous successes both from the theoretical and experimental point of view, conceptual and observational evidence suggests the Standard Models of Particle Physics and Cosmology should be considered incomplete theories, reliable only within their well-defined regime of validity. This dissertation covers various possible extensions of those models from the theoretical, phenomenological and model-building perspective. The topics analyzed range from extra-dimensional approaches to the hierarchy problem, to the AdS/CFT description of perturbative anomaly inflow, and new probes of vacuum energy in neutron stars and gravitational waves.

Beyond the Standard Models of Particle Physics and Cosmology

by

Gabriele Rigo

B.S. Physics, Università degli Studi di Trieste, 2015

M.S. Physics, Syracuse University, 2017

DISSERTATION

Submitted in partial fulfillment of the requirements for the degree

of Doctor of Philosophy in Physics

Syracuse University

May 2021

Acknowledgements

I would like to take this opportunity to acknowledge all the people that have supported me through the years leading up to the completion of my Ph.D.

First and foremost, I am extremely grateful to my advisor, Jay, for being a huge inspiration with his enthusiasm and curiosity for the laws of physics, and for all the hours spent together in front of a blackboard or a screen. I am proud of calling myself your student.

I would also like to thank all the members of the Syracuse particle physics group: Simon, Jack, Scott, Carl, Bal. You have taught me there are so many different ways to be an excellent physicist.

I am sincerely thankful to Claudia and Britton for agreeing to join my thesis defense committee, and for their insightful questions and comments. I had the great pleasure to further discuss some of the topics that contributed to this thesis with my collaborators John, Seung, Brando and Raffaele.

I am grateful to everyone in the Cornell particle phenomenology group: thank you for creating such a welcoming and inspiring environment, and for giving me the opportunity to meet some of the most talented and brilliant people I know. I want to mention in particular Yuval, Maxim, Sungwoo, Gabriel, Stefan, Jeff, Sal, Ofri, Gowri, Ameen. A special thank you

goes to Csaba, for his support and invaluable insight on so many topics, physics-related and otherwise.

It was a great pleasure to share this journey with all the colleagues I overlapped with in the physics department at SU. I am especially thankful to Cem, who is still one of my closest collaborators and extensively contributed to some of the work discussed in this thesis. A honorable mention goes to Ogan, Gizem, Brandon, Eva and Bharath, as we all had the privilege of calling Room 363 our office at some point through the years. I am also very grateful for all the interactions and coffees shared with Francesco, Judah, Mahesh, Harris, Arvind, Kenny, Pinaki, Asad, Goksu, Tianna and Maxx.

I find the sense of community and excitement surrounding a school or a conference to be truly one of the most unique and fulfilling aspects of particle physics. Thanks to those experiences, I had the pleasure to meet some incredible people, and I am grateful that my friendships with Cristina, Anna-Maria, Francesco, Kim, Rashmish, Simone, Alessandro, Olmo, Luca and Matteo have been reaching far beyond the extent of those activities.

I am hugely grateful to all my friends from Italy for their continuous support and for all the joy they bring me: Danny, Mattia, Alessandro, Domenico, Marco, Leonardo, Davide, Alberto, Simone, Lorenzo, Eleonora, Marta, Aurelia, Rachele, Marta. Thank you for always giving me one more reason to look forward to coming back home.

I am deeply grateful, Margaret, for how you make me feel extremely fortunate to have you by my side. Thank you for always giving me one more reason to look forward to what's coming next.

Finally, none of this would have been possible without my family's unconditional love. I am thinking of my grandma Giulia, my aunt Paola, and Claudia: thank you for showing

me again and again, each in your own way, the value of encouragement and support even through the most challenging of times. And of course to my father Idelmo, my mother Marisa and my sister Annachiara: you are the greatest inspirations of all. It gives me great pride to constantly witness, even from so far apart, the immense strength and determination you have displayed. Everything I have achieved, I owe it to growing up next to you.

To my family.

Contents

List of Figures

List of Tables

List of Publications

Chapters 2–5 of this dissertation consist of work originally described in the following papers:

[1] C. Eröncel, J. Hubisz, G. Rigo, "Self-Organized Higgs Criticality", *JHEP* **03**, 046 (2019) [arXiv:1804.00004 [hep-ph]].

[2] C. Eröncel, J. Hubisz, G. Rigo, "Radion-Activated Higgs Mechanism", *Phys. Rev. D* **101**, 055041 (2020) [arXiv:1912.11053 [hep-ph]].

[3] S. Hong, G. Rigo, "Anomaly Inflow and Holography" [arXiv:2012.03964 [hep-th]].

[4] C. Csáki, C. Eröncel, J. Hubisz, G. Rigo, J. Terning, "Neutron Star Mergers Chirp About Vacuum Energy", *JHEP* **09**, 087 (2018) [arXiv:1802.04813 [astro-ph.HE]].

Chapter 1

Introduction

The Standard Model of Particle Physics (SM) can be regarded as one of the most successful theories in the history of modern physics, arguably thanks to the following reasons: it provides a unified and minimal framework that encapsulates a century of development in quantum field theory (QFT), and it generates countless predictions that have been tested to exceptional precision by a multitude of experimental probes. In the present Introduction we will review the elements, as well as the downsides and limitations, of the SM, and anticipate how various possible extensions of the SM itself can lead to a more complete understanding of the phenomena at the core of particle physics and cosmology.

1.1 Review of the Standard Model

Quantum field theory is the unified description of quantum mechanics and special relativity in terms of the fundamental building blocks known as quantum fields. Those fields are typically defined at every point of spacetime, and are characterized by their transformation properties

under the Lorentz symmetry of flat spacetime. Through experiments performed under various conditions, physicists are able to probe the characteristics and behavior of the particles that arise from the excitations of quantum fields. This well-established procedure allows to relate the experimental data to the details of the underlying theory, and viceversa to accurately predict the outcome of a wide range of experiments in terms of a given theoretical model. Such a continuous feedback mechanism has enabled particle physics to thrive and improve for almost a century both from the theoretical and from the experimental side.

Gauge theories are an example of a class of theories that have proven to be especially useful in the context of QFT. A gauge symmetry is not a fundamental symmetry of Nature, or of any physical theory. Rather, it should be interpreted as the redundancy that arises from choosing a particular description of the interactions between degrees of freedom, in which Lorentz invariance is manifest. However, the advantage of resorting to such a description is that the theory is completely determined once only a few key ingredients are specified, namely:

- the symmetries of the Lagrangian and the symmetry breaking pattern;
- the matter content and its transformation properties under the symmetries.

Through years of historical development, physicists have realized that three of the four fundamental interactions and their phenomenological consequences are very well accounted for by writing down a gauge theory with the appropriate symmetries and matter content. In the case of the Standard Model, the gauge (local) symmetry is postulated to be $G_{\rm SM} = \mathrm{SU}(3)_{\rm C} \times \mathrm{SU}(2)_{\rm L} \times \mathrm{U}(1)_Y$, spontaneously broken as $G_{\rm SM} \to \mathrm{SU}(3)_{\rm C} \times \mathrm{U}(1)_{\rm EM}$, where the generator of $\mathrm{U}(1)_{\rm EM}$ is $Q_{\rm EM} \equiv T_3 + Y$. Specifically, the various factors correspond to the

quantum chromodynamics (QCD), weak and hypercharge gauge groups. The last two elements are also collectively referred to as the electroweak (EW) group. At low energies, the EW symmetry is broken down to the gauge group responsible for the electromagnetic interactions that we observe.

Having determined what the symmetries of the SM are, we now turn to the matter content. There are three generations of fermions that differ in their masses and flavor quantum numbers, but are otherwise completely analogous. Those are labelled Q_{L_i}, U_{R_i}, D_{R_i}, L_{L_i}, E_{R_i}, with $i \in \{1, 2, 3\}$ the generation index. There is famously a single scalar field, namely the Higgs field, which has been for many years the last missing piece of the SM, until the experimental discovery of the Higgs boson at CERN in 2012 [1, 2]. All these elements are listed in Table 1.1, together with their transformation properties under the gauge group.

Notice that so far we have not listed any gauge bosons. This is because their existence is guaranteed, and in fact required, by the properties of the gauge symmetry, and as such they don't need to be separately added to the theory. Moreover, their interactions with the matter fields take a very specific form. The gauge group of the SM implies the presence of $8 + 3 + 1 = 12$ gauge bosons, one for each generator, and those are also included in Table 1.1.

1.1.1 The Standard Model Lagrangian and Spectrum

Now that we have introduced all the elements we need, we can write down the most general renormalizable Lagrangian that is consistent with the symmetries:

$$\mathcal{L}_{\text{SM}} = \mathcal{L}_{\text{kin}} + \mathcal{L}_{\text{Yuk}} + \mathcal{L}_{H}. \tag{1.1.1}$$

Table 1.1: Matter and gauge content of the Standard Model. Here **1**, □ and **Ad** represent the trivial, fundamental and adjoint representations for the non-Abelian gauge group, respectively.

	$\mathrm{SU}(3)_\mathrm{C}$	$\mathrm{SU}(2)_\mathrm{L}$	$\mathrm{U}(1)_Y$
Left-handed quarks Q_{L_i}	□	□	$+1/6$
Right-handed up-type quarks U_{R_i}	□	**1**	$+2/3$
Right-handed down-type quarks D_{R_i}	□	**1**	$-1/3$
Left-handed leptons L_{L_i}	**1**	□	$-1/2$
Right-handed leptons E_{R_i}	**1**	**1**	-1
Higgs scalar H	**1**	□	$+1/2$
Gluons G^a_μ	**Ad**	**1**	0
Weak gauge bosons W^a_μ	**1**	**Ad**	0
Hypercharge gauge boson B_μ	**1**	**1**	0

Let us just quote what each individual term looks like. $\mathcal{L}_\mathrm{kin}$ contains the kinetic terms for gauge bosons, fermions and Higgs field:

$$\begin{aligned}\mathcal{L}_\mathrm{kin} = &-\frac{1}{4}G^a_{\mu\nu}G^{a\mu\nu} - \frac{1}{4}W^b_{\mu\nu}W^{b\mu\nu} - \frac{1}{4}B_{\mu\nu}B^{\mu\nu} \\ &+ i\overline{Q}_{L_i}\not{D}Q_{L_i} + i\overline{U}_{R_i}\not{D}U_{R_i} + i\overline{D}_{R_i}\not{D}D_{R_i} + i\overline{L}_{L_i}\not{D}L_{L_i} + i\overline{E}_{R_i}\not{D}E_{R_i} \\ &+ (D_\mu H)^\dagger (D^\mu H).\end{aligned} \tag{1.1.2}$$

Here D denotes the appropriate covariant derivative.

$\mathcal{L}_\mathrm{Yuk}$ describes the Yukawa interactions between the Higgs and the fermions, and is responsible also for the flavor structure and CP-violating phenomena:

$$\mathcal{L}_\mathrm{Yuk} = Y^d_{ij}\overline{Q}_{L_i}HD_{R_j} + Y^u_{ij}\overline{Q}_{L_i}\widetilde{H}U_{R_j} + Y^e_{ij}\overline{L}_{L_i}HE_{R_j} + \text{h.c.}\,, \tag{1.1.3}$$

where $\widetilde{H} \equiv i\sigma_2 H^\dagger$.

$\mathcal{L}_H$ is the scalar potential for the Higgs field:

$$\mathcal{L}_H = -m_H^2|H|^2 - \lambda|H|^4. \tag{1.1.4}$$

Notice the absence of explicit mass terms for the fermions, since the symmetries of the theory forbid them. However, fermion and (some) gauge boson masses are generated through the Higgs mechanism [3–5]. For $m_H^2 < 0$, and below the scale of electroweak symmetry breaking (EWSB), the Higgs condenses to a new minimum in its potential and acquires a vacuum expectation value (VEV). Specifically, the Higgs field can be parametrized as

$$H(x) = \frac{1}{\sqrt{2}} \exp\left(2i\frac{\pi^a(x)\tau^a}{v}\right)\begin{pmatrix} 0 \\ v + h(x) \end{pmatrix}, \tag{1.1.5}$$

where $v^2 = -m_H^2/\lambda$. This VEV is responsible for the symmetry breaking pattern, and fermion and gauge boson masses are generated through the Yukawa and covariant derivative terms, respectively. The massive excitation $h(x)$ of the field $H(x)$ around the new vacuum is what is conventionally referred to as the Higgs boson. After EWSB, the spectrum of the SM can then be expressed in terms of the low energy degrees of freedom.

1.2 Beyond the Standard Model

Despite its impressive success and broad range of applications, we have a considerable amount of evidence suggesting that the Standard Model is not the ultimate theory of Nature. Some of the most notable examples are:

- **Neutrino masses**: the SM does not account for neutrino masses. However, neutrino oscillation experiments have proven that they indeed have a small, nonzero mass.

- **Dark matter**: a plethora of cosmological observations point to the existence of a different type of matter than what is described by the SM, which by itself makes up for 27% of the energy density in the Universe. Its microscopic nature and interactions with the SM are not yet entirely understood.

- **Dark energy**: observation of supernova explosions provide evidence that our Universe is currently expanding at an accelerated rate. This translates into an amount of so-called dark energy that accounts for 68% of the total energy density, leaving only 5% to conventional SM matter. Dark matter and dark energy are essential elements of the Standard Model of Cosmology, also referred to as Λ_{CDM}.

- **Baryon asymmetry**: the SM lacks a mechanism that is able to quantitatively explain the observed overabundance of matter over antimatter in the Universe.

- **Gravity**: of the four fundamental forces, gravity is the only one that is not accounted for in the SM. Moreover, we have strong evidence suggesting that quantum gravitational effects become dominant at the scale $M_{\mathrm{Pl}} \sim 10^{18}\,\mathrm{GeV}$.

On top of those observational challenges, the Standard Models of Particle Physics and Cosmology also suffer from a few conceptual and theoretical issues. These problem don't necessarily render the SMs inconsistent with phenomenological data, but rather beg for a deeper understanding of the underlying phenomena, possibly in terms of a more fundamental and complete theory. Two examples that will play a significant role in the rest of this

dissertation are the hierarchy problem and the cosmological constant problem. Overall, this suggests that we should regard the SM not as the fundamental theory of Nature, but rather as an effective field theory (EFT) that works very well in explaining a wide range of phenomena at (relatively) low energies. A large amount of research in theoretical high energy physics is devoted to finding extensions of the SM that allow to explain some of the discrepancies between the SM itself and the aforementioned experimental and theoretical considerations.

1.2.1 The Hierarchy Problem

The hierarchy problem can be thought of as the issue with the UV sensitivity of the Higgs mass, or more in general of any elementary scalar. Unlike with fermions and gauge bosons, whose masses are protected against radiative corrections by symmetry, the mass of an elementary scalar is quadratically sensitive to the physical scales of the quantum theory. Another equivalent interpretation is that there is no obstacle to continuously deforming a massless scalar QFT to a massive one, since in both cases the scalar is associated with a single degree of freedom. Computing one-loop radiative corrections up to the scale Λ results in

$$\delta m_H^2 = \frac{\Lambda^2}{16\pi^2}\Big(6\lambda + \frac{9}{4}g_2^2 + \frac{3}{4}g_Y^2 - 6y_t^2 + \dots\Big). \tag{1.2.1}$$

In any extension of the SM that contains physical UV scales (like $M_{\rm Pl}$ to account for quantum gravity) this is a disaster: it means that the parameters have to be fine-tuned to an absurd degree in order to obtain the required cancellation and reproduce the physical Higgs mass measured from experiment. Historically physicists have invoked many possibilities in order to explain the mechanism at the core of the hierarchy problem, each of them with an associated

set of new states and experimental signals. Some of those rely on the existence of new kinds of symmetries, like supersymmetry [6] and composite Higgs models/warped extra dimensions [7–12]. Others rely on anthropics arguments [13], or on dynamical relaxation mechanisms [14]. However, so far none of these models have found experimental verification, and resorting to less conventional ideas has progressively become more and more popular in recent years.

1.2.2 The Cosmological Constant Problem

From the point of view of the SM, a constant term in the Lagrangian doesn't play any significant role in terms of physics. However, as soon as the theory is coupled to gravity, such a term has important cosmological consequences, and in fact it contributes as a cosmological constant (CC) term to the Einstein equations of general relativity:

$$G_{\mu\nu} + \Lambda g_{\mu\nu} = \kappa T_{\mu\nu}. \tag{1.2.2}$$

Such a cosmological constant term can drive the accelerated expansion of the Universe, and in fact its contribution to the energy density does not dilute in time like matter and radiation do. For those reasons, it is considered a candidate for explaining the accelerated expansion originally measured from supernovae, and more recently thanks to the *Planck* space observatory [15]. However, this is also problematic as the operator associated with the CC is a relevant one, and similarly to the Higgs mass it is sensitive to the UV physical scales of the theory. Assuming the presence of physical states at the Planck scale famously results

in a theoretical prediction that is massively inconsistent with the experimental value:

$$\frac{\Lambda}{M_{\rm Pl}^4} \sim \left(\frac{10^{-3}\,\text{eV}}{10^{18}\,\text{GeV}}\right)^4 = 10^{-120}. \tag{1.2.3}$$

There are not very many compelling proposals for how to solve the CC problem. Possibly the most convincing one is based on anthropics and the existence of a multitude of vacua [16] (the so-called multiverse), some of which have a CC that is as small as the one observed in our Universe.

1.2.3 Anomalies in the Standard Model and Its Extensions

Even in the context of the SM, gauge and gravitational anomaly cancellation serves as an important consistency check on the particle content of the theory. In fact, gauge anomalies lead to unitarity violation, in the sense that the Ward identity associated with the symmetry is violated and unphysical modes can be produced. On the other hand, global anomalies do not render a theory inconsistent, rather they are often source of interesting physics. The most famous example in the SM consists of the decay $\pi^0 \to \gamma\gamma$. It follows that, also in theories beyond the Standard Model, anomalies can lead to inconsistencies of the description or to interesting new phenomena [17].

From the theoretical point of view, the fact that anomalies depend on robust and nonperturbative features constitutes a powerful tool in probing the details of the theory itself, even in cases in which a perturbative description is not available.

1.3 Outline of the Dissertation

The aim of this dissertation is to describe a number of different ways to tackle the problems in the SM and study its possible extensions. The rest of this work is organized as follows:

- Chapter 2 presents an approach to the hierarchy problem in which masslessness of the Higgs is linked to the minimum of an effective potential for a modulus field. In this way Higgs criticality can become an attractor as a special point of the theory not in terms of symmetry, but rather in terms of dynamics.

- Motivated partly by the analysis of Chapter 2, Chapter 3 studies the dynamics of various extra-dimensional models with multiple scalar fields in the bulk, and derives general results about radius stabilization mechanisms for the size of the extra dimension.

- Still in the context of the AdS/CFT correspondence, Chapter 4 describes a systematic approach to the perturbative anomaly inflow of a bulk Chern-Simons theory in five-dimensional AdS space. In particular, we carefully construct the holographic dual interpretation and show how many interesting phenomena like 't Hooft anomaly matching and Wess-Zumino-Witten terms naturally emerge from a unified description in the 5D theory.

- Finally, Chapter 5 suggests a fascinating new strategy to test the physics of vacuum energy, thanks to the possible role played by high-density QCD in the cores of the most massive neutron stars. It then focuses on how to extract related information from the gravitational waves emitted during neutron star merger events.

Chapter 2

Self-Organized Higgs Criticality

2.1 Introduction

The Higgs instability in the electroweak sector of the Standard Model (SM) appears thus far to be of the simplest variety, with the Higgs sector residing "unnaturally" close to a critical point seemingly unprotected by symmetry and well described by mean field theory. The Higgs sector is associated with a Landau-Ginzburg theory of a symmetry breaking phase transition. The Higgs field of the Standard Model develops a vacuum expectation value (VEV) due to a relevant operator (the Higgs mass term) having the "wrong sign" in the infrared which destabilizes the origin in field space. The naturalness issue, or the hierarchy problem, is the statement that in units of the much larger fundamental scales in the problem, i.e. the Planck or GUT scales, the bare mass must be tuned to an absurd degree to accommodate the observed value for the VEV and the mass of the Higgs particle, and that quantum corrections spread this sensitivity among fundamental parameters. That is, quantum effects make the Higgs mass similarly sensitive to, for example, the value of the top quark Yukawa coupling.

As a consequence it is expected that low energy effective theories with Higgs sectors like that of the SM are extraordinarily rare when there are other large physical scales present.

Most proposed resolutions of this problem invoke new symmetries requiring new particles with fixed interactions that ameliorate the sensitivity of the Higgs mass to larger mass scales. The paucity of new particles at the TeV scale has sown growing doubt that this is the way nature has created a low electroweak scale.

In this work, we begin an investigation of the possibility that the critical point for Higgs sectors like that of the SM can arise naturally not due to symmetry, but rather because of a self-organization principle, as suggested in [18]. This is inspired by critical behavior that has been observed in a wide variety of seemingly unrelated physical systems in nature [19, 20], with the canonical example being the sandpile. In this example, a pile of sand is created and sustained by slowly pouring sand from a funnel onto a fixed point. The sand self-organizes into a cone with opening angle fixed by microscopic interactions between grains. Perturbations, even if only involving a single grain of sand, result in avalanches at all scales, following a power law distribution. After the avalanche, when the system has removed the perturbation, the cone of sand is in a new configuration, but still critical so long as sand continues to be slowly added. Such "self-tuning" is also thought to arise at earthquake fault lines, river bifurcations, and temporally near financial market crashes [21]. It has been key to describing some astrophysical phenomena as well [22]. It has been hypothesized that these phenomena of criticality at the threshold of "catastrophic failure" can be related to an instability arising from critical exponents becoming complex, corresponding to discrete scale invariance [23]. This possibly suggests an approach to the Higgs fine-tuning problem in extra-dimensional models in AdS space, where similar features appear when the Breitenlohner-Freedman (BF) bound [24]

is violated, leading to complex scaling dimensions and a complete loss of conformality in a hypothetical 4D dual [25].

Typically, in the examples we have in statistical physics, criticality is "self-organized" by temporal loading of the system: the slow addition of sand grains at a pile's apex, gradual stress building at faults due to tectonic drift, etc. In relativistic theories, this slow temporal loading can be exchanged with mild spatial gradients, and in 5D, through the AdS/CFT duality [26], spatial translation and gradients can be, in turn, related to scale transformations and renormalization group evolution. This further suggests an approach where the instability associated with complex scaling dimensions is reached dynamically through slow renormalization group evolution, or, in a 5D dual, via growth of a deformation of AdS space that leads to eventual violation of the BF bound. This has a parallel in some perturbative 4-dimensional theories where dimensional transmutation directs the Higgs potential [27]. In models such as the MSSM, the instability of the electroweak sector can be arrived at through quantum corrections [28–30]: RG flow from some microscopic theory seemingly devoid of instabilities evolves to an IR theory where a Higgs picks a non-vanishing condensate.

Stepping away from the background motivation, we can state generally that the eventual goal of this line of research is to have a zero for the Higgs mass term coinciding (or nearly coinciding) with a minimum in the potential for an extra-dimensional modulus field over a wide range of extra-dimensional input parameters. In this case Higgs criticality would be a dynamical attractor for the theory without extreme sensitivity to fundamental constants. In other words, such a 5D system *self-tunes* to the critical point of its 4D low energy effective Higgs theory. This is similar to the way in which the strong CP problem is resolved by the

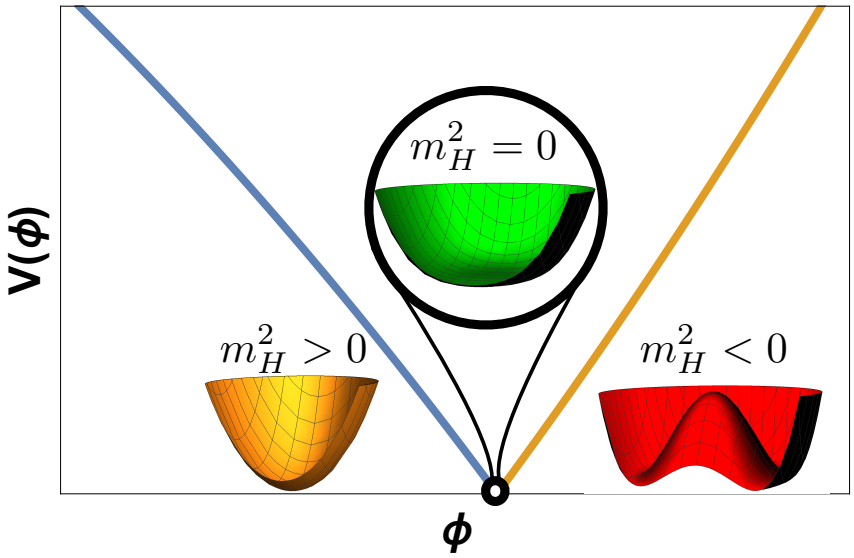

Figure 2.1: This figure exhibits a cartoon of a potential for a modulus field, ϕ, where the singular minimum matches on to a critical point at which the mass of a physical light Higgs field fluctuation passes through zero. On either side of the singular point, the Higgs boson mass is finite and positive, but on one side the mass squared for the field is negative, with the instability driving spontaneous symmetry breaking.

axion hypothesis where the axion field promotes the CP phase to a dynamical field whose potential minimum resides at the point where CP is conserved in QCD, and also to models which solve the hierarchy problem using cosmological dynamics and slightly broken shift symmetries [14].

To be properly identified as self-organization, in the most conservative application of this label, criticality near the minimum of the potential must be robust under reasonable variation of model input parameters: we are looking for a theory with a near-critical Higgs *region*. From the perspective of the low energy theory, at energy scales below the modulus VEV, the lightness of the Higgs would be in apparent violation of effective field theory principles and power counting, that is, a violation of the principle of locality of scales.[1] This could be reconciled by the fact that in a microscopic 5D theory, quantum corrections might renormalize

[1]Such violation has been observed before in a toy model with discrete scale invariance [31], another suggestive connection to self-organized critical systems.

the potential for the Higgs and modulus field simultaneously, shifting the *location* of the minimum, but not the property that the physical Higgs boson is light at that minimum. A cartoon is shown in Figure 2.1. We emphasize that this has not yet been realized in a dynamical model in this work, but rather is a longer term goal in which this paper could be a crucial first step.

To realize such a scenario, there first must be a feedback mechanism, such that when the Higgs field develops a VEV, the potential for the modulus responds, as shown in Figure 2.1. This is somewhat akin to the way thresholds can play an important role in Casimir energies, as in, for example [32]. If this feedback is itself the origin of the minimum of the potential, with the minimum being at or near the critical value at which the Higgs VEV turns on, the modulus field will be attracted to the minimum, where the mass of the Higgs fluctuation is small or vanishing.

In one "toy" and one fully dynamical construction, we investigate the mutual potential of a modulus field (in our case, the radion of a Randall-Sundrum (RS) 2-brane model [33]) and a 5D Higgs field. The models are constructed so that the value of the modulus field vacuum expectation value influences the Higgs stability criterion. Specifically, we consider scenarios where the Higgs instability is linked to dynamical violation of the BF bound far from the UV boundary of the RS geometry through interactions with the modulus field.

The CFT dual of this picture corresponds to the theory described above: one which is conformal in the deep UV, without instabilities, and which contains a near marginal deformation that drives a slow running of the scaling dimension of an operator in this approximate CFT [34, 35]. There is an interplay between two operators, $\mathcal{O}_\epsilon$, a near marginal operator, and $\mathcal{O}_H$. Similar to the way dynamical symmetry breaking for the Higgs can

occur via radiative corrections, here an analogous instability is reached in the RG flow for the dual picture, with the scaling dimension for the operator $\mathcal{O}_H$ becoming complex, and causing an "unhealthy" [36] limit cycle-like behavior in the RG flow that is terminated by condensation of operators in the approximate CFT, breaking the approximate conformal invariance spontaneously.

Curiously, in the models studied here, a nontrivial cosmology may be a common feature of the classical ground state. In the 5D picture, the metric and scalar fields must include a cosmology for the low energy 4D effective theory in order to satisfy the metric junction conditions for the two brane model, unless UV and IR brane tensions are tuned. We suspect this is due to a frustration mechanism similar to that which causes striped and other inhomogeneous phases to appear in some high T_c superconductors [37], and may lead in this case to a time-dependent vacuum state [38, 39]. Studies of holographic superconductivity have identified such phases when the BF bound is violated deep in the interior of asymptotically AdS geometries due to non-trivial gauge and gravitational field backgrounds [40]. In other words, the resolution of the RG limit cycle instability may have its imprint in the low energy theory as a limit cycle in time evolution. We have left a full exploration of the time dependence for future work, however we do speculate on the possible relevance of this feature for cosmology [41, 42].

The article is organized as follows: In Section 2.2, we set the stage with a discussion of a possible effective theory for a dilaton vacuum expectation value that has features that we find in our holographic model, and which points towards a new way to set the confinement scale in an approximately conformal theory. In Section 2.3, we describe a 5D toy holographic implementation of these ideas that leaves out certain backreaction terms, with a bulk Higgs

mass that is given *explicit* dependence on the extra-dimensional coordinate. In Section 2.4, we show how to promote this simplest model to a dynamical one, where the effective Higgs mass evolves due to a coupling to a "driving" scalar which picks a coordinate-dependent VEV. In Section 2.5 we discuss in more detail a possible approximate CFT interpretation of the 5D model, and make some connections to generalized BKT scaling discussed in [25]. In Section 2.6, we briefly discuss connections to self-organized critical models in statistical physics, to catastrophic failure modes of these systems, and future implementation of these ideas into an extension of the SM. Finally, we discuss aspects of the cosmology of the model, part of which involve speculation that can be more fully resolved with future work, in Section 2.7.

2.2 Preliminaries: The Frustrated Dilaton

We begin by considering an effective theory of a dilaton that has aspects of the behavior of the more detailed holographic models we consider. In an approximately scale-invariant theory that undergoes spontaneous breaking, the potential that sets the scale of that breaking is a (nearly) scale-invariant quartic: $V_{\text{dil}} = \alpha(f) f^4$, where α has some weak dependence on f that encodes the amount of explicit breaking. This potential can have a nontrivial minimum at small values of f if α obeys some basic properties.

It is important to note that in this effective theory, f is a summed total scale of conformal breaking, and relations between individual VEVs are hidden in this potential. In other words, many operators could be simultaneously condensing which all contribute to conformal breaking. In addition, if there is some small breaking of conformal invariance, there can be

nontrivial relations between these operator VEVs that are not encoded in the total dilaton potential.

Now we note that it could be the case that there is simply no solution that satisfies the relation between VEVs in the approximate CFT for a total f below some critical value, $f < f_{\text{crit}}$. How does the theory exit the CFT in this case? The dilaton is frustrated – internally, it seeks to satisfy the relations between operator VEVs, providing a lower limit to the total breaking scale. On the other hand, in the low energy theory, a smaller or vanishing f is preferred.

As a very simple example of this, we could consider two VEVs f_ϕ and f_{higgs} where at some critical value of decreasing f_ϕ, f_{higgs} begins to turn on:

$$f_{\text{higgs}}^2 = \begin{cases} -\frac{\lambda f_\phi - \mu^2}{\lambda_H} & \lambda f_\phi - \mu^2 < 0 \\ 0 & \text{otherwise} \end{cases} .$$

Such behavior occurs in the "relaxion" models of electroweak symmetry breaking. Note however, that we are not specifying a global potential for this behavior, but instead are merely providing an ad hoc relationship between operator VEVs that might arise inside of the approximate CFT. In the holographic models we consider, f_ϕ corresponds to the VEV of a marginally relevant operator, and f_{higgs} to the VEV of an operator whose scaling dimension is driven into the complex plane.

If these VEVs contribute to an effective dilaton potential as $V_{\text{dil}} \approx \alpha(f_\phi^4 + f_{\text{higgs}}^4)$ (as though they are both from operators with scaling dimension near 4), the potential will be globally minimized when $f_\phi^2 = \frac{\lambda}{2\lambda_H f_\phi} f_{\text{higgs}}^2$ if the relationship between VEVs is maintained. A

large hierarchy between f_{higgs} and f_ϕ can be created by having a small value of λ_H, and the dilaton potential appears to be minimized at some f_{crit} while enforcing the relation.

We note that the dilaton potential itself does not enforce the relation between the VEVs, which is instead specified by some dynamics that is part of the UV completion of the dilaton effective theory. This can create a puzzle from the perspective of the low energy theorist, which sees only the total breaking scale f, not the interrelations between the individual f's that contribute. The low energy observer would think that $f = 0$ should minimize the pure quartic potential, but instead the theory gets "trapped" at a larger f. Of course these relations between VEVs would require some breaking of scale invariance, and the potential would not be precisely quartics.

There may be a connection here to the concept of frustrated phase separation in condensed matter physics, a phenomenon where (for example) high T_c superconductivity is blocked due to long range Coulomb interactions, and the theory resolves the tension by creating an intermediate phase which spontaneously breaks translation invariance, creating "stripes" [37]. Here, Higgs condensation may be blocked by quasi-long range dilaton interactions, and there may be some analog of these striped phases that resolves the frustration that is important for cosmology.

With this hypothetical scenario as context and motivation, we begin our holographic studies.

2.3 Toy Model: Explicitly Varying Higgs Mass

To illustrate a basic model with the features we seek, we work in 5D asymptotically anti-de Sitter space without a UV brane, and give the Higgs a bulk mass term that varies *explicitly* with the extra-dimensional coordinate. We strongly emphasize that this is a toy model that easily illustrates some curious features that help motivate the more realistic model in Section 2.4. Specifically, this model leaves out backreaction between the Higgs and the (here unspecified) dynamics that give rise to the varying mass term, while in Section 2.4, this backreaction is taken fully into account.

The metric can be written as (setting the AdS curvature near the AdS boundary, k, to 1) [43]:

$$ds^2 = \frac{1}{z^2}\left[dx_4^2 - \frac{dz^2}{G(z)}\right]. \tag{2.3.1}$$

The coordinate z ranges from 0 at the AdS boundary to an IR brane at $z = z_1$, and for $z \to 0$, the function G has the asymptotic behavior $G(z) \to 1$ and $G'(z) \to 0$. Away from $z = 0$, the function G encodes the effects of gravitational backreaction due to nontrivial bulk physics such as condensates. We are restricting our ansatz for the background to solutions obeying 4D Lorentz invariance.

The action is given by

$$\begin{aligned} S = &\int d^4x dz \sqrt{g}\left[|\partial_M H|^2 + \frac{6}{\kappa^2} - m^2(z)|H|^2 - \frac{1}{2\kappa^2}R\right] \\ &- \int d^4x z^{-4} m_0^2 |H|^2\Big|_{z\to 0} - \int d^4x z^{-4} V_1(|H|)\Big|_{z\to z_1}, \end{aligned} \tag{2.3.2}$$

with $\kappa^2 = 1/(2M_{\rm Pl}^3)$. The bulk mass function is chosen to a have fixed value in the limit

$z \to 0$, and decreases monotonically and slowly as z increases:[2]

$$m^2(z) = -4 + \delta m^2 - \lambda z^\epsilon. \tag{2.3.3}$$

Note that $m^2 = -4$ corresponds to the Breitenlohner-Freedman bound, and δm^2 is taken to be a positive quantity so that the $z \to 0$ limit is well-defined.[3] We note that past work explored constant Higgs bulk mass at or near the BF bound [44, 45] with interesting implications for radius stabilization. A possible relationship between the BF bound and scalars with suppressed mass in lattice studies of theories at the boundary of the conformal window was discussed in [46]. For the IR brane potential, we take

$$V_1(|H|) = T_1 + \lambda_H |H|^2 \Big(|H|^2 - v_H^2 \Big), \tag{2.3.4}$$

where T_1 is the tension of the brane. The Higgs may, for some regions of parameter space, pick a nonvanishing vacuum expectation value, $\langle H \rangle = \phi(z)/\sqrt{2}$, where the Higgs VEV has a nontrivial profile along the z-coordinate.

Restricting to solutions that obey 4D Lorentz invariance, the 5-5 component of the Einstein equations relate the metric function G to the behavior of the Higgs VEV in the bulk:

$$G = \frac{-\frac{\kappa^2}{6} V(\phi)}{1 - \frac{\kappa^2}{12} (z\phi')^2}, \tag{2.3.5}$$

[2] It is not difficult to arrange for this type of z-dependent mass term to arise dynamically, rather than through this forced explicit breaking of the isometries of AdS. We give examples in Section 2.4.

[3] If the mass is taken below the BF bound as $z \to 0$, perturbations solving the scalar equation of motion oscillate rapidly in the UV, indicating the need for an ultraviolet cutoff, such as a brane that cuts off the small z region of the spacetime [25].

and they can be further employed to reduce the effective potential for the classical background configuration to a pure IR boundary term [47]:

$$V_{\rm rad} = \frac{1}{z_1^4}\left[V_1(\phi) + \frac{6}{\kappa^2}\sqrt{G}\right]. \tag{2.3.6}$$

There is generally a UV contribution from the brane at z_0 as well, but it vanishes as $z_0^{2\sqrt{\delta m^2}}$ in the $z_0 \to 0$ limit, with the exception of a constant term which is tuned to give vanishing effective cosmological constant. We also note that the remaining components of Einstein's equations in the bulk do not give additional information on G, being equivalent to the scalar field equation of motion for the z-dependent background, and that for the purposes of calculation of the effective potential for the size of the extra dimension, we fix the 4D portion of the metric to be flat. This amounts to satisfying vanishing variation of the action with respect to those metric components in a trivial manner, requiring that the variations themselves vanish: $\delta g_{\mu\nu} = 0$.

For small values of the Higgs VEV, or alternatively weak 5D gravity, this effective radion potential reduces to

$$V_{\rm rad} = \frac{1}{z_1^4}\left[V_1(\phi) + \frac{6}{\kappa^2} - \frac{1}{4}m^2(z_1)\phi^2(z_1) + \frac{1}{4}z_1^2\phi'^2(z_1)\right]. \tag{2.3.7}$$

The scalar field equation of motion in the limit of small κ^2 is

$$\phi'' - \frac{3}{z}\phi' - \frac{1}{z^2}\frac{\partial V}{\partial \phi} = 0, \tag{2.3.8}$$

with energetic favorability of a nontrivial solution depending on the boundary conditions,

which are (again in the small κ^2 limit):

$$z\phi'|_{z=z_{0,1}} = \pm\frac{1}{2}\frac{\partial V_{0,1}(\phi)}{\partial\phi}. \tag{2.3.9}$$

Near the AdS boundary $z \to 0$, the solutions are power law in z, with the expected behavior $\phi \propto z^{2\pm\sqrt{\delta m^2}}$, where the two different scaling laws correspond to two different boundary conditions or definitions of the action [48]. The scaling law z^{Δ_+} is more generic, with fine-tuning of BCs (or supersymmetry) required to obtain the scaling with power law Δ_-. The full solution for all z, including the effects of the changing bulk mass, is

$$\phi \sim \phi_\pm z^2 J_{\pm\nu}\left(\frac{2\sqrt{\lambda}}{\epsilon}z^{\epsilon/2}\right), \tag{2.3.10}$$

where $\nu \equiv 2\sqrt{\delta m^2}/\epsilon$. For $m_0^2 \neq 2-\sqrt{\delta m^2}$, only the $+$ solution is relevant, while for the special case $m_0^2 = 2-\sqrt{\delta m^2}$, the field behavior is given by the $-$ solution. Choosing the special case corresponds in the holographic picture to fine-tuning the coefficient of an operator $O_H^\dagger O_H$ to force the RG flow to go "backwards" compared to the more generic $+$ scaling solution [25, 49], or in other words, tuning so that the theory sits at a UV fixed point.

Choice of the UV boundary condition does not much affect the discussion, and we choose to display the effects of the first of these two solutions, taking $m_0^2 = 0$.

For large values of z, and small ϵ, the asymptotics of the Bessel function exhibit log-periodicity on top of scaling when z is past the point where the BF bound is surpassed by the evolving bulk mass:

$$\phi \propto z^{2-\epsilon/4}\cos\Big(\sqrt{\lambda}\log z + \gamma\Big). \tag{2.3.11}$$

This log-periodic power law behavior may be a common feature in systems where criticality is self-organized [23].

The condition for formation of a condensate is met when the IR brane boundary condition favors a nontrivial value for the coefficients of the bulk solution:

$$\frac{1}{\epsilon}\Big(\lambda_H v_H^2 - 4\Big) \geq \frac{x J'_\nu(x)}{J_\nu(x)}, \tag{2.3.12}$$

where $\nu \equiv 2\sqrt{\delta m^2}/\epsilon$ and $x \equiv 2\sqrt{\lambda} z_1^{\epsilon/2}/\epsilon$. Equality is associated with the presence of the exact critical point. Note that equality is satisfied at many values of z_1 due to quasi-periodicity of the right-hand side at large z_1. We label the i-th critical point as $z_{\rm c}^i$. The emergence of a massless degree of freedom at these critical points can be seen in the small momentum behavior of the bulk correlator for the Higgs fluctuations. Working in the unbroken phase, the Green's equation for scalar fluctuations is given by

$$\left[\partial_z^2 + p^2 - \frac{3}{z}\partial_z - \frac{m^2(z)}{z^2}\right] G\Big(z, z'; p^2\Big) = iz\delta(z - z'). \tag{2.3.13}$$

At the point of criticality, for small p^2, the Green's function in terms of an eigenfunction decomposition takes the form

$$G\Big(z, z'; p^2\Big) \approx \frac{\psi_0(z)\psi_0^*(z')}{p^2} - \sum_{i=1}^{\infty} \frac{\psi_i(z)\psi_i^*(z')}{m_n^2}, \tag{2.3.14}$$

where $\psi_0(z)$ solves the 5D equation of motion for $p^2 = 0$, and thus takes the same functional form as the VEV, $\phi(z)$. The m_n are the usual KK-mode masses. As we discuss in further detail below, the m_n^2 are not guaranteed to be positive at all of the critical points, and in fact

only one, the smallest z_c critical point, z_c^1 has a positive spectrum.

As the Higgs VEV turns on, the character of the radion potential also changes dramatically. Of primary interest is the behavior of the radion potential near the region of z_1 where the Higgs VEV is just turning on. A linearized approximation of the Higgs contribution to the potential gives the leading contribution in the immediate neighborhood of criticality. The function for $\phi(z_1)^2$ is analytic, and near its zeros, say one at $z_1 = z_c^1$, we have

$$\phi(z_1)^2 \approx \sigma^2\left(\frac{z_1}{z_c^1} - 1\right), \tag{2.3.15}$$

where σ^2 is a positive function of the parameters of the theory:

$$\sigma^2 = \frac{-4m^2(z_c^1) + \lambda_H v_H^2(\lambda_H v_H^2 - 8)}{2\lambda_H}. \tag{2.3.16}$$

The radion potential in the regime just after the VEV turns on is given by

$$V_{\text{rad}} \approx \frac{1}{z_1^4}\left[\delta T_1 + \frac{\lambda_H \sigma^4}{8}\left(\frac{z_1}{z_c^1} - 1\right)\right]. \tag{2.3.17}$$

The radion potential is thus piecewise, and if we look in the vicinity of the critical point, it takes the form

$$V_{\text{rad}} \approx \begin{cases} \dfrac{1}{z_1^4}\delta T_1 & z_1 < z_c^1 \\ \dfrac{1}{z_1^4}\left[\delta T_1 + \dfrac{\lambda_H \sigma^4}{8}\left(\dfrac{z_1}{z_c^1} - 1\right)\right] & z_1 > z_c^1 \end{cases}, \tag{2.3.18}$$

where δT_1 is the mistune between the IR brane tension and the bulk cosmological constant. We note that quantum corrections will spread z-dependence from the scalar mass to the cosmological constant term, and the background will no longer be pure AdS. These small

corrections will modify the background potential away from a pure quartic - this is not, however, important for the features we draw attention to in this model. In the next section, the background potential is modified away from a pure quartic by a Golderberger-Wise type potential.

At the critical point, there is a kink discontinuity in the radion potential.[4] The contribution of the Higgs condensate to the radion potential is also positive definite. In order for the derivative of the radion potential to change sign, creating a kink *minimum*, an additional condition for the radion quartic (the IR brane mistune) must hold:

$$0 < \delta T_1 < \frac{1}{128\lambda_H}\left[4m^2\left(z_c^1\right) - \lambda_H v_H^2\left(\lambda_H v_H^2 - 8\right)\right]^2. \tag{2.3.19}$$

These requirements are satisfied relatively robustly under variation of the input parameters. In Figure 2.2, we show an example of the radion potential, where we have taken $\delta T_1 = 1$, $\delta m^2 = 1$, $\lambda = \epsilon = 0.1$, $v_H^2 = 0$, and $\lambda_H = 1/8$.

There are two plots in the figure: in the first, on the left, we show a close-up that focuses on the critical value of the radion VEV. On the right, we zoom out. Unsurprisingly, it appears that there are multiple such minima, and that the first one is metastable. This is due to the quasi-periodicity of the Higgs VEV solution at large values of z. Closer examination of the theory in these regions shows that there are unresolved tachyon instabilities associated with Higgs fluctuations. In these regions, no VEVs are formed, but there are solutions to the scalar equation of motion with negative mass squared, as we show in the next subsection.

[4] We note that this kink feature is due to the fact that we are deliberately ignoring backreaction between the Higgs and the dynamics that creates the varying mass term. The properties of the critical point differ in complete models, and we begin a study of an explicit example in Section 2.4.

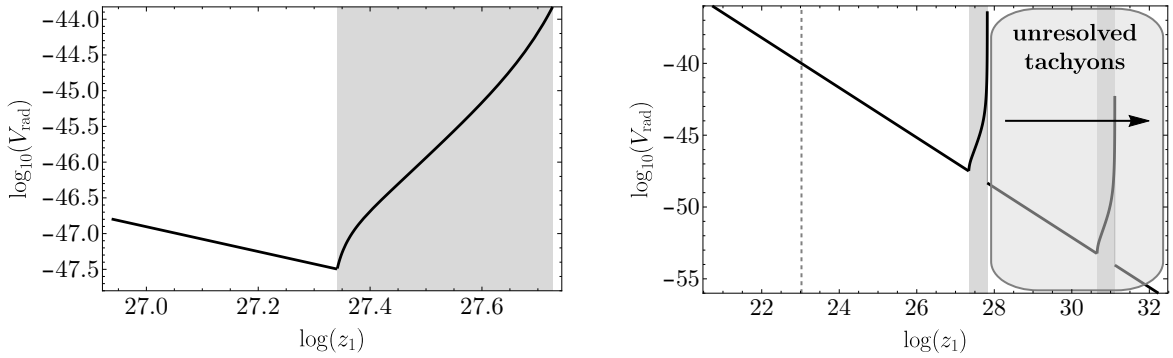

Figure 2.2: Here we display the radion potential, $V_{\rm rad}(z_1)$. In the white region, the Higgs VEV is vanishing, and the radion potential is a pure quartic. In the gray region, $\phi(z_1) \neq 0$, and the contribution of the Higgs to the radion potential causes a kink-like minimum to appear at the critical points. In the first plot, we have zoomed in on the first minimum, corresponding to the smallest z_1 for which the criticality conditions are met. In the second plot, we zoom out, showing other potential minima. These are unhealthy, in that the theory at this point contains unresolved tachyons. The dashed vertical line in the second plot corresponds to the value of z at which the evolving bulk Higgs mass passes the BF bound.

Before studying the instabilities, it is worthwhile to explore the behavior of the effective potential under variations of the fundamental parameters. Crucial to the success of the model as one of self-organized Higgs criticality is the existence of a broad critical region, over which the Higgs remains light. In Figure 2.3, we examine the behavior of the radion potential under variations of the IR brane Higgs mass squared, encoded in v_H^2. We see that with changing v_H^2, the location of the minimum is relatively constant, however there is a crucial value of v_H^2 past which the location of the minimum moves away from the kink in the potential. The region of parameter space where the minimum resides at the kink is a critical region, as there is a zero mode Higgs for all values of $v_H^2 < v_H^2(\text{crit})$.

In the next subsection, we comment on properties of this kink minimum in the effective radion potential, in particular those related to the metric ansatz that we have enforced.

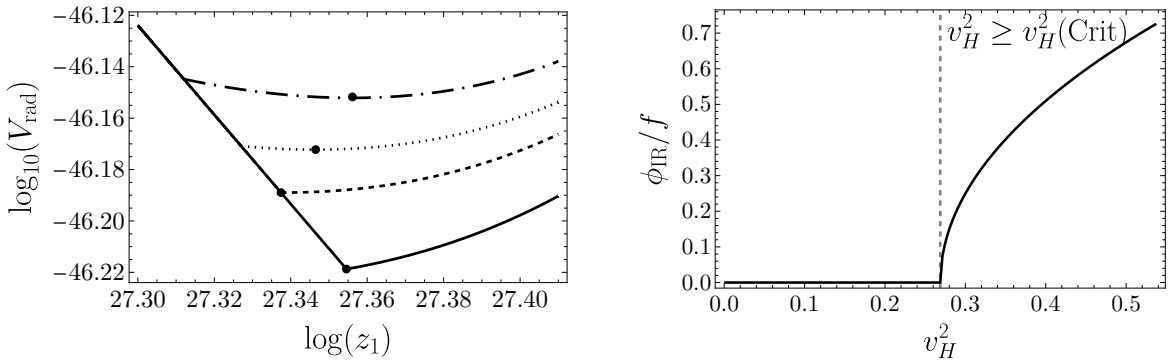

Figure 2.3: Here we show, on the left, the dependence of the potential on the IR brane parameter v_H^2 in the vicinity of the first critical point. The curves correspond to $v_H^2 = -1$ (solid), $v_H^2 = v_H^2(\text{crit})$ (dashed), $v_H^2 = 1$ (dotted), and $v_H^2 = 2$ (dot-dashed). The dots indicate the minimum of the potential. The minimum moves into the region where the Higgs VEV is nonzero after some critical point $v_H^2(\text{crit})$. On the right, we show the value of the Higgs field on the IR brane in units of the scale $f = z_{\rm min}^{-1}$, where $z_{\rm min}$ is the location of the minimum of the radion potential. The VEV (and Higgs mass/inverse of the correlation length), which is proportional to $\phi_{\rm IR}$, is vanishing below $v_H^2(\text{crit})$, and grows quickly after the critical point is exceeded.

2.3.1 Metric Boundary Conditions

In calculating the radion potential in Eq. (2.3.7), we have imposed the boundary conditions for the scalar fields, but we have neglected the metric junction conditions on the branes, which enforce

$$\sqrt{G(z_0)} = \frac{\kappa^2}{6} V_0, \qquad \sqrt{G(z_1)} = -\frac{\kappa^2}{6} V_1. \tag{2.3.20}$$

This is equivalent to having the UV brane and IR brane contributions to the effective potential separately vanish [50, 51]:

$$\begin{aligned} \tilde{V}_{\rm UV} &= V_0 - \frac{6}{\kappa^2}\sqrt{G_0} = 0, \\ \tilde{V}_{\rm IR} &= V_1 + \frac{6}{\kappa^2}\sqrt{G_1} = 0, \end{aligned} \tag{2.3.21}$$

where we have defined $V_{\rm rad} = \frac{1}{z_0^4}\tilde{V}_{\rm UV} + \frac{1}{z_1^4}\tilde{V}_{\rm IR}$. In fact, these conditions are not satisfied for any values of z in the above potential. These conditions should be interpreted as consistency conditions for our metric ansatz, in which we have forced the metric to exhibit 4D Lorentz

invariance so that we can interpret the result as a Lorentz-invariant 4D effective potential for the modulus field. In terms of variation of the scalar-Einstein-Hilbert action, we have satisfied vanishing variation of the action by keeping the variations of the 4D metric components $\delta g_{\mu\nu}$ themselves to be zero, and in so doing, Eq. (2.3.20) is no longer a constraint on the solution.

In the usual Goldberger-Wise scenario, the second of the two conditions in Eq. (2.3.20) is met automatically at the minimum of the potential, with the value of the size of the extra dimension being set by its solution. The first is then arranged for by tuning (equivalent to the usual tuning of the bare cosmological constant to small values). From this, we can roughly interpret the time dependence away from the minimum of the usual Goldberger-Wise potential as a combination of cosmological acceleration and oscillations of the stabilized radion. The situation is quite different in the case of the potential described above. At the kink minimum generated by the Higgs contribution, these junction conditions cannot both be met unless two tunings are performed – both the bare cosmological constant and the mistune in the IR brane tension.

This doesn't necessarily mean that the region where the kink is a minimum is forbidden, but rather tells us that once inside this region, a dynamical geometry is unavoidable, and must be included in a fully consistent calculation of the spectrum of the low energy theory. In other words, in a theory with fully dynamical gravity, the ansatz for the background *must* be relaxed to include a nontrivial 4D cosmology. In Section 2.7, we discuss this issue of a dynamic cosmology further, and speculate on its resolution and interpretation.

We further note that the same behavior occurs in the case of the dynamical scalar model considered in Section 2.4, although the kink feature is absent.

2.3.2 Instabilities

Here we briefly examine the stability of fluctuations for different values of the position of the IR brane. Summarizing the results first: the minimum for smallest z_c and neighboring values of the radion VEV is always a "healthy" minimum where there are no unresolved tachyonic states. However, past the first region where the Higgs VEV resolves the tachyon, there are apparently instabilities without condensates to rectify them, or the condensates are insufficient to prevent all of them. In this case, the approximation of a static 5D description is not a good one, and the theory must resolve the tachyon with some more dramatic dynamics. We comment briefly on this in Section 2.6, and a more complete analysis of this region is part of future work.

We can inspect the tachyon instabilities through examination of the spectrum of Higgs fluctuations. The equation of motion for these, presuming a vanishing Higgs VEV, is given by

$$h''(z) - \frac{3}{z}h'(z) - \frac{1}{z^2}\Big(-4 + \delta m^2 - \lambda z^\epsilon\Big)h(z) = -m^2 h(z), \tag{2.3.22}$$

with IR boundary condition given by

$$h'(z_1) = \frac{1}{2z_1}\lambda_H v_H^2 h(z_1). \tag{2.3.23}$$

The UV boundary condition we impose is that the solution must asymptote to the behavior given in Eq. (2.3.10), on the + branch. Equivalently, one could impose $z_0 h'(z_0) = m_0^2 h(z_0)/2$ for some non-tuned value of m_0^2, and subsequently take the limit as $z_0 \to 0$. The result is similar.

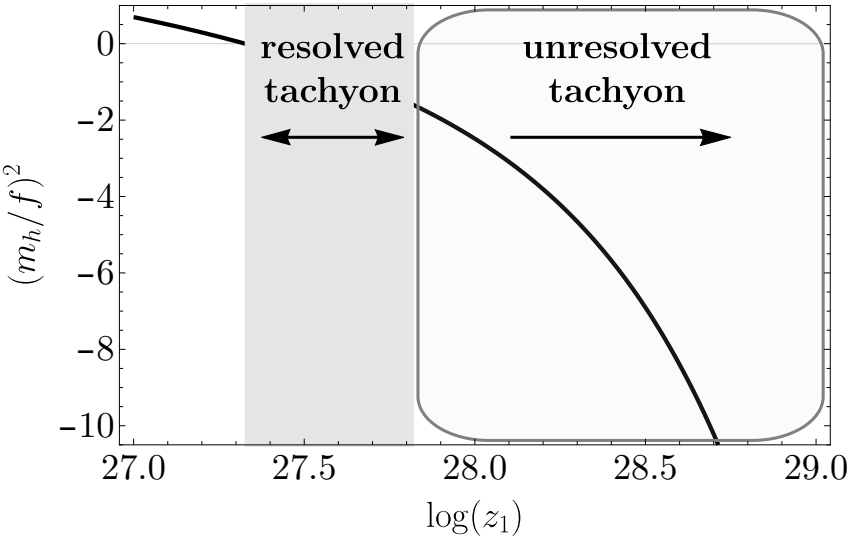

Figure 2.4: Here we show the lowest eigenvalue associated with the Higgs fluctuations, the solutions to Eq. (2.3.22) with the boundary conditions associated with the IR brane-localized Higgs potential. The region where the Higgs VEV resolves a single tachyon is shaded, and the physical Higgs fluctuation here is in fact massive. This is the first critical region, where there is only one tachyon to be resolved. An unresolved tachyon emerges for larger z_1, when the Higgs VEV turns off, indicating a fundamental instability.

Solving the boundary value problem gives the spectrum of states. In Figure 2.4, we display the lowest eigenvalue, expressed as the ratio $(m_h/f)^2$, where $f^{-1} = z_1$. The region where the Higgs VEV resolves the tachyon is shaded, and there Higgs fluctuations are massive. At larger z_1, outside the gray region where there is no Higgs condensate, there is a tachyon that persists. It appears that the condensate can rectify the tachyon so long as the mode is not *too* tachyonic. For larger z_1, the problem grows still worse: in the neighborhood of the n-th critical value of z_1, there are $n-1$ unresolved tachyons.

Due to the presence of unresolvable tachyons for larger z_1, we focus our main attention on values of z_1 where there is either no tachyon, at $z_1 < z_c^1$, or there is a single tachyon that is resolved by the vacuum expectation value for the Higgs field, $z_1 \gtrsim z_c^1$.

It is interesting that the first minimum appears metastable, with other minima at larger

values of z_1, but lower effective potential energy, as seen in Figure 2.2. We comment further on this in Section 2.6. However, we must not take this region of large z_1 too seriously. For one, the vacuum expectation value for the Higgs diverges at the end of the first condensate region, and the theory cannot be trusted there, where gravitational backreaction will be very large. It is not obvious that the geometry can be considered at all past this point.

Additionally, as discussed in the previous subsection, we have not taken into account the required time dependence in the solution. It is not obvious that the same instabilities will be present once the ansatz for the background is relaxed to allow for a dynamical background.

Finally, we have enforced a rigid dependence of the mass on the z-coordinate, which is not likely to be possible in a self-contained fully dynamical model. It is likely that this rigidity of the mass profile is responsible for the kinked behavior of the potential at the critical point. Backreaction between the dynamics that drives the mass and the Higgs VEV may smooth out the potential. This is confirmed in a fully dynamical model explored in the next section.[5]

2.4 Dynamical Model

In the previous section, the varying bulk mass for the Higgs was taken as an input, breaking the isometries of AdS explicitly, and we took the UV brane to the AdS boundary. In this section we show how similar physics can be derived in a dynamical and more realistic model with a UV brane where the interplay of a Goldberger-Wise-like scalar field and a bulk Higgs on an AdS background generates a similar physics result. This model has the benefit of being fully dynamical, of having a possible CFT dual that is easier to interpret, and having a

[5]We thank Prashant Saraswat and Michael Geller for useful comments on the first version of this pre-print that led us to more fully explore the details of the dynamical model.

modulus potential that does not exhibit the kink of the previous toy model. The 5D Higgs profile can no longer be solved for analytically, and so we perform a numerical study.

This model has two bulk scalar fields, a real scalar, $\phi_{\rm d}$, the "driving scalar", in addition to a Higgs scalar. The fields are coupled in such a way that a varying VEV of the scalar $\phi_{\rm d}$ drives the effective bulk mass of the Higgs, making it a function of the extra-dimensional coordinate. The 5D action is given by

$$\begin{aligned} S = &\int d^4x dz \sqrt{g}\Big[|\partial_M H|^2 + \frac{1}{2}(\partial_M \phi_{\rm d})^2 + \frac{6}{\kappa^2} - \Big(m_H^2 - \lambda\phi_{\rm d}\Big)|H|^2 - \frac{1}{2}m_{\phi_{\rm d}}^2\phi_{\rm d}^2 - \frac{1}{2\kappa^2}R\Big] \\ &- \int d^4x z^{-4} V_0(\phi_{\rm d}, |H|)\Big|_{z\to z_0} - \int d^4x z^{-4} V_1(\phi_{\rm d}, |H|)\Big|_{z\to z_1}. \end{aligned} \tag{2.4.1}$$

The brane potentials are assumed to take the form $V_{0,1} = \delta T_{0,1} + V_{0,1}^{\phi_{\rm d}} + V_{0,1}^H$. For the brane Higgs potentials, we take

$$V_0^H = m_0^2|H|^2, \qquad\qquad V_1^H = \lambda_H|H|^2\Big(|H|^2 - v_H^2\Big). \tag{2.4.2}$$

The potential here is quite similar to that in [14], however in this model, there are no very small parameters, and this is a 5D bulk potential – the effective bulk potential in the 4D theory is of course related, but not in one-to-one correspondence. There is a mild approximate shift symmetry in the bulk for the $\phi_{\rm d}$ scalar – a slightly suppressed bulk mass parameter as utilized in the Goldberger-Wise stabilization mechanism [52], and a perturbative bulk interaction with the 5D H field.

The equation of motion for $\phi_{\rm d}$ is given by

$$\phi_{\rm d}'' - \frac{3}{z}\phi_{\rm d}' - \frac{1}{z^2}\left(m_{\phi_{\rm d}}^2\phi_{\rm d} - \frac{\lambda}{2}\phi_h^2\right) = 0, \tag{2.4.3}$$

which is a simple linear non-homogeneous equation for a given Higgs background, ϕ_h, and the solution is given by

$$\phi_{\rm d} = z^\epsilon\left(\phi_\epsilon + \frac{\lambda}{4(2-\epsilon)}\int_{z_0}^{z}\phi_h^2(\tilde{z})\tilde{z}^{-1-\epsilon}d\tilde{z}\right) + z^{4-\epsilon}\left(\phi_4 - \frac{\lambda}{4(2-\epsilon)}\int_{z_0}^{z}\phi_h^2(\tilde{z})\tilde{z}^{-5+\epsilon}d\tilde{z}\right), \tag{2.4.4}$$

where $\epsilon = 2 - \sqrt{4 + m_{\phi_{\rm d}}^2}$. We take ϵ to be small and positive, but not tiny, e.g. $\epsilon = \mathcal{O}(0.1)$, corresponding to a small tachyonic bulk mass for $\phi_{\rm d}$. There are two contributions to the solution – the solution to the homogeneous part of Eq. (2.4.3), and the integrals that solve the nonhomogeneous part from a non-vanishing Higgs VEV.

The Higgs equation of motion is given by

$$\phi_h'' - \frac{3}{z}\phi_h' - \frac{1}{z^2}\big(m_H^2 - \lambda\phi_{\rm d}\big)\phi_h = 0, \tag{2.4.5}$$

which can, in principle, be expressed as a single nonlinear integro-differential equation by inserting the solution to the $\phi_{\rm d}$ boundary value problem.

The radion potential, again assuming small gravitational backreaction, now takes contri-

butions from both fields, and is given in general by

$$\begin{aligned} V_{\rm rad} &= \frac{1}{z_0^4}\left[V_0 - \frac{6}{\kappa^2}\sqrt{G_0}\right] + \frac{1}{z_1^4}\left[V_1 + \frac{6}{\kappa^2}\sqrt{G_1}\right] \\ &\approx \frac{1}{z_0^4}\left[\delta T_0 + V_0^{\phi_{\rm d},0} + V_0^H + \frac{1}{4}m_H^2(z_0)\phi_{h,0}^2 - \frac{1}{4}z_0^2\phi'^2_{h,0} + \frac{1}{4}m_{\phi_{\rm d}}^2\phi_{{\rm d},0}^2 - \frac{1}{4}z_0^2\phi'^2_{{\rm d},0}\right] \\ &\quad + \frac{1}{z_1^4}\left[\delta T_1 + V_1^{\phi_{\rm d},1} + V_1^H - \frac{1}{4}m_H^2(z_1)\phi_{h,1}^2 + \frac{1}{4}z_1^2\phi'^2_{h,1} - \frac{1}{4}m_{\phi_{\rm d}}^2\phi_{{\rm d},1}^2 + \frac{1}{4}z_1^2\phi'^2_{{\rm d},1}\right]. \end{aligned} \tag{2.4.6}$$

Using the analytic solution for $\phi_{\rm d}$ in terms of the function ϕ_h from Eq. (2.4.4), supplemented by the boundary conditions for $\phi_{\rm d}$, one can express the entire radion potential purely in terms of the solution to the ϕ_h equation of motion.

We first specify to a model where much can be done analytically to show some basic results in this model. We take the IR brane potential for the $\phi_{\rm d}$ scalar to be a localized mass term, $V_1^{\phi_{\rm d}} = -\epsilon\phi_{\rm d}^2$. If we assume this value for the mass, and if the Higgs VEV is taken to be zero, the solution is $\phi_{\rm d} = v_0(z/z_0)^\epsilon$. Without the Higgs contribution, the radion potential is just a scale-invariant quartic. We then assume a UV brane potential that fixes v_0 to some value (a stiff-wall-type boundary condition). In this background, ignoring the nonhomogeneous part of $\phi_{\rm d}$ in the Higgs equation of motion, the solution for the Higgs VEV is the same as described in the previous section.

Also, in the case of the model under consideration, there are considerable simplifications of the radion potential. Specifically, all of the $\phi_{\rm d}$ terms in the IR brane contribution cancel after imposing the boundary condition $z\phi'_{\rm d} = \epsilon\phi_{\rm d}$, which arises from the boundary potential we have chosen for $\phi_{\rm d}$.

The radion potential, expressed purely in terms of the boundary values of and integrals

over the solution to the Higgs equation of motion, is

$$\begin{aligned} V_{\rm rad} = \frac{1}{z_0^4}\Bigg[\delta\tilde{T}_0 + \frac{m_0^2}{2}\phi_{h,0}^2 + \frac{1}{4}\Big(m_H^2 - \lambda v_0\Big)\phi_{h,0}^2 - \frac{1}{4}\Big(z_0\phi_{h,0}'\Big)^2 - \frac{1}{2}\epsilon v_0 z_0^{4-\epsilon} I_4 - \frac{1}{4}\Big(z_0^{4-\epsilon} I_4\Big)^2\Bigg] \\ + \frac{1}{z_1^4}\Bigg[\delta\tilde{T}_1 - \frac{1}{4}\Bigg\{m_H^2 - \lambda\Big(\frac{z_1}{z_0}\Big)^\epsilon\Bigg(v_0 + \frac{z_0^\epsilon}{2(2-\epsilon)} I_\epsilon - \frac{z_0^{4-\epsilon}}{2(2-\epsilon)} I_4\Bigg)\Bigg\}\phi_{h,1}^2 \\ + \frac{1}{4}\lambda_H \phi_{h,1}^2\Big(\phi_{h,1}^2 - 2v_H^2\Big) + \frac{1}{4}\Big(z\phi_{h,1}'\Big)^2\Bigg], \end{aligned} \tag{2.4.7}$$

where I_ϵ and I_4 are the following integrals:

$$\begin{aligned} I_\epsilon =& \frac{\lambda}{2}\int_{z_0}^{z_1} \phi_h^2(\tilde{z})\tilde{z}^{-1-\epsilon} d\tilde{z}, \\ I_4 =& \frac{\lambda}{2}\int_{z_0}^{z_1} \phi_h^2(\tilde{z})\tilde{z}^{-5+\epsilon} d\tilde{z}. \end{aligned} \tag{2.4.8}$$

This expression is exact up to contributions from gravitational backreaction, which we are here neglecting.

We note that one can show analytically by expanding the solution near the critical point that the kink of the previous section is removed by the backreaction of the Higgs VEV onto the driving scalar.

In the limit of tiny Higgs VEV, the Higgs background is well approximated by the solution that assumes $\phi_{\rm d} = v_0(z/z_0)^\epsilon$, which was explored in the previous section:

$$\phi_h = z^2\Bigg(\phi_+ J_\nu\Bigg(z^{\epsilon/2}\frac{2\sqrt{\lambda v_0}}{\epsilon}\Bigg) + \phi_- J_{-\nu}\Bigg(z^{\epsilon/2}\frac{2\sqrt{\lambda v_0}}{\epsilon}\Bigg)\Bigg), \tag{2.4.9}$$

where $\nu = 2\sqrt{\delta m^2}/\epsilon$, with $\delta m^2 = m_H^2 + 4$. This is sufficient for determining the critical point, however, for the purposes of evaluating the effective potential, a full numerical solution is necessary. That is, past the critical point, the Higgs background looks similar to this profile,

but the differences due to the nonlinearities need to be incorporated in order to correctly determine the radion potential.

In the next subsection, we embark on a full numerical analysis of the coupled equations, working with a more common setup for the $\phi_{\rm d}$ scalar, where its boundary values are set to $v_{0,1}$ on the UV/IR branes.

2.4.1 Stiff Wall Model

In the stiff wall limit, the boundary conditions for $\phi_{\rm d}$ are $\phi_{\rm d}(z_{0,1}) = v_{0,1}$. Thus, the value of the bulk Higgs mass varies from $m_H^2(z_0) = m_H^2 - \lambda v_0$ on the UV brane to $m_H^2(z_1) = m_H^2 - \lambda v_1$ in the IR. It is not difficult to arrange for the effective Higgs mass to vary such that it crosses the BF bound somewhere in the bulk, and evolves from power law behavior in the UV to a log-periodic power law in the IR. For small values of z_1, the AdS tachyon is not reached, however, for larger values, the tachyon eventually must emerge and be resolved by condensation of some sort. In order to understand this process fully, we embark on a numerical exploration of solutions to the scalar equations of motion.

We note that the bulk equations governing the behavior of $\phi_{\rm d}$ and ϕ_h are nonlinear, and that one must take care in seeking out solutions to the scalar equations of motion. Existence and uniqueness are not guaranteed in the case of the general nonlinear boundary value problem. Due to this complication, we do not search for solutions with fixed z_1, but rather search for solutions with varying values of the Higgs VEV. We note that there is always a solution with $\phi_h = 0$ – the solution to the linear Goldberger-Wise problem with just the $\phi_{\rm d}$ scalar.

To numerically investigate the solutions, we generalize the bulk equations to accommodate a sort of shooting method. That is, we search for solutions to the boundary value problem at hand by scanning over a range of initial value problems until we find a global solution. To do so, we write the solution to the Higgs as $\phi_h = h_0 f_h(z)$ with $f_h(z_0)$ set to some arbitrary value. The coefficient h_0 does not appear explicitly in the Higgs equation of motion, as for fixed $\phi_{\rm d}$, that equation is linear. It does, however, appear in the $\phi_{\rm d}$ equation:

$$\begin{aligned} &f_h'' - \frac{3}{z} f_h' - (m_H^2 - \lambda\phi_{\rm d}) f_h = 0, \\ &\phi_{\rm d}'' - \frac{3}{z}\phi_{\rm d}' - (\epsilon^2 - 4\epsilon)\phi_{\rm d} + \frac{\lambda}{2} h_0^2 f_h(z)^2 = 0. \end{aligned} \tag{2.4.10}$$

We shoot from the UV brane, enforcing the UV brane boundary conditions for f_h and $\phi_{\rm d}$, which in our cases of study are $f_h'(z_0) = m_0^2 f_h(z_0)/(2z_0)$ and $\phi_{\rm d}(z_0) = v_0$. We then use a prechosen value of h_0 to define each solution. The magnitude of h_0 closely tracks the low energy effective Higgs VEV as a fraction of the KK scale. As $f_h(z_0)$ is fixed arbitrarily, the only remaining condition is on $\phi_{\rm d}'$, the correct value for which will be determined by shooting. The value of z_1 for a $\phi_{\rm d}'$ guess is chosen by finding the point in the bulk at which the IR brane boundary condition for the Higgs is met: $h_0^2 = 1/f_h(z)^2\left(v_H^2 - \frac{2f_h'(z)}{\lambda_H z f_h(z)}\right)$. Of course at that z_1, it will not usually be the case that the IR boundary condition for $\phi_{\rm d}$ is met, so we repeat the process by shooting with different values of $\phi_{\rm d}'$ until both the Higgs and $\phi_{\rm d}$ boundary conditions are solved at the same value of z_1. In summary, for a given input Higgs VEV, we obtain a value for z_1 and the associated bulk profiles for ϕ_h and $\phi_{\rm d}$.

It is useful to characterize each solution in terms of some parameter with physical meaning to a low energy observer, and we choose the effective Higgs VEV, evaluated by integrating

the Higgs solution squared over a hypothetical flat zero-mode gauge boson wave function with appropriate metric factors:

$$\left(\frac{v_{\text{eff}}}{f}\right)^2 = z_1^2 h_0^2 \int_{z_0}^{z_1} \frac{1}{z^3} f_h^2(z) dz. \tag{2.4.11}$$

We find that the types of solutions one obtains can be divided into two classes based on the value of the IR brane-localized Higgs mass, determined by taking different values for v_H^2. If v_H^2 is taken to be very negative, corresponding to a non-tachyonic brane-localized Higgs mass squared, there is no solution for nonzero Higgs VEV with $z_1 > z_c$. Instead, with increasing Higgs VEV (roughly h_0 in our numerical analysis), the solution requires *smaller* values of z_1. This then means that for a given value of $z_1 < z_c$, there may be two solutions, one with positive effective 4D Higgs mass squared/vanishing VEV, and the other with nonvanishing Higgs VEV. For more positive values of v_H^2, a different behavior is possible, e.g. where the value of z_1 at first increases as the Higgs VEV is turned on, and then turns around, so that at some particular z_1 value, there are two possible values of the effective Higgs VEV.

None of this should be too surprising from the perspective of the 4D CFT dual. The value of z_1 represents some total scale of conformal breaking through the relation $z_1 \sim 1/f$ where f should be some additive combination of all vacuum expectation values in the system that break approximate conformal invariance spontaneously. The bulk $\phi_d|H|^2$ interaction has enforced a relationship between the multiple f's (in this case, dual to the ϕ_d and ϕ_h scalar solutions), and lifted the constraint of uniqueness present in theories without bulk scalar interactions. In other words, the nonlinearity of the boundary value problem has allowed for multiple solutions for a given z_1, and thus different ways for the bulk theory to produce a

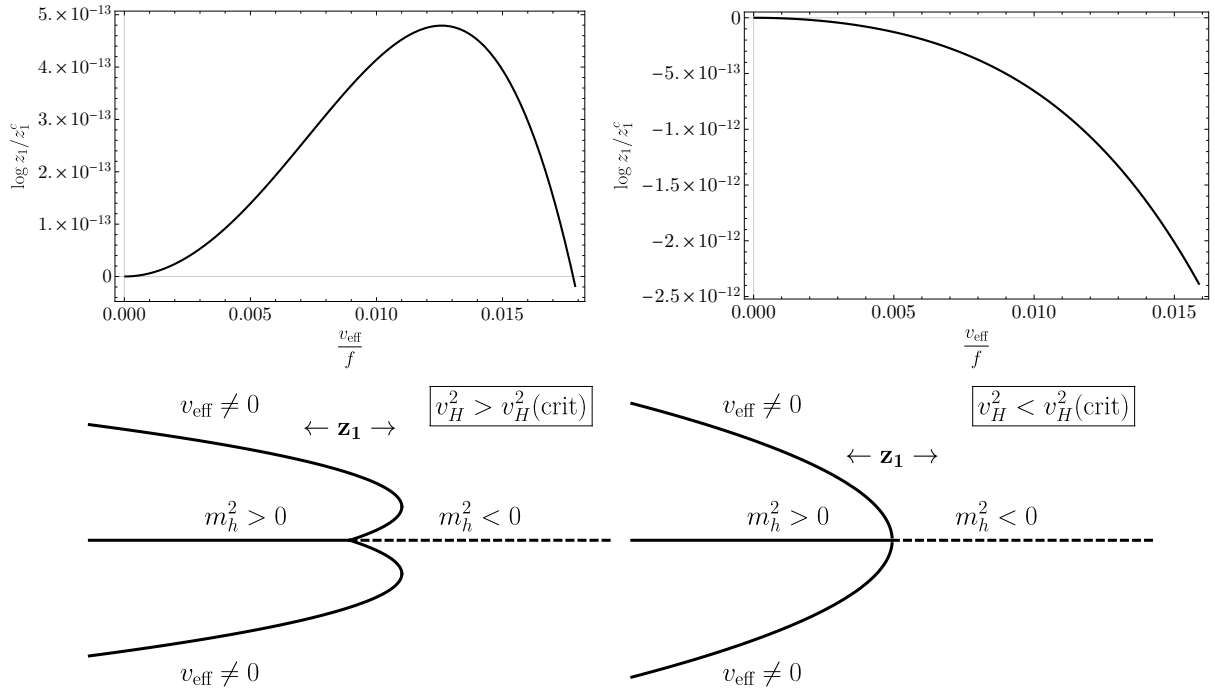

Figure 2.5: In this plot, we show the effective VEV as a function of z_1. On the left, we show it for a value of v_H^2 that is very close to "critical," but with $v_H^2 > v_H^2(\text{crit})$. In this case, for small Higgs VEV $z_1 > z_c$. On the right, we display it for v_H^2 more negative than the critical value, and in this case, for all values of the Higgs VEV, we find $z_1 < z_c$. We also sketch the "bifurcation" diagrams for each of these scenarios as a function of z_1, where the solid lines represent the stable scalar configurations and the dashed line represents the background solution with unresolved tachyon(s). The branching point corresponds to $z_1 = z_c$.

given total $f \sim 1/z_1$. In Figure 2.5, we show for two different values of v_H^2 that are close to a critical value (but on either side) the relationship between z_1 and the effective VEV. We note that the Higgs VEV grows extremely fast near the critical point.

This matches onto the first part of our preliminary discussion of the dilaton effective theory in Section 2.2. Extremization of the scalar part of the action corresponds in the dual picture to sorting out the correct relationship between the vacuum expectation values of operators in the approximate CFT. This relationship must now be fed into the total radion effective potential.

Now we consider the radion potential for this model. Plugging in the results from the

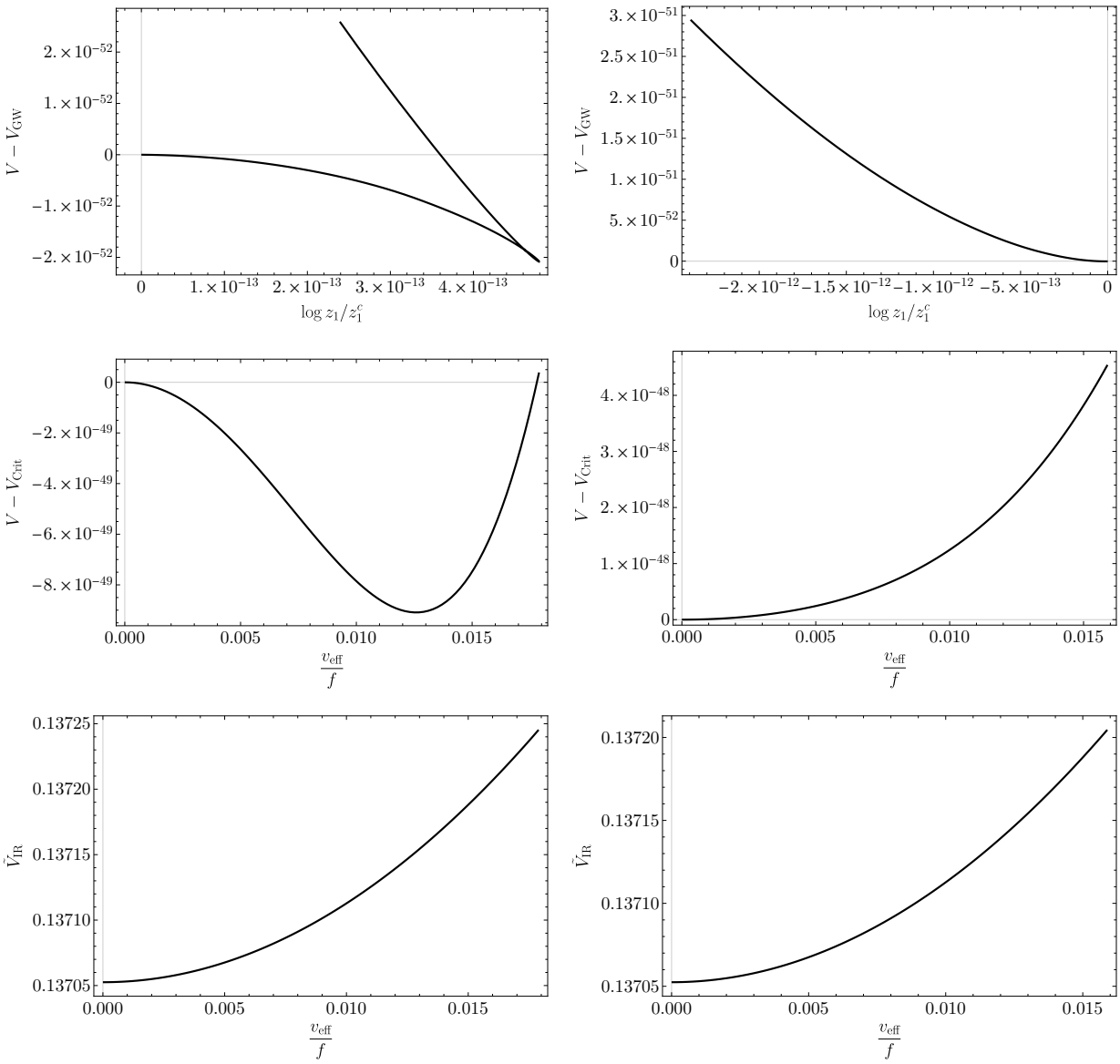

Figure 2.6: In this plot, we show the radion potential for two different values of v_H^2 near $v_H^2(\text{crit})$. In the column on the left, $v_H^2 > v_H^2(\text{crit})$. We have taken $\epsilon = v_0 = 1/10$, $m_H^2 = -3.9$, $v_0 = 1$, $\delta T_1 = -1/10$, $\lambda = 1/3$, $m_0^2 = 4.1$, and $\lambda_H = 1/8$. The critical point is between $v_H^2 = -16.5830$ and $v_H^2 = -16.5831$, and the two columns correspond respectively to these two values of v_H^2 that straddle $v_H^2(\text{crit})$. In descending order, the plots display: the difference between the radion potentials with and without a Higgs VEV as a function of $\log z_1/z_1(\text{crit})$, the same potential with $V_{\rm crit}$ being its value at the critical z_1, but instead as a function of $v_{\rm eff}/f$, and finally the value of $\tilde{V}_{\rm IR}$, defined in Eq. (2.3.21), indicating the degree of mismatch of the metric junction condition on the IR brane. There is no discernible difference in these two plots on either side of the critical value of v_H^2, and there is certainly no zero.

numerical solutions, we find that for $v_H^2 > v_H^2(\text{crit})$, there are solutions to the scalar equations of motion and boundary conditions with $z_1 > z_c$. For all $v_H^2 < v_H^2(\text{crit})$, there is a minimum in the effective radion potential *at* $z_1 = z_c$, the value of z_1 where the Higgs fluctuation is massless. We note that this is under the constraint that values of z_1 where there is an unresolved tachyon are disallowed.[6]

In Figure 2.6, we display the results of the radion potential for two values of v_H^2 near the critical value. We show the potential both as a function of z_1 and as a function of v_{eff}/f. In this plot, V_{GW} denotes the GW contribution to the radion potential, while V_{crit} is the radion potential at the critical z_1. For the subcritical case, the location of the potential minimum is at an energy which is lower than if the Higgs VEV is turned off – symmetry breaking is the preferred configuration for that value of z_1.

One can now make contact with the dilaton effective potential discussed in Section 2.2. The value of $1/z_1$ for a given solution corresponds to the total scale of symmetry breaking, with the KK-mode masses of the extra-dimensional theory corresponding to its value. Larger values of z_1 have scalar instabilities. Ignoring this region, the radion potential is minimized at the largest value of z_1 that accommodates a solution to the scalar equations of motion.

In Figure 2.7, we display the behavior of the model with subcritical v_H^2, focusing on the value of the Higgs VEV in the approach to Higgs criticality. The Higgs VEV, roughly the inverse correlation length in the low energy theory, appears to depend linearly on $\sqrt{v_H^2 - v_H^2(\text{crit})}$ in the approach.

In Figure 2.8, we display the behavior of the model with supercritical values of v_H^2, focusing

[6]Dynamics of the system *will* move the IR brane into this region - the true vacuum is not simply one in which the brane rests at z_c. Going past the critical value of v_H^2, there is likely a phase transition of the system that cannot be encapsulated under the static ansatz that was the starting point for this analysis. We speculate on its nature in Section 2.7, leaving a full analysis of the $v_H^2 < v_H^2(\text{crit})$ region for future work.

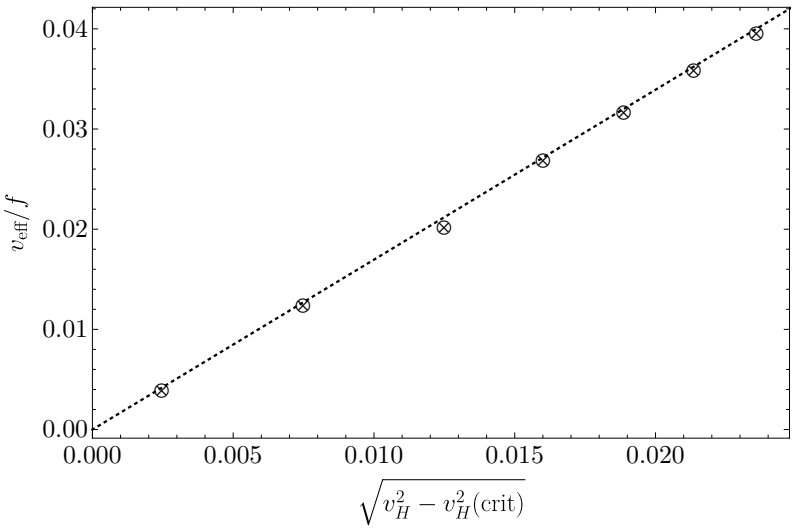

Figure 2.7: In this plot, we display the behavior of $v_{\rm eff}/f$ at the minimum of the radion potential for subcritical $v_H^2 > v_H^2(\rm crit)$ as it approaches the critical region. The dashed line is a linear fit to the numerical data forced to pass through the origin by adjusting $v_H^2(\rm crit)$. The critical value is determined in this manner to be $v_H^2(\rm crit) = -16.58305605$

on the value of the second derivative of the radion potential at the minimum. The second derivative remains positive for all v_H^2 values less than the critical one, and so the minimum of the potential along the line where the Higgs boundary conditions are met coincides with the Higgs critical point.

While the radion potential has a smooth minimum (as a function of the effective Higgs VEV) in this dynamical model on either side of the critical value of v_H^2, we again find that it does not generally satisfy the $\mu\nu$ components of Einstein's equations, specifically the metric junction conditions $\sqrt{G_{0,1}} = \pm\frac{\kappa^2}{6}V_{0,1}$.

Of course one could fine-tune both tensions to meet both metric junction conditions, as is done in the original unstabilized Randall-Sundrum model, however one should first ask what physical phenomena occur when such tuning is not performed. In the RS model, the mistunes lead to either collapse or runaway of the branes, however in this case, it seems

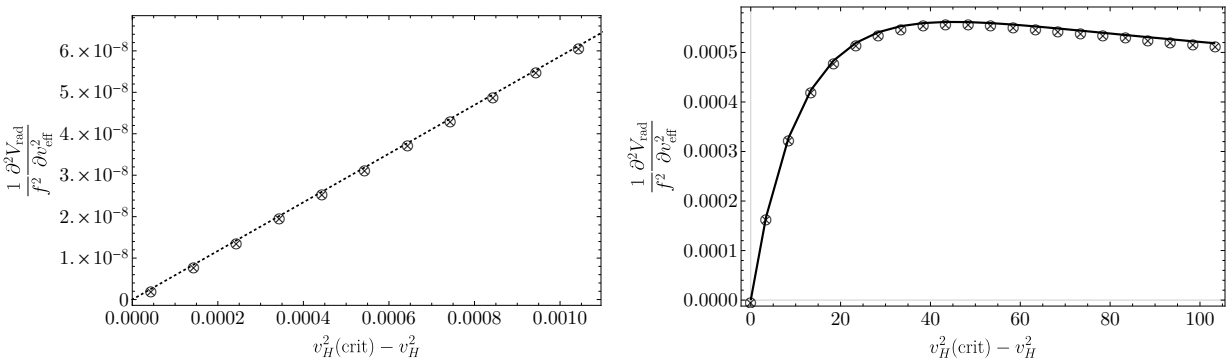

Figure 2.8: In this Figure, we display the curvature of the radion potential as a function of the effective Higgs VEV for $v_H^2 < v_H^2(\text{crit})$. In the plot on the left, we focus on v_H^2 close to the critical value, while on the right, we display the curvature for a wider range of $v_H^2 < v_H^2(\text{crit})$. Near the critical v_H^2, the behavior is well described by a line intersecting with the origin, with the critical value here determined to be $v_H^2(\text{crit}) = -16.58305645$, apparently consistent with the value determined on the sub-critical side in Figure 2.7 up to numerical errors in the solving routine.

unlikely that the same behavior occurs, as the potential does not exhibit obvious runaway directions. What seems more likely is that the background solution obtained after relaxing the metric ansatz to include bent branes (e.g. nontrivial time dynamics). This is discussed further in Section 2.7.

2.5 CFT Interpretation

Here we comment on the 4-dimensional CFT interpretation of this model. The dual of this picture has a parallel in weakly coupled models where electroweak symmetry breaking is driven radiatively, as is the case in the MSSM [28]. In such cases, the electroweak scale arises via dimensional transmutation, with renormalization group effects creating the instability that is rectified by the vacuum expectation value of the Higgs in spite of the microscopic theory having no explicit scales.

In the picture under consideration, a similar instability is reached when the scaling

dimensions of operators in a quasi-conformal theory are pushed towards and potentially into the complex plane through renormalization group flow. Such complex scaling dimensions are a usual part of the description of theories with a discrete scale invariance, thus we have a picture where a theory evolves off of a standard nontrivial UV fixed point and begins to exhibit discrete scale invariance in the IR. Discrete scale invariance is found in the IR behavior of the Higgs profile, where the Higgs behaves approximately as

$$\phi \propto z^{2-\epsilon/4} \cos\Big(\sqrt{\lambda} \log z + \gamma\Big). \tag{2.5.1}$$

The solution is simple scaling under the discrete transformation $z \to z \exp\Big(2\pi/\sqrt{\lambda}\Big)$, corresponding to a discrete scale transformation $\mu \to \mu \exp\Big(-2\pi/\sqrt{\lambda}\Big)$. While at first glance interesting, discrete scaling behavior is forbidden in the deep IR [36], and is expected to be terminated in some way – likely by the formation of condensates and a transition scale past which RG flow resumes more standard behavior. Indeed, the study of the scalar fluctuations in Section 2.3 shows that if one tries to continue the bulk too far into the regime of log-periodic behavior, additional tachyons emerge that are, at least in the toy 5D theory of Section 2.3, unresolved.

In the dynamical model of Section 2.4, the driving scalar field $\phi_{\rm d}$ plays the role dual to an operator whose coupling runs slowly, slightly deforming the CFT, with the deformation growing in the infrared. This running backreacts, in general, on the theory, and can generate a running for scaling dimensions of other operators in the theory. The bulk trilinear coupling between the Higgs and the scalar $\phi_{\rm d}$ is the pathway for this backreaction.

The running scaling dimension of the operator associated with the bulk Higgs is dual to

the 5D z-dependence of the effective 5D mass of the Higgs in the background of the scalar, $\phi_{\rm d}$, and the instability associated with complex scaling dimensions and discrete scale invariance is dual to supersaturation of the Breitenlohner-Freedman bound. Since the effective mass begins above the BF bound, the far UV behavior is that of a normal CFT without instabilities, where the operators have normal real scaling dimensions. It is only in the IR behavior, where scaling dimensions become complex, that an instability emerges.

This class of instability, without the dynamical aspect we explore, was investigated in work by Kaplan, Lee, Son, and Stephanov [25] along with a proposed AdS dual. In this work, it was conjectured that the loss of conformality as a function of some descriptor of the theory, such as the number of massless QCD flavors, can be thought of as due to the annihilation of two fixed points (UV and IR) under variations of that parameter. They posit that such a theory could contain some operator O that has different scaling dimensions at the two fixed points, $\Delta_{\rm UV,\,IR}$, and these scaling dimensions smoothly merge and become complex when the external descriptor is moved past some critical value. It was pointed out in this work that the behavior of the theory under this transition is closely similar to scaling behavior associated with finite temperature topological phase transitions of the sort studied by Berezinskii, Kosterlitz, and Thouless (BKT) [53, 54]. In these models, there is a critical line, with the theory being conformal for a finite range of descriptor, and with a gap turning on smoothly past the point where conformality is lost. These two scaling dimensions, $\Delta_{\rm UV,\,IR}$, correspond in the 5D AdS dual to the two solutions to the scalar equations of motion in the $z \to 0$ region, each of which has different scaling properties given by $\Delta_{\rm UV}$ and $\Delta_{\rm IR}$. In 5D, the loss of conformality corresponds to the merging of these two scaling solutions at the Breitenlohner-Freedman bound as the bulk mass is taken through $m^2 = -4$. Below the

BF bound, the theory requires a UV cutoff, and also predicts an IR scale associated with rectification of a tachyon instability through condensation of bulk fields, corresponding in the holographic picture to a VEV for the operator O.

The 5D model we have described has given dynamics to this picture, where what was an external parameter has been promoted to a coupling in the theory which has nontrivial RG evolution. In Figure 2.9, we give a cartoon of what the model we explore achieves. In [25], in the case that parameters are chosen to put the theory in a conformal window, there are explicit UV and IR fixed points, both nontrivial. Moving in and out of the conformal window is achieved by varying those external parameters, with the fixed points merging at its threshold. In the case of our model, the idea is that the theory begins at or flows quickly to an IR fixed point which has been demoted by a slightly relevant deformation of the theory to a quasi-fixed point. The theory tracks this IR quasi-fixed point until it disappears after annihilating its associated UV quasi-fixed point. Under further RG flow, scaling dimensions become complex with a corresponding discrete scaling law, the theory becomes unstable, and the instability is potentially resolved by condensates. The theory can also begin and remain near the UV quasi-fixed point, in principle, corresponding to taking the tuned boundary condition for the bulk scalar that picks out the other slower-growing solution.

When the instability is rectified by condensates, the approximate conformal invariance is broken spontaneously. There are different options for this breaking. The Higgs itself can form a vacuum expectation value, likely along with condensates of the operator that is driving the theory towards the instability. This option gives a Higgs mass and 4D effective VEV that is not typically suppressed in comparison with the 5D KK scale or its dual picture compositeness scale. There are other options, however. It is known that the phase structure

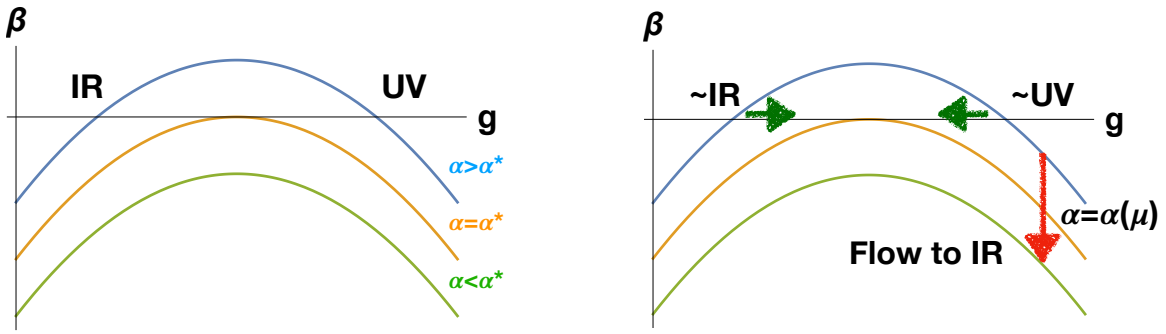

Figure 2.9: Here we show a cartoon of an approximate CFT dual of our 5D model. On the left is the picture of fixed points annihilating under continuous variation of some descriptor of the theory, as explored in [25]. On the right is our picture of quasi-fixed points annihilating under renormalization group evolution.

of superconductivity can be quite rich, allowing for condensates with inhomogeneous spatial configurations such as stripes or crystalline structure, and this has been reproduced in the holographic context [40].

A dynamical dilaton field, corresponding to the condensates of operators in the CFT and fluctuations about these points in field space, has a potential that depends on which operators take on VEVs, and its potential selects the most attractive channel for resolving the tachyon. The extra-dimensional modulus field, the radion, is the dual to this dilaton. Finding the classical extrema of the 5D effective potential corresponds to identifying the vacuum state of the dual CFT.

When sourced operators with nontrivial scaling dimension take on vacuum expectation values, approximate conformal invariance is spontaneously broken, and the dilaton potential is nontrivial (more than a scale-invariant quartic). If the potential has a nontrivial minimum, the resulting mass of the dilaton particle is proportional to the degree of explicit breaking of conformal symmetry. In our picture, as a function of the gap of the CFT associated with a VEV of a marginally relevant operator O_ϵ, an IR tachyon instability eventually emerges

for smaller values of $\langle O_\epsilon \rangle$, in the regime of discrete scale invariance. At this point the VEV $\langle O_H \rangle$ turns on in addition to $\langle O_\epsilon \rangle$.

The kink in the toy model of Section 2.3, or its cousin, the non-existence of solutions with nonvanishing Higgs VEV past some critical z_1 in the dynamical model of Section 2.4, are the most curious features of this setup. These behaviors appear to be strongly tied to the type of instability that is dominant in the model. The tachyon that emerges due to the renormalization group instability/violation of the BF bound appears to be a necessary component for novel behavior of the potential. This hypothesis is supported by what is observed in Figure 2.3, and in the behavior of the scalar solutions in Section 2.4. Taking, for example, v_H^2 to be large, giving a large 4D tachyonic mass to the Higgs on the brane, gives a more standard kind of picture where a Higgs condensate turns on and determines the brane location. However, for smaller or negative v_H^2, when there is no longer a 4D brane-localized tachyon, there is a turnaround in the behavior of the solutions. For v_H^2 below the critical value, it is the bulk mass falling below the BF bound that is the more important component of the instability.

2.6 Discussion

2.6.1 Connections to Condensed Matter and Statistical Physics

The construction we explore potentially gives a new way to think about self-organized criticality in the fields where it was first explored and named [19]. The scaling of perturbations ($1/f$ flicker noise in the literature), and the instabilities associated with catastrophic failure

and its possible connection to an emergent discrete scale invariance have their signatures in the purported holographic dual we have proposed. The $1/f$ so-called "flicker" noise (in fact $1/f^{\alpha}$, where α can depend on the system under consideration) is simply the signature of criticality itself [20] – a fixed point where perturbations exhibit scaling laws. There should be CFTs describing the coarse-grained effective theory of such systems where criticality is self-organized, and there could be AdS dual descriptions of such theories. The scaling laws associated with the self-organized critical point are associated in this case to the scaling behavior of field solutions in AdS space. The above discussion applies to any critical point, not just self-organized ones. However, the particular 5D picture we have presented here appears to have features which place it close to systems with self-organization. These share the commonality that the systems in question are brought to the point of some sort of failure mode that leads to time dynamics, typically a form of adjustment. It has been suggested that the development of the adjustment behavior can be associated, in the coarse-grained theory, with scaling dimensions of the critical point being driven into the complex plane, and creating a discrete scale invariance, with fluctuations obeying a log-periodic power law. In the context of quantum field theory, it is known that such scaling laws are not allowed, and have instabilities associated with them [36]. In our picture these instabilities map to the region in the radion potential in which there are unresolved tachyons. Should the system be placed at these points of instability, it is, at the moment, unknown what the response of the system will be.

2.6.2 Incorporation of the Standard Model

The eventual goal is to embed this class of Higgs sector into a theory which accommodates the rest of the SM field content, and where the Higgs resides not precisely at the point of criticality, but instead picks a VEV and breaks the electroweak gauge symmetry spontaneously. This may occur as a result of finite radiative corrections, or perhaps through nontrivial feedback due to explicit breaking of conformal invariance in the SM (for example, from confinement and chiral symmetry breaking in QCD), or in extensions of it (as in [14]). If the SM can accommodate such a Higgs sector, a key calculation will be the Higgs cubic coupling in the context of the manner in which its potential is generated, as this will be eventually probed by colliders. As we will discuss in the next section, cosmology of such an extension of the SM could be very interesting. As we have emphasized, we have not yet fully identified the vacuum state, which we argue must be time-dependent unless tuning is performed.

2.7 Speculation: Cosmology

The phenomenology of this scenario, if employed by nature in creating a low electroweak scale, is expected to be quite novel. Cosmology stands out as a particularly interesting area, due to the interplay between the radion and the Higgs. Metastability of the self-organized critical state is a vital consideration, although possibly resolved trivially by details of the deformation that drives self-organization or by a more complete model without a hard wall. A very interesting possibility is that dynamics of the radion could "rock" the early universe across the electroweak phase transition, sourcing a stochastic gravitational wave background, and creating an era of the early universe with an exotic equation of state (leading to modified

constraints on inflationary scenarios and/or moduli masses) [55]. This may be interesting also from the standpoint of baryo- and leptogenesis.

Even more curious features are likely to emerge under a full calculation of the classical background, which we have left for future work. As we have emphasized, in writing down a 4D Lorentz-invariant radion potential, we have been required to do some violence to the theory. That is, we have calculated the potential under the presumption that the metric slices are flat. However, at the minima we have identified, the consistency conditions for a flat metric ansatz on the boundaries of the space, that both the UV and IR contributions to the radion potential separately vanish at the minimum, cannot be met without tuning. Bent 4D slices thus appear to be an integral part of the full solution to the theory at or near Higgs criticality. The theory is telling us that, as part of the resolution of the AdS tachyon, it breaks Lorentz invariance spontaneously at long distances. It is interesting to speculate at the form that this takes without (at least in this work) undertaking a detailed calculation.

Pessimistically, we might imagine that the solution could be a runaway. This seems unlikely from the following consideration of the dynamical model discussed in Section 2.4: one could imagine adjusting the bulk cubic coupling λ between $\phi_{\rm d}$ and the Higgs, increasing it starting from some small value. The system would then reside at the minimum of the Goldberger-Wise potential created by the VEV of the $\phi_{\rm d}$ scalar, and the Higgs would have positive mass squared. One would in this case start in an unbroken phase with a massive Higgs field near the KK scale, and a completely static geometry (presuming the usual single tuning of the UV brane tension). Increasing the coupling would move the turn-on of the Higgs VEV ever closer to the minimum of the Goldberger-Wise potential, the critical z_1 value approaching the minimum from large z_1. The lowest-lying Higgs excitation would then

gradually move to the bottom of the spectrum. There is a fine-tuned value of λ where the Higgs extremum coincides exactly at the minimum of the GW potential. The theory at this point, as the usual solution to the theory at the Goldberger-Wise minimum tells us, has a massive radion. Due to the adjustment of λ, it also has a (finely-tuned) massless Higgs. The only nearby instability in the low energy theory seems like the usual one associated with the Higgs phase transition. Further increase in λ either results in a Higgs VEV and symmetry breaking of the usual sort, or a more novel transition. It would appear the latter is a good possibility in some fraction of the parameter space of the model.

We have shown that the change in the radion potential due to the Higgs contribution creates a new minimum and for large negative v_H^2, there appears to be an onset of a novel type of transition that does not satisfy the usual metric junction condition. This means that the transition is not likely a normal Higgs one, but rather could be a transition to a spontaneously Lorentz-violating dynamical background. The radion should still be stabilized by its mass if we remain close to the boundary of the critical region. Therefore if it moves, it likely oscillates rather than runs away, acting "trapped" [56].[7] Amusingly, such a "trapped" modulus, the oscillating radion field, might look cosmologically similar to non-relativistic matter from the standpoint of the low energy theory: a Bose-Einstein condensate of radion particles. Deeper into the critical Higgs region, as the metric junction conditions become further from being satisfied, this time dependence may become very complicated, involving a mixture of the many degrees of freedom in the model. A simulation including full backreaction may be needed. It will be interesting to see more clearly what the low energy theory looks like with further study.

[7] We thank Ofri Telem for suggesting the possibility of an oscillating radion background.

In short, the resolution of the IR-emergent AdS tachyon appears to require a spontaneous breakdown of 4D Lorentz invariance possibly a time-dependent oscillatory vacuum state. In the language of condensed matter physics and superconductivity literature, the theory would be resolving the instability by entering a "striped phase" at long distances with oscillations of the radion state breaking time translation invariance. The generic phenomenon of classical spontaneous breakdown of time translation invariance was investigated in [38], with a quantum mechanical version explored in [39]. These striped phases in condensed matter systems appear to arise in the presence of a frustration in the system where competing phenomena strive to set the vacuum state. In the case of our radion model, there are two competing "minima" of the potential: one where the radion is at a global minimum set by the Goldberger-Wise mechanism, but the Higgs is unstable, and the other where the Higgs field is stabilized, but the 5D gravity sector is not at an extremum of the action. The outcome in some condensed matter systems is to resolve such tension by entering a translation invariance-breaking striped phase, and we are suggesting similar physics may be at work in resolution of this AdS tachyon, although the breaking could be of time-translation invariance. A picture of these competing extrema is shown in Figure 2.10.

This sort of time dependent vacuum state and its application to cosmology was first explored in [41], with important recent followup work concerning stability of this scenario in [42].

In the 4D CFT language, there may be strongly coupled quasi-conformal 4D theories with a dynamically generated gap that have aspects of matter-Λ cosmology built into their ground state at long distances due to frustration of the dilaton. Classical breaking of time-translation invariance in the 5D theory corresponds to its quantum mechanical counterpart in the 4D

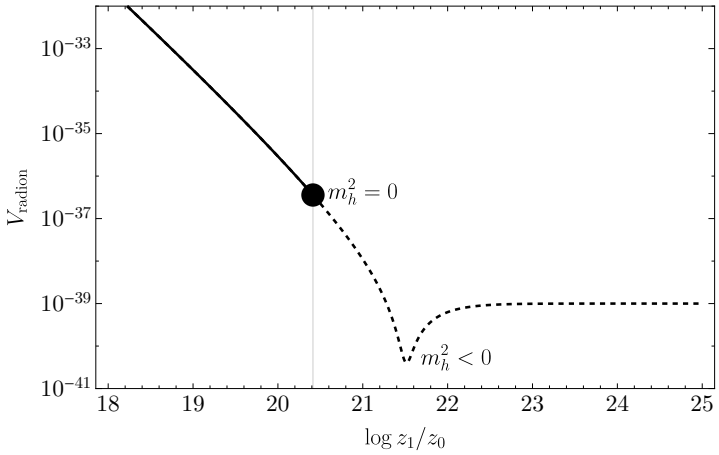

Figure 2.10: Here we show the radion potential. The dashed line is the potential if the Higgs VEV is left vanishing. There is a minimum of this potential where the metric ansatz for the IR brane is satisfied, but it corresponds to an unstable Higgs configuration. The solid line is the region where the effective Higgs mass squared in the low energy theory is positive. At the dot, the mass vanishes, and if $v_H^2 < v_H^2(\text{crit})$, the potential of the radion is minimized if the unstable Higgs region is forbidden. The gravity sector is not extremized here – the metric junction condition on the IR brane is not met.

dual. The apparent puzzle of the light and seemingly unprotected Higgs in the critical region may be that it is the Goldstone boson of this breaking, a type of phonon, perhaps making the lightness of the Higgs directly connected to the presence of a cosmology with non-relativistic matter and dark energy content.

A better understanding of the dynamical aspects of this class of Higgs model is definitely required to make these statements more firm, but there seem to be some quite promising avenues to pursue.

2.8 Conclusions

We have discussed a new possible approach to the Higgs hierarchy problem. The model is in part inspired by attempts to model aspects of self-organized criticality in condensed matter

systems in which it has been hypothesized that some classes of these critical states on the brink of catastrophic failure contain critical exponents that are becoming complex under loading of the system, leading to discrete scale invariance and instabilities.

We have explored 5D constructions that have features that are similar to the behavior just described. It has made us directly confront the AdS tachyon, associated with violation of the Breitenlohner-Freedman bound, and search for the manner in which field theory might resolve it. In this model, the resolution takes the form of an IR brane with characteristics that depend on the 5D fundamental parameters. We found that there is are large regions of the parameter space where a novel type of transition appears to be taking place.

A dynamical cosmology is an unavoidable consequence of the model when placed inside or near this region. Time evolution appears crucial to resolution of the AdS tachyon in this model. This could be a feature rather than a bug, tying together puzzling aspects of fundamental particle physics with puzzling features of cosmology in a novel way. It remains to be seen what the Higgs vev and spectrum will be once this time evolution is completely taken into account, and whether its effective mass and/or vacuum expectation value are tied in some interesting way to aspects of the cosmology.

Top priorities are to further investigate the cosmological dynamics, determine whether this type of setup can be utilized as an extension of the Standard Model, study its novel phenomenological implications and constraints if so, and to seek an embedding in a more complete microscopic theory.

Chapter 3

Radion-Activated Higgs Mechanism

3.1 Introduction

The mass of the Higgs is far smaller than dimensional analysis predicts given that there are so far no experimental signatures of new physics indicating new symmetries near the electroweak scale. This suggests that there may be some degree of fine tuning of parameters to achieve consistency with observations. Of course, the Higgs mass problem is not the only one of the Standard Model. The SM offers no explanation of large fermion mass hierarchies, of dark matter, of the matter/anti-matter asymmetry, etc. Strong dynamics, and/or field theories in higher-dimensional spacetimes offer resolutions or at least interesting reformulations of many of these problems, along with partially ameliorating the Higgs hierarchy problem.

The Higgs mass couples to singlet sectors in many extensions of the electroweak sector, which can put the the hierarchy problem into a new light [14]. The question is no longer "Why is the Higgs light?" Rather, the correct question is "Why does a small Higgs mass coincide with the global (or a cosmologically metastable) minimum of the scalar potential?"

Such scalars are generic features in models with additional compact spatial dimensions [33]. In these models, there are typically moduli that are gauge singlet states with non-trivial couplings to matter required by higher dimensional general covariance [52, 57]. Stabilization of these moduli is typically non-trivial as the moduli can be interpreted as Goldstone bosons of spontaneously broken spacetime symmetries. Providing a potential for them often requires new scalar degrees of freedom whose dynamics serve to explicitly break the spacetime symmetries, demoting the moduli to pseudo-Goldstone bosons.

In this work, we explore the relationship between extra-dimensional radius stabilization and the Higgs mass. In particular, the modulus of Randall-Sundrum models (the "radion") generally plays a crucial role in determining the value of the Higgs vacuum expectation value. The same goes for the reverse: the Higgs VEV itself will backreact on the geometry, and feed into the total effective potential for the radion.

This first motivates the development of a formalism for dealing with multi-scalar models of 5D RS model radius stabilization. This is the focus of the first part of this work. We show that even in cases of complicated bulk dynamics with many interacting scalar fields, the classical effective potential lives on the boundary. Making the assumption that the 5D action is of Einstein-Hilbert form with minimal couplings to bulk scalar fields, we calculate the classical potential to all orders in the 5D gravitational coupling constant.

The criteria for minimization of this effective potential determine aspects of the physics such as the Kaluza-Klein scale, and the masses of light resonances. We study these criteria, and provide conditions for extremization of this potential that fully include geometric backreaction effects.

We then apply this formalism to a few illustrative examples of the Higgs mechanism in

RS models. Given the lack of signals for extra-dimensional resonances in collider experiments, we look for models which achieve moderate separation of scales between the electroweak scale and the scale associated with the IR brane $f/v \gtrsim \mathcal{O}(10)$. The Higgs mass term is generally a function of the brane separation. Thus, in order to achieve a light Higgs, the minimum of the modulus potential must coincide with the region where the Higgs mass is small. We expect (and find) that tuning is involved in these cases. For example, such a coincidence problem may require that the IR brane mistune (between the brane tension and the bulk cosmological constant) be adjusted to high degree in order to keep the Higgs light. We explore the type and degree of tuning required in a few examples in which there is non-trivial interplay between electroweak symmetry breaking and radius stabilization.

As noted in [58], fine tuning can have dramatic phenomenological consequences when parameters of the Standard Model are set by the dynamics of a modulus field. These consequences influence both early universe cosmology and collider physics. Cosmology can be dramatically changed by interplay of Higgs and modulus field, with oscillations of the coupled scalar system leading to repercussions for gravity waves, and constraints on inflationary models. It is with this in mind that we choose models whose parameter space explore the full range of classes of mixed modulus-Higgs potential. The specifics of these classes are expanded on in the introduction to Section 3.3.

The example models we study are as follows:

- Higgs on the IR brane, Goldberger-Wise scalar stabilizing field in the bulk;
- Higgs in the bulk, with mass near the Breitenlohner-Freedman bound [24], stabilizing the geometry (studied previously in [44, 45]);

- Both Higgs and Goldberger-Wise stabilizing field in the bulk.

For simplicity of presentation, these models are all studied to lowest non-trivial order in the gravitational backreaction, where neither the Higgs or Goldberger-Wise scalar develop VEVs that are comparable to the AdS curvature.

An important result from these studies is that mass mixing between the Higgs and radion is completely generic. Mass mixing occurs in different ways: through symmetry-allowed couplings between a Goldberger-Wise field and the Higgs, or from mixing of the Higgs with the 5D gravity sector through backreaction.[1] It occurs both when the Higgs is purely localized on the IR brane through couplings to the Goldberger-Wise field, or when the Higgs is in the bulk of the extra dimension. This mixing is different in the various classes of Higgs-radion potential, and influences the spectrum of light scalar modes.

In Section 3.2 we discuss general properties of multi-scalar stabilization, giving conditions under which the geometry is stabilized. In Section 3.3, we explore the construction, phenomenology, and spectra of three different models where the Higgs is coupled to the extra-dimensional radion. In Section 3.4 we discuss a CFT interpretation of different multi-scalar stabilization models. In Section 3.5 we conclude.

3.2 General Properties of the Radion Potential

Before analyzing particular models, we first study some general properties of radius stabilization when there is more than one 5D scalar field that has non-vanishing vacuum expectation value. In such cases, the radion potential is affected by backreaction of all of these VEVs

[1] This is in addition to kinetic mixing, which can occur through couplings of the Higgs to either the 5D curvature, or to the extrinsic curvature of the IR brane [59].

onto the geometry. In what follows, we consider arbitrary backreaction onto the geometry, however we presume that the action is of Einstein-Hilbert form, with no higher curvature operators.

The generic problem is one of N real scalar fields minimally coupled to gravity in 5D space with negative cosmological constant $\Lambda_5 = -6k^2/\kappa^2$. The bulk geometry can be described with metric

$$\mathrm{d}s^2 = e^{-2A(y)}\,\mathrm{d}x_4^2 - \mathrm{d}y^2\,, \tag{3.2.1}$$

where we have presumed flat 4D slices. The space is cut off on both sides by branes at positions y_0 and y_1.

All dimensionful quantities are understood to be expressed in units of the AdS curvature: $k = 1$. For perturbative control of the 5D gravity theory, the 5D Newton constant must be small: $\kappa^2 = \frac{1}{2M_5^3} \sim \mathcal{O}(1/10)$. The action is:

$$\begin{aligned} S = &\int \mathrm{d}^4x\,\mathrm{d}y\,\sqrt{g}\left[\frac{1}{2}\sum_i(\partial_M\phi_i)^2 - V(\{\phi_i\}) - \frac{1}{2\kappa^2}R\right] \\ &- \int \mathrm{d}^4x\,\sqrt{-g_0}V_0(\{\phi_i\})\Big|_{y=y_0} - \int \mathrm{d}^4x\,\sqrt{-g_1}V_1(\{\phi_i\})\Big|_{y=y_1}, \end{aligned} \tag{3.2.2}$$

where the scalar potential includes the bulk cosmological constant term.

The bulk Einstein equations relate derivatives of $A(y)$ to the scalar fields in the following way:

$$\begin{aligned} A'^2 &= \frac{\kappa^2}{12}\sum_i \phi_i'^2 - \frac{\kappa^2}{6}V(\{\phi_i\}), \\ A'' &= \frac{\kappa^2}{3}\sum_i \phi_i'^2. \end{aligned} \tag{3.2.3}$$

The scalar curvature is given by

$$R = 20A'^2 - 8A''. \tag{3.2.4}$$

In the absence of scalar field VEVs, or in the limit of small κ^2, the space is AdS.

Plugging the result for the scalar curvature, and for the scalar terms into the action above, we find that the bulk portion is a derivative, and thus can be expressed as a boundary term:

$$S_{\text{bulk}} = \frac{2}{\kappa^2}\int \mathrm{d}^4x\,\mathrm{d}y\,\frac{\partial}{\partial y}\left[e^{-4A(y)}A'(y)\right] = \frac{2}{\kappa^2}\int \mathrm{d}^4x\left[e^{-4A(y_0)}A'(y_0) - e^{-4A(y_1)}A'(y_1)\right]. \tag{3.2.5}$$

The factor of 2 is from integration over the circle. We note that on the boundaries, there must be a jump in the derivative of the metric. This can be seen most easily from the orbifold perspective, where on either side of an orbifold fixed point, you must have $A(y_{0,1})_+ = A(y_{0,1})_-$ and $A'(y_{0,1})_+ = -A'(y_{0,1})_-$. This leads to a term in the scalar curvature R which is a delta function, as you must have $A''(y_{0,1}) \supseteq \pm 2\delta(y_{0,1} - y)A'(y_{0,1})$. Inclusion of the delta function term in the scalar curvature gives additional boundary contributions to the effective action.

Including all terms, the effective potential can now be expressed as a pure boundary term [47]:

$$V_{\text{eff}} = e^{-4A(y_0)}\left[V_0(\{\phi_i(y_0)\}) - \frac{6}{\kappa^2}A'(y_0)\right] + e^{-4A(y_1)}\left[V_1(\{\phi_i(y_1)\}) + \frac{6}{\kappa^2}A'(y_1)\right]. \tag{3.2.6}$$

where, at the moment, none of the boundary conditions have been imposed, nor even the bulk scalar equations of motion, which are given by:

$$\phi_i'' = 4A'\phi_i' + \frac{\partial V}{\partial \phi_i}. \tag{3.2.7}$$

The scalar boundary conditions are given (in these coordinates) as:

$$\phi_i' \Big|_{y_0,y_1} = \pm \frac{1}{2} \frac{\partial V_{0,1}}{\partial \phi_i} \Big|_{y_0,y_1} . \tag{3.2.8}$$

The boundary Einstein equations (the metric junction conditions that match the geometry to the brane-localized stress-energy) are

$$A' \Big|_{y_0,y_1} = \pm \frac{\kappa^2}{6} V_{0,1} \Big|_{y_0,y_1} , \tag{3.2.9}$$

which correspond to the UV and IR terms in the effective potential vanishing individually.

One can associate the brane separation with the vacuum expectation value of the radion. The metric boundary condition at y_1 can be thought of as setting the VEV of the radion. That is, one varies y_1 until the IR brane contribution to the effective potential vanishes. We show in the next Subsection that it is always the case that the minimum in the static effective potential corresponds to vanishing $V_{\rm IR}$ after all scalar bulk and boundary equations of motion are imposed.[2]

At this point we can impose the scalar field equations of motion. For a single scalar field, if we impose the bulk equations, the effective potential is then a function of the two remaining freedoms in the scalar field (its value and derivative, on, for example, the UV brane), and the position of the IR brane. If one further imposes the scalar boundary conditions on both of the two branes, then only the value of y_1 remains, to be determined by minimizing the effective potential with respect to it. However, we might be interested in a more intuitive

[2]However, it curiously remains possible that extrema or saddles arise where neither the scalar or metric conditions are satisfied (and this occurs in some models [60]). This may be due to nearby extrema which do not satisfy the ansatz of a Lorentz invariant background.

measure of the effective potential, particularly when taking into account the multiple scalar degrees of freedom, where we expect to have a multidimensional scalar potential.

We advocate an approach inspired by holography, where the effective potential is measured in terms of field values on the UV brane only. In this case, the procedure we should take to find the effective potential is as follows:

- pick a particular value of y_1;
- impose the IR boundary conditions, eliminating N of the $2N$ scalar boundary conditions. N degrees of freedom remain, e.g. the values of the fields on the UV brane;
- we are left with N scalar boundary values and the free value of y_1. Ideally, one would then, for constant UV field values, minimize the effective action over y_1.

This last step is difficult to implement in practice. However, if at least one of the scalar fields (say ϕ_N) has "stiff" boundary conditions in the UV, then one instead imposes that UV brane condition, leaving $N-1$ scalar degrees of freedom on the UV brane. The value of y_1 corresponds to the last degree of freedom, so that one has $V_{\text{eff}}(\phi_1(y_0), \cdots, \phi_{N-1}(y_0); y_1)$.

3.2.1 Derivative of the Radion Potential

We are interested in finding stable configurations of the branes, where the effective potential is minimized. We explore here the conditions for minimization, showing analytically that they correspond in most, but not all, cases to vanishing of the IR portion of the effective potential.

Employing the above procedure, imposing the IR brane boundary conditions for the scalar fields the derivative of the effective potential with respect to y_1 takes a particularly simple

form:

$$\frac{\mathrm{d}V}{\mathrm{d}y_1} = e^{-4A(y_0)} \sum_i \left(\frac{\partial V_0}{\partial \phi_i}(y_0) - 2\phi_i'(y_0) \right) \frac{\mathrm{d}\phi_i}{\mathrm{d}y_1}(y_0) - 4e^{-4A_1} \frac{\mathrm{d}A_1}{\mathrm{d}y_1} \left[V_1 + \frac{6}{\kappa^2} A_1' \right]. \tag{3.2.10}$$

The first term is vanishing if the boundary conditions for the scalars on the UV brane are imposed. The second term is vanishing if the metric junction condition in the IR is imposed. We thus note that this formula implies that extremization of the action implies (as it must, of course) extremization of the effective potential. However, the converse is not necessarily the case. It may be that this expression vanishes where the two terms cancel against each other and neither metric nor scalar boundary conditions are met. We hypothesize that this may occur when there are extrema of the action "nearby" in configuration space that do not obey the static, homogeneous, and isotropic ansatz that was the starting point for this analysis of the effective action.

We note that there is a method that generalizes the well known superpotential method for stabilization [61] to include multiple scalar fields. This method guarantees a solution in which the effective potential is extremized.

3.3 Examples of Radion-Induced Symmetry Breaking

We now explore some specific simple models that illustrate different classes of multi-scalar potentials where a Higgs instability occurs over some region of radius values. We are particularly interested in models where some tuning has been performed to obtain mild or large hierarchies between the electroweak scale and the KK scale. Broadly speaking, there are

3 classes of tunings distinguished by the shape of the 2-dimensional scalar potential. These are as follows:

- All parameters of the 5D theory are of order 1 (in units of the AdS curvature for dimensionful couplings). Tuning is achieved by making the symmetry breaking critical point extremely close to the minimum of the radion potential.

- The Higgs potential has only mild dependence on the radion VEV. Tuning is achieved by arranging the Higgs effective mass term to be small over a large range of radius, including at the minimum of the radion potential.

- The radion potential itself is very shallow due to tuning. The Higgs VEV then contributes sizably to the stabilization, and even small Higgs VEV successfully stabilizes the geometry for large KK scale.

In Figure 3.1, we display the basic pictures of these three types of 2D scalar potentials.

These different types of tunings have implications for phenomenology. For example, there may be consequences for cosmology, affecting the manner in which the early universe electroweak phase transition takes place [62–64], and possibly playing a crucial role during post-inflationary reheating [58]. Additionally, the different tunings have implications for the mass spectrum of the lightest scalar modes, and for general considerations about vacuum energy [65, 66]. For example, the radion mass may be typically lighter or heavier than the Higgs for the different classes of model.

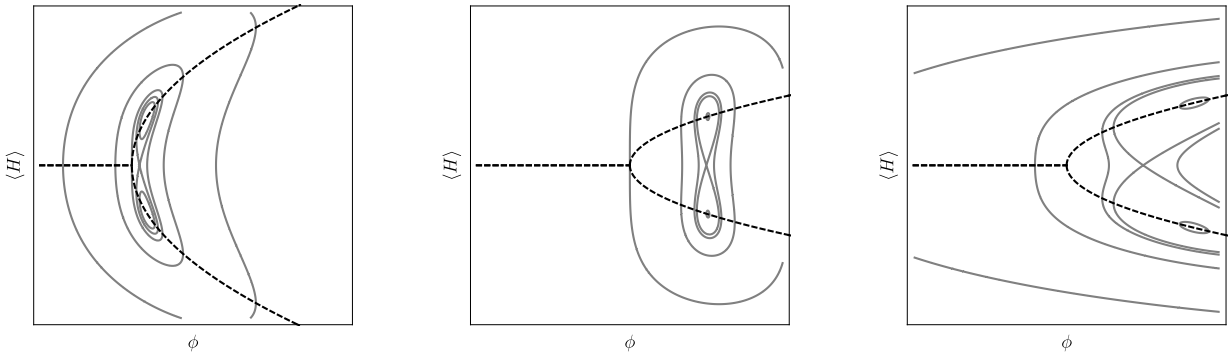

Figure 3.1: In this figure, we roughly characterize the different types of potentials in the space of the radion and the Higgs VEVs. Each plot shows a potential as a function of a modulus VEV, ϕ, and a Higgs VEV. Dashed lines indicate points at which the Higgs potential is minimized with ϕ held constant. In the first image, all couplings are order 1, however, the minimum of the modulus potential is tuned to be close to the critical point for the Higgs. In the second, the dependence of the Higgs potential on the modulus field is weak, and the bare Higgs mass is taken to be somewhat small. In the final plot, the modulus potential without the Higgs is very flat, and thus the backreaction of the Higgs onto the modulus potential is the dominant feature in the potential.

3.3.1 Higgs on the Brane

We now want to consider the case in which the interactions between the Higgs and the GW scalar take place on the IR brane. We assume no bulk interactions between the fields. This can be done with a Higgs which is either in the bulk or completely localized on the IR brane. We first consider the latter.

When the Higgs is localized on the IR brane, the only field that propagates in the bulk is the Goldberger-Wise (GW) scalar. The bulk action is then

$$S_{\text{bulk}} = \int \mathrm{d}^5x\, \sqrt{g} \left(\frac{1}{2} g^{MN} \partial_M \Phi\, \partial_N \Phi + \frac{6}{\kappa^2} - \frac{1}{2} m_\Phi^2 \Phi^2 - \frac{1}{2\kappa^2} R \right). \tag{3.3.1}$$

We take $m_\Phi^2 \equiv \epsilon(\epsilon - 4)$, where ϵ is taken to be $\mathcal{O}(1/10)$ in order to generate exponential hierarchies without severe tuning. The bulk action is supplemented by brane-localized

Lagrangian terms, including a kinetic term and potential for the Higgs on the IR brane:

$$S_{\text{brane}} = -\int \mathrm{d}^4x\,\sqrt{-g_0}\,V_0(\Phi)\Big|_{y=y_0} - \int \mathrm{d}^4x\,\sqrt{-g_1}\left(|\partial_\mu H|^2 - V_1(\Phi,|H|)\right)\Big|_{y=y_1}. \tag{3.3.2}$$

We presume the following form for the brane-localized potentials:

$$\begin{aligned} V_0 &= T_0 + \gamma_0(\Phi - v_0)^2, \\ V_1 &= T_1 + \lambda_H|H|^2(|H|^2 - v_H^2 - \lambda\Phi) + \gamma_1(\Phi - v_1)^2. \end{aligned} \tag{3.3.3}$$

These include brane tensions and localized mass terms for the Goldberger-Wise stabilizing field that displace the VEV from the origin. In addition, there is a standard potential for the IR brane-localized Higgs with an additional trilinear coupling to the Goldberger-Wise field. This last term is crucial for our purposes, as it couples the Higgs field to the radius.

We then solve the equation of motion (3.2.7), supplemented by the boundary conditions (3.2.8), under the assumption of an x-independent background VEV, $\langle\Phi\rangle = \phi(y)$. Putting everything together we get the effective dilaton potential of Equation (3.2.6) in the case of a single bulk scalar field, with the added contributions of the brane-localized Higgs.

We consider the small backreaction limit, $\kappa \ll 1$. In this case, $A' \approx 1$ and the bulk equation of motion can be solved in general to give

$$\phi(y) = \phi_\epsilon e^{\epsilon y} + \phi_4 e^{(4-\epsilon)y}. \tag{3.3.4}$$

The coefficients are fixed by imposing the boundary conditions. We adopt a stiff wall boundary condition for the GW field on the UV brane, corresponding to the limit $\gamma_0 \to \infty$, which fixes

$\phi_0 \equiv \phi(y=0) = v_0$.

The IR brane potential contains the interaction between the GW scalar and the Higgs. We do not take the stiff wall limit for the GW scalar on the IR brane, so $\phi_1 \equiv \phi(y_1)$ is not fixed at v_1. Through the trilinear coupling to Φ, the brane-localized Higgs mass is then a function of y_1. The equation of motion for the Higgs background that minimizes the effective potential energy is

$$2\langle H\rangle^2 \equiv v^2(y_1) = \begin{cases} 0 & v_H^2 + \lambda\phi_1 < 0 \\ v_H^2 + \lambda\phi_1 & v_H^2 + \lambda\phi_1 > 0, \end{cases} \tag{3.3.5}$$

while the boundary condition for $\phi(y)$ is

$$\phi_1' = -\gamma_1(\phi_1 - v_1) + \frac{1}{4}\lambda\lambda_H v^2(y_1). \tag{3.3.6}$$

If we impose only the IR boundary condition for ϕ, leaving the Higgs VEV free (not imposing Equation (3.3.5)), we can explore the two dimensional effective potential as a function of v and y_1.

In the small backreaction limit, the effective potential for the system is

$$V_{\text{eff}} = e^{-4y_0}\left(V_0 - \frac{6}{\kappa^2} - \frac{1}{4}\phi_0'^2 - \frac{\epsilon(4-\epsilon)}{4}\phi_0^2\right) + e^{-4y_1}\left(V_1 + \frac{6}{\kappa^2} + \frac{1}{4}\phi_1'^2 + \frac{\epsilon(4-\epsilon)}{4}\phi_1^2\right). \tag{3.3.7}$$

For small y_1 values, it can be arranged that $v_H^2 + \lambda\phi_1 < 0$, and the origin in Higgs field space is a stable minimum: $\langle H\rangle = 0$.

In this region, the effective potential (after imposing the Higgs equation of motion) is

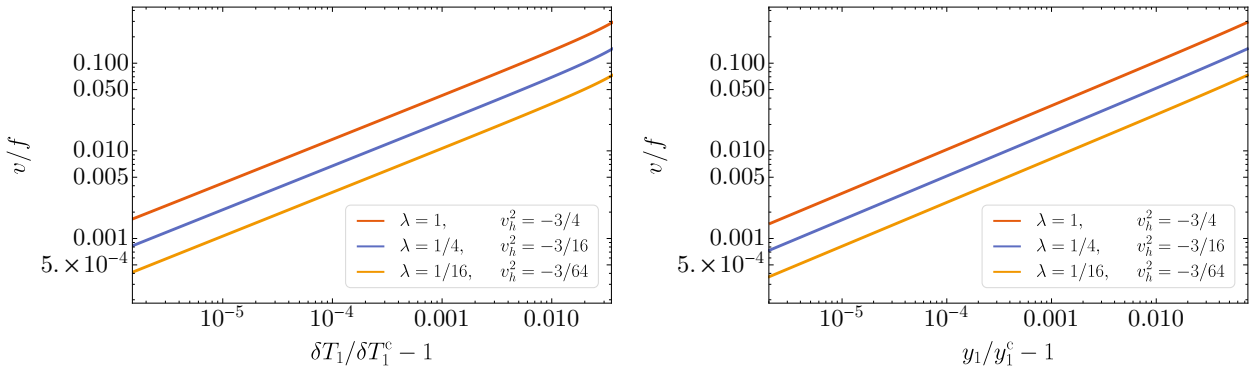

Figure 3.2: Higgs VEV in units of the symmetry breaking scale f and its dependence on various parameters of the model. On the left, we show the variation as a function of the IR brane mistune δT_1. On the right, we display it in terms of how close the minimum of the radion potential is to y_1^c, the critical point in the extra dimension where the interplay between the GW scalar and the Higgs first triggers electroweak symmetry breaking. We have taken $v_0 = 1/10$, $v_1 = 2$, $\gamma_1 = 1$, $\lambda_H = 1/8$, $\kappa = 1/50$. The different curves are obtained by fixing the ratio λ/v_H^2, so that equal values of ϵ correspond to equal values of y_1^c.

determined by the single GW field and its backreaction onto the geometry.

On the other hand, for larger y_1 values, the Higgs may develop a VEV. For example, when ϵ is taken to be small and we set $\gamma_1 = 0$, we can approximate the electroweak symmetry breaking condition as

$$y_1 \gtrsim \frac{1}{\epsilon} \log\left(-\frac{v_H^2}{\lambda v_0}\right). \tag{3.3.8}$$

Minimizing the effective potential with respect to y_1 relates the Higgs VEV to the symmetry breaking scale. The effective VEV, in units of the Kaluza-Klein scale f, scales with δT_1, the IR brane mistune, as

$$\frac{v}{f} \approx \left(\frac{64\delta T_1}{\lambda_H(16 - \lambda^2\lambda_H)}\right)^{1/4}. \tag{3.3.9}$$

In Figure 3.2 we quantify the amount of tuning associated with a given Higgs VEV v. The Higgs VEV is fixed in the following way: first we identify the effective 4D scale of gravity, i.e. the Planck scale, via $M_{\rm Pl}^2 \approx 1/(2\kappa^2)$, as a consequence of the warped geometry. For a given value of κ, we then reproduce the experimentally measured hierarchy between the Planck

and the weak scale, $\log(M_{\rm Pl}/v) \approx 38.4$. We scan over f by changing $\epsilon \sim 1/10$, so that the corresponding values of y_1 provide a large range of Kaluza-Klein scales. To obtain a small v/f, parameters must be chosen so that the global minimum of the effective potential is very close to the critical point for electroweak symmetry breaking. We denote the critical values of the 5D parameters with the superscript "c". We display this information in two different ways: on the left, as a function of δT_1, which is the physical parameter that needs to be tuned to adjust the location of the minimum of the effective potential. On the right, as a function of y_1, the location of the minimum itself, which is more useful to visually determine how close the minimum has to be to the critical point. As expected from the analytic estimate of Equation (3.3.9), a small Higgs VEV requires a very small mistune in the brane tension against the bulk cosmological constant.

Mass Spectrum

In order to understand the spectrum of the theory, we consider fluctuations around the background solutions for the metric and the two scalar field profiles to linearized order. In particular, we parametrize the various degrees of freedom as

$$\begin{aligned} \Phi(x,y) &= \phi(y) + \varphi(x,y), \\ H(x) &= \frac{1}{\sqrt{2}}[v + h(x)]\exp(i\alpha), \\ \mathrm{d}s^2 &= e^{-2A(y)-2F(x,y)}\eta_{\mu\nu}\,\mathrm{d}x^\mu\,\mathrm{d}x^\nu - (1+2F(x,y))^2\,\mathrm{d}y^2\,. \end{aligned} \tag{3.3.10}$$

It is possible to show that, when having only one scalar field in the bulk, the whole set of linearized Einstein equations, together with the equations of motion for the scalar fields,

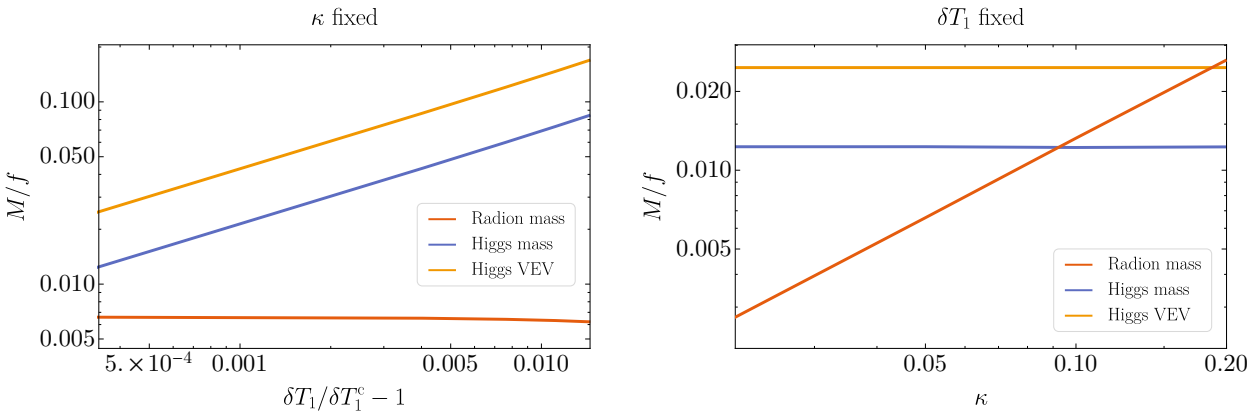

Figure 3.3: Dependence of the mass scales in the theory on various parameters of the model. On the left, we show how for a fixed value of κ the IR brane mistune controls the Higgs mass and VEV, while the radion mass is essentially unchanged. On the right, we see that the radion mass is dependent on the amount of backreaction. The parameters are the same as in Figure 3.2.

reduces to a single homogeneous differential equation for F in the bulk [51]:

$$F'' - 2A'F' - 4A''F - 2\frac{\phi''}{\phi'}F' + 4\frac{\phi''}{\phi'}A'F = e^{2A}\Box F. \tag{3.3.11}$$

We also have to specify the boundary conditions. When considering a stiff wall UV brane boundary condition for the background GW field ($\gamma_0 \to \infty$), the UV boundary condition is $F_0' = 2A_0'F_0$. The IR boundary condition for F can be obtained by combining the following equations:

$$\begin{aligned} \phi'\varphi &= \frac{3}{\kappa^2}(F' - 2A'F), \\ -2\varphi_1' &= \frac{\partial^2 V_1}{\partial\phi^2}\varphi_1 + \frac{\partial^2 V_1}{\partial\phi\partial h}h + 2F_1\frac{\partial V_1}{\partial\phi}, \\ \Box h + e^{-2A_1}&\left(\frac{\partial^2 V_1}{\partial\phi\partial h}\varphi_1 + \frac{\partial^2 V_1}{\partial h^2}h\right) = 0. \end{aligned} \tag{3.3.12}$$

Notice that the mass eigenvalue appears both in the bulk equation and in the boundary condition because of the presence of the brane-localized Higgs kinetic term which leads to the $\Box \equiv \partial_\mu\partial^\mu$ operator.

Solutions are parametrized by 3 unknowns. Two are integration constants associated with the second order equation for F, and the third is the eigenvalue. One integration constant can be fixed by choosing a convenient normalization, and the other is eliminated by imposing the UV brane boundary condition. To find the eigenvalues, we employ a shooting method and determine the mass eigenvalues for which the IR boundary condition is satisfied. We find that the spectrum contains a light radion and Higgs along with a KK tower due to the bulk GW field.[3][4]

Figure 3.3 shows the mass spectrum obtained by solving Equation (3.3.11) supplemented by the boundary conditions (3.3.12). Once again, we fix v to the electroweak value and we scan over f by varying $\epsilon \sim 1/10$. We can see how the mass of the Higgs fluctuation tracks the Higgs VEV and is controlled by the amount of mistune (left subfigure), while the radion mass is determined by the backreaction parameter κ (right subfigure). On the other hand, the Higgs and radion masses are essentially insensitive to changes in κ and δT_1, respectively. The lightest particle in the spectrum can be either the Higgs or the radion, depending on the choice of parameters. This is in contrast to the results of Subsection 3.3.3, where we consider only the Higgs in the bulk, and the radion is constrained to be the lightest state in the spectrum.

3.3.2 Two Bulk Fields

In this Subsection, we consider the case where both fields, GW scalar Φ and the Higgs H, propagate in the bulk. For simplicity, we assume that they are uncoupled, despite such a

[3] As usual, there is no separate KK tower for the radion field, as these modes are eaten by the massive KK gravitons.

[4] Recent work also utilizes a new approach to get the full potential for the lightest scalar mode, going beyond the mass eigenvalue [67].

coupling being allowed by the symmetry. However, they still interact indirectly through gravity, as both fields backreact on the geometry. We assume that the Higgs is localized towards the IR brane by taking its bulk mass close to (but above) the Breitenlohner-Freedman bound $m_H^2 = -4$. Note that the bulk mass is constant.

The bulk action is given by

$$S_{\text{bulk}} = \int \mathrm{d}^5x\, \sqrt{g}\Big(\frac{1}{2}\partial^N\Phi\partial_N\Phi + \partial^N H^\dagger \partial_N H + \frac{6}{\kappa^2} - \frac{1}{2}m_\Phi^2\Phi^2 - m_H^2|H|^2 - \frac{1}{2\kappa^2}R\Big). \quad (3.3.13)$$

Again we take $m_\Phi^2 \equiv \epsilon(\epsilon - 4)$ with $\epsilon \sim \mathcal{O}(1/10)$, and we also define $\nu^2 \equiv 4 + m_H^2$ with $\nu \sim \mathcal{O}(1/10)$. This bulk action is supplemented by brane-localized Lagrangian terms

$$S_{\text{brane}} = -\int \mathrm{d}^4x\, \sqrt{-g_0}V_0(\Phi, |H|)\Big|_{y=y_0} - \int \mathrm{d}^4x\, \sqrt{-g_1}V_1(\Phi, |H|)\Big|_{y=y_1}. \quad (3.3.14)$$

The brane-localized potentials are given by the following:

$$\begin{aligned} V_0(\Phi, |H|) &= T_0 + \gamma_0(\Phi - v_0)^2 + m_0^2|H|^2, \\ V_1(\Phi, |H|) &= T_1 + \gamma_1(\Phi - v_1)^2 + \lambda_H|H|^2(|H|^2 - v_H^2). \end{aligned} \quad (3.3.15)$$

In this Subsection, we work in the simplifying limit $\gamma_{0,1} \to \infty$, which sets the UV/IR boundary conditions for the GW field as $\Phi(y = y_0) = v_0$ and $\Phi(y = y_1) = v_1$ respectively.

We write the VEVs for the GW and the Higgs field respectively as $\langle\Phi\rangle = \phi(y)$ and $\langle|H|\rangle = v(y)/\sqrt{2}$. Presuming small metric backreaction, the bulk equations of motion for the

scalars are given by

$$\begin{aligned} \phi'' - 4\phi' - \epsilon(\epsilon-4)\phi = 0, \\ v'' - 4v' - (-4+\nu^2)v = 0. \end{aligned} \tag{3.3.16}$$

The GW field ϕ has the same profile as in the previous Subsection, which is given by (3.3.4) where the coefficients ϕ_ϵ and ϕ_4 are fixed by the boundary conditions $\phi(y_0 = 0) = v_0$ and $\phi(y_1) = v_1$. The solution for the Higgs VEV can be conveniently expressed as

$$v(y) = v(y_1)e^{2(y-y_1)}\left(\frac{e^{\nu y} - re^{-\nu y}}{e^{\nu y_1} - re^{-\nu y_1}}\right), \tag{3.3.17}$$

where $v(y_1)$ and r are integration constants which will be determined by the Higgs boundary conditions generated by the brane potentials (3.3.15):

$$\begin{aligned} v'(y_0) &= \frac{m_0^2}{2}v(y_0), \\ v'(y_1) &= \frac{\lambda_H}{2}v(y_1)\Big(v_H^2 - v^2(y_1)\Big). \end{aligned} \tag{3.3.18}$$

The UV boundary condition fixes r as

$$r = \frac{m_0^2 - 4 - 2\nu}{m_0^2 - 4 + 2\nu}. \tag{3.3.19}$$

The constant $v(y_1)$, the Higgs VEV on the IR brane, is determined by the IR boundary condition which has two solutions. One of them is the trivial one $v(y_1) = 0$ corresponding to unbroken electroweak symmetry. By defining $m_1^2 \equiv \lambda_H v_H^2$, the second solution is given by

$$v^2(y_1) = \frac{1}{\lambda_H}\left[(m_1^2 - 4 - 2\nu) + \frac{4\nu(m_0^2 - 4 - 2\nu)}{(m_0^2 - 4 - 2\nu) - e^{2\nu y_1}(m_0^2 - 4 + 2\nu)}\right], \tag{3.3.20}$$

provided that the term inside brackets is positive. In this case, the above solution is the preferred one, corresponding to broken electroweak symmetry.

If the Higgs has a nonzero VEV, it contributes to the 4D effective potential (3.3.7) by a term given by

$$V_{\text{eff}}^{v} = \left[\frac{m_0^2}{2}v^2 - \frac{1}{4}v'^2 + \frac{1}{4}m_H^2 v^2\right]\Big|_{y=0} + e^{-4y_1}\left[\frac{\lambda_H}{2}v^2\left(\frac{v^2}{2} - v_H^2\right) + \frac{1}{4}v'^2 - \frac{1}{4}m_H^2 v^2\right]\Big|_{y=y_1} \tag{3.3.21}$$

By using the Higgs solution (3.3.17) and the boundary conditions (3.3.19) and (3.3.20), the above expression takes a very simple form:

$$V_{\text{eff}}^{v} = -\frac{\lambda_H}{4}v^4(y_1)e^{-4y_1}. \tag{3.3.22}$$

We can directly see that it is negative definite, therefore if there is a solution with a non-trivial VEV, then it will be energetically favored.

Parameter Space for Electroweak Symmetry Breaking

By inspecting the function $v^2(y_1)$, we can see that it has a singularity at

$$y_1^s = \frac{1}{2\nu}\log\left(\frac{m_0 - 4 - 2\nu}{m_0^2 - 4 + 2\nu}\right), \tag{3.3.23}$$

since the denominator of the second term in (3.3.20) diverges. In the region of parameter space where $m_0^2 - 4 < -2\nu$, y_1^s is positive, hence physical. As a result, the effective potential will be unbounded from below at $y_1 = y_1^s$. This singularity is an artifact of neglecting the backreaction of the Higgs on the geometry, which cannot be done in the vicinity of y_1^s.

Nevertheless, since we want to continue to work in the small backreaction limit, we will exclude the $m_0^2 - 4 < -2\nu$ from our parameter space.

For the rest of the discussion, we will assume $m_0^2 - 4 > -2\nu$ and define $\alpha_{0,1} \equiv m_{0,1}^2 - 4 - 2\nu$ for notational simplicity. By taking the derivative of (3.3.20) with respect to y_1, we find

$$\frac{\partial v^2(y_1)}{\partial y_1} = \frac{1}{\lambda_H} \frac{8\alpha_0 \nu^2 (\alpha_0 + 4\nu) e^{2\nu y_1}}{[\alpha_0 - e^{2\nu y_1}(\alpha_0 + 4\nu)]^2}. \tag{3.3.24}$$

This tells us that $v^2(y_1)$ is either monotonically increasing or decreasing depending on the sign of α_0. We will consider the former case in this particular example.

In order to have symmetry breaking, we need $\lim_{y_1 \to \infty} v^2(y_1) > 0$ which implies $\alpha_1 > 0$. Additionally, the symmetry will be unbroken in the UV if $v^2(y_1 = 0) < 0$, or $\alpha_0 > \alpha_1$. In this case there is a "critical" position of the IR brane, $y_1 = y_1^c$, where the effective Higgs mass squared term is vanishing. This point corresponds to $v^2(y_1 = y_1^c) = 0$ and is given by

$$y_1^c = \frac{1}{2\nu} \log\left(\frac{\alpha_0(\alpha_1 + 4\nu)}{\alpha_1(\alpha_0 + 4\nu)}\right). \tag{3.3.25}$$

A convenient measure of the size of the Higgs VEV is the mass that would be given to a gauge field by the Higgs mechanism. For small backreaction, this can be approximated by

$$\left(\frac{v_{\text{eff}}}{f}\right)^2 = \int_{y_0}^{y_1} \mathrm{d}y \, e^{-2(y - y_1)} v(y)^2, \tag{3.3.26}$$

where $f = e^{-y_1}$ is the conformal symmetry breaking scale, i.e. the KK scale.

The full effective potential can be expressed as the sum of the UV and IR contributions:

$$V_{\text{eff}}(y_1) = e^{-4y_0} V_{\text{eff}}^{\text{UV}}(y_1) + e^{-4y_1} V_{\text{eff}}^{\text{IR}}(y_1). \tag{3.3.27}$$

The condition for an extremum of the effective potential is that $V_{\text{eff}}^{\text{IR}}$ vanishes, provided that the scalar boundary conditions (3.2.8) are satisfied. Such a point, let us denote it by y_1^{ext}, is a minimum provided that

$$V''_{\text{eff}}(y_1)\Big|_{y_1=y_1^{\text{ext}}} > 0. \tag{3.3.28}$$

Since the Higgs contribution to the effective potential scales as the fourth power of the Higgs VEV, we can neglect it for finding the extremum points and their stability. Then we can approximate $V_{\text{eff}}^{\text{IR}}$ by

$$V_{\text{eff}}^{\text{IR}}(y_1) \approx \delta\tilde{T}_1 - v_0 v_1 (2-\epsilon)(4-\epsilon) e^{\epsilon y_1} + v_0^2 (2-\epsilon)^2 e^{2\epsilon y_1}, \tag{3.3.29}$$

where in the second line we absorbed all the y_1-independent terms into the definition of $\delta\tilde{T}_1$. The extremum of the potential is determined by the solution of the quadratic equation:

$$\delta\tilde{T}_1 - v_0 v_1 (2-\epsilon)(4-\epsilon) f_{\text{ext}}^{-\epsilon} + v_0^2 (2-\epsilon)^2 f_{\text{ext}}^{-2\epsilon} = 0, \tag{3.3.30}$$

where $f_{\text{ext}} = \exp\{-y_1^{\text{ext}}\}$ denotes the conformal breaking scale at the extremum point y_1^{ext}. To determine the stability, we need to calculate the full effective potential. Again ignoring

Higgs contributions, it can approximately be expressed as

$$V_{\text{eff}}(f) \approx \delta\tilde{T}_0 + \delta\tilde{T}_1 f^4 - 4v_0 v_1(2-\epsilon)f^{4-\epsilon} + 2v_0^2(2-\epsilon)f^{4-2\epsilon}. \tag{3.3.31}$$

Since $V''_{\text{eff}}(y_1)$ and $V''_{\text{eff}}(f)$ have the same sign, we can calculate the latter. Then, the stability condition reads

$$12\delta\tilde{T}_1 - 4v_0 v_1(2-\epsilon)(3-\epsilon)(4-\epsilon)f_{\text{ext}}^{-\epsilon} + 2v_0^2(2-\epsilon)(3-2\epsilon)(4-2\epsilon)f_{\text{ext}}^{-2\epsilon} > 0. \tag{3.3.32}$$

Finally, we replace $\delta\tilde{T}_1$ with the solution of (3.3.30). Then we find that the extremum point f_{ext} is stable if

$$f_{\text{ext}} < \left(\frac{(v_1/v_0)(4-\epsilon)}{4-2\epsilon}\right)^{-1/\epsilon}. \tag{3.3.33}$$

Mass Spectrum

In this Subsection, we will work out the mass spectrum when both fields are propagating in the bulk. We will parameterize the fluctuations of the metric and the field in the same way as in Subsection 3.3.1, except now the Higgs field does also depend on the bulk coordinate y:

$$H(x,y) = \frac{1}{\sqrt{2}}[v(y) + h(x,y)]\exp\{i\alpha\}. \tag{3.3.34}$$

In this case, the linearized Einstein equations for fields F, h, φ take the form

$$12A'^2F - 6A''F - 6A'F' + F'' = -\frac{\kappa^2}{3}\left[2VF + 3F(\phi'^2 + v'^2) - \frac{\partial V}{\partial \phi}\varphi - \frac{\partial V}{\partial v}h - \phi'\varphi' - v'h'\right] - \frac{\kappa^2}{3}\sum_{j=0,1}\left(4V_jF - \frac{\partial V_j}{\partial \phi}\varphi - \frac{\partial V_j}{\partial v}h\right)\delta(y - y_j), \tag{3.3.35}$$

$$4A'F' + e^{2A}\Box F = -\frac{\kappa^2}{3}\left(4VF + \frac{\partial V}{\partial \phi}\varphi + \frac{\partial V}{\partial v}h - \phi'\varphi' - v'h'\right), \tag{3.3.36}$$

$$\partial_\mu(3F' - 6A'F) = \kappa^2\partial_\mu(\phi'\varphi + v'h), \tag{3.3.37}$$

where all derivatives of the bulk and brane potentials are evaluated on the background scalar VEVs. The $\mu 5$-equation can directly be integrated to give

$$F' - 2A'F = \frac{\kappa^2}{3}(\phi'\varphi + v'h). \tag{3.3.38}$$

By combining the $\mu\nu$- and 55-equations in the bulk we obtain

$$F'' - 2A'F' + e^{2A}\Box F = \frac{2\kappa^2}{3}(\phi'\varphi' + v'h'). \tag{3.3.39}$$

Matching the singular terms in the $\mu\nu$-equation gives the junction conditions for F:

$$[F']_i = \frac{2\kappa^2}{3}V_iF + \frac{\kappa^2}{3}\left(\frac{\partial V_i}{\partial \phi}\varphi + \frac{\partial V_i}{\partial v}h\right). \tag{3.3.40}$$

By using the boundary conditions for the background solution, one can show that this is equivalent to the $\mu 5$-equation so it provides no new constraints.

The linearized scalar field equations are given by

$$e^{2A}\Box\varphi - \varphi'' + 4A'\varphi' + \frac{\partial^2 V}{\partial\phi^2}\varphi = -6F'\phi' - 4\frac{\partial V}{\partial\phi}F, \tag{3.3.41}$$

$$e^{2A}\Box h - h'' + 4A'h' + \frac{\partial^2 V}{\partial v^2}h = -6F'v' - 4\frac{\partial V}{\partial v}F, \tag{3.3.42}$$

together with the boundary conditions

$$[\varphi' - 2\phi' F]_i = \frac{\partial^2 V_i}{\partial\phi^2}\bigg|_\phi \varphi, \tag{3.3.43}$$

$$[h' - 2v' F]_i = \frac{\partial^2 V_i}{\partial v^2} h. \tag{3.3.44}$$

So far, there are three second order differential equations, (3.3.39)(3.3.41) and (3.3.42), which need to be solved simultaneously. However, we can use the $\mu 5$-equation (3.3.38) to eliminate φ from the system. Then (3.3.39) becomes

$$F'' - 2A'F' - 4A''F - 2\frac{\phi''}{\phi'}F' + 4A'\frac{\phi''}{\phi'}F = e^{2A}\Box F + \frac{2\kappa^2}{3}\left(v'' - \frac{\phi''}{\phi'}v'\right)h. \tag{3.3.45}$$

To find the mass spectrum, we expand both F and h into their Kaluza-Klein (KK) modes by

$$F(x,y) = \sum_n F_n(y)R_n(x), \tag{3.3.46}$$

$$h(x,y) = \sum_n h_n(y)R_n(x), \tag{3.3.47}$$

where each KK mode in the above expansions satisfies $\Box R_n = -m_n^2 R_n$. Using (3.3.42) and

(3.3.45), we write the system of differential equations to determine the mass spectrum as

$$F_n'' - 2A'F_n' - 4A''F_n - 2\frac{\phi''}{\phi'}F_n' + 4A'\frac{\phi''}{\phi'}F_n + e^{2A}m_n^2 F_n = \frac{2\kappa^2}{3}\left(v'' - \frac{\phi''}{\phi'}v'\right)h_n, \tag{3.3.48}$$

$$h_n'' - 4A'h_n' - \left(\frac{\partial^2 V}{\partial v^2} - e^{2A}m_n^2\right)h_n = 6F_n'v' + 4\frac{\partial V}{\partial v}F_n. \tag{3.3.49}$$

This system of differential equations have five integration constants; two from each equation plus the eigenvalue. Two of them are fixed by the boundary condition (3.3.44), which reads

$$h_n' - 2v'F_n = \pm\frac{1}{2}\frac{\partial^2 V_{0,1}}{\partial v^2}h_n, \quad +/- \text{ is for the UV/IR brane.} \tag{3.3.50}$$

In the case of stiff-wall boundary conditions, (3.3.43) sets $\varphi = 0$ on both branes. Then, (3.3.40) implies the relation

$$F_n' - 2A'F_n = \frac{\kappa^2}{3}v'h_n, \quad \text{on the branes.} \tag{3.3.51}$$

The remaining integration constant can be fixed by normalizing both F_n and h_n by a common factor, since the system is invariant under such a scaling.

The rest of this Subsection is devoted to solving this system of equations to zero and leading order in the backreaction. We will assume that κ is small enough so that the background field profiles are accurately expressed by their zero backreaction solutions. We shall investigate the validity of this assumption later.

Mass Spectrum with Backreaction Neglected

First, we will study the mass spectrum in the $\kappa^2 \to 0$ limit. This means that we will search for the mass eigenvalues which remain finite after this limit. We will denote these eigenvalues and their corresponding eigenvector components F_n and h_n by the superscript (0). Then (3.3.48) and (3.3.49) become

$$\left(F_n^{(0)\prime} - 2F_n^{(0)}\right)' - 2\frac{\phi''}{\phi'}\left(F_n^{(0)\prime} - 2F_n^{(0)}\right) + e^{2y}\left(m_n^{(0)}\right)^2 F_n^{(0)} = 0, \tag{3.3.52}$$

$$h_n^{(0)\prime\prime} - 4h_n^{(0)\prime} - \left(\frac{\partial^2 V}{\partial v^2} - e^{2y}\left(m_n^{(0)}\right)^2\right)h_n^{(0)} = 6F_n^{(0)\prime}v' + 4\frac{\partial V}{\partial v}F_n^{(0)}. \tag{3.3.53}$$

The $\mu 5$-component of the Einstein equations (3.3.38) tells us that $F_n^{(0)\prime} - 2F_n^{(0)} \propto \kappa^2$. Then (3.3.52) implies $F_n^{(0)} \propto \kappa^2$ too. Hence, the mass spectrum in the $\kappa^2 \to 0$ limit is given by the differential equation

$$h_n'' - 4h_n' + (m_n^2 e^{2y} - m_H^2)h_n = 0, \tag{3.3.54}$$

with boundary conditions

$$h_n' = \pm\frac{1}{2}\frac{\partial^2 V_{0,1}}{\partial v^2}h_n, \tag{3.3.55}$$

where $+/-$ for UV/IR brane, and we have omitted the superscripts for brevity.

We see that the fluctuations F and h are decoupled from each other in this limit, which is expected since there is no explicit coupling between the GW and the Higgs field. In the absence of backreaction, each field does not know about the existence of the other.

The solution of (3.3.54) is given in terms of Bessel functions:

$$h_n = e^{2y}[J_\nu(m_n e^y) + cY_\nu(m_n e^y)], \tag{3.3.56}$$

where c is a constant which is determined by the UV boundary condition. The mass eigenvalue is fixed by the IR boundary condition. After applying both, we find that the mass spectrum is given by the roots of

$$b_v(m_n) = \tilde{J}^1_\nu(m_n) - \frac{\tilde{J}^0_\nu(m_n)}{\tilde{Y}^0_\nu(m_n)}\tilde{Y}^1_\nu(m_n), \tag{3.3.57}$$

where we defined

$$\tilde{X}^0(m_n) \equiv \left(\frac{\partial^2 V_0}{\partial v^2} - 4\right)X_\nu(m_n) - m_n(X_{\nu-1}(m_n) - X_{\nu+1}(m_n)), \tag{3.3.58}$$

$$\tilde{X}^1(m_n) \equiv \left(\frac{\partial^2 V_1}{\partial v^2} + 4\right)X_\nu(m_n) + m_n e^{y_1}(X_{\nu-1}(m_n e^{y_1}) - X_{\nu+1}(m_n e^{y_1})), \tag{3.3.59}$$

with $X = \{J, Y\}$. The Higgs mass is the smallest m_n which satisfy $b_v(m_n) = 0$.

The Higgs sector of the model is specified by five parameters; m_0^2, m_1^2, λ_H, ν and f. Two of them can be fixed in terms of the others, by setting the effective Higgs VEV (3.3.26) and the Higgs mass to 246 GeV and 126 GeV respectively. We have chosen to keep m_0^2, ν and f free, and calculate m_1^2 and λ_H in terms of the rest. We show the results in Figure 3.4. One can see that a fair amount of tuning is needed in the IR brane mass parameter of the Higgs. One might get the impression that the tuning is less severe when we lower the ν parameter, or increase the hierarchy between the electroweak and conformal breaking scales. But in that

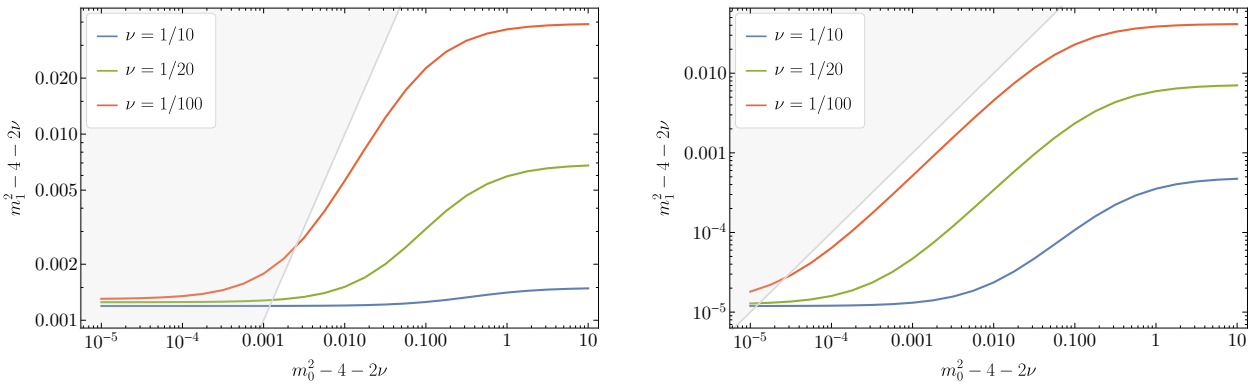

Figure 3.4: In this figure, we are plotting the necessary value of m_1^2 in order to get $v_{\rm EW} = 246$ GeV and $m_h = 126$ GeV, as a function of m_0^2. The hierarchy between the electroweak and the conformal breaking scale is $f/v_{\rm EW} = 10$ and $f/v_{\rm EW} = 100$ for the left and right plot respectively. In the shaded region, there is no "critical region", i.e. the electroweak symmetry is broken, even if the IR brane is very close to the UV brane.

case, the tuning between the GW and the Higgs sector does increase, as we shall see shortly.

Since the GW contribution dominates the effective potential, the minimum is mainly determined by the GW sector. Therefore, one can choose a particular value for the IR mistune δT_1, such that the minimum coincides with $y_1^{\rm c}$, as long as (3.3.33) is satisfied. We denote this "critical" mistune by δT_1^c. Then, a convenient parameter to measure the tuning between the GW and the Higgs sector is $|\delta T_1/\delta T_1^c| - 1$.

In Figure 3.5, we show the required tuning on the parameter space where the electroweak symmetry breaking is activated by the radion. The procedure to obtain these plots is as follows: We have set the GW sector parameters to be $v_0 = 1/50$, $v_1 = 1$ and $\epsilon = 1/10$. Then we set the conformal breaking scale to be $f = 10(50)$ TeV for the left(right) plot. For each point on the $\alpha_0 - \alpha_1$ plane, we fix the Higgs parameters such that $v_{\rm eff} = 246$ GeV and $m_h = 126$ GeV. Finally, we solve for δT_1 such that $V_{\rm eff}^{\rm IR} = 0$.

Different points in Figure 3.5 which share the same $\alpha_0 = m_0^2 - 4 - 2\nu$ values are obtained by varying ν. For a fixed α_0, larger ν values correspond to larger $\alpha_1 = m_1^2 - 4 - 2\nu$, thus

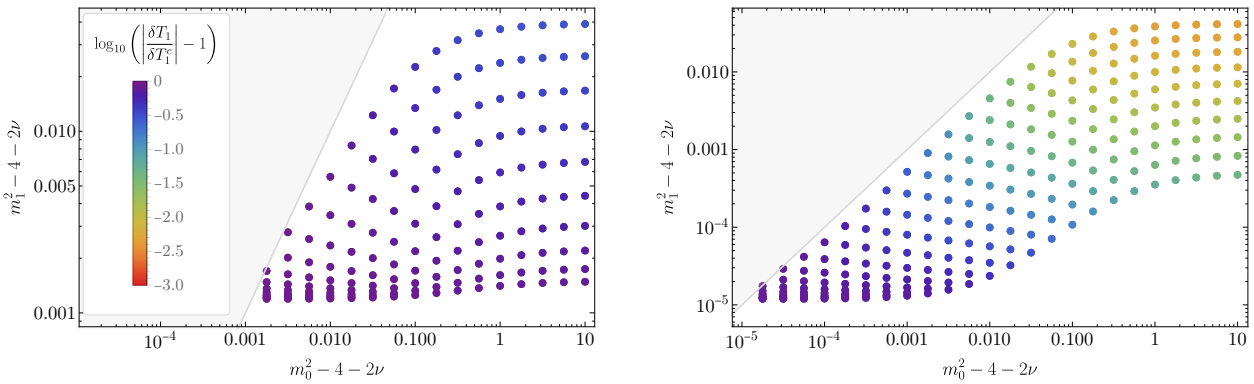

Figure 3.5: These plots show the amount of tuning required between the Higgs and the GW sector when the breaking scale is set to $f = 10$ TeV (left figure) and $f = 50$ TeV (right figure). Different points which have the same α_0 value are obtained by varying ν which is decreasing as one goes up on the vertical axis. We can observe that the tuning increases as we go the the top-right region of the $\alpha_0 - \alpha_1$ plane. Also increasing the breaking scale increases the tuning, which is expected.

ν increases as one goes up on the vertical axis. As one can see more clearly in the plot on the right, tuning between the GW and the Higgs sectors does also increase in this direction. Therefore, as one relaxes the tuning in the m_1^2 parameter, the tuning in δT_1 becomes larger.

The Radion Mass

To calculate the radion mass, we make the following ansatz for the radion wavefunction, and the radion mass eigenvalue:

$$F_r = e^{2A}\left(1 + \kappa^2 \tilde{F}_r\right) \quad \text{and} \quad m_r^2 = \kappa^2 l_r^2. \tag{3.3.60}$$

By plugging this ansatz into (3.3.45), and keeping only the terms which are at leading order in κ^2 we find

$$\tilde{F}_r'' + \tilde{F}_r'\left(2 - 2\frac{\phi''}{\phi'}\right) = \frac{2}{3}\left[(\phi'^2 + v'^2) + \left(v'' - \frac{\phi''}{\phi'}v'\right)h_r e^{-2y}\right] - e^{2y} l_r^2. \tag{3.3.61}$$

The solution of this equation is

$$\tilde{F}_r'(y) = \frac{1}{u(y)}\left[\frac{2}{3}\int_0^y \mathrm{d}y'\, u(y')(\phi'^2 + g_v(y')) - l_r^2 \int_0^y \mathrm{d}y'\, u(y')e^{2y} + \tilde{F}_r'(0)\right], \tag{3.3.62}$$

where

$$u(y) = \exp\left\{\int_0^y \mathrm{d}y' \left(2 - 2\frac{\phi''}{\phi'}\right)\right\} \quad \text{and} \quad g_v(y) = v'^2 + \left(v'' - \frac{\phi''}{\phi'}v'\right)h_r e^{-2y}. \tag{3.3.63}$$

The function $u(y)$ can be obtained analytically:

$$u(y) = \left(\frac{\phi'(0)}{\phi'(y)}\right)^2 e^{2y}. \tag{3.3.64}$$

By plugging this result into (3.3.62) and evaluating it at $y = y_1$, we can write an expression for the radion mass:

$$\frac{l_r^2}{f^2} = \left(\int_0^{y_1} \mathrm{d}y\, \frac{e^{4(y-y_1)}}{\phi'(y)^2}\right)^{-1}\left[\frac{1}{3} + \frac{2}{3}\int_0^{y_1} \mathrm{d}y\, \frac{g_v(y)}{\phi'^2}e^{2(y-y_1)} + \left(\frac{\tilde{F}'(0)e^{-2y_1}}{\phi'(0)^2} - \frac{\tilde{F}'(y_1)}{\phi'(y_1)^2}\right)\right], \tag{3.3.65}$$

where we have dropped the e^{-2y_1} term after evaluating the integral $\int_0^{y_1} \mathrm{d}y\, e^{2(y-y_1)}$. The boundary values for $\tilde{F}_r'$ can be expressed in terms of the boundary values for h_r using the junction conditions given in (3.3.40). Since $\varphi = 0$ on the branes in the case of stiff wall boundary conditions, these give

$$\tilde{F}_r' = \frac{1}{3}v' h_r e^{-2y}, \quad \text{on the branes.} \tag{3.3.66}$$

Plugging this result into (3.3.65) gives

$$\frac{l_r^2}{f^2} = \left(\int_0^{y_1} \mathrm{d}y\, \frac{e^{4(y-y_1)}}{\phi'^2}\right)^{-1} \left[\frac{1}{3} + \frac{2}{3}\int_0^{y_1} \mathrm{d}y\, \frac{g_v(y)}{\phi'^2} e^{2(y-y_1)} + \frac{1}{3}\left(\frac{v'(0)h_r(0)}{\phi'(0)^2} - \frac{v'(y_1)h_r(y_1)}{\phi'(y_1)^2}\right)e^{-2y_1}\right]. \tag{3.3.67}$$

The first term in this expression is the radion mass in the absence of the Higgs VEV, which can be calculated analytically. Ignoring the terms which are proportional to e^{-2y_1} and higher, it is given by

$$\frac{l_{r,0}^2}{f^2} \equiv \frac{1}{3}\left(\int_0^{y_1} \mathrm{d}y\, \frac{e^{4(y-y_1)}}{\phi'^2}\right)^{-1} = \frac{4}{3}\epsilon(2-\epsilon)^2 v_0^2 e^{\epsilon y_1}\left[\frac{(v_1/v_0)(4-\epsilon)}{4-2\epsilon} - e^{\epsilon y_1}\right]. \tag{3.3.68}$$

We note that this result confirms the stability condition we have derived in (3.3.33).

In the case of nonzero Higgs VEV, the radion mass receives contributions due to its mixing with the Higgs, which are given by the remaining terms in (3.3.67). To calculate them, all we need is the profile for the field h_r. It can be obtained by solving (3.3.42) together with the boundary condition (3.3.44) in the small backreaction limit. By using the ansatz (3.3.60), the equation of motion and the boundary condition for $\tilde{h}_r \equiv h_r e^{-2y}$ are given respectively by

$$\tilde{h}_r'' - \nu^2 \tilde{h}_r = 4[3v' + (-4+\nu^2)v] = 4(v'' - v'), \tag{3.3.69}$$

and

$$(\tilde{h}_r' + 2\tilde{h}_r) - 2v' = \pm\frac{1}{2}\frac{\partial^2 V_{0,1}}{\partial v^2}\tilde{h}_r, \quad +/- \text{ on the UV/IR brane.} \tag{3.3.70}$$

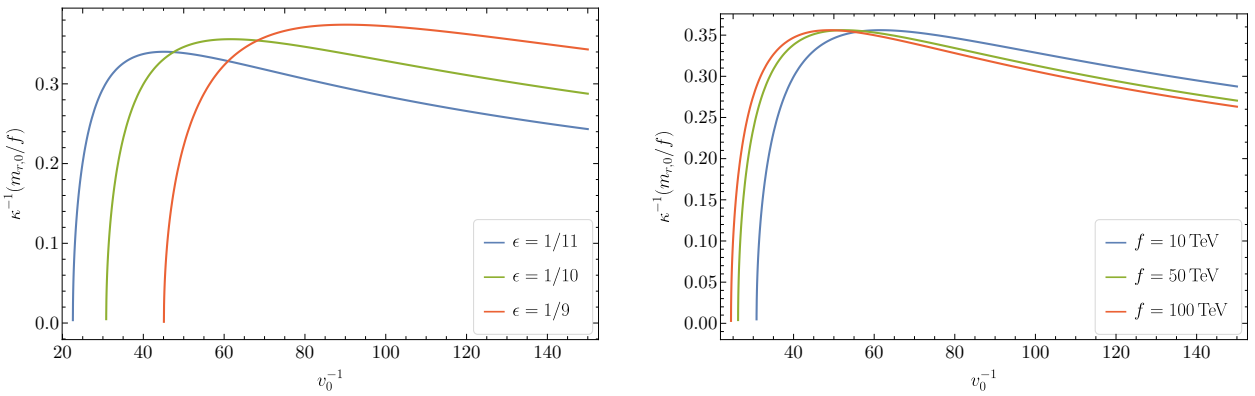

Figure 3.6: In these plots, we show the values of the radion mass rescaled with the breaking scale f and backreaction parameter κ. In both plots, we fix $v_1 = 1$ and vary v_0. On the left figure, we fix the breaking scale to $f = 10\,\text{TeV}$ and plot for various values of ϵ. On the right figure, we fix $\epsilon = 1/10$ and plot for various values of the breaking scale.

This equation can be solved exactly, and its solution can be plugged into (3.3.67) to determine the correction to the radion mass due to Higgs-Radion mixing. The expression for the correction is fairly complicated, but it can be easily seen that it scales with $v^2(y_1) \sim v_{\text{eff}}^2/f^2$, so they are heavily suppressed compared to the leading term inside the brackets of (3.3.67). Hence we conclude that, for the parameter space we are interested in, the radion mass is given by (3.3.68) to a very good approximation. We are showing the radion mass as a function of GW parameters in Figure 3.6.

The Validity of Small Backreaction

At the beginning of this Subsection, we have ignored the backreaction of gravity when obtaining the solutions for the VEVs of both field, and we have used those solutions to calculate the mass spectrum. Now, we shall check the validity of this approximation.

In this model, the field profiles in the bulk have different scales. While the GW field starts with $\mathcal{O}(0.01)$ and ends with $\mathcal{O}(1)$, the Higgs field scales as $\sim v(y_1)e^{-2y_1}$ and $\sim v(y_1)$ near the UV and IR branes respectively. Therefore, the backreaction of the GW field on the

Higgs profile can be sizable, due to the fact that the GW field heavily dominates throughout the bulk. Hence, we should analyze the backreaction carefully, and determine the largest value of κ, so that the results we have derived so far remain valid.

In order to study the backreaction, we need to use the general form of the equation of motion which is given by (3.2.7). The function $A'(y)$ is given by (3.2.3), which for this model reads

$$A' = \sqrt{1 + \frac{\kappa^2}{12}[\phi'^2 + v'^2 - \epsilon(\epsilon-4)\phi^2 - (-4+\nu^2)v^2]}. \tag{3.3.71}$$

We are only interested in the backreaction of the GW field to leading order. Therefore we approximate A' as

$$A' \approx 1 + \frac{\kappa^2}{24}\Big(\phi'^2 - \epsilon(\epsilon-4)\phi^2\Big). \tag{3.3.72}$$

This function peaks on the IR brane, thus we can use its IR value to determine the strength of the backreaction. Hence we estimate the size of the corrections as

$$\frac{\kappa^2}{24}\Big(\phi'^2(y_1) - \epsilon(\epsilon-4)\phi^2(y_1)\Big) \approx \frac{\kappa^2}{24} \times \mathcal{O}(1), \tag{3.3.73}$$

Although this number seems quite small, it has a significant effect on the Higgs VEV as we shall see below.

The Higgs VEV on the IR brane is determined by the IR boundary condition for the

Higgs, which can be rearranged to have the form

$$\frac{v^2(y_1)}{v_H^2} = 1 - \frac{2}{\lambda_H v_H^2}\frac{v'(y_1)}{v(y_1)}. \tag{3.3.74}$$

The Higgs parameters we have used in this Subsection typically have $\lambda_H^{-1} \approx 17$ and $m_1^2 \approx 4$ to satisfy $v_{\rm EW} = 246\,{\rm GeV}$ and $m_h = 126\,{\rm GeV}$. This sets $v_H^2 = \lambda_H^{-1} m_1^2 \approx 68$. So the number on the LHS of (3.3.74) is very small. Therefore, a delicate cancellation between two $\mathcal{O}(1)$ parameters is needed. This equation encodes the tuning required to get a Higgs VEV that is suppressed compared with the KK scale. For a fixed set of 5D parameters, Equation (3.3.74) effectively gives the Higgs VEV as a function of y_1, which is the position of the IR brane that minimizes the effective potential. One can alternatively see that there is a large sensitivity to 5D parameters. For example, by increasing the value of the 5D Newton constant, κ^2 even slightly, one finds that the Higgs VEV will change significantly because of the sensitivity of the cancellation to small changes.

To see explicitly how large the backreaction parameter κ can be, let us assume that we want to know $v^2(y_1)$ to a 10% accuracy. Then a rough upper bound for κ can be given by

$$\frac{\kappa^2}{24}\Big(\phi'^2(y_1) - \epsilon(\epsilon-4)\phi^2(y_1)\Big) \lesssim 0.1 \times \frac{v^2(y_1)}{v_H^2}. \tag{3.3.75}$$

For a hierarchy $f/v_{\rm eff} \sim 10$, we get $\kappa \lesssim \mathcal{O}(1) \times 10^{-3}$.

In the next Subsection, we will study the same model but without the GW field. Then the only source of the backreaction is due to the Higgs field itself. In that case, we need to

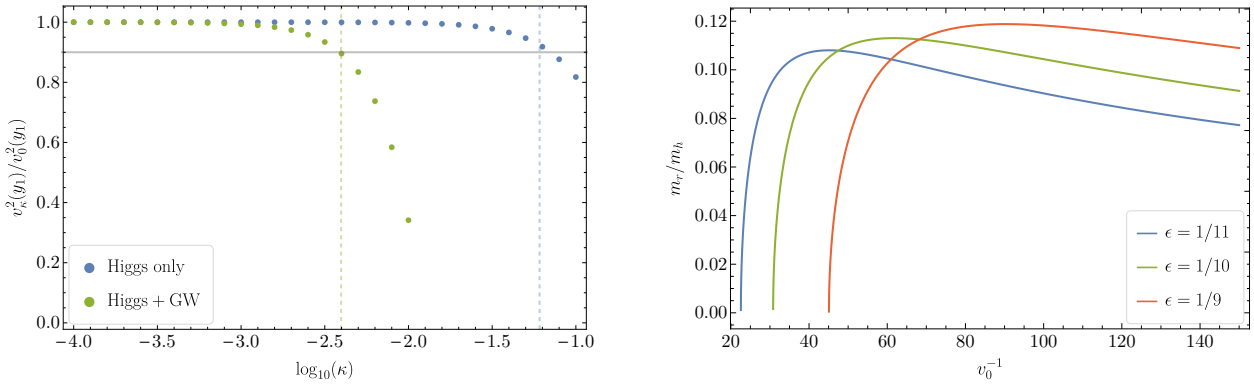

Figure 3.7: On the left figure, we show the ratio between $v^2(y_1)$ obtained by solving (3.2.7) numerically with nonzero backreaction, and the analytical result (3.3.20) obtained by neglecting the backreaction. The green dots show the results for the model of this Subsection, where both GW and the Higgs are in the bulk, while the blue dots are the results for the model of the next Subsection, where only the Higgs is in the bulk. The green and blue dashed vertical lines show the upper bound estimates for κ calculated via (3.3.75) and (3.3.76) respectively. The gray line corresponds to a ratio of 0.9 which we have assumed in our estimates. On the right figure, we plot the Radion-Higgs mass ratio for $\kappa = 4 \times 10^{-3}$. The parameters for these plots are $v_0 = 1/50$, $v_1 = 1$, $\epsilon = 1/10$, $f = 10\,\text{TeV}$, $m_0^2 = 43/10$, $\nu = 1/10$ unless otherwise specified. The remaining free parameters are fixed such that $v_{\text{EW}} = 246\,\text{GeV}$ and $m_h = 126\,\text{GeV}$.

replace the GW field in the above expression by the Higgs field:

$$\frac{\kappa^2}{24}\Big(v'^2(y_1) - (-4+\nu^2)v^2(y_1)\Big) \lesssim 0.1 \times \frac{v^2(y_1)}{v_H^2}. \tag{3.3.76}$$

The term inside the parentheses on the LHS is $\sim 8v^2(y_1)$, thus the bound on κ in this model is given by

$$\kappa \lesssim \sqrt{0.1 \times \frac{3}{v_H^2}} \sim \mathcal{O}(1) \times 10^{-2}. \tag{3.3.77}$$

On the left plot of Figure 3.7, we show the ratio $v_\kappa^2(y_1)/v_0^2(y_1)$ as a function of κ, where $v_\kappa^2(y_1)$ is the Higgs VEV square on the IR brane found by numerically solving (3.2.7) with nonzero backreaction, and $v_0^2(y_1)$ is the analytical result with no backreaction given in

(3.3.20). The green and blue dots show the results for models of this and the next Subsection respectively. The green and blue dashed vertical lines denote the bounds calculated via (3.3.75) and (3.3.76) respectively, while the gray line shows the $v_\kappa^2(y_1)/v_0^2(y_1)$ ratio of 0.9, which we have used in our estimates. We can see that the backreaction has a much bigger effect when both GW and the Higgs are in the bulk, and our estimates agree with the numerical results quite well.

On the right plot of Figure 3.7, we show the Radion-Higgs mass ratio by assuming $\kappa = 4 \times 10^{-3}$. We see that, if we insist on staying in the regime where the backreaction can be neglected, then the radion mass is about an order of magnitude smaller than the Higgs mass. The radion can be made heavier by increasing the backreaction, but one needs a full numerical analysis of the mass spectrum, which is beyond the scope of this work.

3.3.3 Higgs in the Bulk

In this Subsection, we will study a model where the Higgs is the only stabilizing field in the bulk. This model has two major differences compared to the one in the previous Subsection where both the Goldberger-Wise and the Higgs fields were propagating in the bulk. First, the parameter space for electroweak symmetry breaking receives another constraint due to the fact that now the Higgs is responsible for radius stabilization. This means that we don't have the freedom of adjusting Goldberger-Wise parameters to get a stable minimum; instead, we demand that the Higgs parameters $\alpha_{0,1}$ and ν satisfy additional conditions which we shall derive below. The second main difference will be the radion mass, which now depends only on the Higgs parameters.

Parameter Space for Electroweak Symmetry Breaking

We will be using the notation introduced in Subsection 3.3.2 and assume $\alpha_0 > 0$ so that (3.3.24) is positive definite. From (3.3.22), we can write the effective potential everywhere as

$$V_{\text{eff}}(y_1) = \begin{cases} e^{-4y_1}\delta T_1, & \text{No EWSB} \\ e^{-4y_1}\left[\delta T_1 - \frac{\lambda_H}{4}v^4(y_1)\right], & \text{EWSB,} \end{cases} \tag{3.3.78}$$

where we have tuned $\delta T_0 = 0$. By taking the derivative and setting it to zero, we find that at an extremum point $y_1 = y_1^{\text{ext}}$, the IR brane mistune is given by

$$\delta T_1^{\text{ext}} = \frac{\lambda_H}{8}v^2(y_1^{\text{ext}})\left[2v^2(y_1^{\text{ext}}) - \frac{\partial v^2(y_1)}{\partial y_1}\bigg|_{y_1=y_1^{\text{ext}}}\right]. \tag{3.3.79}$$

In order to not have a runaway solution in the UV, i.e. to have a global minimum, we demand that this term is positive. Then the second derivative of V_{eff} at $y_1 = y_1^{\text{ext}}$, where δT_1 is replaced by δT_1^{ext} is given by

$$V''_{\text{eff}}(y_1^{\text{ext}}) = e^{-4y_1}\frac{\lambda_H}{2}\left[v^2(y_1)\left(4\frac{\partial v^2(y_1)}{\partial y_1} - \frac{\partial^2 v^2(y_1)}{\partial y_1^2}\right) - \left(\frac{\partial v^2(y_1)}{\partial y_1}\right)^2\right]\bigg|_{y_1=y_1^{\text{ext}}}. \tag{3.3.80}$$

By using explicit expression for $v^2(y_1)$, it is possible to show that $\delta T_1^{\text{ext}} > 0$ implies $V''_{\text{eff}}(y_1^{\text{ext}}) > 0$, so we can use the former. Then we obtain the following constraint on the parameter α_1:

$$\alpha_1 > \frac{4\alpha_0\nu[(1+\nu)(\alpha_0+4\nu)e^{2\nu y_1} - \alpha_0]}{[(e^{2\nu y_1}-1)\alpha_0 + 4\nu e^{2\nu y_1}]^2}\bigg|_{y_1=y_1^{\text{ext}}}. \tag{3.3.81}$$

We are showing the effect of this constraint on the Higgs parameter space in Figure 3.8. In

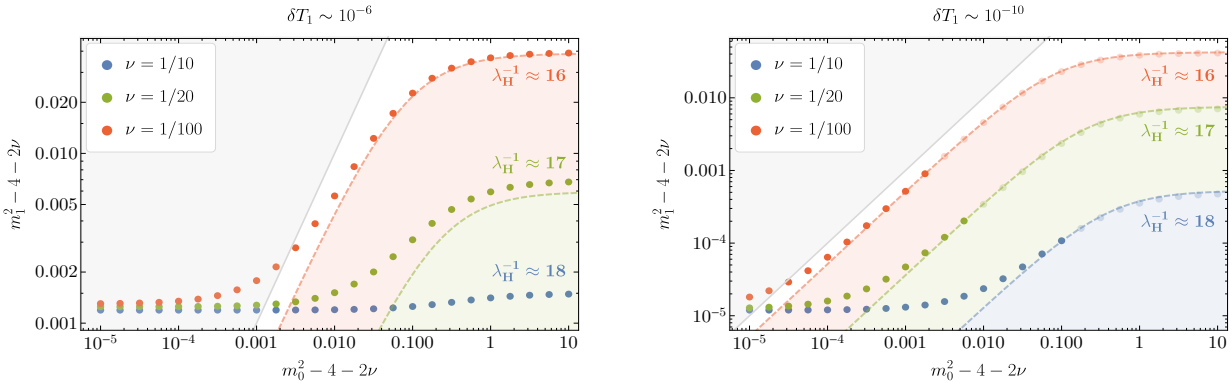

Figure 3.8: In this figure, the circles denotes possible $\{\alpha_0, \alpha_1\}$ pairs characterized by $v_{\rm EW} = 246\,\text{GeV}$ and $m_h = 126\,\text{GeV}$. The hierarchy between the electroweak and the conformal breaking scales is $f/v_{\rm EW} = 10$ and $f/v_{\rm EW} = 100$ for the left and right plot respectively. The gray shaded area denotes the region in parameter space where there is no "critical" value of y_1. The color shaded areas are the regions where the condition for global minimum (3.3.81) is violated. To improve clarity, we are showing the $\{\alpha_0, \alpha_1\}$ pairs corresponding to these regions with semi-transparent circles.

these plots, we are plotting m_1^2 in terms of m_0^2 such that the electroweak scale is $v_{\rm EW} = 246\,\text{GeV}$ and the Higgs mass is $m_h = 126\,\text{GeV}$. The methods and the equations for determining m_1^2 are identical to the Goldberger-Wise and Higgs model studied in the previous Subsection. The semi-transparent circles correspond to the points where the constraint (3.3.81) is not satisfied, hence those points should be excluded from the parameter space. We can see that the constraint becomes more stringent as one decreases ν and increases the breaking scale f.

The Radion Mass

The radion mass can be calculated by following the procedure described in Subsection 3.3.2. For this model we find

$$\frac{l_r^2}{f^2} = \frac{1}{3}\left(\int_0^{y_1} \mathrm{d}y\, \frac{e^{4(y-y_1)}}{v'(y)^2}\right)^{-1}\left[1 - \frac{\tilde{h}_r(y_1)}{v'(y_1)} + \frac{\tilde{h}_r(0)}{v'(0)}e^{-2y_1}\right], \tag{3.3.82}$$

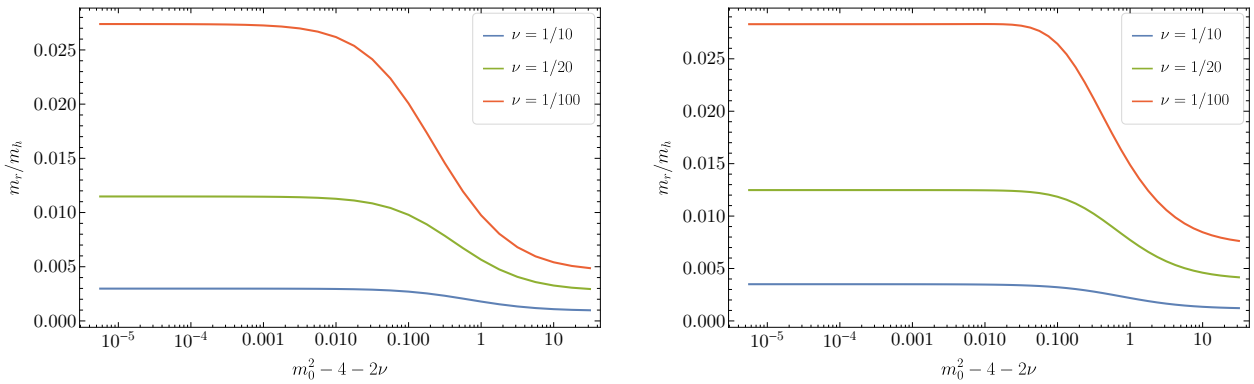

Figure 3.9: In this figure, we are plotting the ratio between the radion mass and the Higgs mass as a function of α_0 by assuming $\kappa = 6 \times 10^{-2}$. The breaking scale is $f = 10\,\text{TeV}$ and $f = 50\,\text{TeV}$ on the left and right figure respectively. The Higgs parameters are fixed such that $v_{\text{EW}} = 246\,\text{GeV}$ and $m_h = 126\,\text{GeV}$.

where $\tilde{h}_r$ is the solution to equations (3.3.69) and (3.3.70). Again, the full solution is analytical, but fairly complicated. Nevertheless, we can get a good insight by calculating the factor which multiplies the term inside the brackets. It is given by

$$I \equiv \frac{1}{3}\left(\int_0^{y_1} \mathrm{d}y\, \frac{e^{4(y-y_1)}}{v'(y)^2}\right)^{-1} = \frac{4v^2(y_1)m_0^2\nu^2 e^{-2\nu y_1}}{3(e^{2\nu y_1}-1)(m_0^2-4+2\nu)}\left[\frac{e^{2\nu y_1}(2+\nu)-r(2-\nu)}{(1-re^{-2\nu y_1})^2}\right], \quad (3.3.83)$$

where $r = \frac{m_0^2-4-2\nu}{m_0^2-4+2\nu}$. We find that the term inside the brackets varies between 1.0 and 1.4 in the parameter space we are using. We show the results of the Radion-Higgs mass ratio in Figure 3.9 as a function of $\alpha_0 = m_0^2 - 4 - 2\nu$, under the assumption that $\kappa = 6 \times 10^{-2}$. To make the plots we have used the full analytical result given in (3.3.82). We can see that in this model, the radion is two to three orders of magnitude lighter than the Higgs. Since the effect of the backreaction is not as significant as in the previous model, we expect that a significantly light radion is a property of this model, even with backreaction.[5]

It might seem surprising that decreasing ν increases the radion mass. To understand the

[5]Note that radion masses at the GeV scale and above are still largely unconstrained by the latest experimental results, as shown by the detailed analysis of [68].

effect of this parameter, it is useful to study the quantity I in detail. Since $f \sim \mathcal{O}(10\,\text{TeV})$, we have $y_1 \sim \mathcal{O}(30)$. Choosing $\nu \approx 1/10$ implies $e^{2\nu y_1} \sim \mathcal{O}(1000)$ hence we can assume $e^{2\nu y_1} \gg 1$. In this approximation, I becomes

$$I \approx \frac{4}{3} v^2(y_1) \frac{m_0^2(2+\nu)\nu^2}{m_0^2 - 4 + 2\nu} e^{-2\nu y_1}, \quad e^{2\nu y_1} \gg 1. \tag{3.3.84}$$

In this regime, the radion mass is heavily suppressed by $e^{-2\nu y_1}$, which is $\mathcal{O}(10^{-3})$, in addition to suppression by $v^2(y_1)$ and ν^2. On the other hand, if $\nu \sim 1/100$, then $e^{2\nu y_1} \sim \mathcal{O}(1)$. In this case, we can evaluate I at the leading order in ν. The result is

$$I \approx \frac{8}{3} v^2(y_1) \frac{m_0^2 \nu^2}{m_0^2 - 4} \frac{e^{2\nu y_1}}{(e^{2\nu y_1} - 1)^2}, \quad \nu \ll 1. \tag{3.3.85}$$

We see that the exponential suppression is absent in this case, hence the radion is heavier in this regime.

3.4 CFT Interpretation

Field theories in AdS admit an interpretation in terms of a 4D strongly coupled CFT (or approximate CFT) dual [26, 69]. In this Section, we discuss a CFT interpretation of multi-scalar stabilization models.

It is useful to first recall the CFT interpretation of the original unstabilized Randall-Sundrum construction [33], and then the simplest stabilization mechanism introduced by Goldberger and Wise [52, 57]. We then discuss the specific interpretation of multi-scalar models with emphasis on those where there are critical points for symmetry breaking in the

moduli space for the radion.

The original 2-brane RS model with weak 5D gravity has an interpretation as a large-N approximate CFT where the conformal symmetry is spontaneously broken. The radion degree of freedom corresponds to the dilaton – the Goldstone boson of spontaneously broken conformal invariance. The classical equations of motion (Einstein's equations) rule out a static geometry unless the UV and IR brane tensions are individually tuned against the bulk cosmological constant. These two tunings represent (respectively) the need to have a vanishing bare cosmological constant so that there is no explicit breaking of conformal invariance, and the vanishing of the dilaton quartic, an allowed coupling that would otherwise destabilize the conformally non-invariant vacuum state. In other words, as is well known [70], spontaneous breaking of exact conformal invariance without breaking Poincaré invariance requires a flat direction.

Even in this case, with both tunings performed (and ignoring quantum effects)[6], the continuum of physically inequivalent vacua (the moduli space of inter-brane separations) present a problem for creating a low energy description that resembles our Standard Model. Thus, a model must incorporate a stabilization mechanism. The simplest such mechanism posits a bulk scalar field that develops a vacuum expectation value, deforming the geometry through gravitational backreaction. If this scalar has an approximate shift symmetry, violated by (for example) a small bulk mass term, its VEV grows slowly, and backreaction effects are sizable only deep into the bulk of AdS. This backreaction leads to an effective potential for the inter-brane separation, and stabilization is achieved dynamically without tuning of the IR

[6] In fact, even with both UV and IR brane tunings performed, quantum corrections will generally lead to a nonzero Casimir potential between the branes.

brane tension (the UV tuning must still be performed, or enforced by additional symmetries to obtain static geometries). The slow growth of the scalar VEV in the UV region of the geometry ensures that the generated hierarchy is exponentially large.

This 5D picture is dual to 4D dimensional transmutation in which a nearly marginal operator (not necessarily classically marginal as is the case for asymptotic freedom) is given a nonzero coupling constant. Its logarithmic evolution breaks conformal invariance explicitly, leading to the dynamical generation of an infrared scale where either the theory has flowed very far away from the UV fixed point [34, 35], or has flowed to a point where the effective dilaton quartic has become small [47, 71].

There is a similar class of 5D models where, in the 4D CFT dual, it is a composite operator that serves as the nearly marginal deformation of the CFT. This occurs in the case where there is a 5D field with mass near the Breitenlohner-Freedman bound, which (in 5D) is $m^2 = -4$ in units of the AdS curvature [25, 48, 72]. The corresponding operator $\mathcal{O}$ in the CFT dual has dimension $\Delta \sim 2$, such that at large N, the composite operator $\mathcal{O}^\dagger\mathcal{O}$ has dimension $\Delta \sim 4$. Thus, turning on this composite operator corresponds at large N to a nearly marginal deformation of the CFT. The model we discuss where only the Higgs is in the bulk is of this form, where it is the Higgs vacuum expectation value that backreacts on the geometry and stabilizes the inter-brane separation.

To understand the CFT interpretation of radion-induced Higgs criticality, it is first necessary to review the interpretation of the UV brane and field dynamics there. In models with a UV brane, the interpretation is that there are two sectors of the theory, a fundamental sector and a CFT sector, and that these sectors mix.

First, we review the basics of the correspondence without the UV brane (or with the UV

brane taken to the boundary of AdS). In this case the correspondence links field configurations on the boundary of AdS (which are not integrated over in the higher dimensional partition function) to sources for a dual CFT:

$$Z_{\mathrm{CFT}}[J(x) = \phi(x, z = 0)] = \int [\mathcal{D}\phi]_{\mathrm{bulk}} \exp[iS(\phi)]. \tag{3.4.1}$$

The CFT with sources could be described by a Lagrangian of the form $\mathcal{L}_{\mathrm{CFT}} = \mathcal{L}^0_{\mathrm{CFT}} + J(x)\mathcal{O}_{\mathrm{CFT}}$.

When the UV brane is introduced, the path integral has no restriction – effectively the sources are promoted to dynamical fields that mix with the CFT, and the new dual 4D Lagrangian is of the form

$$\mathcal{L} = \mathcal{L}_{\mathrm{fundamental}}(\phi(x)) + \mathcal{L}^0_{\mathrm{CFT}} + \lambda\phi(x)\mathcal{O}. \tag{3.4.2}$$

The CFT and fundamental sector mix with each other. Through the mixing, spontaneous breaking of conformal invariance in the CFT sector from VEVs of CFT operators, $\langle\mathcal{O}\rangle$, is communicated to the fundamental sector. The size of these VEVs corresponds in 5D to the position of the IR brane. Integrating out the CFT (or bulk, in the 5D picture) degrees of freedom leads to an effective theory for the fundamental degrees of freedom in which parameters of the EFT, like the Higgs mass squared term, are a function of y_1. This y_1 dependence can be such that the EFT crosses phase boundaries for symmetry breaking transitions as y_1 is varied.

In short, the 5D theory with two branes is dual to a 4D theory where a fundamental

and CFT sector are coupled to each other, and where the CFT is spontaneously broken by operator VEVs. The coupling between the two allows a "CFT-induced criticality", where CFT operator VEVs induce instabilities in the fundamental sector. In 5D, the instabilities leading to non-trivial VEVs are induced by varying the position of the IR brane.

In the case of using this picture as a model for electroweak physics, the effective Higgs mass squared term is, in the 4D picture, a function of CFT operator VEVs. For certain values of these VEVs, the effective mass squared may become negative, and induce electroweak breaking. In 5D, the mass squared of the lowest lying state of the bulk Higgs can become negative for ranges of y_1, such that electroweak symmetry breaking is induced by the radion VEV.

3.5 Conclusions

We have explored radius stabilization in the context of 5D models in warped space with multiple scalar fields. General results for multi-scalar models are derived to all orders in backreaction for 5D Einstein-Hilbert gravity. We suggest a holography-inspired approach to the multi-scalar potential, and additionally derive a superpotential method for creating static geometries with multiple bulk scalar fields.

Of particular interest given recent experimental results are the phenomenological implications of Higgs fine tuning. We explored 5D models focusing on obtaining a hierarchy between extra-dimensional excitations and the electroweak symmetry breaking scale. 5D models with such a hierarchy are close to the critical point for the electroweak sector, and thus, generically, the radion will be a dynamical degree of freedom that scans the Higgs phase transition.

Three examples were presented where the radion scans the effective Higgs mass parameter across a symmetry breaking phase transition:

- A model with the Higgs on the IR brane, where a bulk Goldberger-Wise scalar couples to the Higgs and scans its effective mass.
- A model with only a Higgs field in the bulk, where coupling to the radion arises through geometrical backreaction.
- A model with both Higgs and a Goldberger-Wise scalar in the bulk.

These three models cover a range of types of modulus-Higgs potential that give a hierarchy between extra-dimensional resonances and the electroweak scale.

The models presented are an important step in understanding electroweak symmetry breaking in the context of holographic composite Higgs models, particularly those where the Higgs is light in comparison to the compositeness scale. An important message is that the tuning of the Higgs itself has implications in terms of cosmology and collider phenomenology through the manner of the Randall-Sundrum/electroweak early universe physics and the low lying spectrum of scalar states.

The formalism we have developed for multi-scalar stabilization models is relevant for all theories in which the Higgs emerges as a mode that is light in comparison with the compactification scale. In general, the Higgs plays a non-trivial part in stabilization, and this work helps further elucidate the connection between the compactification scale and that of electroweak physics.

Chapter 4

Anomaly Inflow and Holography

4.1 Introduction

Fermion anomalies have played an important role in a plethora of different aspects in theoretical physics. The discovery of the one-loop triangle anomaly of Adler, Bell, and Jackiw (ABJ) [73, 74] taught us that fermion anomalies not only have direct implications on observable phenomena such as $\pi^0 \to \gamma\gamma$, but also provide strong constraints on consistent quantum field theories. That chiral anomalies do not receive any renormalization beyond one-loop (Adler-Bardeen theorem [75], see also [76] for a review) was then beautifully realized in 't Hooft anomaly matching argument [77] showing that fermion anomalies can yield non-trivial consequences in the spectrum of the infrared (IR) phase of the confining gauge theory. Applications of anomaly matching (together with other sets of techniques) resulted in tremendous success in uncovering phases and dualities of supersymmetric gauge theories [78–80]. In theories with spontaneously broken global symmetries, the chiral anomalies of the ultraviolet (UV) phase of the theory are maintained in the IR by the (gauged) Wess-

Zumino-Witten (WZW) action [81, 82]. This also led to an elegant resolution of the puzzle of CP-violation, e.g. $K^+K^- \to \pi^+\pi^-\pi^0$, which is absent in any order in chiral perturbation theory [82]. In string theory, the requirement of anomaly cancellation was crucial in arriving at the conclusion that for any supersymmetric theory in 10D with gravity and gauge supermultiplets, the only allowed gauge groups are $SO(32)$ or $E_8 \times E_8$ [83, 84].

Fermion anomalies in spacetime dimension $D = 2n$ often find their natural description from a higher-dimensional setup. Notably, the form of chiral anomalies compatible with the Wess-Zumino consistency condition [81] can be constructed by starting from an Abelian anomaly in $2n + 2$ dimensions and subsequently arriving at (non-Abelian) anomalies in $2n$ dimensions via the descent equations [85–89] (see also [17, 90]). As an intermediate step of the descent formalism, one finds that the relevant quantity in $2n + 1$ dimensions is the Chern-Simons (CS) action.

A deeper physical insight of the descent procedure was then realized by the idea of *anomaly inflow* originally discovered in [91]. In its perturbative version, the bulk CS theory is not gauge-invariant when the theory is defined on a manifold with boundary. This variance is then cancelled by fermions localized on the boundary, making the overall bulk plus boundary theory consistent. A non-perturbative version of the anomaly inflow was discussed in [92, 93] in the context of topological phases of matter, and its full justifications were presented recently in [94] (see also [95]). Many condensed matter systems that exhibit non-trivial topological phases can be described by and hence are the physical realizations of anomaly inflow [92]. One of the first example of topological phases of matter is the integer quantum Hall effect [96], which admits a description in terms of $U(1)$ CS theory in the $(2 + 1)$D bulk

of the material [95, 97]:

$$S \sim \kappa \int A \wedge F, \quad \kappa \in \mathbb{Z}. \tag{4.1.1}$$

This is not gauge-invariant if the material has a physical boundary, and the resulting variance coincides with the first Chern class $\propto \int \frac{i}{2\pi} F$. This contribution is cancelled by the chiral anomaly of localized fermions on the $(1+1)$D boundary charged under $U(1)$ (called "edge modes"). The combined system of bulk + boundary is anomaly-free and the quantized Hall conductance is proportional to κ.

In the language of anomaly inflow, 11D M-theory can also be thought of as being "topological matter". In the bulk of 11D spacetime, the 3-form superpartner of the metric field C (with 4-form field strength $G = dC$) has the coupling

$$S \sim \int_{11\text{D}} C \wedge G \wedge G, \tag{4.1.2}$$

and again this is not invariant in the presence of the boundary. The anomaly inflow is then completed by the introduction of "edge modes" which in this case are shown to be a 10D E_8 gauge supermultiplet [98, 99].

For completeness, we also mention that there have been many works with regard to anomalies in orbifold field theories, see for example [100–106]. Anomalies in orbifold gauge theories have a "shape" independent of extra-dimensional profiles and are localized on the boundaries. It may be instructive to recall the form of the anomaly in a theory with $S^1/(\mathbb{Z}_2 \times \mathbb{Z}_2')$ orbifold. Consider a $U(1)$ gauge theory with bulk fermions with boundary conditions (BC) denoted as (α_0, α_1), where $\alpha_i = \pm$ for $i = 0(1)$ means Neumann $(+)$ or

Dirichlet $(-)$ BC for the left-handed Weyl component of the 5D spinor at the UV (IR) boundary brane. For instance, $(+,+)$ gives rise to a left-handed zero mode, while the choice $(-,-)$ results in a right-handed zero-mode. Other choices do not lead to any zero mode. In this notation, the anomaly of a bulk fermion is given by [106]

$$\mathcal{A}(x,z) = \left(\frac{Q^3}{48\pi^2} F_{\mu\nu}\tilde{F}^{\mu\nu}\right)\frac{1}{2}[\alpha_0\delta(z-z_0) + \alpha_1\delta(z-z_1)]. \tag{4.1.3}$$

Here, the expression in parenthesis is the 4D $U(1)$ chiral anomaly with charge Q. The corresponding 5D anomaly is split between UV and IR boundaries with equal size, and the sign is determined by the BC. From this, one sees that for $(+,+)$ or $(-,-)$ (like in the case of a $S^2/\mathbb{Z}_2$ orbifold), the anomaly function integrated over the extra dimension does not vanish. Such an anomaly in the orbifold theory is often referred to as a "globally non-vanishing" anomaly, and it arises from the zero mode. In this case, the cancellation of 4D anomalies is sufficient to render the full 5D theory consistent [100]. For other choices of BC such as $(+,-)$ or $(-,+)$, however, the 5D anomaly function integrates to zero and is denoted as "globally vanishing" anomaly. Importantly, in this case, 4D anomaly cancellation is not enough, and in fact, there is no anomaly in the 4D effective field theory (EFT) [101, 106]. While the 4D EFT is free of anomaly, the 5D theory nonetheless has localized anomalies. These anomalies may be cancelled by localized fermions, or localized higher-dimensional Wess-Zumino counter terms [106]. Sometimes, they are cancelled by bulk Green-Schwarz mechanisms [102, 103]. In some cases, anomaly inflow by the bulk CS action can restore consistency of the theory. In this sense, anomalies in orbifold gauge theories are certainly related to anomaly inflow, but the two are not equivalent.

In this paper, we study in detail the physics of anomaly inflow in AdS_5, and in particular obtain its holographic dual interpretations in terms of strongly coupled 4D (deformed) CFT. Of course, this can be equally phrased as a study of the AdS/CFT duality of a bulk CS theory. Yet another equivalent characterization, by now completely redundant, is the bulk AdS description corresponding to the anomaly of 4D CFT. We find our analysis has several important motivations. First off, ever since its first discovery [91], interest in anomaly inflow was revived and has increased recently both in the condensed matter theory and high energy theory communities, also thanks to the powerful machinery of the Dai-Freed theorem [107] and generalized symmetries [108]. See for instance [92, 93] for the exposition of the subject written in a high energy theorist's language. Many surprising results are revealed by thorough explorations of anomaly inflow using modern techniques. While the anomaly inflow itself is largely insensitive to the specific form of the metric, the choice of AdS_5 for the bulk metric nevertheless has a nice advantage. Namely, in this case, in addition to the standard features of anomaly inflow, i.e. cancellation of "problems" between the bulk and boundary physics, an additional description emerges. That is, the combination of bulk + boundary can be interpreted as a unified description in terms of holographic 4D field theory. The dual 4D CFT consists of a strongly interacting CFT and external degrees of freedom, and the physics of anomaly inflow is dual to the interplay between these two sectors which results in a shared anomaly. As such, understanding holographic aspects of anomaly inflow seems well-justified. Of course, CS theory in the context of AdS/CFT and its implications in terms of anomaly in $SU(4)$ R-symmetry current were discussed in [69]. Subsequently, AdS/CFT of trace and chiral anomaly were studied for example in [109–114]. To our knowledge, however, a systematic study of holography for anomaly inflow, especially for non-supersymmetric theories which are

more relevant in particle physics model building and phenomenology, are much less explored (see however [106, 115, 116]). Moreover, we found the introduction of UV and IR boundaries (branes) to lead to a remarkably rich description in the context of AdS/CFT. For one, most of particle physics models in AdS_5 were constructed with both UV and IR branes [33] or even with additional branes [117], and understanding the holographic version of anomaly inflow in a similar setup can provide more straightforward applications in particle physics. On a more theoretical side, anomaly inflow in AdS/CFT has been studied much less in the presence of UV and IR branes, and nevertheless we would like to emphasize that they provide excellent theoretical "tools", leading to a much richer story for anomaly inflow. Namely, with Neumann BC, the UV brane allows to introduce the concept of "weakly gauging" of the global symmetry of the 4D CFT, resulting in "dynamical" source fields. On the other hand, the IR brane makes it possible to incorporate the phenomena of "confinement" and "spontaneous symmetry breaking". In this way, even setting aside its usage in particle phenomenology, the UV and IR branes with their associated boundary conditions offer invaluable theoretical handles and we are able to explore full facets of anomaly inflow holographically.

In fact, we have found that anomaly inflow with Neumann IR-BC in AdS_5 is the holographic realization of 't Hooft anomaly matching. To this end, it was important to realize that in this case the variance generated by the bulk CS theory is cancelled by *localized* degrees of freedom on the boundaries. In the end, we show how anomaly matching occurs for both purely global ('t Hooft type) and weakly gauged (ABJ type) symmetries. These results, therefore, led us to speculate that fermion anomalies from holographic anomaly inflow are necessarily free of mixed anomalies with confining large-N_s gauge symmetries of the dual CFT. These are discussed in section 4.5.

On the other hand, when the IR-BC is chosen so that a subgroup H_1 of the bulk gauge group G satisfies Neumann BC, while the coset G/H_1 is set to Dirichlet BC, the 4D dual theory describes spontaneous symmetry breaking $G \to H_1$ (whether weakly gauged or not). In this case, we show that in the low energy effective theory, the WZW action naturally appears and achieves anomaly matching. One key difference compared to the previous case with fully Neumann IR-BC is that in the current choice there are no IR brane-localized terms that are required by 5D consistency. This then is related to the fact that anomaly cancellation is done not by IR brane-*localized* degrees of freedom, but rather by *delocalized* modes, i.e. Goldstone modes which holographically correspond to a 5D Wilson line $\Sigma \sim \exp(i \int dz A_z(x,z))$. This may represent a less conventional feature of anomaly inflow. Discussion along these lines is presented in section 4.6.

To complete the outline of this paper, we first mention that in section 4.2 we describe the basic setup of the gauge theory with CS action in a slice of AdS_5. We then in section 4.3 describe the non-perturbative version of anomaly inflow in terms of the APS η-invariant [118], reducing it eventually to the perturbative version by means of the APS index theorem [118]. It may be worth mentioning, however, that the rest of the paper is readable independently of the discussion in section 4.3. Reading the last part of section 4.3 should be enough background for the rest of the paper. In section 4.4, we perform the gauge fixing in a way that the holographic aspects of the theory become apparent. In particular, we compute the holographic partition function, which we use in later sections to study anomaly inflow. As described above, sections 4.5 and 4.6 contain our main results. In section 4.7 we discuss the issue of quantization conditions for the CS level.

4.2 Gauge theory in a slice of AdS_5

In the rest of the paper, we wish to study a gauge theory in a slice of five-dimensional anti-de Sitter space, AdS_5. In particular, our prime interest is to study a gauge theory in the presence of a Chern-Simons action and to understand its 4D CFT dual interpretation. Most of what we discuss will go through whether or not the theory includes the usual gauge kinetic terms. In the absence of the gauge kinetic term, the 5D theory is purely topological. As we will discuss in section 4.3 such a topological field theory may be thought of as being induced by integrating out massive Dirac fermions in the bulk *perturbatively* [119–121]. We, however, do not need to specify a particular UV completion.

When the theory includes both the gauge kinetic and CS terms, the action for the gauge group G is given by

$$\begin{aligned} S = S_0 + S_{\rm CS}, \qquad\qquad S_0 = -\frac{1}{2g_5^2}\int d^5x\sqrt{g}\,{\rm Tr}\Big[F_{MN}F_{LS}g^{ML}g^{NS}\Big], \\ S_{\rm CS} = c\int d^5x\,\epsilon^{MNPQR}\,{\rm Tr}\Big(A_M\partial_N A_P\partial_Q A_R + \frac{3}{2}A_MA_NA_P\partial_Q A_R + \frac{3}{5}A_MA_NA_PA_QA_R\Big), \end{aligned} \tag{4.2.1}$$

where the metric takes the form (with mostly minus convention, $\eta_{\mu\nu} = {\rm diag}(+,-,-,-)$)

$$ds^2 = a(z)^2\Big(dx^2 - dz^2\Big), \qquad a(z) = \frac{1}{kz}. \tag{4.2.2}$$

Here, k is the compactification scale. The theory is defined on the interval $z_0 \le z \le z_1$. At the boundaries, we put 3-branes that we call *UV brane* and *IR brane*, respectively.

It is often convenient to adopt a differential form notation to simplify expressions. In these terms, the gauge connection is a 1-form $A \equiv A_M^A T^A dX^M$ and the field strength is a

2-form $F = dA + A^2 = \frac{1}{2}F^A_{MN}T^A dX^M dX^N$. In this notation, the wedge product symbols are suppressed, e.g. $A^2 = A \wedge A$. For instance, the CS action can be written as

$$S_{\rm CS} = c\int {\rm Tr}\Big(AdAdA + \frac{3}{2}A^3 dA + \frac{3}{5}A^5\Big). \tag{4.2.3}$$

At the moment, the overall coefficient c, called the *level*, is considered to be a free parameter. In section 4.7, we will show that it is quantized by anomaly cancellation requirements. The 5D CS action is the integral of the *canonical* form $\omega_5^{(0)}(A)$,

$$S_{\rm CS} = c\int_{\rm 5D} \omega_5^{(0)}(A). \tag{4.2.4}$$

The canonical CS term $\omega_5^{(0)}(A)$ is related to the 6D Abelian anomaly $\Omega_6(A) = {\rm Tr}(F^3)$ and 4D (non-Abelian) chiral anomaly $\omega_4^{(1)}(\alpha, A)$ via descent equations as $\Omega_6 = d\omega_5^{(0)}(A)$ and $\delta_\alpha \omega_5^{(0)}(A) = d\omega_4^{(1)}(\alpha, A)$. One has the freedom to add local counter terms to this, and this leads to the *shifted* CS action, $\omega_5^{(0)} \to \tilde{\omega}_5^{(0)} = \omega_5^{(0)} + dB_4$. The resulting 4D anomaly is then a shifted anomaly.

Suitable gauge-invariant boundary conditions (BC) can be obtained by studying the variation of S_0. This leads to

$$\delta S_0 = \frac{2}{g_5^2}\int dz d^4x \ {\rm Tr}[\delta A^\mu (aD^\nu F_{\nu\mu} + D_z(aF_{\mu z}))] + {\rm Tr}[\delta A^z D^\mu (aF_{\mu z})] \tag{4.2.5}$$

$$+ \frac{2}{g_5^2}\int_{\rm UV} d^4x \ {\rm Tr}[\delta A^\mu a F_{\mu z}] - \frac{2}{g_5^2}\int_{\rm IR} d^4x \ {\rm Tr}[\delta A^\mu a F_{\mu z}]. \tag{4.2.6}$$

Eq. (4.2.5) gives the bulk equations of motion (EOM), while eq. (4.2.6) is the boundary EOM

and provides the BC. A vanishing boundary variation is achieved by either setting $\delta A^\mu = 0$ (Dirichlet BC) or $F_{\mu z} = 0$ (Neumann BC).[1] While in the orbifold construction $S^1/\mathbb{Z}_2$ the UV and IR BC are correlated, we are treating the extra-dimensional direction as an interval (or $S^1/(\mathbb{Z}_2 \times \mathbb{Z}_2')$) and we are free to choose UV and IR BC independently.

4.3 Anomaly inflow

In this section, we review the basic idea of anomaly inflow. However, we first remark that the discussion in the rest of paper can be understood in a mostly self-contained manner with a minimal conceptual picture of anomaly inflow. Readers primarily interested in anomaly inflow by bulk CS theory and its AdS/CFT interpretations, therefore, may read a brief discussion below around eq. (4.3.12) and (4.3.13) and safely skip the rest of this section.

A non-perturbative formulation of anomaly inflow was given in a recent paper [94]. In the non-perturbative version, anomaly inflow is described in terms of the η-invariant of Atiyah, Patodi, and Singer (APS) [118]. The idea is the following: we start with a bulk *massive* fermion $\Psi(x, z)$ coupled to a background gauge field and gravity. We, however, will focus only on the gauge field part. The goal is to compute the partition function of this theory with some *local* (and chiral) BC. Examples of such local BC are $P_{\rm R}\Psi|_{\rm UV} = 0$ and $P_{\rm L}\Psi|_{\rm IR} = 0$ and so on, where $P_{\rm L/R} = \frac{1}{2}(1 \mp \gamma^5)$ is the chiral projection operator. Since we have two boundaries, and adopting the interval formulation (or $S^1/(\mathbb{Z}_2 \times \mathbb{Z}_2')$), we impose independent UV and IR BC. We denote the BC that keeps the LH component of Ψ (i.e. RH component projected out) as "L", while the BC that keeps the RH component as "R". For instance,

[1] In the axial gauge $A_z = 0$, the condition $F_{\mu z} = 0$ becomes $\partial_z A_\mu = 0$, a usual form of Neumann BC. Also, once a BC for A_μ is specified, that of A_z is fixed by the bulk EOM.

writing a general BC as (α_0, α_1), the choice (L, R) means that the bulk Ψ is projected onto LH (RH) component on the UV (IR) brane. Calling the bulk Y and boundaries W_0 and W_1, the path integral of a bulk massive fermion with the BC (α_0, α_1) may be written as[2]

$$Z[Y, (\alpha_0, \alpha_1)] = \langle \alpha_0 | Y | \alpha_1 \rangle \equiv \int_{(\alpha_0, \alpha_1)} \mathcal{D}\Psi \mathcal{D}\bar{\Psi}\ e^{-S}. \tag{4.3.1}$$

The states $|\alpha_{0(1)}\rangle$ defined on the Hilbert space of the boundary incorporate the BC. The meaning of this statement is as follows. Let us consider the example of L-UV-BC. Writing the boundary Dirac operator as $\mathcal{D}_W$ and chirality operator as γ^τ with $\{\gamma^\tau, \mathcal{D}_W\} = 0$, the bulk fermion Ψ can be expanded in terms of modes of $\mathcal{D}_W$,

$$\mathcal{D}_W \psi_{L,a} = \lambda_a \psi_{R,a},\ \mathcal{D}_W \psi_{R,a} = \lambda_a \psi_{L,a},\ \gamma^\tau \psi_{L/R,a} = \mp \psi_{L/R,a}. \tag{4.3.2}$$

The mode expansion is given by

$$\Psi = \sum_a (A_{L,a} \psi_{L,a} + A_{R,a} \psi_{R,a}), \tag{4.3.3}$$

where the fermionic operators coefficients $A_{L/R,a}$ are annihilation operators for LH (RH) modes. In terms of this, L-UV-BC is a condition on the UV value such that the RH modes are fixed to be zero, while the LH mode is unconstrained. The latter condition may be rephrased as its "conjugate momentum" mode being fixed to be zero.[3] Hence, $\langle \alpha_0 = L|$ is

[2] See [94, 95] for the description of path integral in terms of state overlaps and for more details.

[3] Recall that a plane wave in position space corresponds to a delta function in its conjugate momentum space, and vice versa.

defined by the properties

$$\langle L|A_{R,a} = 0, \quad \text{and} \quad \langle L|A^{\dagger}_{L,a} = 0. \tag{4.3.4}$$

Going back to the evaluation of the partition function eq. (4.3.1), we note that, in general, the bulk Dirac operator is not self-adjoint in the presence of a boundary. In order for the Dirac operator to be self-adjoint, hence to result in a well-defined real spectrum, a special class of *global* BC, called APS-BC [118], should be imposed. Without going into too much technical details, we simply quote the result here, referring to [94, 95] for more details. Provided the geometry near the boundary is $\sim [z_0, \epsilon) \times W_0$ (similarly for the IR boundary) and $|m|\epsilon \gg 1$ (i.e. the bulk mass m is much larger than the curvature scale), the Euclidean path integral near the boundary is effectively a projection to the vacuum $e^{-\epsilon|m|} \approx |\Omega\rangle\langle\Omega|$ and the partition function eq. (4.3.1) can be computed in the limit $|m| \to \infty$ to get

$$\begin{aligned} Z[Y, (\alpha_0, \alpha_1)] &= \langle \alpha_0|\Omega\rangle\langle\Omega|Y|\Omega\rangle\langle\Omega|\alpha_1\rangle \\ &= \frac{\langle \alpha_0|\Omega\rangle\langle\Omega|\mathrm{APS}\rangle}{|\langle\Omega|\mathrm{APS}\rangle|^2} \langle \mathrm{APS}|Y|\mathrm{APS}\rangle \frac{\langle \mathrm{APS}|\Omega\rangle\langle\Omega|\alpha_1\rangle}{|\langle\Omega|\mathrm{APS}\rangle|^2}. \end{aligned} \tag{4.3.5}$$

We used $e^{-\epsilon|m|} \approx |\Omega\rangle\langle\Omega|$ and that in the limit $|m| \to \infty$ the Hilbert space becomes effectively one-dimensional. In particular, this implies $|Y\rangle \propto |\mathrm{APS}\rangle \propto |\Omega\rangle$, where $|Y\rangle$ is the path integral over Y (recall that path integration over Y gives a state vector in the Hilbert space on the boundary). The first and the last factor in eq. (4.3.5) are UV and IR boundary contributions and the middle term is identified as the bulk contribution. $|\mathrm{APS}\rangle$ is a state in the Hilbert space of the boundary that incorporates the required APS-BC. As shown in [94], the boundary contributions are related to $\left|\mathrm{Det}\mathcal{D}^{\pm}_{W}\right|$, where $\mathcal{D}^{\pm}_{W}$ is the chiral Dirac operator on the boundary $W_{0(1)}$ and its exact nature depends on the BC and associated localized

modes.[4] For us, the precise form of the boundary contributions are not important.[5] Instead, we are interested in the bulk contribution, $\langle \text{APS}|Y|\text{APS}\rangle$. This is just a path integral over Y with APS-BC. As mentioned above, the bulk Dirac operator $\mathcal{D}_Y$ with APS-BC is self-adjoint and its spectrum is well-defined and real. The massive fermion now can be integrated out non-perturbatively, and the phase of the partition function can be determined. In fact, this is one of the important reasons to rewrite the partition function in the form of eq. (4.3.5). Formally, the path integral of Ψ with negative mass $-m$ ($m > 0$) is $\text{Det}(\mathcal{D}_Y - im)$. Using Pauli-Villars (PV) regularization (with positive mass $+M$ ($M > 0$)), we get

$$\langle \text{APS}|Y|\text{APS}\rangle = \prod_a \frac{\lambda_a - im}{\lambda_a + iM} = \prod_a \frac{\lambda_a}{\lambda_a + iM} \prod_a \frac{\lambda_a - im}{\lambda_a}. \tag{4.3.6}$$

Each factor of the form $\prod_a \lambda_a/(\lambda + iM)$ is recognized as the partition function of a massless fermion in PV-regularization. In the limit $M \gg |\lambda_a|$, each term has a phase $-i\frac{\pi}{2}\text{sign}(\lambda_a)$ and the overall phase is therefore $-i\frac{\pi}{2}\sum_a \text{sign}(\lambda_a)$. This formal expression, which requires a regularization, is known as the APS η-invariant. Similarly, in the limit $m \to \infty$, the phase of the second factor is found to be also $-i\frac{\pi}{2}\sum_a \text{sign}(\lambda_a)$. Therefore, the phase of the bulk term is given by[6]

$$\text{phase of } \langle \text{APS}|Y|\text{APS}\rangle = -i\pi \sum_a \text{sign}(\lambda_a)|_{\text{reg}} = -i\pi\eta_Y. \tag{4.3.7}$$

[4] A study of non-perturbative anomaly inflow in extra-dimensional particle physics models and its connection with "anomalies in orbifold field theories" will be presented elsewhere [122].

[5] To be clear, the precise form of the boundary term is very important. In fact, because the boundary term is $\left|\text{Det}\mathcal{D}_W^{\pm}\right|$, and not say $\text{Det}\mathcal{D}_W^{\pm}$, the non-perturbative anomaly inflow formula eq. (4.3.8) provides the unique determination of the phase of the boundary partition function, provided eq. (4.3.8) is independent of the choice of Y (i.e. absence of anomaly).

[6] The phase of eq. (4.3.6) is indeed regularized. For $\lambda_a \gg M, m$, the phase is 0 and the sum over the entire "UV" modes is trivial. In addition, for the zero mode (if the Dirac operator does have zero modes), the phase is given by (setting $m = M \to \infty$) $-i\pi$. In this sense, in PV regularization, $\text{sign}(\lambda_a = 0) = +1$.

If we instead had chosen a positive mass $+m$, the phase of the PV-regularized (with negative mass $-M$) partition function would be just minus that of eq. (4.3.7). Using this, the integration of the bulk massive fermion non-perturbatively eq. (4.3.5) may be written as

$$Z[Y,(\alpha_0,\alpha_1)] = Z_0 \cdot e^{\mp i\pi\eta_Y} \cdot Z_1, \tag{4.3.8}$$

where $Z_{0(1)}$ are the boundary contributions, while the exponentiated η-invariant is the bulk contribution. This is the formula for the non-perturbative version of anomaly inflow. A perturbative version can be obtained from this thanks to the APS index theorem [118]. For a closed manifold X of dimension $d+2$[7], according to the Atiyah-Singer index theorem [123], the index of the Dirac operator, the number of positive chiral zero modes minus the number of negative chiral zero modes, is equal to

$$\mathrm{ind}(\mathcal{D}_X) = n_+ - n_- = \int_X I_{d+2}, \quad I_{d+2} = \hat{A}(R)\mathrm{tr}\,\exp\left(\frac{iF}{2\pi}\right)\Big|_{d+2}, \tag{4.3.9}$$

where $\hat{A}(R)$ is the Dirac genus of the manifold (R being the Ricci curvature)[8] and $\mathrm{tr}\,\exp\left(\frac{iF}{2\pi}\right)$ is the Chern character (F is the field strength 2-form). If, on the other hand, the manifold X has a boundary, the relevant formula is the APS index theorem [118],

$$\mathrm{ind}(\mathcal{D}_X) = \int_X I_{d+2} - \frac{\eta_{\partial X}}{2}, \tag{4.3.10}$$

[7]We imagine a theory defined on a d-dimensional spacetime W ($d=4$ in our case), which itself is a boundary of a $d+1$ manifold Y (bulk of AdS_5). We then define a $d+2$-dimensional manifold X, whose boundary is $\partial X = Y \cup -Y'$; since Y has a boundary, we combine Y with Y' where $\partial Y' = W = \partial Y$ to form a closed manifold $Y \cup -Y'$ (where $-Y'$ is the orientation reversal of Y).

[8]For an explicit form of $\hat{A}(R)$ see e.g. [124, 125].

where the η-invariant contribution may be interpreted as the boundary correction. In the perturbation theory we are focusing on here, it is straightforward to see that (taking $d = 4$)

$$e^{i\pi\eta_Y} = \exp\Big(i\frac{1}{48\pi^2}\int_Y \omega_5^{(0)}(A)\Big), \tag{4.3.11}$$

that is, the bulk term in eq. (4.3.8) turns into the 5D CS action in the perturbative limit. The perturbative anomaly inflow is performed by the interplay of the bulk CS interaction and the boundary modes. In fact, this is our starting point for the rest of the paper. We study the anomaly inflow of various CS theories and obtain its dual CFT descriptions.

In order to illustrate the point, let us consider the simple example of a $U(1)$ CS theory in a slice of AdS_5:

$$S_{\rm CS} = c\int_{\rm 5D} AdAdA = c\int_{\rm 5D} AFF. \tag{4.3.12}$$

Under a gauge transformation, $A \to A + dv$ and $F \to F$, and CS action changes by

$$\delta S_{\rm CS} = c\int_{\rm IR} vFF - c\int_{\rm UV} vFF. \tag{4.3.13}$$

To get eq. (4.3.13) we performed an integration by parts and used $dF = 0$. We see that the CS theory defined on a manifold with boundary is not gauge invariant, and the variance terms induced on the boundary have the form of chiral anomaly. In order to make the 5D theory consistent, such surface terms need to be cancelled, and one way to achieve this is to introduce boundary localized fermions (edge modes) charged under $U(1)$. This is the essential feature of perturbative anomaly inflow and can be generalized to more complicated (and interesting) cases. Below, we study various CS theories, including non-Abelian and/or

mixed CS theories, with special emphasis on their holographic dual descriptions. While the description given so far makes the interplay between bulk and boundary physics clear, it is not yet the optimal one for a holographic study. For this reason, in the next section, we first discuss a description of the gauge theory in which the AdS/CFT duality becomes apparent.

4.4 Holographic partition function

In this section, we discuss the gauge fixing issue, adopting the axial gauge. Since we are interested in the holographic study, we perform the gauge fixing in such a way that the holographic nature of the AdS_5 gauge theory becomes manifest: we derive the gauge-fixed holographic partition function $Z^{\text{g.f.}}$. Our discussion in this section is influenced by the work of [115]. We, however, generalize it to arbitrary UV and IR boundary conditions. In addition, when the UV-BC is chosen to be Neumann for some non-trivial subgroup $H_0 \subset G$, we show that there is a residual gauge redundancy, requiring further (brane-localized) gauge fixing.[9]

Let us consider a very general situation. We take the bulk gauge group to be G. We imagine a general BC by which G is broken down to $H_0 \subset G$ on the UV brane and to $H_1 \subset G$ on the IR brane. In this case, the full 5D gauge symmetry is given by

$$G_B = \{g(x,z) \in G \mid \hat{g} \equiv g(x,z_0) \in H_0, \bar{g} \equiv g(x,z_1) \in H_1\}. \tag{4.4.1}$$

The dual 4D CFT then has a global symmetry group G, which is spontaneously broken to H_1 by confinement at the scale associated with the IR brane location. $H_0 \subset G$ on the UV brane

[9] In [126], in the context of AdS/QCD without a CS term, a discussion was presented in which a field redefinition, instead of gauge fixing, is used. Both approaches produce agreeing results when expected.

is dual to the fact that the H_0 part of G is weakly gauged, featuring an explicit breaking of G by gauging. The inclusion of the 5D CS action further incorporates the anomaly structure into the 4D dual gauge theory.

We denote the Lie algebra of G as $\mathbf{g}$. Similarly, $\mathbf{h}_0$ is the Lie algebra of H_0 and we denote the space generated by the coset G/H_0 generators to be $\mathbf{k}_0$. Likewise, $\mathbf{h}_1$ is the Lie algebra of H_1 and $\mathbf{k}_1$ denotes the space spanned by the generators of the coset G/H_1. Generators of $\mathbf{g}$ are written as $T^A \in \mathbf{g}, A = 1, \ldots, \mathrm{Dim}[\mathbf{g}]$. Likewise, $T^i_m \in \mathbf{h}_m$ and $T^a_m \in \mathbf{k}_m, m = 0, 1$ are the unbroken and broken generators, respectively.

Before gauge fixing, the holographic partition function of a gauge theory of eq. (4.4.1) takes the form

$$Z[B^a] = \int \mathcal{D}B^i \; \mathcal{Z}\Big[B^A\Big], \tag{4.4.2}$$

$$\mathcal{Z}\Big[B^A\Big] = \int \mathcal{D}A_\mu(x,z)|^{\hat{A}=B}_{\bar{A}:\begin{bmatrix}(F)^i_1=0\\ \\ (A)^a_1=0\end{bmatrix}} \mathcal{D}A_z(x,z)\; e^{iS[A_\mu(x,z),A_z(x,z)]}. \tag{4.4.3}$$

Let us explain the notation we used in these expressions. First, $\mathcal{Z}\Big[B^A\Big]$ is the partition function with UV boundary value of the bulk gauge field A taken to be B^A. Here, we suppressed the Lorentz index for the sake of brevity. The superscript A runs over *all* generators. This statement about the UV-BC is also written schematically as the superscript "$\hat{A} = B$" in eq. (4.4.3). The subscript in the same equation denotes instead the IR-BC. $(F)^i_1 = 0$ means $F_{\mu z} = 0$ for $T^i_1 \in \mathbf{h}_1$. The expression $(A)^a_1 = 0$ can be understood in the same way. As it is, $\mathcal{Z}\Big[B^A\Big]$ is the holographic partition function with Dirichlet UV-BC for all generators. In

order to obtain the partition function corresponding to eq. (4.4.1), we need to promote the background source for the $T_0^i \in \mathbf{h}_0$ to dynamical fields. This is done by path integrating over the fields B^i. Once this is done, then the partition function depends only on B^a, the background fields associated with $T_0^a \in \mathbf{k}_0$. The final result of this whole procedure is summarized by eq. (4.4.2) and (4.4.3).

As a next step, we want to incorporate the axial gauge, $A_z = 0$. As usual, this is done by inserting the following gauge-fixing factor into eq. (4.4.2):

$$\begin{aligned} 1 &= \int \mathcal{D}A_z \; \delta(A_z) = \int \mathcal{D}g \; \mathrm{Det}\left[\frac{\delta A_z^g}{\delta g}\right] \; \delta(A_z^g) \\ &= \int \mathcal{D}\Sigma_1(x) \; \mathcal{D}h_1(x) \; \mathcal{D}h_0(x) \; \mathcal{D}g|^{\hat{g}=h_0}_{\bar{g}=\Sigma_1 \circ h_1} \; \mathrm{Det}[D_z(A_z)] \; \delta(A_z^g), \end{aligned} \tag{4.4.4}$$

where $A^g \equiv g(d + A)g^{-1}$ is the gauge transformation of the gauge connection A by $g \in G$. To obtain the last line, we used the fact that for a compact group G and a closed subgroup H the integration over the group manifold can be split into H and G/H parts with proper left invariant Haar measures [115, 127]. In particular, for the coset part, the G-invariant measure on G/H can be expressed as [127]

$$\mathcal{D}\Sigma = \prod_a \left(\Sigma^{-1} d\Sigma\right)^a, \tag{4.4.5}$$

where $(\Sigma^{-1}d\Sigma)^a$ is defined via $(\Sigma^{-1}d\Sigma)_k = (\Sigma^{-1}d\Sigma)^a T^a$, $T^a \in \mathbf{k}$. The G-invariance is seen

by noting that under an arbitrary $g \in G$, $(\Sigma^{-1}d\Sigma)_k$ transforms as[10]

$$\Big(\Sigma^{-1}d\Sigma\Big)_k \to h^{-1}(g,\Sigma)\Big(\Sigma^{-1}d\Sigma\Big)_k h(g,\Sigma). \tag{4.4.7}$$

In the above, $h(g,\Sigma) \in H$ is defined by $g\Sigma = \Sigma^g(g,\Sigma)h(g,\Sigma)$. If we had used a naive (non-invariant) measure $\prod_a d\xi_a$ (recall $\Sigma = e^{-\xi_a T^a}$), then G-invariance of the quantum theory could be restored by adding a proper term $\int \mathcal{L}(\xi)$ to the action. The role of this term is to precisely cancel the non-invariance of the naive measure.

The gauge redundancy by G_B can be singled out by the following change of variable: $g \to g = \tilde{\Lambda} \circ g'$, where $\hat{\tilde{\Lambda}} = \tilde{\Lambda}(x, z_0) = 1$ and $\bar{\tilde{\Lambda}} = \tilde{\Lambda}(x, z_1) = \Sigma_1(x)$.[11] After inserting the transformed version of eq. (4.4.4) into eq. (4.4.2) we get

$$Z[B^a] = \int \mathcal{D}B^i \; \mathcal{Z}\Big[B^A\Big], \tag{4.4.8}$$

$$\mathcal{Z}\Big[B^A\Big] = \int \Big[\mathcal{D}h_0 \, \mathcal{D}h_1 \, \mathcal{D}g'|^{\hat{g}'=h_0}_{\bar{g}'=h_1}\Big] \, \mathcal{D}\Sigma_1(x)\mathcal{D}A_\mu(x,z)|^{\hat{A}=B}_{\bar{A}:\begin{bmatrix}(F)^i_1=0\\ \\ (A)^a_1=0\end{bmatrix}} \mathcal{D}A_z(x,z)$$

$$\times \; \mathrm{Det}[D_z(A_z)] \; \delta\Big(A_z^{\tilde{\Lambda}\circ g'}\Big) \; e^{iS[A_\mu(x,z),A_z(x,z)]}. \tag{4.4.9}$$

[10] On the other hand, $\big(\Sigma^{-1}d\Sigma\big)_h$ transforms inhomogeneously as

$$\big(\Sigma^{-1}d\Sigma\big)_h \to h^{-1}(g,\Sigma)\big(\Sigma^{-1}d\Sigma\big)_h h(g,\Sigma) + h^{-1}dh. \tag{4.4.6}$$

[11] The existence of such $\tilde{\Lambda}(x,z)$ is guaranteed provided $\pi_4(G/H) = 0$. This is understood by observing that $\tilde{\Lambda}$ is effectively an extension of $\Sigma_1(x)$ defined on S^4 (IR brane) to a 5D disk D_5. If $\pi_4(x) = 0$, then every coset element admits an extension to D_5. If, on the other hand, $\pi_4(G/H)$ is non-trivial, then while a $\Sigma(x)$ belonging to the trivial class of $\pi_4(G/H)$ can be extended to D_5, any $\Sigma(x)$ in the non-trivial elements can at best be deformed into a representative of the corresponding class and the resulting object is defined on $S^4 \times [0,1]$ [128]. For simplicity, we assume $\pi_4(G/H) = 0$ in what follows.

Notice that $\left[\mathcal{D}h_0\,\mathcal{D}h_1\,\mathcal{D}g'|^{\hat{g}'=h_0}_{\bar{g}'=h_1}\right]$ is nothing but the integration over G_B, the gauge redundancy we hope to remove from the path integral.

We proceed further with a change of variable: $A' = A^{\tilde{\Lambda}\circ g'}$. This simplifies the argument of the delta function, making the evaluation of the A_z-integral trivial. Taking into account the changes of UV-BC, IR-BC, and performing the A_z-integral using the delta function, we arrive at

$$Z[B^a] = \int_{G_B}\left[\mathcal{D}h_0\,\mathcal{D}h_1\,\mathcal{D}g'|^{\hat{g}'=h_0}_{\bar{g}'=h_1}\right]\int \mathcal{D}B^i\,\mathcal{D}\Sigma_1(x)\mathcal{D}A'_\mu(x,z)|^{\hat{A}'=B^{h_0}}_{\bar{A}':\begin{bmatrix}\left((F'_1)^{\Sigma_1^{-1}}\right)^i=0\\ \left((A'_1)^{\Sigma_1^{-1}}\right)^a=0\end{bmatrix}}$$
$$\times\; e^{iS\left[(A'_\mu)^{(\tilde{\Lambda}\circ g')^{-1}}(x,z),0^{(\tilde{\Lambda}\circ g')^{-1}}\right]}. \tag{4.4.10}$$

To get eq. (4.4.10) we used the fact that, upon A_z-integration, $\mathrm{Det}[D_z(A_z)] \to \mathrm{Det}[\partial_z]$ and dropped this irrelevant constant. We also used the H_1-invariance of the IR-BC to simplify its form. Notice that now the second argument (fifth component) in the action is a pure gauge contribution, which in general does not vanish.

Let us now analyze how the latest form of the partition function depends on h_0 and g'. First of all, when H_0 is not trivial, there is a residual gauge freedom that needs to be fixed. The existence of this residual gauge redundancy is seen by the appearance of the extra integration over h_0 compared to the case with a trivial H_0. A more careful statement can be made as follows. The bulk axial gauge fixing coincides with the condition $A'_z = g(\partial_z + A_z)g^{-1} = 0$. This is a condition on g, selecting a specific gauge orbit. The solution to this equation is the

Wilson line

$$g = P \exp\Big(\int_{z_0}^{z} dz' \, A_z(x, z') \Big), \tag{4.4.11}$$

stretched from the UV brane to a point in the bulk at z.[12] This g successfully removes any A_z component everywhere in the bulk except at $z = z_0$ where g becomes 1. For the Dirichlet UV-BC, this is not an issue since the UV brane preserves no gauge symmetry. If, however, the UV-BC involves a non-trivial H_0, this indicates that the bulk axial gauge fixing is not complete, and we need to add a brane-localized gauge fixing term to eliminate the residual gauge freedom. Since the details of this extra gauge fixing do not affect our discussion below in any crucial way, we simply set $h_0 = 1$ and drop the integration over h_0. This is also equivalent to properly reinterpreting the gauge fixing constraint in eq. (4.4.4), so that instead of integrating over the entire gauge manifold, we pick a specific gauge orbit.

The advantage of this approach is that it also allows us to more easily study the g' transformation appearing in the action. We know that there are different contributions to $S[A_\mu, A_5]$, namely the gauge and CS action. The former is by assumption gauge invariant. The latter in general is not, but nevertheless we can use the fact that its variation only contributes as a boundary term to the variation of the full action, and therefore only depends on the boundary values of g'. Thus, by setting $h_0 = 1$, and by assuming from now on that the CS action satisfies $\omega_5^{(0)}(A_h) = 0$, i.e. the CS action (hence the associated anomaly $\omega_4^{(1)}$) vanishes when the gauge field A is restricted to its H_1 part, we can conclude that the full action $S[A_\mu, A_5]$ is invariant under any $g' \in G_B$ transformation. The property $\omega_5^{(0)}(A_h) = 0$ is referred to as an anomaly-free embedding (AFE) of $H_1 \subset G$.

[12] An equivalent solution is the Wilson line from the IR brane to a bulk point at z. Our argument can be applied to both cases.

After dropping the g' transformation from eq. (4.4.10), we make one last change of variable, which moves the Σ_1 dependence from the IR-BC to the UV-BC. We set $A_\mu = (A'_\mu)^{\Sigma_1^{-1}}$ to obtain

$$Z[B^a] = \int_{G_B} \left[\mathcal{D}h_0\, \mathcal{D}h_1\, \mathcal{D}g' \Big|_{\bar{g}'=h_1}^{\hat{g}'=h_0}\right] \int \mathcal{D}B^i\, \mathcal{D}\Sigma_1(x)\mathcal{D}A_\mu(x,z) \Big|_{\bar{A}:\begin{bmatrix} F_1^i=0 \\ A_1^a=0 \end{bmatrix}}^{\hat{A}=B^{\Sigma_1^{-1}}} e^{iS\left[A^\Lambda(x,z)\right]}, \quad (4.4.12)$$

where now $A_M = \{A_\mu, 0\}$ indicates a 5D vector with vanishing fifth component, and $\Lambda = \tilde{\Lambda}^{-1} \circ \Sigma_1$, with $\hat{\Lambda} = \Sigma_1$ and $\bar{\Lambda} = 1$. At this point, we want to make a couple of comments. First, we note that the integrand becomes completely independent of any G_B element and the integral over G_B (the infinite gauge redundancy) will be cancelled between the numerator and the denominator in any observable computation. Therefore, as usual, we can simply drop that factor. Second, since we have chosen the axial gauge, we do not need ghost fields to exponentiate the determinant factor. Third, the transformation parameter $\Lambda(x,z)$ can be thought of as an interpolating function between a coset element $\hat{\Lambda}$ and a trivial element $\bar{\Lambda}$. As we mentioned before, such an element exists whenever $\pi_4(G/H) = 0$.

We finally arrive at the gauge-fixed holographic partition function for arbitrary choice of UV and IR BC:

$$Z^{\text{g.f.}}[B^a] = \int \mathcal{D}B^i\, \mathcal{D}\Sigma_1(x)\mathcal{D}A_\mu(x,z) \Big|_{\bar{A}:\begin{bmatrix} F_1^i=0 \\ A_1^a=0 \end{bmatrix}}^{\hat{A}=B^{\Sigma_1^{-1}}} e^{iS\left[A^\Lambda(x,z)\right]}. \quad \text{(general UV-BC, IR-BC)} \quad (4.4.13)$$

Using this general formula, we can obtain results for special cases. Two particularly relevant

ones are (i) pure Dirichlet UV-BC and pure Neumann IR-BC and (ii) pure Dirichlet UV-BC and mixed IR-BC with a G/H_1 symmetry breaking pattern. In the first case, we simply remove the integration over B^i and Σ_1 and set $\Sigma_1 = 1$ (hence $\Lambda = 1$ as well). In the second case, while we remove the B^i-integral, we keep Σ_1 and Λ as they are. We obtain[13]

$$Z^{\text{g.f.}}\left[B^A\right] = \int \mathcal{D}A_\mu(x,z)|^{\hat{A}=B}_{\bar{A}:F^A=0}\, e^{iS[A(x,z)]}, \quad \text{(D-UV-BC, N-IR-BC)} \tag{4.4.14}$$

$$Z^{\text{g.f.}}\left[B^A\right] = \int \mathcal{D}\Sigma_1(x)\mathcal{D}A_\mu(x,z)|^{\hat{A}=B^{\Sigma_1^{-1}}}_{\bar{A}:\begin{bmatrix} F_1^i=0 \\ \\ A_1^a=0 \end{bmatrix}}\, e^{iS\left[A^\Lambda(x,z)\right]}. \quad \text{(D-UV-BC, } G/H_1\text{-IR-BC)} \tag{4.4.15}$$

4.5 Unbroken symmetry and 't Hooft anomaly matching

Having developed the necessary formalism to study gauge theories in a slice of AdS_5 holographically, we now turn to the holography of anomaly inflow. In this section, we focus on the case where the IR-BC is purely Neumann. In its 4D dual CFT, this corresponds to the global symmetry (either weakly gauged or not) unbroken by the vacuum condensate. The case of mixed IR-BC with the breaking pattern G/H_1 will be the subject of the next section.

4.5.1 Purely global symmetry

We first study the case with pure Dirichlet UV-BC. The dual CFT then has a purely global symmetry G, without any gauging. In particular, the relevant partition function is eq. (4.4.14) and the B^A associated with all $T^A \in \mathbf{g}$ are non-dynamical background fields.

[13] We have confirmed the following results by separate explicit computations.

In order to study the (in)variance of the theory, we check how the partition function transforms as we vary the source fields. Considering an infinitesimal transformation $g \approx 1-\alpha$, the partition function transforms as

$$\begin{aligned} Z^{\text{g.f.}}\left[\left(B^A\right)^\alpha\right] &= \int \mathcal{D}A_\mu(x,z)|^{\hat{A}=B^\alpha}_{\bar{A}:F^A=0}\, e^{iS_0[A]+iS_{\text{CS}}[A]} \\ &= \int \mathcal{D}A_\mu(x,z)|^{\hat{A}=B}_{\bar{A}:F^A=0}\, e^{iS_0[A]+iS_{\text{CS}}[A^\alpha]}, \end{aligned} \tag{4.5.1}$$

where we made a change of variable $A \to A^\alpha$ and used the G-invariance of the gauge action S_0 and of the IR-BC. In addition, given a UV-localized group element $g(x) \approx 1-\alpha(x)$ acting on the source B, we extended it to a 5D one as $\alpha(x,z) = \alpha(x)$.[14] From the second line of this equation, it is clear that the (in)variance of the partition function when the UV-BC is purely Dirichlet is fully determined by the transformation of the CS action. Using eq. (4.2.4) and

$$\int_{5\text{D}} \delta_\alpha \omega_5^{(0)}(A) = \int_{5\text{D}} d\omega_4^{(1)}(\alpha, A) \tag{4.5.2}$$

we obtain

$$Z^{\text{g.f.}}\left[\left(B^A\right)^\alpha\right] = e^{-ic\int_{\text{UV}}\omega_4^{(1)}(\alpha,B)} \int \mathcal{D}A_\mu(x,z)|^{\hat{A}=B}_{\bar{A}:F^A=0}\, e^{iS_0[A]}\, e^{ic\int_{\text{IR}}\omega_4^{(1)}(\alpha,\bar{A})}\, e^{iS_{\text{CS}}[A]}. \tag{4.5.3}$$

Here, since the UV brane-localized variance term is independent of A_μ, we factor it out of the path integral. We also observe that the partition function is not invariant under the transformation. Before we proceed any further, however, we first need to discuss one problem. That is, under the transformation, the integrand picks up an IR brane-localized variance

[14] In the case of G/H_1 discussed in section 4.6, an extra subtlety appears regarding the extension of a 4D local gauge group element to a 5D one.

term. Recalling that the bulk gauge symmetry G is unbroken at the IR brane, such an IR brane-localized variance is not acceptable.[15] In order to remedy this issue, we introduce an IR-localized effective action, $\Gamma_{\rm IR}\left[\bar{A}\right]$, which under an infinitesimal transformation A^α shifts by an opposite anomaly factor to cancel the bulk-generated anomaly factor:

$$e^{i\Gamma_{\rm IR}\left[\bar{A}^\alpha\right]} = e^{-ic\int_{\rm IR}\omega_4^{(1)}(\alpha,\bar{A})}e^{i\Gamma_{\rm IR}\left[\bar{A}\right]}. \tag{4.5.4}$$

Such an effective action may be obtained by first introducing an anomalous set of 4D Weyl fermions charged under G and localized on the IR brane. Integrating out the fermions then generates $\Gamma_{\rm IR}\left[\bar{A}\right]$:

$$e^{i\Gamma_{\rm IR}\left[\bar{A}\right]} \equiv \int \mathcal{D}\psi\mathcal{D}\bar{\psi}\; e^{iS_{\rm IR}\left[\bar{A},\psi,\bar{\psi}\right]}. \tag{4.5.5}$$

In this case, however, the coefficient c cannot be arbitrary, and in fact, must be an integral multiple of the coefficient of the chiral anomaly due to a single Weyl fermion. This leads to the *quantization* condition for the CS level c. This issue will be discussed in section 4.7.

The UV-localized variance term, on the other hand, is perfectly fine: G is completely broken on the UV brane. In terms of the modified partition function $\tilde{Z}^{\rm g.f.}$ with $\Gamma_{\rm IR}$ inserted, the transformation rule for the holographic partition function is therefore given by

$$\begin{aligned}
\tilde{Z}^{\rm g.f.}\left[B^A\right] &= \int \mathcal{D}A_\mu(x,z)|^{\hat{A}=B}_{\bar{A}:F^A=0}\; e^{iS_0[A]+iS_{\rm CS}[A]}\; e^{i\Gamma_{\rm IR}\left[\bar{A}\right]}, \\
\tilde{Z}^{\rm g.f.}\left[\left(B^A\right)^\alpha\right] &= e^{-ic\int_{\rm UV}\omega_4^{(1)}(\alpha,B)}\;\tilde{Z}^{\rm g.f.}\left[B^A\right].
\end{aligned} \tag{4.5.6}$$

[15] In fact, there is an alternative to this view point. Since the 5D gauge theory is intrinsically non-renormalizable, it is at best an effective field theory. An effective gauge theory with non-vanishing gauge anomaly can still be consistently quantized below a cut-off scale and the associated cut-off scale can be estimated by the knowledge of the anomaly [127]. A study of a 5D $U(1)$ gauge theory along this line was presented in [106].

In order to obtain the dual 4D CFT interpretation, we now view $\tilde{Z}^{\text{g.f.}}\left[B^A\right]$ as the partition function of a 4D CFT with classical source $\left(B^A\right)_\mu$ coupled to the CFT current operators J^μ. The phase factor in eq. (4.5.6) shows that the global symmetry G of the CFT is anomalous. This anomalous global symmetry G is unbroken by confinement, a fact dual to the pure Neumann IR-BC. Furthermore, the appearance of both the UV- and IR-localized anomaly factors in eq. (4.5.3), with same magnitude but opposite signs, encodes what we might call a *'t Hooft anomaly matching*. In order to see this explicitly, as is usually done, let us first weakly gauge G. This is done by switching the UV-BC to be purely Neumann. Under this change, what we called the source fields B before now turn into dynamical fields, and the UV-localized variance needs to be cancelled just like we did for the IR-localized anomaly factor. We proceed as we did for the IR-localized anomaly term, by introducing a UV-localized effective action $\Gamma_{\text{UV}}[B]$, which again may be obtained by integrating out UV-localized 4D Weyl fermions. In order to achieve gauge anomaly cancellation, we require

$$e^{i\Gamma_{\text{UV}}[B^\alpha]} = e^{+ic\int_{\text{UV}}\omega_4^{(1)}(\alpha,B)}\, e^{i\Gamma_{\text{UV}}[B]}. \tag{4.5.7}$$

The full partition function then becomes

$$\tilde{Z}^{\text{g.f.}} = \int \mathcal{D}B^A\, e^{i\Gamma_{\text{UV}}[B]}\, \mathcal{D}A_\mu(x,z)|^{\hat{A}=B}_{\hat{A}:F^A=0}\, e^{iS_0[A]+iS_{\text{CS}}[A]}\, e^{i\Gamma_{\text{IR}}\left[\bar{A}\right]}. \tag{4.5.8}$$

As expected, the partition function is independent of any B fields, and the symmetry property of the theory is tested by making a change of variable (or field redefinition) in the form of a G-transformation and check whether it results in an anomalous change to the original theory

or not.

The 4D interpretation goes as follows. The 4D confining gauge theory (in fact deformed CFT) has a weakly gauged symmetry G. In addition to the CFT preons, there is an anomalous set of external fermions (UV-localized fermions that induce $\Gamma_{\rm UV}$) charged under G. While CFT and external sector are not individually G-anomaly free, these two contributions, nonetheless, cancel, making the gauging of G legal. Importantly, these external fermions need not couple to the confining CFT gauge force, and they are spectator fermions. Along the renormalization group (RG) flow, while the chiral anomaly does not get renormalized, the CFT sector undergoes confinement. By assumption, G is not broken, and the original anomaly of the CFT preons should be reproduced by a spectrum of massless composite fermions. These composite fermions are the IR brane-localized fermions we introduced in 5D to cancel the IR-localized variance. For these reasons, the choice of Neumann IR-BC and the resulting requirement of cancelling the IR-localized variance term by 4D fermions on the IR brane is the holographic realization of 't Hooft anomaly matching.

One perhaps interesting feature deduced from the above discussion is that the anomaly inflowed from the bulk CS theory must be the one that has vanishing mixed anomaly between global G and confining gauge group G_s of the CFT. In order to make this point clear, we may consider a $U(1)$ CS theory in the bulk. The variances induced on the boundaries are dual to a $U(1)^3$ anomaly of the global symmetry. If this global $U(1)$ current had a Adler-Bell-Jackiw (ABJ) type anomaly [73, 74] with the confining gauge force of the CFT, then the spectators would be necessarily coupled to the strong interaction as well, and as a result, 't Hooft argument for the anomaly matching would not hold. However, we have seen that, with Neumann IR-BC, anomaly inflow by the bulk CS action always comes with an

IR-localized variance term in addition to the UV variance term: 't Hooft anomaly matching is automatically at play. As we discuss in section 4.5.2, this fact holds even if G is weakly gauged.

4.5.2 Partially gauged symmetry

In this section, we consider the anomaly inflow with a mixed UV-BC in which a subgroup $H_0 \subset G$ takes a Neumann BC, while the coset G/H_0 has a Dirichlet BC. In order to make the discussion as concrete as possible, we consider a product group $G = G_1 \times G_2$, where $G_1 = U(1)$ and G_2 is any compact simple Lie group. We choose UV-BC such that one factor group takes Neumann while the other takes Dirichlet BC. This choice is interesting because it admits a non-trivial mixed CS action, hence a mixed anomaly interpretation in the dual 4D picture. A lot of qualitative features we describe below apply to more general cases and an explicit analysis with arbitrary choice of $G \to H_0$ can be achieved straightforwardly.

In the 4D dual description, the CFT has a global $G = G_1 \times G_2$ symmetry and one factor group (either G_1 or G_2) is weakly gauged. We present both cases, one with gauged G_1 and the other with gauged G_2. With pure Neumann IR-BC, none of these symmetries are broken at the confinement scale. The anomaly inflow from the mixed CS action will get a 4D interpretation in terms of G_1-G_2 mixed anomaly, while inflow by the pure CS actions corresponds to pure G_1 and/or G_2 anomalies.

Let us choose $G_2 = SU(2)$. Any other choice of G_2 will require a very similar discussion.[16] The bulk CS action consists of two contributions: pure $U(1)$ and mixed $U(1)$-$SU(2)$. The

[16] One exceptional property of the group $SU(2)$ is that it has vanishing $d^{abc} \propto \mathrm{Tr}[T^a\{T^b, T^c\}]$ and the pure $SU(2)$ CS action vanishes identically. This feature is dual to the fact that there is no perturbative $SU(2)$ anomaly in 4D.

form of the mixed CS action can be obtained by first embedding $U(1)$ and $SU(2)$ into a simple compact Lie group $G_{\rm GUT}$. Once this is done, then the GUT gauge field A can be written as a sum $A = V + W$ in terms of the $U(1)$ gauge field V and the $SU(2)$ gauge field W. The mixed CS action can be read off from the CS action of A [129]. In terms of the *canonical* $\omega_5^{(0)}(A)$, after a couple of integrations by parts, we get (including the pure $U(1)$ CS action)

$$S_{\rm CS}[V,W] = c_1 \int_{\rm 5D} VdVdV + c_{12} \int_{\rm 5D} 3{\rm Tr}\Big[VF_W^2\Big] + d{\rm Tr}\Big[\Big(2VWdW + \frac{3}{2}VW^3\Big)\Big], \quad (4.5.9)$$

where $F_W = dW + W^2$ is the $SU(2)$ field strength 2-form. Notice that the last term, obtained as a result of integration by parts, is a brane-localized term. The virtue of this form for the CS action is that the bulk CS actions are manifestly $SU(2)$-invariant and any non-trivial $SU(2)$ transformations are from the boundary terms. It may be worth mentioning that a priori the two CS levels c_1 and c_{12} are independent and are subject to separate quantization conditions (see section 4.7).

Under $U(1)$ and $SU(2)$ transformations, the CS action changes as

$$\begin{aligned}\delta_{\alpha_1} S_{\rm CS} = {} & c_1 \int_{\rm IR} \alpha_1 d\bar{V}d\bar{V} + c_{12} \int_{\rm IR} \Big(3{\rm Tr}\Big[\alpha_1 F_{\bar{W}}^2\Big] - {\rm Tr}\Big[\alpha_1\Big(2d\bar{W}d\bar{W} + \frac{9}{2}d\bar{W}\bar{W}^2\Big)\Big]\Big) \\ & - c_1 \int_{\rm UV} \alpha_1 d\hat{V}d\hat{V} - c_{12} \int_{\rm UV} \Big(3{\rm Tr}\Big[\alpha_1 F_{\hat{W}}^2\Big] - {\rm Tr}\Big[\alpha_1\Big(2d\hat{W}d\hat{W} + \frac{9}{2}d\hat{W}\hat{W}^2\Big)\Big]\Big),\end{aligned} \quad (4.5.10)$$

$$\begin{aligned}\delta_{\alpha_2} S_{\rm CS} = {} & c_{12} \int_{\rm IR} {\rm Tr}\Big[2\bar{V}d\alpha_2\Big(d\bar{W} - 2\bar{W}^2\Big) + \frac{9}{2}\bar{V}\Big(d\alpha_2\bar{W}^2\Big)\Big] \\ & - c_{12} \int_{\rm UV} {\rm Tr}\Big[2\hat{V}d\alpha_2\Big(d\hat{W} - 2\hat{W}^2\Big) + \frac{9}{2}\hat{V}\Big(d\alpha_2\hat{W}^2\Big)\Big].\end{aligned} \quad (4.5.11)$$

Next we discuss two cases, one with gauged G_1 and the other with gauged G_2 in turn.

$G = G_1 \times G_2$ with gauged G_1

We first consider the case with Neumann UV-BC for $U(1)$ and Dirichlet UV-BC for $SU(2)$. The relevant partition function is

$$Z^{\text{g.f.}}\left[B^A\right] = \int \mathcal{D}B^i \, \mathcal{D}A_\mu|^{\hat{A}=B}_{\hat{A}:F^A=0} \, e^{iS_0+iS_{\text{CS}}}, \tag{4.5.12}$$

with S_{CS} given in eq. (4.5.9). In this case, $B^i = \hat{V}$ and $B^a = \hat{W}$. Since the full $G = G_1 \times G_2$ is unbroken on the IR brane, we need to cancel the anomaly factors there. In the 4D dual description, the c_1-term in eq. (4.5.10) corresponds to the $U(1)^3$ anomaly, while the c_{12}-terms in eq. (4.5.10) and (4.5.11) represent the mixed anomaly. One way to eliminate the IR-localized variance is to introduce IR-localized Weyl fermions charged under both $U(1)$ and $SU(2)$. The requirement is that this set is anomalous in such a way that their $U(1)^3$ and mixed anomalies cancel the CS-generated variance terms. In order to present another possibility, however, we take a slightly different path.

We can add a local counter terms $dB_4(A_0, A_1)$ to the bulk CS term in such a way that the CS action becomes invariant under an $H_0 \subset G$ transformation. In particular, this works well for the product group. Applying this to the mixed CS action, in the current example, we take $A_0 = V$ and $A_1 = A = V + W$. The shifted mixed CS action $\omega_5^{(0)} \to \tilde{\omega}_5^{(0)}(V, A) = \omega_5^{(0)}(A) - \omega_5^{(0)}(V) + dB_4(V, A)$ is then invariant under a $U(1)$ transformations. To be more precise, we first note that $\omega_5^{(0)}(A)$ contains the pure $U(1)$ CS action as well as the mixed CS action. Using a short notation for the mixed CS action as $\omega_5^{(0)}(\text{mixed}) = \omega_5^{(0)}(A) - \omega_5^{(0)}(V)$,

what we really do is

$$\begin{aligned} S_{\rm CS} &= c_1 \int \omega_5^{(0)}(V) + c_{12} \int \omega_5^{(0)}(\text{mixed}) \\ &\to c_1 \int \omega_5^{(0)}(V) + c_{12} \int \tilde{\omega}_5^{(0)}(V,A) \\ &= c_1 \int \omega_5^{(0)}(V) + c_{12} \int \Big[\omega_5^{(0)}(\text{mixed}) + dB_4(V,A)\Big]. \end{aligned} \tag{4.5.13}$$

Notice that in $\tilde{\omega}_5^{(0)}(V,A)$ there is a cancellation between two $U(1)$ CS actions, and effectively the procedure is equivalent to adding a local counter terms dB_4 to the original mixed CS action. An important property we recover is that this shifted CS action is invariant under a $U(1)$ transformation. We will write the shifted CS action as $\tilde{S}_{\rm CS} = S_{\rm CS} + S_{\rm CT}$, where $S_{\rm CT}$ is the action for the counter terms. In order to show the $U(1)$-invariance more explicitly, we first note that the explicit form of the counter term B_4 in this case is given by

$$\begin{aligned} S_{\rm CT} &= c_{\rm CT} \int_{\rm 5D} dB_4(V,A), \\ B_4(V,A) &= \text{Tr}\Big[VWdW + \frac{1}{2}VW^3\Big]. \end{aligned} \tag{4.5.14}$$

One may notice that these two terms in B_4 are exactly the same as the boundary terms in eq. (4.5.9), only the relative coefficients differ. Also, eventually, $c_{\rm CT} = c_{12}$ as is evident from eq. (4.5.13). Here, we use a separate notation temporarily to make one important point below. Explicit computations show that with counter term added, the shifted CS action

transforms according to

$$\begin{aligned}\delta_{\alpha_1}\tilde{S}_{\rm CS} &= c_1\int_{\rm IR}\ \alpha_1 d\bar{V}d\bar{V} + c_{12}\int_{\rm IR}\ \Big(1-\frac{c_{\rm CT}}{c_{12}}\Big){\rm Tr}\Big[\alpha_1 F_{\bar{W}}^2\Big] \\ &\quad - c_1\int_{\rm UV}\ \alpha_1 d\hat{V}d\hat{V} - c_{12}\int_{\rm UV}\ \Big(1-\frac{c_{\rm CT}}{c_{12}}\Big){\rm Tr}\Big[\alpha_1 F_{\hat{W}}^2\Big], \qquad (4.5.15)\\ \delta_{\alpha_2}\tilde{S}_{\rm CS} &= c_{12}\int_{\rm IR}\ \Big(2+\frac{c_{\rm CT}}{c_{12}}\Big){\rm Tr}\Big[\bar{V}d\alpha_2 d\bar{W}\Big] - c_{12}\int_{\rm UV}\ \Big(2+\frac{c_{\rm CT}}{c_{12}}\Big){\rm Tr}\Big[\hat{V}d\alpha_2 d\hat{W}\Big]. \qquad (4.5.16)\end{aligned}$$

It is observed that the mixed anomaly terms are such that in units of c_{12} the "sum" of $U(1)$ and $SU(2)$ variations is fixed, $(1-c_{\rm CT}/c_{12})+(2+c_{\rm CT}/c_{12})=3$, regardless of the size of the counter term. In contrast, the "difference" is not fixed, and in fact is proportional to the size of the counter term [127]. We also confirm that with $c_{\rm CT}=c_{12}$, the shifted *mixed* CS action is indeed invariant under $U(1)$ transformations: all the mixed anomaly is attributed to the $SU(2)$ currents.

We now introduce a set of IR-localized Weyl fermions charged under both $U(1)$ and $SU(2)$ such that their chiral anomaly cancels the CS-induced variance terms. Equivalently, we add $\Gamma_{\rm IR}\big[\bar{V},\bar{W}\big]$ which transforms as

$$\begin{aligned} e^{i\Gamma_{\rm IR}\left[\bar{V}^{\alpha_1},\bar{W}\right]} &= e^{-ic_1\int_{\rm IR}\ \alpha_1 F_{\bar{V}}^2}\ e^{i\Gamma_{\rm IR}\left[\bar{V},\bar{W}\right]}, \\ e^{i\Gamma_{\rm IR}\left[\bar{V},\bar{W}^{\alpha_2}\right]} &= e^{-ic_{12}\int_{\rm IR}\ 3{\rm Tr}\left[\bar{V}d\alpha_2 d\bar{W}\right]}\ e^{i\Gamma_{\rm IR}\left[\bar{V},\bar{W}\right]}. \end{aligned} \qquad (4.5.17)$$

Considering the UV-localized variance term, since only the $U(1)$ factor takes Neumann BC, we only need to cancel the pure $U(1)^3$ variance term. Hence, on the UV brane, we add a set of Weyl fermions charged under $U(1)$ only. The UV brane-localized effective action, upon

integrating out these fermions, is then required to transform as

$$e^{i\Gamma_{\rm UV}[\hat{V}^{\alpha_1}]} = e^{+ic_1 \int_{\rm UV} \alpha_1 F_{\hat{V}}^2} \, e^{i\Gamma_{\rm UV}[\hat{V}]}. \tag{4.5.18}$$

Moving on to the 4D dual interpretation, at the UV scale, the theory consists of a CFT sector and a set of external fermions. The CFT has a global symmetry group $G = SU(2)\times U(1)$, of which the $U(1)$ factor is weakly gauged. The external fermions are charged under the $U(1)$ gauge force. The $U(1)^3$ gauge anomaly is cancelled between the two contributions from the CFT and the external sector. There is a non-vanishing $U(1)$-$SU(2)$ mixed anomaly of ABJ type, which comes only from the CFT sector. Naively, depending on the UV regulator, the mixed anomaly can be shared among gauge and global currents. In particular, if the gauge current is anomalous, we have an issue with gauging the $U(1)$ factor. However, we added local counter terms proportional to $B_4(V, A)$, so that we moved all the mixed anomaly to the global $SU(2)$ currents. In this way, the gauged $U(1)$ symmetry is free of any mixed anomalies. Thanks to this feature, the external fermions need not carry the global $SU(2)$ quantum numbers. This is an analog of what occurs in QCD: there the anomaly computed from the Feynman diagrams (*consistent anomaly*) results in the non-conservation of both vector and axial-vector currents. However, by adding an appropriate counter term (*Bardeen's counter term*), the vector current becomes conserved and all the mixed anomaly is moved to the axial-vector current (*covariant anomaly*) [130].

As the theory RG runs to the IR scale, the CFT sector confines and the anomalies are matched by massless composite fermions. Notice that in the current example, the $U(1)$ factor is physically gauged. Nevertheless, anomaly matching arguments go through since $U(1)$ is not

a confining force. As for the $SU(2)$ part, as usual, we formally weakly gauge it, and introduce extra external spectator fermions to cancel the mixed anomaly. This mixed anomaly is also reliably reproduced by the massless composite fermions in the IR. Our holographic study of anomaly inflow, therefore, shows that in a confining gauge theory, the anomaly associated with a weakly gauged symmetry in the UV (i.e. $U(1)$ gauge anomaly carried by the composite sector) as well as the ABJ anomaly (i.e. mixed $U(1)$-$SU(2)$) are matched by the composite spectrum in the IR.

$G = G_1 \times G_2$ with gauged G_2

In this case, we take $A_0 = W$ and $A_1 = A$. The counter term $B_4(W, A)$ is similarly given by

$$B_4(W, A) = -\mathrm{Tr}\Big[2VWdW + \frac{3}{2}VW^3\Big]. \tag{4.5.19}$$

This exactly cancels the boundary terms in eq. (4.5.9) and the shifted CS action becomes manifestly $SU(2)$ invariant. Under a $U(1)$ transformation, we get

$$\delta_{\alpha_1}\tilde{S}_{\mathrm{CS}} = c_1 \int_{\mathrm{IR}} \alpha_1 F_{\bar{V}}^2 + c_{12} \int_{\mathrm{IR}} 3\mathrm{Tr}\Big[\alpha_1 F_{\bar{W}}^2\Big] - (\mathrm{UV}), \tag{4.5.20}$$

where the UV-localized variance terms are obtained from the IR-localized terms with the replacement $\bar{V}, \bar{W} \to \hat{V}, \hat{W}$. In this case, there is no gauge anomaly. All the anomalies are on the global current, either pure global $U(1)^3$ or ABJ-type mixed anomalies. On the IR, since G is preserved, we again need to include brane-localized fermions. On the UV, on the other hand, thanks to the counter term B_4, no $SU(2)$ variance term shows up and there's no

need to add anything.

The 4D interpretation is straightforward. The CFT has a global symmetry group $G = SU(2) \times U(1)$ and $SU(2)$ is weakly gauged. While there are global $U(1)^3$ and mixed anomalies, a proper counter term is added in such a way that the gauged $SU(2)$ is free of any mixed anomaly. We can again formally weakly gauge the $U(1)$ part and add spectator fermions. In the IR, when the CFT confines, composite fermions achieve 't Hooft anomaly matching, the 4D dual of IR-localized fermions. Once again, our holographic study of anomaly inflow indicates that an ABJ anomaly in the UV, when the gauged external legs are weakly interacting, is matched by the composite spectrum in the IR. While in the previous section it was $U(1)$ that was weakly gauged, here it is a non-Abelian group, namely $SU(2)$, and the same analysis can be performed with any non-Abelian group.

4.6 Spontaneously broken symmetry and Wess-Zumino-Witten action

In this section, we consider the possibility that the IR-BC breaks G down to $H_1 \subset G$. In its holographic 4D CFT dual, this corresponds to the spontaneous breaking of the symmetry group G down to H_1 by confinement. If the UV-BC is Dirichlet for all G, the bulk gauge group is dual to a *global* symmetry of the 4D CFT. On the other hand, choosing Neumann UV-BC for all G corresponds to a *weakly gauged* symmetry. A slightly less trivial case can be analyzed by choosing Dirichlet UV-BC for some of the generators, and Neumann UV-BC for the rest. For instance, if we choose Neumann UV-BC for a subgroup $H_0 \subset H_1$, and Dirichlet

for the rest, the dual picture is that of a CFT with global symmetry G spontaneously broken to H_1 by vacuum condensate, and a subgroup $H_0 \subset H_1$ is weakly gauged. This is very much like what happens in QCD. There, G is the chiral symmetry $G = SU(3)_L \times SU(3)_R$, which is broken to $H_1 = SU(3)_V$ by the quark condensate. Moreover, $U(1)_{\rm EM} \subset H_1$ is weakly gauged.

Using the result of section 4.4, we start with eq. (4.4.13), which we report below again for convenience:

$$Z^{\text{g.f.}}\Big[B^A\Big] = \int \mathcal{D}B^i \; \mathcal{Z}\Big[B^A\Big] = \int \mathcal{D}B^i \; \mathcal{D}\Sigma_1(x)\mathcal{D}A_\mu(x,z)|^{\hat{A}=B^{\Sigma_1^{-1}}}_{\bar{A}:\begin{cases} F_1^i=0 \\ \\ A_1^a=0 \end{cases}} \; e^{iS\left[A^\Lambda(x,z)\right]}, \tag{4.6.1}$$

where $\hat{\Lambda} = \Sigma_1$ and $\bar{\Lambda} = 1$. Before we delve into a detailed discussion of the two separate cases (Dirichlet UV-BC vs Neumann UV-BC) let us study the gauge transformation properties of $\mathcal{Z}\Big[B^A\Big]$. Once this is understood, it's easier to focus on a specific case.

The action consists of the gauge kinetic term, S_0, and of the CS action, which for now we set to its *canonical* version $S_{\rm CS} = c\int \omega_5^{(0)}(A)$. Also, for the sake of simplicity, we will just write $\bar{A}$ for the IR-BC. For example, IR-BC after a gauge transformation by $h \in H$ will be denoted as $\bar{A}^h$, and this means $(F_1^h)^i = 0$ for the unbroken generators and $(A_1^h)^a = 0$ for the broken ones. Under $\hat{g} \in G$ on the UV brane, $\mathcal{Z}\Big[B^A\Big]$ transforms as

$$\begin{aligned}
\mathcal{Z}\Big[\big(B^A\big)^{\hat{g}}\Big] &= \int \mathcal{D}\Sigma_1 \int \mathcal{D}A_\mu|^{\hat{A}=B^{\Sigma_1^{-1}\circ\hat{g}}}_{\bar{A}} \; e^{iS_0\left[A^\Lambda\right]+iS_{\rm CS}\left[A^\Lambda\right]} \\
&= \int \mathcal{D}\Sigma_1^{\hat{g}} \int \mathcal{D}A_\mu|^{\hat{A}=B^{(\Sigma^{\hat{g}})^{-1}\circ\hat{g}}}_{\bar{A}} \; e^{iS_0\left[A^{\Lambda^g}\right]+iS_{\rm CS}\left[A^{\Lambda^g}\right]} \\
&= \int \mathcal{D}\Sigma_1 \int \mathcal{D}A_\mu|^{\hat{A}=B^{h(\hat{g},\Sigma)\circ\Sigma^{-1}}}_{\bar{A}} \; e^{iS_0\left[A^{\Lambda^g}\right]+iS_{\rm CS}\left[A^{\Lambda^g}\right]}.
\end{aligned} \tag{4.6.2}$$

In the second line, we made a change of integration variable $\Sigma_1 \to \Sigma_1^{\hat{g}}$, and used the fact that the integration measure on G/H_1 is the left invariant Haar measure to get the third line.

We mention that we extend a given $\hat{g}(x) \approx 1 - \hat{\alpha}(x)$ on the UV brane to 5D such that $g(x, z_0) = \hat{g}$ and $g(x, z_1) = \bar{g} \in H_1$ [115]. The reason for the latter condition is simply that on the IR brane H_1 is the only unbroken gauge group. Such an extension of gauge element exists provided $\pi_4(G/H)$ is trivial, which we assume in the paper. This can be understood by first decomposing $g = \Sigma_1 h,\ \Sigma_1 \in G/H_1,\ h \in H_1$, and realizing that the desired extension is equivalent to the deformation that takes a coset element on the UV brane into a trivial element, i.e. H_1-element, on the IR brane.

In order to make the overall transformation more manifest, next we make a change of variable: $A \to A^{h(g,\Sigma)}$. The partition function becomes

$$\begin{aligned} \mathcal{Z}\Big[\big(B^A\big)^{\hat{g}}\Big] &= \int \mathcal{D}\Sigma_1 \int \mathcal{D}A_\mu|_{\hat{\bar{A}}=B^{\Sigma_1^{-1}}}\ e^{iS_0[A]+iS_{\rm CS}\left[A^{\Lambda^g \circ h}\right]} \\ &= \int \mathcal{D}\Sigma_1 \int \mathcal{D}A_\mu|_{\hat{\bar{A}}=B^{\Sigma_1^{-1}}}\ e^{iS_0[A]+iS_{\rm CS}\left[A^{g\circ\Lambda}\right]}, \end{aligned} \tag{4.6.3}$$

where we used the H_1-invariance of the IR-BC and the G-invariance of S_0. We also used $g\Lambda = \Lambda^g h(g,\Lambda)$ to rewrite the argument of the CS action. Hence, we see that the theory is not invariant under a given $g \in G$ transformation, and in particular, its non-invariance comes from the bulk CS action. In order to understand the form of the transformation, it is sufficient to study the infinitesimal version. Under $\hat{g} \approx 1 - \hat{\alpha}$, we get

$$\begin{aligned} \mathcal{Z}\Big[\big(B^A\big)^{\hat{g}}\Big] &= \int \mathcal{D}\Sigma_1 \int \mathcal{D}A_\mu|_{\hat{\bar{A}}=B^{\Sigma_1^{-1}}}\ e^{iS_0[A]+iS_{\rm CS}\left[A^\Lambda\right]+i\delta_\alpha S_{\rm CS}\left[A^\Lambda\right]} \\ &= e^{-ic\int_{\rm UV}\omega_4^{(1)}(\hat{\alpha},B)} \int \mathcal{D}\Sigma_1 \int \mathcal{D}A_\mu|_{\hat{\bar{A}}=B^{\Sigma_1^{-1}}}\ e^{iS_0[A]+iS_{\rm CS}\left[A^\Lambda\right]}\ e^{+ic\int_{\rm IR}\omega_4^{(1)}(\bar{\alpha},A_h)}. \end{aligned} \tag{4.6.4}$$

We used that $A_\mu(x,z_0)=\hat{A}_\mu=B_\mu^{\Sigma_1^{-1}}$ and $A_\mu(x,z_1)=\bar{A}_\mu=A_h$, where A_h is the restriction of the gauge field to $\mathbf{h}_1$. It may be worth mentioning that with $(A)^{g\circ\Lambda}=(A^\Lambda)^g$ we denote the whole gauge transformation of A^Λ as a single gauge connection, i.e. $\Big(A^\Lambda\Big)^g=g\Big(d+A^\Lambda\Big)g^{-1}$.

In order to restore 5D consistency, we need to modify the theory to remove the IR-localized variance term. This may be attained by adding an appropriately anomalous set of localized 4D fermions. Alternatively, the problem is solved if the subgroup H_1 is an anomaly-free embedding (AFE). Anomaly-free embedding means $\omega_5^{(0)}(A_h)=0$, i.e. the CS action (hence associated anomaly $\omega_4^{(1)}$) vanishes when the gauge field A is restricted to its H_1 part. In what follows, we take the second path.[17] In addition, we also promote $\omega_5^{(0)}(A)\to\tilde{\omega}_5^{(0)}(A_h,A)$ so that the bulk CS action is invariant under H_1 transformations. When it comes to the UV-localized variance term, the required amendment and associated dual interpretation depends on the UV-BC.

4.6.1 Purely global symmetry

When all of G satisfies Dirichlet BC on the UV brane, from a 5D perspective, there is no induced UV surface terms as a result of a gauge transformation. Hence, once we cure the IR brane-localized non-invariance, the 5D theory is consistent. Denoting the shifted CS action as $\tilde{S}_{\rm CS}=c\int\tilde{\omega}_5^{(0)}(A_h,A)$, eq. (4.6.4) becomes

$$\begin{aligned} Z^{\rm g.f.}\Big[B^A\Big]&=\int\mathcal{D}\Sigma_1\int\mathcal{D}A_\mu|_{\hat{A}}^{\hat{A}=B^{\Sigma_1^{-1}}}\ e^{iS_0[A]+i\tilde{S}_{\rm CS}\left[A^\Lambda\right]}\\ \to Z^{\rm g.f.}\Big[\Big(B^A\Big)^{\hat{\alpha}}\Big]&=e^{-ic\int_{\rm UV}\tilde{\omega}_4^{(1)}(\hat{\alpha},B)}\ Z^{\rm g.f.}\Big[B^A\Big]. \end{aligned} \tag{4.6.5}$$

[17] In fact, in the derivation of eq. (4.6.1) it was already assumed that H_1 is AFE.

We remark that while the theory is not invariant under $\hat{\alpha} \in \mathbf{k}_1$ transformations, the anomalous phase $\tilde{\omega}_4^{(1)}(\hat{\alpha}, B)$ vanishes for $\hat{\alpha} \in \mathbf{h}$ transformations.

In the dual 4D CFT, we interpret this as an anomalous global symmetry G of the CFT. More precisely, the global symmetry G is spontaneously broken at the confinement scale by the vacuum condensate, and while the unbroken group H_1 is free of anomalies (thanks to the counter term we added), the anomaly associated with G/H_1 is captured by the above phase factor. Since $H_1 \subset G$ is already anomaly-free, it can be gauged if wanted. In 5D, this is equivalent to the statement that we can freely switch the UV-BC to Neumann without needing extra modifications.

We have seen that if $H_1 \subset G$ is an AFE, no IR brane-localized state is needed. Given that the UV phase has a non-trivial anomaly, this raises a question about anomaly matching. In QCD, the chiral anomaly in the UV quark phase is matched in the IR hadronic phase by the gauged WZW term of Nambu-Goldstone bosons (NGBs) [82]. It is then natural to ask if this feature can be seen in the current framework. After all, since we take Dirichlet UV-BC for all G, all of G/H_1 describes physical NGBs in the dual 4D CFT. It can be shown that the answer to this question is yes, but with some subtleties. To see this, we first rewrite the (shifted) CS action in the partition function as

$$\tilde{\omega}_5^{(0)}\Big(\big(A^\Lambda\big)_h, A^\Lambda\Big) \to \tilde{\omega}_5^{(0)}(A_h, A) + \Big(\tilde{\omega}_5^{(0)}\Big(\big(A^\Lambda\big)_h, A^\Lambda\Big) - \tilde{\omega}_5^{(0)}(A_h, A)\Big) = \tilde{\omega}_5^{(0)}(A_h, A) + \frac{\mathcal{L}_{\text{WZW}}}{c}. \tag{4.6.6}$$

First of all, the new version is trivially equal to the original CS action. In order to see how the expression in parenthesis is indeed the wanted WZW action, we note that it vanishes

trivially as $\Sigma_1 \to 1$, and it depends only on the (UV) boundary value.[18] Hence, it satisfies two of the three conditions for it to qualify as the WZW action. For the last requirement, i.e. solving the anomalous Ward identity, it is sufficient to show that $\tilde{\omega}_5^{(0)}(A_h, A)$, as part of the partition function, is invariant under G-transformations. This is achieved rather easily. One just recalls that under an arbitrary $g \in G$ transformation, the change of the partition function is captured by $A \to A^{h(g,\Sigma_1)}$ in the CS terms. For $\tilde{\omega}_5^{(0)}(A_h, A)$ this corresponds to just $\tilde{\omega}_5^{(0)}((A_h)^{h(g,\Sigma_1)}, A^{h(g,\Sigma_1)})$, which is invariant. Therefore, the expression in parenthesis is indeed the WZW term. For the same reason, in the splitting $\tilde{\omega}_5^{(0)}(A_h, A) + \mathcal{L}_{\text{WZW}}/c$, the first term is invariant under any $g \in G$ transformation, and the non-invariance is completely encoded in the WZW term.

Crucially, in the partition function, e.g. eq. (4.6.5), the path integral variable $\Sigma_1(x)$ depends only on the 4D spacetime coordinates, and upon integrating over the bulk, we get the holographic effective action which depends on $\Sigma_1(x)$ as well as on the boundary value B. In particular, as we just showed, the WZW action only depends on the boundary value, and it can be taken out of the integral over $A_\mu(x, z)$:

$$\begin{aligned} Z^{\text{g.f.}}\Big[B^A\Big] &= \int \mathcal{D}\Sigma_1(x)\; e^{iS_{\text{WZW}}\left[B^A,\Sigma_1\right]} \int \mathcal{D}A_\mu|^{\hat{A}=B^{\Sigma_1^{-1}}}_{\bar{A}}\; e^{iS_0[A]+i\tilde{S}_{\text{CS}}[A]} \\ &= \int \mathcal{D}\Sigma_1(x)\; e^{iS_{\text{WZW}}\left[B^A,\Sigma_1\right]}\; e^{iS_{\text{h},0}\left[B^A,\Sigma_1\right]}. \end{aligned} \tag{4.6.7}$$

In the above, $S_{\text{h},0}$ is the holographic effective action obtained by integrating out the bulk degrees of freedom. With pure Dirichlet UV-BC, this action describes the chiral perturbation theory (see for example [126]) of massless NGBs. The physical NGB fields $\Sigma_1(x)$ correspond

[18] $d\Big(\tilde{\omega}_5^{(0)}\big((A^\Lambda)_h, A^\Lambda\big) - \tilde{\omega}_5^{(0)}(A_h, A)\Big) = \Omega_6(A^\Lambda) - \Omega_6(A) = 0.$

to the Wilson line of the zero mode A_5, and hence constitute the low energy degrees of freedom. From this discussion, therefore, it is clear that, in the deep IR after integrating out all massive hadronic states (i.e. integrating out the bulk in 5D), the anomaly of the global symmetry is maintained by the WZW term of NGBs.

We wish to emphasize the differences of the WZW action we obtained in the holographic context compared to the discussion in the context of $2n$-dimensional spacetime. There, the WZW term is given as $\tilde{\omega}^{(0)}_{2n+1}(A_h, A) - \tilde{\omega}^{(0)}_{2n+1}\Big((A^{\Lambda^{-1}})_h, A^{\Lambda^{-1}}\Big)$, and the non-invariance comes from the first term, while the second term is invariant. Here, on the other hand, the WZW term is given by eq. (4.6.6), and the non-invariance is from $\tilde{\omega}^{(0)}_5(A^{\Lambda}_h, A^{\Lambda})$, the naive shifted CS term being invariant. Of course, this is in part because here the $g \in G$ transformation is effectively in terms of $h(g, \Sigma_1)$.

A slightly more explicit expression for the WZW action is obtained as follows. Since we assume that H_1 is an anomaly-free embedding (AFE) in G, the d-symbol, $d^{ijk} \propto \mathrm{Tr}[\{T^i, T^j\}T^k]$, vanishes for H_1. We can write

$$\begin{aligned} \omega^{(0)}_5(A^{\Lambda}) &= \tilde{\omega}^{(0)}_5(0, A^{\Lambda}) = \tilde{\omega}^{(0)}_5(\Lambda^{-1}d\Lambda, A) \\ &= \omega^{(0)}_5(A) - \omega^{(0)}_5(\Lambda^{-1}d\Lambda) + dB_4(\Lambda^{-1}d\Lambda, A). \end{aligned} \tag{4.6.8}$$

To get the second equality, we used $\tilde{\omega}^{(0)}_{2n+1}((A_h)^g, A^g) = \tilde{\omega}^{(0)}_{2n+1}(A_h, A)$ with $g = \Lambda^{-1}$. The WZW action then is obtained to be

$$S_{\mathrm{WZW}}[\Sigma_1, B]/c = -\int_{5D} \omega^{(0)}_5(\Lambda^{-1}d\Lambda) + \int_{\partial(5D)} B_4\Big(\Lambda^{-1}d\Lambda, A\Big) + B_4\Big((A^{\Lambda})_h, A^{\Lambda}\Big) - B_4(A_h, A). \tag{4.6.9}$$

We can use this to extract the pure NGB WZW terms. For this, we just set $A = 0$. Since B_{2n} vanishes if one or both of the arguments are set to zero, we get

$$S_{\text{WZW}}[\Sigma_1, B = 0]/c = -\int_{5D} \omega_5^{(0)}\left(\Lambda^{-1}d\Lambda\right) + \int_{\partial(5D)} B_4((\Lambda d\Lambda^{-1})_h, \Lambda d\Lambda^{-1}). \tag{4.6.10}$$

For small $\xi(x)^a$, we expand $\Sigma_1(x) = e^{-\xi(x)} \approx 1 - \xi^a(x)X^a$, and in particular, $\Sigma_1 d\Sigma_1^{-1} = d\xi + \mathcal{O}(\xi^2)$. The point is that infinitesimally, $\Sigma_1 d\Sigma_1^{-1} = d\xi \in \mathbf{k}$ (i.e. $(\Lambda d\Lambda^{-1})_h = 0$), and the B_4 term does not contribute. Using $U = \Lambda^{-1}d\Lambda \approx -d\xi$, straightforward steps lead to

$$\begin{aligned} S_{\text{WZW}}[\xi, B = 0]/c &= -(-1)^5\frac{1}{10}\int_{5D} \text{Tr}\left[(d\xi)^5\right] + \mathcal{O}(\xi^6) \\ &= -\frac{1}{10}\int_{\text{UV}} \text{Tr}\left[\xi(x)(d\xi(x))^4\right] + \mathcal{O}(\xi^6). \end{aligned} \tag{4.6.11}$$

A direct comparison with the existing literature such as [131] can be made by noting that for chiral symmetry, the parametrization $\Sigma = e^{-2i\xi}$ is used (note the factor of 2). Also, as we show in section 4.7, the overall coefficient consistent with the quantization condition is $c = \frac{\kappa}{24\pi^2}$ with $\kappa \in \mathbb{Z}$ (see also [129, 132]). Taking into account the factor 2^5 from the difference in GB parametrization, we get

$$S_{\text{WZW}}[\xi, B = 0] = -\frac{2}{15\pi^2}\kappa\int_{\text{UV}} \text{Tr}\left[\xi(x)(d\xi(x))^4\right] + \mathcal{O}(\xi^6), \qquad \xi = \frac{\Pi(x)}{F_\pi}. \tag{4.6.12}$$

This agrees with [131].

4.6.2 Gauged symmetry

In this section, we gauge some part of the group G, and analyze the resulting anomaly inflow. This is done by taking Neumann UV-BC for some of the generators of $\mathbf{g}$. We will first consider the case in which we only gauge a subgroup $H_0 \subset H_1$. This is an analog of QCD, and we will obtain a *gauged* version of the WZW action as the low energy effective action, as we expect. The gauged WZW action includes terms that match ABJ and 't Hooft anomalies [82]. We then move on to analyze the most general possibility. We consider a situation in which a subgroup $H_0 \subset G$ which is not a proper subset of H_1 is gauged. This is a prototypical situation for dynamical symmetry breaking of the electroweak group of the SM [90, 133]. Here, we focus on the topological terms in such a theory, and show, among other things, that the (would-be) NGBs associated with the gauged generators can be removed by means of field redefinitions.

Gauging a subgroup $H_0 \subset H_1$: analog of QCD

Let us first consider the case in which the UV-BC for the subgroup $H_0 \subset H_1 \subset G$ is taken to be Neumann, while the rest G/H_0 is set to be Dirichlet. The relevant partition function is eq. (4.6.1) with the shifted CS action and $B_\mu^i \in \mathbf{h}_0$. As we discussed in section 4.6.1, the shifted CS action is invariant under any H_1 transformations. This in turn implies that under any gauged $H_0 \subset H_1$ transformations, the shifted action is automatically invariant as well. Therefore, we do not need to add any UV brane-localized effective action: with $\omega_5^{(0)}(A) \to \tilde{\omega}_5^{(0)}(A_h, A)$ the 5D theory is consistent. Using eq. (4.6.4), the change in the

partition function under an infinitesimal G/H_1 transformation $\hat{\gamma} \in \mathbf{k}_1$ is found to be

$$\begin{aligned} Z^{\text{g.f.}}\Big[(B^a)^{\hat{\gamma}}\Big] &= \int \mathcal{D}\Big(B^i\Big)^{\hat{\gamma}} \int \mathcal{D}(\Sigma_1)^{\hat{\gamma}} \mathcal{D}A_\mu|_{\hat{A}}^{\hat{A}=B^{\left(\Sigma_1{}^{\hat{\gamma}}\right)^{-1}\circ\hat{\gamma}}} \; e^{iS_0[A]+\tilde{S}_{\text{CS}}\left[A^\Lambda(x,z)\right]} \\ &= \int \mathcal{D}B^i \int \mathcal{D}\Sigma_1 \mathcal{D}A_\mu|_{\hat{A}}^{\hat{A}=B^{h(\hat{\gamma},\Sigma_1)\circ\Sigma_1^{-1}}} \; e^{iS_0[A]+\tilde{S}_{\text{CS}}\left[A^\Lambda(x,z)\right]}. \end{aligned} \tag{4.6.13}$$

Here, we changed the integration variables $B^i \to (B^i)^{\hat{\gamma}}$ and $\Sigma_1 \to \Sigma_1^{\hat{\gamma}}$ and used the invariance of the left-invariant Haar measure. In the second line, we used $g\Sigma_1 = \Sigma_1^g \, h(g,\Sigma_1)$. To extract the anomaly phase, we further redefine $A_\mu \to A_\mu^{h(\hat{\gamma},\Sigma_1)}$ and get

$$\begin{aligned} Z^{\text{g.f.}}\Big[(B^a)^{\hat{\gamma}}\Big] &= \int \mathcal{D}B^i \; e^{-ic\int_{\text{UV}} \tilde{\omega}_4^{(1)}\left(\hat{\gamma},B^i,B^a\right)} \int \mathcal{D}\Sigma_1 \mathcal{D}A_\mu|_{\hat{A}}^{\hat{A}=B^{\Sigma_1^{-1}}} \; e^{iS_0[A]+\tilde{S}_{\text{CS}}\left[A^\Lambda(x,z)\right]} \\ &= \int \mathcal{D}B^i \; e^{-ic\int_{\text{UV}} \tilde{\omega}_4^{(1)}\left(\hat{\gamma},B^i,B^a\right)} \; \mathcal{Z}\Big[B^A\Big]. \end{aligned} \tag{4.6.14}$$

Alternatively, we can write this directly in terms of the WZW action, where the partition function is expressed as

$$Z^{\text{g.f.}}\Big[B^A\Big] = \int \mathcal{D}B^i \int \mathcal{D}\Sigma_1 \; e^{iS_{\text{WZW}}\left[B^A,\Sigma_1\right]} \; e^{iS_{\text{h},0}\left[B^A,\Sigma_1\right]}. \tag{4.6.15}$$

Recall that $S_{\text{h},0}$ is the holographic effective action and is invariant under any G transformation (see eq. (4.6.7)): any variance comes from the WZW action. Eq. (4.6.14) turns into

$$Z^{\text{g.f.}}\Big[(B^a)^{\hat{\gamma}}\Big] = \int \mathcal{D}B^i \; e^{-ic\int_{\text{UV}} \tilde{\omega}_4^{(1)}\left(\hat{\gamma},B^i,B^a\right)} \int \mathcal{D}\Sigma_1 \; e^{iS_{\text{WZW}}\left[B^A,\Sigma_1\right]} \; e^{iS_{\text{h},0}\left[B^A,\Sigma_1\right]}. \tag{4.6.16}$$

This form of transformation makes the following 4D dual interpretation very transparent.

In the 4D dual CFT, we have a global symmetry G which is broken down to $H_1 \subset G$ by confinement. In addition, $H_0 \subset H_1$ is weakly gauged. In the strongly interacting CFT,

we regulate the UV-divergences such that H_1 is anomaly-free. The advantage of such a choice is that the gauged symmetry H_0 is automatically anomaly-free. However, there can still be anomalies in global currents. In particular, we can have mixed anomalies among global and gauged currents as well as pure global anomalies. Thanks to the proper local counter terms added (i.e. choice of UV-regulator), the mixed anomalies come entirely from the global currents. Under a global transformation $\hat{\gamma} \in \mathbf{k}_1$, the CFT is anomalous and the anomaly is captured by the phase factor in eq. (4.6.16). We emphasize that the anomaly factor depends on both the classical source B^a and the gauged dynamical field B^i. In detail, this single anomaly phase contains both pure global anomalies as well as mixed global-gauge anomalies. This of course is equivalent to the statement that the WZW action contains local operators that match chiral anomalies of the UV phase [82]. For example, in QCD, the gauged WZW Lagrangian contains $\mathcal{L}_{\text{WZW}} \supset n\frac{e^2}{24\pi^2 F_\pi}\pi^0 F\tilde{F}$, which on one hand explains the $\pi^0 \to \gamma\gamma$ decay, and on the other hand, reproduces the ABJ anomaly when the quantization condition $n = N_c = 3$ is chosen. The QCD WZW Lagrangian also contains $\mathcal{L}_{\text{WZW}} \supset -\frac{2}{3}ie\frac{n}{\pi^2 F_\pi^3}\epsilon^{\mu\nu\rho\sigma}A_\mu\partial_\nu\pi^+\partial_\rho\pi^-\partial_\sigma\pi^0$, which in turn reproduces the QCD VAAA anomaly for $n = N_c = 3$. Once we specify G, H_1, and H_0, our formalism allows explicit computations of all of these.

General analysis

In this section, we consider the most general possibility in which $H_0 \subset G$ is gauged and G is spontaneously broken to H_1. The transformation of the partition function is obtained through a series of similar steps as in section 4.6.2. The final result has the same form as eq. (4.6.14) but the transformation parameter $\hat{\gamma}$ is not constrained to be just $\hat{\gamma} \in \mathbf{k}_1$ and

instead takes any value $\hat{\alpha} \in \mathbf{g}$. There are three different kinds of transformations we need to consider separately. First, under $\hat{\beta} \in \mathbf{h}_1$, the partition function is invariant. As a result, there is no UV-brane surface terms associated with these transformations, hence no "remedy" is needed. Second, we can perform a pure global transformation $\hat{\gamma}$ which is not part of $\mathbf{h}_1$ ($G/(H_0 \cup H_1)$ transformations). For these transformations, the partition function changes in exactly the same manner as in section 4.6.2 and in the 4D dual description we get anomalies in the global currents. Finally, we can consider $\hat{\delta} \in \mathbf{h}_0$ which is not part of $\mathbf{h}_1$ ($H_0 \setminus H_0 \cap H_1$ transformations). For these transformations, we get UV-localized anomaly factors, and given that these generators are not broken on the UV brane, we need to cure this problem. This is done by inserting

$$e^{i\Gamma_{\rm UV}[B^i]} \equiv \int \mathcal{D}\psi \mathcal{D}\bar{\psi}\; e^{iS_{\rm UV}[B^i,\psi,\bar{\psi}]} \tag{4.6.17}$$

into the partition function. As usual, we require it to transform so as to cancel the variance of the third kind (i.e. $\hat{\delta}$ transformations). Specifically, $\Gamma_{\rm UV}[B^i]$ is invariant under both H_1 and $G/(H_0 \cup H_1)$ transformations, whilst it changes under a $H_0 \setminus H_0 \cap H_1$ transformation in an opposite way to the way the bulk action does. The final form of the consistent partition function is then written as

$$Z^{\rm g.f.}\left[B^A\right] = \int \mathcal{D}B^i\; e^{i\Gamma_{\rm UV}[B^i]} \int \mathcal{D}\Sigma_1 \mathcal{D}A_\mu|^{\hat{A}=B^{\Sigma_1^{-1}}}_{\tilde{A}}\; e^{iS_0[A]+i\tilde{S}_{\rm CS}\left[A^\Lambda\right]}. \tag{4.6.18}$$

This is invariant under any $H_0 \cup H_1$ transformations, although under an infinitesimal transformation $g \approx 1 - \hat{\gamma} \in G/(H_0 \cup H_1)$ it changes as

$$Z^{\text{g.f.}}\left[(B^a)^{\hat{\gamma}}\right] = \int \mathcal{D}B^i \; e^{i\Gamma_{\text{UV}}\left[B^i\right]} \; e^{-ic\int_{\text{UV}} \tilde{\omega}_4^{(1)}(\hat{\gamma},B^i,B^a)} \int \mathcal{D}\Sigma_1 \mathcal{D}A_\mu|_{\hat{A}}^{\hat{A}=B^{\Sigma_1^{-1}}} \; e^{iS_0[A]+i\tilde{S}_{\text{CS}}\left[A^\Lambda\right]}. \tag{4.6.19}$$

We are now ready to discuss the dual 4D CFT description. The UV theory consists of the CFT sector and an external sector of Weyl fermions. The subgroup H_0 of G is weakly gauged. In the IR, the CFT sector confines and this breaks G down to a subgroup H_1. Unlike what happens in QCD, this unbroken subgroup H_1 does not need to be aligned with the gauged H_0, a typical situation occurring in dynamical symmetry breaking. We added proper local counter terms to the theory so that the UV-regulator preserves the H_1-symmetry. For this reason, the external fermions in the UV theory form an anomaly-free set under the $H_0 \cap H_1$ gauge forces.

The anomaly story of this theory is rather rich: the anomaly phase in eq. (4.6.19) includes several different classes of anomalies. First, we have the gauge anomaly associated with the unbroken gauge symmetry $H_0 \cap H_1$. The UV CFT is free of this gauge anomaly since the UV-regulator respects the $H_0 \cap H_1$ symmetry (i.e $\omega_5^{(0)}(A) \to \tilde{\omega}_5^{(0)}(A_{\mathbf{h}_1}, A)$). For this reason, the external fermions do not carry any $H_0 \cap H_1$ anomalies. Second, the UV CFT has non-trivial anomalies in the global symmetry G/H_0. However, a subset $H_1 \setminus H_0 \cap H_1 \subset G/H_0$ is anomaly free for the same reason why the gauged $H_0 \cap H_1$ is anomaly free. The remaining global symmetry $G/(H_0 \cup H_1)$ is, however, anomalous and the pure global anomaly or 't Hooft anomaly (e.g. anomaly in $\langle JJJ \rangle$ with all global currents J) is included in the phase in eq. (4.6.19). Third, the UV CFT has non-vanishing gauge anomalies for the broken part

$H_0 \setminus H_0 \cap H_1$. This is cancelled by the chiral anomaly of the external fermions. We see that, generically, external fermions are charged under the gauged H_0, and while they carry non-trivial anomalies under the broken part $H_0 \setminus H_0 \cap H_1$, they form an anomaly-free set under $H_0 \cap H_1$. The anomaly phase in eq. (4.6.19) hence does not contain these anomalies. In fact, we need to look at the $\hat{\delta}$-variation to probe these, and the anomaly phase from the bulk (CFT) is exactly cancelled by that of $\Gamma_{\rm UV}$ (external fermions). There are several mixed anomalies we want to discuss. One of them is the mixed anomaly among gauged $H_0 \cap H_1$ and global $G/(H_0 \cup H_1)$ currents and is present in eq. (4.6.19). The local counter terms added to the theory result in the gauged current being conserved, and all the mixed anomaly is moved to the global currents. Next, there is a mixed anomaly among the gauged $H_0 \setminus H_0 \cap H_1$ and the global $G/(H_0 \cup H_1)$ currents, and eq. (4.6.19) includes these in principle. The requirement is that the addition of external fermions cancels any possible mixed anomaly in the gauged currents, and again all the mixed anomalies are stored in the global currents. In general, there may be also a mixed anomaly among gauged $H_0 \setminus H_0 \cap H_1$ and global $H_1 \setminus H_0 \cap H_1$, and we need to make sure that the mixed anomaly is all attributed to the global symmetry. This, and some of the above mentioned conditions, may require extra local counter terms on the UV brane.

When the CFT sector confines in the IR, the gauge bosons associated with the broken generators acquire mass via the "technicolor" mechanism. Hence, these massive gauge bosons are integrated out in the IR, leaving only massless gauge bosons of $H_0 \cap H_1$. In addition, we have physical NGBs associated with $G/(H_0 \cup H_1)$. The "would-be" NGBs of $H_0 \setminus H_0 \cap H_1$ are eaten by the massive gauge bosons and removed in the unitary gauge. What happens to the external fermions? We recall that they couple to the broken gauge generators, and we

think that they will also become massive and get integrated out. On the other hand, in the IR, we do not have any massless composite fermions in the spectrum, a dual picture of the absence of IR brane-localized fermions in the 5D. Hence, the anomalies of the UV theory described above must be matched by the WZW action made of the physical NGBs and the massless gauge bosons. Explicit confirmation of this deserves a separate designated study and we leave it for future works.

Removing the "would-be" NGBs

As already mentioned in the previous section, the NGBs associated with the broken *gauged* generators are a gauge artifact and can be eliminated in the unitary gauge. In this section, we confirm that this expectation is fulfilled in our holographic description of anomaly inflow. In fact, we show that this is achieved via field redefinitions, or change of integration variables, which is an allowed operation for path-integrated, i.e. dynamical, fields. Recall that the boundary value B for the Dirichlet UV-BC corresponds to a classical source in the 4D dual theory. On the other hand, the boundary value B for the Neumann UV-BC is dual to a dynamical gauge field and is path-integrated. Therefore, we see that for the latter case, the integration field variable can be redefined so as to eliminate the corresponding Σ_1-dependence. Such freedom, however, is absent for the purely global symmetry. In order to illustrate the point in a clean setup, instead of dealing with the most general case, in this section we consider the pure Neumann UV-BC.

Since all of the G generators are gauged, none of Σ_1 corresponds to physical degrees of freedom. Therefore, we should be able to entirely remove the Σ_1-dependence. We first note

that for small NGB field ξ, we can expand $\Sigma_1 \approx 1 - \xi$ and get

$$\begin{aligned}\tilde{S}_{\rm CS}\Big[A^\Lambda\Big] &= c\int_{\rm 5D}\tilde{\omega}_5^{(0)}\Big(\big(A^\Lambda\big)_h, A^\Lambda\Big)\\ &\approx c\int_{\rm 5D}\tilde{\omega}_5^{(0)}(A_h, A) + c\int_{\rm 5D} d\tilde{\omega}_4^{(1)}(\xi, A_h, A).\end{aligned} \tag{4.6.20}$$

Using this, the partition function can be expressed as[19]

$$Z^{\rm g.f.} = \int \mathcal{D}\Sigma_1\mathcal{D}B\; e^{i\Gamma_{\rm UV}[B]}\; e^{-ic\int_{\rm UV}\tilde{\omega}_4^{(1)}\left(\hat{\xi},B^{\Sigma_1^{-1}}\right)}\; \mathcal{D}A_\mu|^{\hat{A}=B^{\Sigma_1^{-1}}}_{\hat{A}}\; e^{iS_0[A]+i\tilde{S}_{\rm CS}[A]}. \tag{4.6.21}$$

The Σ_1-dependence can be eliminated by a change of variable, $B \to B^{\Sigma_1}$. Under this we get

$$\begin{aligned}Z^{\rm g.f.} &= \int \mathcal{D}\Sigma_1\mathcal{D}B^{\Sigma_1}\; e^{i\Gamma_{\rm UV}[B^{\Sigma_1}]}\; e^{-ic\int_{\rm UV}\tilde{\omega}_4^{(1)}(\hat{\xi},B)}\; \mathcal{D}A_\mu|^{\hat{A}=B}_{\hat{A}}\; e^{iS_0[A]+i\tilde{S}_{\rm CS}[A]}\\ &= \int \mathcal{D}\Sigma_1\mathcal{D}B\left(e^{iG_{\rm UV}\left[\hat{\xi},B\right]}\; e^{i\Gamma_{\rm UV}[B]}\right) e^{-ic\int_{\rm UV}\tilde{\omega}_4^{1}(\hat{\xi},B)}\; \mathcal{D}A_\mu|^{\hat{A}=B}_{\hat{A}}\; e^{iS_0[A]+i\tilde{S}_{\rm CS}[A]},\end{aligned} \tag{4.6.22}$$

where $G_{\rm UV}\Big[\hat{\xi}, B\Big]$ is the anomaly functional of the external sector. Hence, we observe that the "would-be" NGB dependence is completely encoded in the two anomaly factors associated with the CFT and external degrees of freedom. In particular, we see that, provided the gauge anomaly cancels, the entire Σ_1-dependence disappears from the whole integrand, and the overall immaterial Σ_1-integral can be dropped. In other words, provided the gauged group is free of anomalies (hence suitable for gauging to begin with), the NGBs are unphysical and removable.

[19] Recall that Λ is the 5D extension of the 4D Σ_1. Likewise, given a 4D $\hat{\xi}$ we extend it to 5D so that $\xi_{\rm UV} = \hat{\xi}$ and $\xi_{\rm IR} = 0$.

4.7 Quantization conditions

The coefficient of the 5D CS action, called CS level, is subject to quantization conditions. A quick and easy way to derive this is by requiring that the variance of the 5D CS action under a gauge transformation is cancelled by the chiral anomaly of the 4D Weyl fermions localized on the boundaries. For simplicity we focus on a $U(1)$ CS theory (see also [132]). We first recall that the *consistent* chiral anomaly[20] takes the form

$$\partial_\mu J^\mu_L = -\frac{1}{48\pi^2} F^{\mu\nu}_L \tilde{F}_{L\mu\nu}, \qquad \partial_\mu J^\mu_R = +\frac{1}{48\pi^2} F^{\mu\nu}_R \tilde{F}_{R\mu\nu}, \tag{4.7.2}$$

with $J^\mu_L = \bar{\psi}_L \gamma^\mu \psi_L$ and $J^\mu_R = \bar{\psi}_R \gamma^\mu \psi_R$. When the Weyl fermions ψ_L and ψ_R have a vector-like coupling to the gauge field, $F_{L\mu\nu} = F_{R\mu\nu}$. The main point here is that the chiral anomaly takes value in units of $\frac{1}{48\pi^2}$. The $U(1)$ CS theory in the bulk takes the form

$$S_{\rm CS} = c \int_{5D} AdAdA. \tag{4.7.3}$$

[20] This is the form of the anomaly one gets from the triangle diagram. It is called *consistent* anomaly since the result is consistent with Feynman diagram computations. In the presence of a single Weyl fermion, this is the only possible form. However, when the theory includes both LH and RH Weyl fermions, one can choose to decompose the currents in *vector* and *axial-vector*. In this case, there is an ambiguity in the form of the anomalous Ward identity. This ambiguity is due to possible local counter term(s) one can add to the theory. Equivalently, it is related to the UV regulator one chooses. A counter term of the form $S_{\rm CT} = \frac{1}{6\pi^2} \int d^4x \epsilon_{\mu\nu\rho\sigma} A^\mu V^\nu \partial^\rho V^\sigma$ can make the vector current conserved, while all of the anomaly is "moved" to the axial current:

$$\partial_\mu J^\mu_V = 0, \qquad \partial_\mu J^\mu_A = \frac{1}{8\pi^2}\left(F^{\mu\nu}_V \tilde{F}_{V\mu\nu} + \frac{1}{3} F^{\mu\nu}_A \tilde{F}_{A\mu\nu} \right). \tag{4.7.1}$$

This form of the anomaly is called *covariant* anomaly since the theory is now invariant under the vector symmetry.

Under gauge transformations, we get

$$\delta S_{\rm CS} = \frac{c}{2}\Big(\int_{\rm IR} d^4x \bar{\alpha} F\tilde{F} - \int_{\rm UV} d^4x \hat{\alpha} F\tilde{F}\Big). \tag{4.7.4}$$

Thus, the cancellation of these variance terms by κ 4D Weyl fermions requires

$$c = \frac{\kappa}{24\pi^2}, \qquad \kappa \in \mathbb{Z}. \tag{4.7.5}$$

For instance, for $\kappa > 0$, the UV-localized variance term can be canceled by κ RH fermions, while the IR-localized terms can be canceled by κ LH fermions.

When the IR-BC is chosen so that the dual 4D picture describes spontaneous symmetry breaking, the relevant quantization condition comes from the argument by Witten in [82] (see also [115]). A proper reinterpretation of Witten's argument in the context of anomaly inflow may be given as follows. First, we recall the instances in which we required the extension of the coset element from a map defined on 4D spacetime S^4 to the 5D bulk. For example, in the derivation of the gauge-fixed holographic effective action, we needed to make a change of variable with the property that $\tilde{\Lambda}_{\rm UV} = 1$ and $\tilde{\Lambda}_{\rm IR} = \Sigma_1 \in G/H_1$. Consequently, we extended the 4D $\Sigma_1(x) \in G/H_1$ to a 5D object $\Lambda(x,z)$ such that $\Lambda_{\rm UV} = \Sigma_1(x)$ and $\Lambda_{\rm IR} = 1$. Also, for any $g \in G$ transformation on the source field B, we assumed the existence of an extension to an element of the bulk gauge group G_B. By a decomposition $g(x) = \gamma(x)h(x), \gamma \in G/H_1, h \in H_1$, such an extension is equivalent to the possibility of deforming $\gamma(x)$ at the UV brane to 1 (i.e. H_1-element) at the IR brane. All these deformations/extensions have to do with the homotopy group $\pi_4(G/H_1)$. When $\pi_4(G/H_1) = 0$, we can extend $\Sigma_1(x)$ to D_5. In what

follows, we will assume this is the case.[21] Even when $\pi_4(G/H) = 0$, there is an important question. Namely, one may consider two different extensions, $\Lambda_1(x, z)$ and $\Lambda_2(x, z)$, and the physics should be the same regardless of the extension chosen. Suppose Λ_1 is defined on D_5 and Λ_2 is defined on D'_5, with the spacetime manifold S^4 being the boundary of both D_5 and D'_5. The equivalence of the two extensions then imposes a quantization condition for the bulk CS action. Calling $S_{\text{CS}i}$ the CS action with Λ_i, $i = 1, 2$, the statement that the quantum action can be multi-valued only if the changes are integral multiples of 2π yields

$$e^{i(S_{\text{CS}1} - S_{\text{CS}2})} = e^{ic\left(\int_{D_5} \omega_5^{(0)} - \int_{D'_5} \omega_5^{(0)}\right)} = e^{ic\int_{S^5} \omega_5^{(0)}} = e^{i2\pi n}. \tag{4.7.6}$$

Therefore, if $\pi_5(G/H_1)$ is trivial, then there is no quantization condition: all choices of $\Lambda(x, z)$ are (topologically) equivalent. If, on the other hand, $\pi_5(G/H_1) \neq 0$, we are forced to choose the coefficient c such that the above requirement is fulfilled. In the context of 4D QCD chiral symmetry breaking, $G = SU(3) \times SU(3)$ and $H_1 = SU(3)_V$, the fifth homotopy group is $\pi_5(G/H_1) = \mathbb{Z}$ and Witten gave the correct normalization for the base 5-sphere [82].[22]

In the holographic description of anomaly inflow, we seem to have another way to determine the level c. Namely, we may use the fact that a single parameter c determines the anomaly of the UV and IR branes by the holographic realization of anomaly matching. Furthermore, changing UV and IR BC is equivalent to gauging (UV-BC) and spontaneous breaking (IR-BC), and it is conceivable that the "norm" of anomaly should not change under these "deformations". For instance, given the bulk CS action, if we choose (partially)

[21] As argued in [128], when $\pi_4(G/H_1)$ is non-trivial, then we can deform $\Sigma_1(x)$ to $\Sigma_a(x)$, a fixed representative of each homotopy class. Even in this case, the WZW action can still be defined with the same conclusions.

[22] Any other element of the $\pi_5(G/H_1)$ is an integer multiple of the base sphere, hence once the integral over the base sphere is fixed, the remaining ones are just integer multiples of the value for the base sphere.

Neumann UV-BC, cancellation of the CS induced anomaly by the UV-localized Weyl fermions fixes the coefficient c. Then, if we choose IR-BC so that G is broken to H_1, we get the WZW action with pre-determined coefficient. In fact, we used this to fix c to be $c = \frac{\kappa}{24\pi^2}$ in section 4.6.1, and successfully obtained the known normalization for the pure NGB WZW action. Furthermore, switching the UV-BC to a different one afterwards leads to a deformed theory with a fixed CS level.

4.8 Conclusions

In this paper, we systematically investigated the perturbative anomaly inflow by the bulk Chern-Simons (CS) theory in five-dimensional anti-de Sitter spacetime (AdS_5). When the bulk geometry is AdS_5, we are granted a holographic dual CFT description, in addition to the usual bulk–boundary interplay. The physics becomes especially rich and interesting once we introduce 3-branes. The UV brane allows us to incorporate "weakly gauging" of the global symmetry and as such the dual CFT possesses Adler, Bell, and Jackiw (ABJ) anomalies [73, 74] as well as 't Hooft anomalies [77]. On the other hand, the phenomena of "confinement" and "spontaneous symmetry breaking" can be introduced once the IR brane is added. Therefore, through its dual description in terms of strongly coupled 4D CFT, anomaly inflow in the presence of UV and IR branes in AdS background captures a variety of features realized by fermion anomalies in quantum field theories. A holographic approach to anomaly inflow turns out to provide an especially economic framework to organize and cover various facets of the fermion anomaly. Namely, one first makes a choice of bulk gauge group, based on the interest in Abelian vs non-Abelian anomaly, and anomaly of a single group vs mixed

anomaly. Then, distinctions between the possible UV and IR BC integrate in a unified setup most, if not all, characteristics of chiral anomalies in confining gauge theories.

We showed that the choice of pure Neumann boundary conditions on the IR brane realizes 't Hooft anomaly matching holographically. We found that both ABJ (Neumann UV-BC) and 't Hooft (Dirichlet UV-BC) anomalies are matched by the composite fermions once 5D gauge invariance is restored by IR brane-localized 4D Weyl fermions. In the case of Neumann UV-BC, the necessary UV brane-localized fermions that restore 5D gauge invariance are physical spectator states. For Dirichlet UV-BC, as in the standard 't Hooft argument for the anomaly matching [77], formally weakly gauging the global symmetry group is achieved by simply switching the Dirichlet UV-BC to Neumann. Once this change is made, then the existence of spectator fermions is required by 5D gauge invariance. Based on our findings that both ABJ and 't Hooft anomalies are matched by composite fermions when the symmetry G is not broken on the IR brane, we infer that anomalies that inflow from the bulk CS theory are necessarily free of mixed anomalies with the confining gauge group of the 4D dual CFT. In the case of a mixed CS theory, taking $U(1) \times SU(2)$ as an example, we demonstrated that proper local counter terms can be added to the bulk CS action so that the mixed $U(1)$-$SU(2)$ anomaly is transferred between $U(1)$ and $SU(2)$ currents. We explicitly showed the form of local counter terms whose role is to attribute the entire mixed anomaly to either the $U(1)$ or $SU(2)$ currents.

We then worked out in detail the case of IR-BC such that the bulk gauge group G is broken down to a subgroup H_1. This choice is dual to a spontaneously broken global symmetry of the CFT. By first considering pure Dirichlet UV-BC (purely *global* symmetry of the CFT), we described how the Wess-Zumino-Witten action [81, 82] naturally arises from

the bulk CS action. In particular, we argued that unlike in the case of Neumann IR-BC, 5D gauge invariance does not require any IR brane-localized modes. Nevertheless, anomaly matching occurs via modes which are delocalized in the entire bulk. These modes, described as Wilson lines along the fifth direction, are indeed Goldstone bosons (GB) of spontaneously broken global symmetry, confirming our expectation based on the standard situation in QCD. When some part of G is weakly gauged, by taking Neumann UV-BC, we discussed how our formulation leads to a unified description of both ABJ and 't Hooft anomalies. In particular, in such a case, we showed explicitly that the "would-be" GBs can be completely removed by means of field redefinitions. This matches the observation that the source fields for the weakly gauged symmetry become dynamical, and the associated GBs are eaten and become longitudinal modes of the gauge bosons of broken generators. In 5D, this is realized by the fact that the sources are path-integrated over once the UV-BC are chosen as Neumann, and this allows for the possibility of performing a change of variable. We also studied a very general case: G broken down to H_0 by UV-BC and G broken down to H_1 by IR-BC. This is a prototypical setup for models of dynamical symmetry breaking, in which a symmetry group G is spontaneously broken to a subgroup H_1 and in addition another subgroup H_0 (not necessarily aligned with H_1) is weakly gauged.

Finally, we discussed the issue of quantization condition for the CS level. We described how such a requirement arises as an anomaly cancellation condition between brane-localized fermions and the bulk CS term when the BC is Neumann. On the other hand, when the BC is Dirichlet, we have reformulated Witten's argument [82] in the context of anomaly inflow in AdS_5 and shown that it indeed agrees with the condition obtained from Neumann BC. Since two distinct 4D theories with unbroken vs broken symmetry correspond to the same

bulk theory in 5D with different BC, we speculated that the quantization condition of CS level might be insensitive to these "deformations" of the theory (i.e. changes of BC). In this sense, our analysis opens up the possibility of fixing the level for one choice of BC, and then studying the theory with different BC and pre-determined normalization condition.

Chapter 5

Neutron Star Mergers Chirp About Vacuum Energy

5.1 Introduction

The recent observations of gravitational waves (GW's) from the merger of neutron stars (NS's) by LIGO/Virgo [134] along with the corresponding electromagnetic observations of the resulting kilonova have reverberated across most areas of physics and astronomy. From the point of view of particle physics the most important consequence of GW170817 and future merger events is our new ability to directly examine the properties of the QCD matter forming the inner layers of NS's, allowing us to use NS's as laboratories for fundamental physics [135–137]. This might also open up new avenues to testing the gravitational properties of vacuum energy (VE) which may also get at the heart of some of the deepest puzzles in fundamental physics [138].

It has long been speculated that there may be a new phase of nuclear matter at the core

of the NS's [139]. If such a phase indeed exists it is expected to be accompanied by a jump in VE [140] of order $\Lambda_{\rm QCD}^4$ (where $\Lambda_{\rm QCD} \sim 200\,{\rm MeV}$ is the usual QCD scale) making NS's the only known objects where VE might make up a non-negligible fraction of the total mass. Therefore studies of the interior structure of NS's can also probe the gravitational properties of VE, possibly shedding light on some of the most interesting open questions in physics: it could provide verification of the equivalence principle for VE. This would be the first test independent of those obtained from the cosmic acceleration of the Universe. Acceleration of the Universe provides information on VE in the low-temperature low density phase of the SM, while NS's could probe a low temperature but very high density phase if it exists in their cores. This could allow us to isolate the QCD contribution to ordinary VE and probe its gravitational properties.

Alongside the exciting advent of the gravitational wave observation era shepherded in by LIGO/Virgo, the Neutron star Interior Composition ExploreR (NICER) mission will soon measure masses and radii of several millisecond pulsars [141]. These measurements as well as the chirps from the inspiral of merging neutron stars can provide information about the equation of state (EoS) of dense nuclear matter. The chirps in particular are sensitive to the tidal deformability of NS's as they approach each other [142–146]. There has already been considerable work on constraining the EoS using the new LIGO/Virgo data [147–151].

There exists an extensive literature focused on trying to put bounds on the nuclear EoS at high densities from neutron star measurements (see for example [152–155]). Some recent theoretical work has focused on modeling possible new phases at the cores of neutron stars by using quasi-particle quarks rather than neutrons to provide the simplest description of the microscopic physics [156–162]. Further work has been done using NS's to constrain "beyond

the Standard Model" physics [135–137].

In this paper we will assume that there is only Standard Model physics involved in the composition of neutron stars, and we will not try to model the microphysics of the putative new phase. Our main goal is to investigate the observable effects of the presence of VE on the GW signal as well as the mass versus radius curve of NS's, possibly providing new experimental probes of VE. To achieve this we will parameterize the effect of the new phase with a jump in the ground state energy due to a QCD phase transition assumed at the core [138, 161, 163, 164]. This new phase would appear at a critical pressure of order $p_c \propto \Lambda_{\rm QCD}^4$, and is expected to also lead to a change of VE [140] of order $\Delta\Lambda \propto \Lambda_{\rm QCD}^4$. We will follow the conventional models for NS's where the EoS is divided into 7 layers, but we modify the innermost layer to take the effect of the phase transition and the appearance of VE at the core into account. Previous studies treat all 7 layers as simple polytropic fluids, but this is expected to be a poor fit to an inner core exhibiting the physics of a new phase of QCD, where the vacuum energy does not vanish. We will then evaluate the tidal Love numbers for such models, varying over the value of the vacuum energy at the core. One important consequence of the new phase (along with the presence of vacuum energy) is that the jump conditions at the boundary of the inner core have to be modified from those traditionally used in NS simulations [161, 163, 164]. We will explore the effect of a difference in energy densities of the two phases that includes a discontinuous, density independent term reflecting the absence of the low density QCD contribution to VE [138]. We will present several models of NS cores and estimate the effect of VE on tidal Love numbers. We find that VE can have a significant effect on NS merger waveforms with high chirp masses, so that such events serve as a probe of the physics of vacuum energy.

While vacuum energy is found to have a significant effect on waveforms, there are currently significant uncertainties both in terms of experimental waveform data and in terms of theoretical expectations for parameters describing the equation of state. Disentangling the effect of the QCD vacuum energy from other high density physics is currently not yet possible, however, the future of gravity wave observation holds great promise in terms of obtaining multiple independent measurements of neutron star observables, significantly tightening constraints on the equation of state of QCD. Additionally, progress may be made on the theory side – QCD is a complete microscopic theory, therefore its high density behavior can be uniquely determined from first principles. The ultimate goal is to use neutron stars as new astrophysical laboratories for studying physics at the density frontier, and determining whether the SM (plus classical gravity) agrees with data, or whether new exotic (gravitational or particle) physics is necessary to explain the observations.

The paper is organized as follows. In Section 2 we present the models we use for nuclear matter in the interior of NS's, along with a detailed discussion of the treatment of the phase transition at the boundary of the innermost layer. Section 3 contains the description of the tidal deformability of NS's. The results of our simulations and the effects of VE on the NS observables are given in Section 4: we show the mass versus radius curves and the tidal deformabilities for three different well-studied NS models and the effects of VE on those observables. Finally we conclude in Section 5.

5.2 Modeling High Density QCD

The main difference between our work and that of previous studies of tidal deformability of NS's is that we will fully account for a phase transition to an exotic phase of QCD in the innermost core region of NS's. Crucially, we take into account the Standard Model expectation that there is a constant shift Λ, independent of baryon number density, in the ground state energy relative to the surrounding layers parametrizing the change in VE due to the phase transition. In the ordinary phase of QCD the nonperturbative condensates of quarks and gluons make contributions [140] of order $(100\,\mathrm{MeV})^4$ to the VE. These contributions, along with those from other sectors of the SM, are canceled by the "bare" cosmological constant down to the observed cosmological constant of order $(\mathrm{meV})^4$:

$$\Lambda_{\mathrm{QCD}}^{\mathrm{SM\,vac}} + \Lambda_{\mathrm{SM\,other}} + \Lambda_{\mathrm{bare}} \simeq (10^{-3}\ \mathrm{eV})^4 \ . \tag{5.2.1}$$

The origin of the mechanism leading to this cancelation remains unknown. In an exotic phase of QCD the QCD contributions to the VE will have order one modifications and hence the precise cancelation will no longer apply:

$$\Lambda_{\mathrm{QCD}}^{\mathrm{exotic}} + \Lambda_{\mathrm{SM\,other}} + \Lambda_{\mathrm{bare}} \simeq \Delta\Lambda \ , \tag{5.2.2}$$

where $\Delta\Lambda$ is the shift in the QCD vacuum energy due to the phase transition. Hence in the absence of a dynamical adjustment mechanism, Standard Model physics predicts a density independent shift in the energy of the exotic phase compared to the ordinary phase, which will serve as a new effective cosmological constant term for this phase. An estimate of the

difference between the VE of the exotic phase and the ordinary vacuum is given by nuclear saturation density: $|\Delta\Lambda| \sim \Lambda_{\rm QCD}^4$ [138]. Such a phase change is strongly suspected to occur at high chemical potential, with theoretical evidence arising from truncated diagrammatic expansions and other approximate methods [157, 162]. The phase change is in fact part of the standard picture of the QCD phase diagram. For many plausible descriptions of the matter in the outer portions of the star, nuclear saturation density is approached near the core of the densest NS's, making it quite possible that the most massive NS's contain cores with an exotic phase. In this section, we give a description of how one can model the QCD equation of state at various pressures, with particular attention paid to the phase transition that may occur in the innermost region.

5.2.1 Modeling the Outer Layers

The physics of neutron stars is an extremely rich field, and there are many details that go into modeling the different regions of NS's. Such an analysis is well beyond the scope of this work, however there are methods for coarse-graining these complexities to obtain an approximate equation of state for nuclear matter up until the phase transition we are interested in. Such an approximation is sufficient for the purposes of making predictions for gravitational wave signals. The most common methodology for modeling the high density nuclear physics region outside the exotic phase core is to separate the neutron star into multiple layers, with each layer satisfying a non-relativistic polytropic equation of state. The parameters of the polytrope are fixed either by matching conditions or by fitting results from more detailed studies.

We follow this established methodology and model the nuclear fluid and its corresponding EoS as a piecewise polytrope where the boundaries between each layer are set by a given value of the pressure. Following previous work [154, 155] we will parametrize the EoS with a total of 7 layers. The Israel junction conditions [165] require that the pressure must always be continuous between layers, even if each side of the boundary is separated by a first order phase transition. It is traditional to parameterize the EoS by assuming that the pressure is given by a power of the mass density $\rho(r) = m_n n(r)$ rather than a power of the energy density (as would be natural for a high-density, relativistic fluid). Since we want to efficiently compare our results with the existing state of the art simulations (some of which have been used as benchmarks for the LIGO/Virgo analysis) we will bow to this tradition and parametrize the EoS as

$$p = K_i \rho^{\gamma_i} \ , \qquad p_{i-1} \leq p \leq p_i \ , \tag{5.2.3}$$

where $i \in \{1, \ldots, 7\}$ for K_i, γ_i and $i \in \{1, \ldots, 6\}$ for p_i. The pressures, p_i, dividing the various layers have a one to one correspondence with the boundaries in the mass density: ρ_i. The Einstein equations contain the energy density, which is related to the mass density via the first law of thermodynamics: $d(\epsilon/\rho) = -p\, d(1/\rho)$. Integrating the first law together with (5.2.3) yields the corresponding energy density:

$$\epsilon = (1 + a_i)\rho + \frac{K_i}{\gamma_i - 1}\rho^{\gamma_i} \ , \tag{5.2.4}$$

where the a_i are integration constants. Note that the appearance of the a_i parameters is a consequence of using a polytropic ansatz for the mass density. Naively, one would think that

using a relativistic polytropic ansatz for the energy density would have led us to a relation with one less free parameter. However another thermodynamical condition, continuity of the chemical potential, would have forced us to reintroduce the baryon number density, and therefore to bring back another parameter. So these simply correspond to different parametrizations of the EoS, and we adopt the one described above in order to follow the traditional approach.

By using 7 layers we have introduced a large number of parameters (γ_i, K_i and a_i). Most of those can be determined by continuity of various quantities at the layer boundaries. For the outer 6 layers we assume the continuity of the energy density at the boundaries, which allows us to determine the a_i's:

$$a_i = \frac{\epsilon(\rho_{i-1})}{\rho_{i-1}} - 1 - \frac{K_i}{\gamma_i - 1}\rho_{i-1}^{\gamma_i - 1} \ . \tag{5.2.5}$$

If the K_1 constant for the outermost layer is known, then the other K_i values (except for the innermost layer) can be determined by the continuity of the pressure:

$$K_i = K_{i-1}\rho_{i-1}^{\gamma_{i-1}-\gamma_i} \ , \qquad i \in \{2, \ldots, 6\} \ . \tag{5.2.6}$$

For the outermost layer, the "crust", we have $p_0 = 0$. Requiring that $\lim_{\rho\to 0} \frac{\epsilon}{\rho} = 1$ (physically this means that the edge of the star is ordinary non-relativistic matter) implies that $a_1 = 0$. Thus the parameterization of the EoS of the NS for the outer layers will require us to specify the critical pressures p_i, all the polytropic exponents γ_i as well as the outermost polytropic constant K_1, while all other parameters will be determined by the continuity conditions.

5.2.2 Modeling the Core and the Effect of VE

For the last layer, we use an equation of state that incorporates physics associated with a change in the QCD vacuum state due to high density. There are two effects expected at this phase transition: a vacuum energy term Λ in the fluid that is independent of baryon number density, and a jump in energy density across the boundary. Unlike in the outer layers, in the exotic phase the nature of the baryonic states may be very different from the usual zero temperature baryons. Since QCD conserves baryon number, for the innermost layer it is more natural to use baryon number density n in place of the mass density as the variable parametrizing the EoS for the central core ($p > p_6$). In this case, the equation of state can be written as:

$$p = \tilde{K}_7 n^{\gamma_7} - \Lambda \ , \tag{5.2.7}$$

$$\epsilon = \tilde{a}_7 n + \frac{\tilde{K}_7}{\gamma_7 - 1} n^{\gamma_7} + \Lambda \ . \tag{5.2.8}$$

Note that the vacuum energy appears with the opposite sign in the energy density and pressure, just as with the cosmological constant. Our goal is to see how sensitive neutron star observables are to the VE shift Λ.

To keep the form of the EoS unchanged in the various layers we can introduce the density $\rho = m_n n$ where m_n is the ordinary neutron mass, and use this rescaled number density for the innermost layer. We can easily see that in terms of this rescaled density the EoS will

have the same form as for the outer layers:

$$p = K_7 \rho^{\gamma_7} - \Lambda \ , \tag{5.2.9}$$

$$\epsilon = (1 + a_7)\rho + \frac{K_7}{\gamma_7 - 1}\rho^{\gamma_7} + \Lambda \ , \tag{5.2.10}$$

where $K_7 = \tilde{K}_7/m_n^{\gamma_7}, (1 + a_7) = \tilde{a}_7/m_n$ are just redefinitions of the unknown constants parametrizing the EoS for the inner layer. We adopt this notation in order to stay close to the standard formalism used in the literature.

Let us now examine in detail the continuity (or jump) of the various quantities at the phase boundary between the sixth and the seventh (innermost) layer. The Israel junction conditions [165] still require that the pressure be continuous:

$$K_7 \rho_+^{\gamma_7} - \Lambda = K_6 \rho_-^{\gamma_6} = p_6 \ , \tag{5.2.11}$$

but due to the appearance of the Λ term this now requires a jump in $\rho(r)$ from ρ_+ to ρ_- (where $\rho_- = \rho_6$) and consequently also in $\epsilon(r)$ from ϵ_+ to ϵ_-. Since QCD conserves baryon number, another quantity that we need to require to be continuous is the chemical potential μ (that is we are assuming chemical equilibrium at the phase boundaries with conserved baryon number). The chemical potential at zero temperature is given by

$$\mu = \frac{\epsilon + p}{n} \ , \tag{5.2.12}$$

where n is again the baryon number density. This relation holds even if the VE is nonzero.

Therefore the jumps from ϵ_+ to ϵ_- and from ρ_+ and ρ_- (in our convention $\rho_+ = m_n n_+$ and $\rho_- = m_n n_-$) are related to each other by

$$\frac{\epsilon_+ + p_6}{\rho_+} = \frac{\epsilon_- + p_6}{\rho_-} \ . \tag{5.2.13}$$

The convexity of the free energy $\left(\frac{\partial^2 F}{\partial V^2}\right)_{T,N} > 0$ can be translated to $\left(\frac{\partial p}{\partial n}\right)_{T,N} > 0$. This latter form implies that the number density increases with pressure, yielding $\rho_+ \geq \rho_-$. This condition together with the continuity of the chemical potential tells us that the jump in energy density should also be positive, i.e. $\epsilon_+ \geq \epsilon_-$.

A typical phase transition will have both $\Delta\epsilon$ and Λ non-vanishing, and this scenario is the focus of our studies. We choose to parametrize the jump in energy density such that it is proportional to the absolute value of the shift in VE:

$$\epsilon_+ - \epsilon_- = \alpha|\Lambda| \ . \tag{5.2.14}$$

For each value of γ_7, α, and Λ, this condition, together with continuity of the chemical potential, fixes the values of K_7 and a_7. This parametrization of the phase transition has the advantage that the $\Lambda = 0$ limit reproduces the results obtained in the literature since both the mass density and the energy density become continuous in this case. In principle, α could be taken to be zero, isolating the effects of vacuum energy from a jump in the energy density, corresponding to a second order phase transition. Here we will assume that the phase transition is first order with an accompanying jump in most quantities across the phase boundary and take $\alpha > 0$. A final consistency condition is that both the full pressure and

the partial pressure of the fluid, $K_7\rho^{\gamma_7}$, must be positive. This implies that Λ must satisfy $-p_6 < \Lambda$.

5.3 Modeling Neutron Stars

After presenting the relevant physics of the dense QCD matter forming the interior of the NS we are now ready to review the usual method for calculating the structure of the interior of the NS. GW emission observed by LIGO/Virgo originates from the inspiral phase, when the stars are far apart relative to their radii. In this stage of the merger, the NS's are still well approximated by nearly spherically symmetric static objects, with deviations described by a linear response in an expansion in spherical harmonics. In this paper we will ignore the effects of NS angular momentum but plan to further investigate that in a future publication. First we briefly review the equations relevant for the spherically symmetric solution and then present an overview of the perturbations due to the gravitational field of the other NS.

5.3.1 Spherically Symmetric Solutions

At lowest order, the stars are spherically symmetric, and their mass distribution is given by the solution to the Tolman-Oppenheimer-Volkoff (TOV) equations [166]. These equations are easily derived by starting with a spherically symmetric metric ansatz

$$ds^2 = e^{\nu(r)}dt^2 - \left(1 - \frac{2Gm(r)}{r}\right)^{-1} dr^2 - r^2 d\Omega^2 \ , \tag{5.3.1}$$

and using the associated Einstein equations assuming a spherically symmetric fluid distribution with pressure $p(r)$ and energy density $\epsilon(r)$. The resulting TOV equations are:

$$m'(r) = 4\pi r^2 \epsilon(r) \ , \tag{5.3.2}$$

$$p'(r) = -\frac{p(r)+\epsilon(r)}{r(r-2Gm(r))} G\Big[m(r) + 4\pi r^3 p(r)\Big] \ , \tag{5.3.3}$$

$$\nu'(r) = -\frac{2p'(r)}{p(r)+\epsilon(r)} \ , \tag{5.3.4}$$

where $'$ denotes differentiation with respect to the radial coordinate r. The TOV metric provides the unperturbed solution around which the gravitational field of the second star will introduce perturbations that can be dealt with using a multipole expansion. From the solution to these equations, one obtains the internal structure of the star: the mass as a function of radius, as well as the thicknesses and masses of the various layers.

5.3.2 Tidal Distortion and Love Numbers

In a neutron star binary, each neutron star experiences gravitational tidal forces due to the other. This force squeezes the stars along the axis passing through both of their centers, and deforms the stars, inducing a quadrupole moment. The size of this induced quadrupole moment is determined by the structure of each neutron star, which can be characterized by its compactness and the stiffness of the EoS. These in turn depend on the physical properties of the dense QCD matter as described by its EoS discussed in the previous section. The effect of the induced quadrupole on gravitational wave data is to change the power emission as a function of time and frequency. Thus LIGO data on NS inspirals contains information

about this tidal deformability, which depends on the equation of state of the matter making up the stars.

A common way to describe the deformability of a star is through the Love number. Love numbers were originally introduced in the study of Newtonian tides [167]. The application of Love numbers to gravitational waves produced in neutron star inspirals was initiated in refs. [142, 143], and further generalized in [168]. Detailed studies of the prospects for gravitational wave detection were provided in [144–146].

In the local rest frame of one star a small tidal field can be described in terms of a Taylor expansion of the Newtonian gravitational potential, or the time-time component of the metric tensor. There are two contributions, one from the effect of the distant star, and the other from the induced quadrupole moment. At large distances (using Cartesian coordinates, x^i) g_{tt} takes the form [144]

$$\frac{1+g_{tt}}{2} \approx \frac{GM}{r} + \frac{3GQ_{ij}}{2r^5}x^i x^j - \frac{1}{2}\mathcal{E}_{ij}x^i x^j \ldots \tag{5.3.5}$$

Here $\mathcal{E}_{ij}$ parametrizes the external tidal gravitational field, and Q_{ij} is the induced quadrupole moment. Both matrices are traceless and symmetric. To linear order in the response, the induced quadrupole is determined by the tidal deformability, λ, defined by

$$Q_{ij} = -\lambda\,\mathcal{E}_{ij}\ . \tag{5.3.6}$$

One can then define a dimensionless quantity k_2 by

$$k_2 = \frac{3}{2}\frac{G\lambda}{R^5} \ , \tag{5.3.7}$$

where R is the radius of the neutron star. This is referred to as the $l = 2$ tidal Love number, and is the main physical observable. The advantage of this parametrization is that the Love number does not vary much with the size of the star, with typical Love numbers ranging from $k_2 = 0.001$ to $k_2 = 1$ as masses and equations of state are varied.

In order to determine k_2, one performs the perturbative expansion of the solutions to the Einstein equations in the presence of an external gravitational field assuming a multipole expansion. Thus inside and near the star we will write the metric perturbation as an expansion in spherical harmonics Y_l^m. Due to the axial symmetry around the axis connecting the centers of the two stars, m is zero, and since the tidal deformation is dominantly quadrupolar, with no dipole, the leading contribution is at $l = 2$ [144]. Hence the full perturbed metric $g_{\alpha\beta} + h_{\alpha\beta}$ (where $g_{\alpha\beta}$ is the metric from (5.3.1)) is written as

$$h_{\alpha\beta} = \text{diag}\Big(e^{\nu(r)}H(r), e^{\mu(r)}H(r), r^2K(r), r^2\sin^2\theta K(r)\Big)Y_2^0(\theta,\phi) \ , \tag{5.3.8}$$

where $e^{\mu(r)}$ and $e^{\nu(r)}$ are the functions in the solution to the unperturbed spherically symmetric metric (5.3.1):

$$e^{\mu}(r) = (1 - 2Gm(r)/r)^{-1} \ , \tag{5.3.9}$$

$$\nu'(r) = -\frac{2p'(r)}{p(r) + \epsilon(r)} \ , \tag{5.3.10}$$

and the Einstein equations relate the functions K and H:

$$K'(r) = H'(r) + H(r)\nu'(r) \ . \tag{5.3.11}$$

Inserting the perturbed metric into Einstein's equations results in a second order differential equation for $H(r)$:

$$\begin{aligned} H'' = 2He^{\mu}\left\{-2\pi G\left[5\epsilon + 9p + \frac{d\epsilon}{dp}(\epsilon + p)\right] + \frac{3}{r^2} + 2G^2 e^{\mu}\left(\frac{m(r)}{r^2} + 4\pi r p\right)^2\right\} \\ + \frac{2}{r}H'e^{\mu}\left\{-1 + \frac{Gm(r)}{r} + 2\pi G r^2(\epsilon - p)\right\}. \end{aligned} \tag{5.3.12}$$

To find solutions, one starts with a series expansion of H very near the core of the star, at small r:

$$H(r) = a\, r^2 + \mathcal{O}\Big(r^4\Big). \tag{5.3.13}$$

The linear term drops out since the solution must be regular at $r = 0$. The size of the coefficient a is linearly proportional to the size of the external perturbation, $\mathcal{E}_{ij}$, and is not an intrinsic property of the star, as is clear from the fact that it is simply a normalization coefficient for the solution to the linear ODE for H. One can thus pick this coefficient arbitrarily in numerically solving for H. The $l = 2$ tidal Love number, on the other hand is an intrinsic property, and the value for a drops out in calculating it. The value for k_2 can be calculated once H is found, and matched at large r onto the metric ansatz in Eq. (5.3.5). It

is given by

$$
\begin{aligned}
k_2 = \frac{8C^5}{5}(1-2C)^2[2+2C(y-1)-y] \\
\times \Big\{ 2C[6-3y+3C(5y-8)] + 4C^3[13-11y+C(3y-2)+2C^2(1+y)] \\
+ 3(1-2C)^2[2-y+2C(y-1)]\log(1-2C) \Big\}^{-1} ,
\end{aligned}
\tag{5.3.14}
$$

where C is the compactness parameter GM/R, and y is obtained from the solution to H evaluated on the surface of the star:

$$
y = \frac{RH'(R)}{H(R)} \ . \tag{5.3.15}
$$

Another dimensionless quantity, known as the dimensionless tidal deformability, is often found in the literature. It is obtained from the definition of k_2 by factoring out the C^5 in front:

$$
\bar{\lambda} = \frac{2k_2}{3C^5} = \frac{\lambda}{G^4M^5} \ . \tag{5.3.16}
$$

5.4 Results and Fits

We are now ready to present our results for the effects of adding a VE component to the innermost layer. We will use several different benchmark EoS's for modeling the NS's and investigate the consequences of the presence of VE in each of those cases. Two of the EoS's are more "conservative" in the sense that the maximum stable NS mass that can be achieved just barely goes above $2M_\odot$ (the maximum NS mass observed thus far is $M = (2.01 \pm 0.04)M_\odot$). The two more conservative models are the AP4 [169] and SLy [153] EoS's, which were also

	SLy	AP4	Hebeler
K_1	9.27637×10^{-6}		See [155]
p_1	$(0.348867)^4$		See [155]
p_2	$(7.78544)^4$		
p_3	$(10.5248)^4$		
p_4	$(40.6446)^4$	$(41.0810)^4$	$(72.2274)^4$
p_5	$(103.804)^4$	$(97.1544)^4$	$(102.430)^4$
p_6	$(176.497)^4$	$(179.161)^4$	$(149.531)^4$
γ_1	1.58425		See [155]
γ_2	1.28733		
γ_3	0.62223		
γ_4	1.35692		
γ_5	3.005	2.830	4.5
γ_6	2.988	3.445	5.5
γ_7	2.851	3.348	3

Table 5.1: The parameters used for each EoS. The exponents γ_i are dimensionless, the various pressures have units of MeV^4, and K_1 is in units of $\text{MeV}^{4-4\gamma_1}$. The Hebeler et al. parametrization [155] uses a semi-analytic expression which is not piecewise polytropic in the outer region of the star, and thus cannot be displayed in the table.

used as benchmarks by LIGO/Virgo [134]. We also consider the less restrictive model of Hebeler et al. [155] which permits larger masses, up to nearly $3M_\odot$. For the AP4 and SLy models we use the piecewise polytropic parametrization for all 7 layers provided by Read et al. [154]. We have tabulated the corresponding parameters in Table 5.1. While the model of Hebeler et al. also uses a piecewise polytropic EoS for the innermost three layers, for the outer four layers corresponding to the crust they use a semi-analytic expression. In their parametrization, the outer crust is modeled by the BPS EoS [170] assuming β equilibrium[1], followed by a layer for which chiral EFT (valid up to the nuclear saturation density around 0.18 baryons/fm^3) is used to obtain the EoS. This semi-analytic expression is consistent with the piecewise polytropic approach of AP4 and SLy.

[1] β-equilibrium corresponds to equal rates of neutron decay and proton capture of electrons.

Varying the EoS leads to more or less compact NS's, whose deformability will also change. The compactness of the NS can be characterized by the radius of a NS with a fixed mass. The deformability describes how much the NS reacts to the presence of the gravitational field of the second NS in the binary merger event and is characterized by the tidal deformability. In the first subsection, we present our results for the mass versus radius, $M(R)$, curves of neutron stars with different nuclear EoS's including the effect of VE, while in the second, we study the tidal deformability and comment on the potential for LIGO/Virgo to discern between models with different assumptions about the change in VE in exotic phases of QCD.

5.4.1 $M(R)$ Results

We first present the results for the mass versus radius curves for the three different benchmark equations of state, whose parameters are displayed in Table 5.1. These three benchmarks cover a realistic range of possible EoS's, with a wide variation in the maximum possible stable neutron star mass. We take care not to violate basic constraints on the behavior of high density QCD matter. For example, when pressures near the center of the star become very large, and relativistic effects dominate, one must ensure that the equation of state does not violate causality. Causality requires that the speed of sound in the fluid does not exceed the speed of light:

$$v_{\rm s} = \sqrt{\frac{dp}{d\epsilon}} \leq 1 \ . \tag{5.4.1}$$

However, using simple EoS models this condition is often violated for very large central pressures. Such violation does not imply the instability of the NS, but is rather an indication that the ansatz for the EoS is no longer a good approximation of the underlying nuclear

physics in that region. Such causality violation would never arise in the true QCD equation of state at very high densities.

The true stability condition for the central pressures that a neutron star can support is given by

$$\frac{\partial M}{\partial p_{\rm center}} > 0 \ . \tag{5.4.2}$$

This constraint arises from considerations of radial pulsation modes of the star, and is directly associated with stability of the fundamental mode of oscillation [171]. The relation in Eq. (5.4.2) above can be violated when the jump in the energy density is too large [163]:

$$\epsilon_+ - \epsilon_- \geq \frac{1}{2}\epsilon_- + \frac{3}{2}p_6 \ . \tag{5.4.3}$$

Above this bound, the mass of the NS no longer increases with increasing core pressure, and the NS is unstable [159–161, 163, 164].

We note that the condition in Eq. (5.4.2) can be satisfied for two stars of the same mass, but different internal pressures [172], corresponding to different phases in the core of the star. In such cases, the critical energy density jump exceeds that in Eq. (5.4.3) at the transition. However, even with this instability, one sometimes finds for $p > p_6$, that there is a disconnected class of solutions that does not exceed the bound in Eq. (5.4.2). The possibility then arises that some of the exotic, disconnected solutions have the same masses as some of the normal, lower pressure solutions.

Which of the two conditions, causality or monotonicity, will limit the central pressure depends on the EoS. For AP4 and SLy, the limit is set by causality. This bound can be

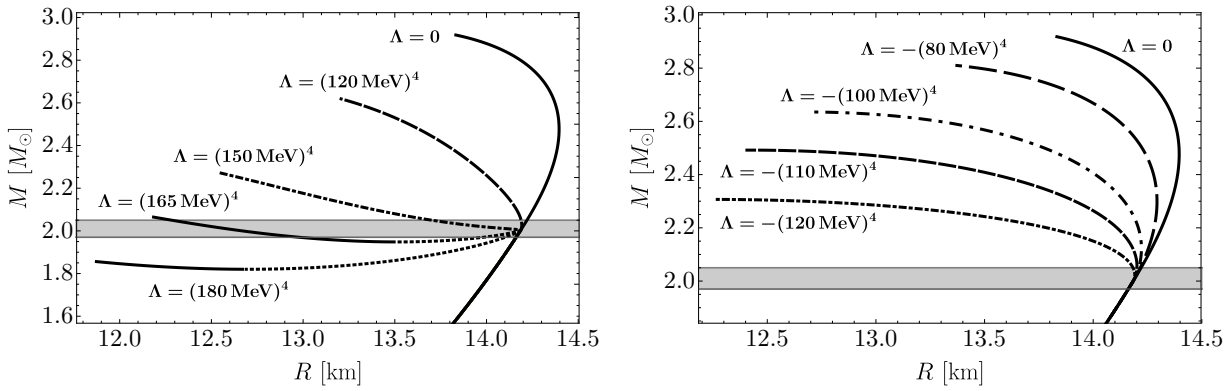

Figure 5.1: Mass versus radius curves corresponding to the stiff parametrization of Hebeler et al. [155] with $\alpha = 3$. Dotted curves in the plot on the left correspond to unstable configurations violating Eq. (5.4.2). Positive values of Λ are shown in the plot on the left, and negative ones on the right.

avoided by modifying the EoS via a "causal extension" [155] into the regions where the pressure exceeds the maximal value set by the causality bound. For the models we are working with, we have found that this extension simply flattens out the curves at the point where causality is violated, and hence does not change the value of the maximum mass significantly. For this reason we have chosen not to make this modification and ended the curves at the point where the speed of sound reaches unity.

The $M(R)$ curve and the effect of VE for the Hebeler et al. EoS [155] are shown in Fig. 5.1. Each curve is obtained by varying the pressure at the center of the star but keeping all of the other parameters fixed. We have fixed $\alpha = 3$ in this plot, as well as all those that follow.[2] When the central pressure is greater than p_6, the value of Λ becomes relevant and the other curves depart from the behavior of the $\Lambda = 0$ case. Dotted parts of the curves correspond to unstable regions, i.e. solutions of the TOV equations in which the stability condition (5.4.2) is violated. The shaded region represents the most massive neutron star measured to date, with

[2]Taking α to be small reduces the change in the curves relative the $\Lambda = 0$ case, however small values of α are not representative of most phase transitions, which are typically accompanied by a change in the energy density as well as the vacuum energy.

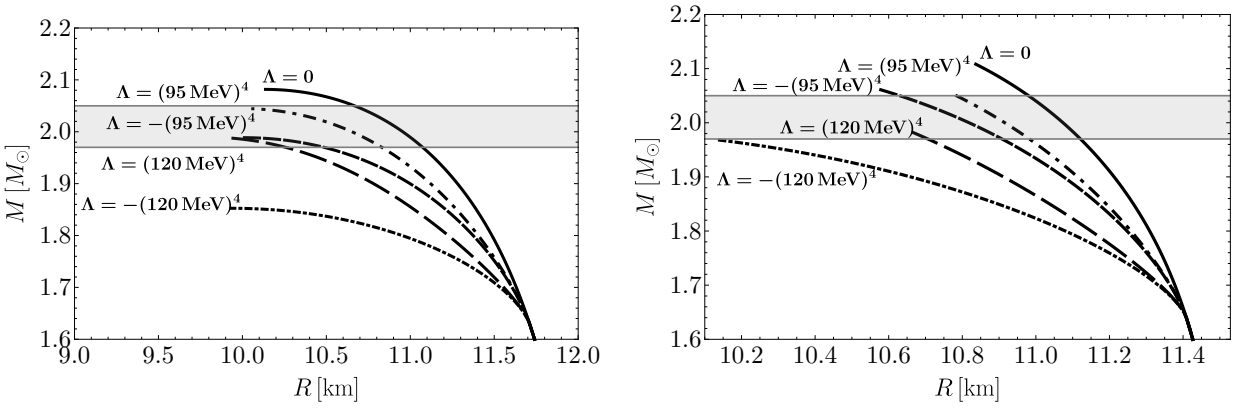

(a) SLy EoS

(b) AP4 EoS

Figure 5.2: $M(R)$ curves for the SLy and AP4 equations of state for various Λ values on the seventh layer. For all the curves, the proportionality constant α in the jump equation (5.2.14) is chosen to be $\alpha = 3$. The gray region shows the allowed mass range of the heaviest neutron star, with mass $(2.01 \pm 0.04)M_\odot$.

a mass of $(2.01 \pm 0.04)M_\odot$ [173]. Notice that for some positive values of Λ, i.e. when the jump in energy density is big enough according to Eq. (5.4.3), we find a second stable region which is disconnected from the main branch, as discussed above. This means that for a given mass, there are two possible types of stars, one with no exotic phase in the core, and another with a significant portion of the star in the new phase. This gives rise to interesting effects, both for $M(R)$ curves and in GW observables. For example, assuming that the $\Lambda = (165\,\mathrm{MeV})^4$ curve is the correct one, it would be possible to observe two $2M_\odot$ neutron stars with significantly different radii. That is, there are two stable configurations for stars with the same mass. It is quite interesting that the physics of QCD may allow for a plethora of different compact objects, with population numbers depending on the conditions of their formation.

Our procedure for introducing the VE for this model is the following. In order to make sure that all values of Λ considered here are compatible with a neutron star mass of $(2.01 \pm 0.04)M_\odot$, we stop the next-to-innermost polytropic region as soon as the mass reaches $2.00M_\odot$. This corresponds to choosing a critical pressure $p_6 \approx (150\,\mathrm{MeV})^4$. Once the critical pressure is

reached, we transition into the innermost polytropic region with a nonzero VE, and we allow for the central pressure to be as high as possible without violating the causality bound.

Next we present results for the AP4 [169] and SLy [153] EoS models. The $M(R)$ curves for the AP4 and SLy models with different values of the VE in the innermost layer are shown in Fig. 5.2. One can again see that up to a certain critical mass, the curves corresponding to different Λ's in the innermost layer do coincide with each other. The reason for this is that below this mass the central pressure is not high enough to enter the exotic high density phase of QCD. The critical pressure for the phase transition to occur is set by p_6 which is an input of the model. For the AP4 and SLy models, $p_6 \approx (179\,\mathrm{MeV})^4$ and $p_6 \approx (176\,\mathrm{MeV})^4$ respectively which correspond to a critical mass of approximately $1.6 M_\odot$ for both models.

The plots for all three EoS's show that the maximal mass of the neutron star decreases for both positive and negative values of VE. This is a generic feature of neutron star models with phase transitions with vacuum energy in our study, and is due to the jump in the energy density across the phase transition. This conclusion is similar to that obtained in previous works that study phase transitions without vacuum energy [174].

5.4.2 Tidal Deformabilities and LIGO/Virgo

Let us now discuss NS observables from GW's emitted during the merger of NS's. The frequency versus time behavior of the waveform of the emitted gravitational wave, usually expressed in terms of the "gravitational wave phase" appearing in the Fourier transform of the chirp, can be determined by an expansion in relativistic effects, starting at Newtonian order, and proceeding to post-Newtonian corrections in the velocity. At dominant Newtonian

order, where the two NS's are approximated by point masses, the waveform depends only on a particular combination of the masses called the chirp mass:

$$\mathcal{M} = \mu^{3/5} M_{\rm tot}^{2/5} = \frac{(M_1 M_2)^{3/5}}{(M_1 + M_2)^{1/5}} \ , \tag{5.4.4}$$

where μ is the reduced mass of the system [175]. For the recently observed merger event, GW170817, the chirp mass was measured to be $\mathcal{M} = 1.188^{+0.004}_{-0.002} M_\odot$.

Since this is the dominant contribution to the waveform, the chirp mass can be determined quite accurately. However, the individual masses must be extracted from higher order velocity corrections to the waveform, and are thus more difficult to constrain. At higher order, spin-couplings are important as well, and without information about the stars' rotational speeds and axes, precise extraction of the masses is impossible. This information is in principle retrievable from measurements of the waveform, but is difficult as it relies on data near the end of the inspiral, where current experiments lose sensitivity, and where full numerical simulation of the merger event may be necessary [176].

At present, the individual masses can only be estimated by using the chirp mass and some assumptions for the angular rotation frequency of the stars. For GW170817 in the low-spin case, the estimated mass range is 1.36–1.60$M_\odot$ for the heavy star and 1.17–1.36$M_\odot$ for the light star, while for the high-spin case, there is considerably more possible variation in the masses: 1.36–2.26$M_\odot$ for the heavy star and 0.86–1.36$M_\odot$ for its less massive partner.

Similarly, it is not yet possible to measure individual tidal deformabilities. However, it is possible to constrain a weighted combination of the individual masses and deformabilities through their contribution to the gravitational wave phase at order v^5. This so-called

"combined dimensionless tidal deformability" is defined as

$$\tilde{\Lambda} = \frac{16}{13}\frac{(M_1 + 12M_2)M_1^4\bar{\lambda}_1 + (M_2 + 12M_1)M_2^4\bar{\lambda}_2}{(M_1 + M_2)^5} \ . \tag{5.4.5}$$

For the recent event GW170817, the current constraint placed on $\tilde{\Lambda}$ is ≤ 800 for the low-spin assumption and ≤ 700 for the high-spin case. In the low-spin case, the neutron star masses are probably too low to contain an exotic QCD phase, and thus event GW170817 would not contain information about VE. Of course, this may not be the case for future merger events, which may involve heavier NS's. In the high-spin case, however, the inner core could be in the exotic phase, and the constraints from GW170817 are relevant for studying VE.

The rest of this section contains our results for the effects of VE on the tidal deformabilities, which will be presented in a series of plots. Each plot will be presented both for the Hebeler et al. EoS, which allows for larger NS masses and hence larger effects from VE, as well as for the AP4 and SLy EoS's, which cut NS masses off at $2M_\odot$ and thus have smaller VE effects.

- Fig. 5.3 shows the individual tidal deformabilities of both NS's and the effect of VE using the Hebeler et al. EoS.

- Fig. 5.4 translates the effects of VE into a fractional shift of the combined tidal deformability $\tilde{\Lambda}$. This plot shows that the effect of VE can be as large as 70% and is generically sizable for the case of the Hebeler et al. EoS.

- Figs. 5.5, 5.6, 5.7 repeat the same analyses for the AP4 and SLy EoS's, where we see that the deviations are generically smaller, but can still reach 25–30% for larger chirp masses.

- Figs. 5.8, 5.9 emphasize the role of the chirp mass: they show the maximal achievable effect of VE as the chirp mass is increased. We can see that observing events with chirp masses above 1.6–1.8$M_\odot$ will be key to observing the effects of VE.

- Fig. 5.10 shows the effect of VE on GW170817 (assuming the Hebeler EoS) where it can significantly change the allowed region of NS masses one would infer from the constraint on the tidal deformability.

The EoS parametrization of Hebeler et al. [155] allows for large possible deviations in the tidal deformability when a VE term is added to the central core in the new phase. In Fig. 5.3, we show the effect of varying the VE term for a selection of three different input chirp masses. The curves are obtained by fixing the chirp mass $\mathcal{M}$ at a few representative values and then scanning over the mass of the heaviest star, M_1. Typically it is found that the heavier the star, the smaller the tidal deformability. This is largely due to the fact that more massive stars typically have smaller radii, and thus respond less to external tidal fields.

We note that the $\Lambda = (165\,\mathrm{MeV})^4$ curve in the third plot is composed of two separate branches, corresponding to the two separate stable stars with equal masses but different radii as explained in the previous section. The branch with the highest values of $\bar{\lambda}_2$ corresponds to only the most massive star laying in the disconnected branch of the $M(R)$ curve, while in the other case both stars in the binary would come from the disconnected branch. Part of the reason why the deviations from the $\Lambda = 0$ curve are significant here can be found directly in Fig. 5.1. Since there the maximum mass for the $\Lambda = 0$ curve is close to $3M_\odot$, the curves that correspond to a nonzero Λ can depart significantly without being excluded by the measurement of the most massive neutron star, $(2.01 \pm 0.04)M_\odot$.

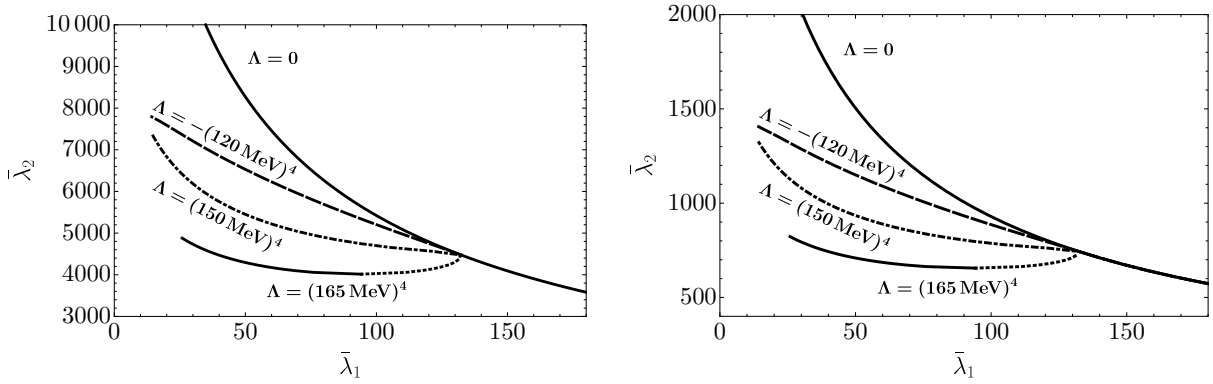

(a) $\mathcal{M} = 2^{-1/5} 1.4 M_\odot \approx 1.22 M_\odot$

(b) $\mathcal{M} = 2^{-1/5} 1.7 M_\odot \approx 1.48 M_\odot$

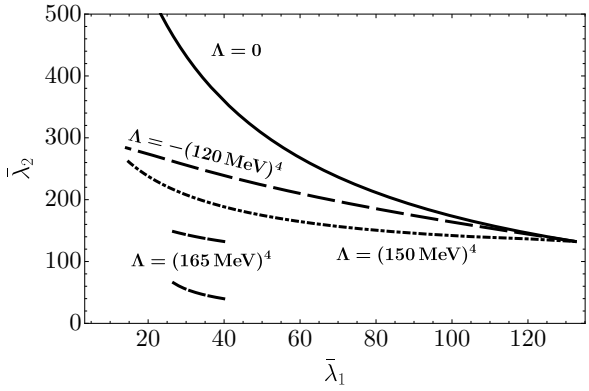

(c) $\mathcal{M} = 2^{-1/5} 2.0 M_\odot \approx 1.74 M_\odot$

Figure 5.3: Tidal deformabilities for the Hebeler et al. parametrization with $\alpha = 3$. Each plot corresponds to a different chirp mass. Dotted parts of the curves with $\Lambda = (165\,\mathrm{MeV})^4$ correspond to unstable configurations. In all cases, the deviation from the $\Lambda = 0$ curve is significant.

As we are most interested in the changes brought about by considering non-vanishing VE, it is useful to introduce a variable that quantifies the relative shift in $\tilde{\Lambda}$ due to VE:

$$\delta \equiv \frac{\tilde{\Lambda} - \tilde{\Lambda}_0}{\tilde{\Lambda}_0} \ , \tag{5.4.6}$$

where $\tilde{\Lambda}_0$ is the value of $\tilde{\Lambda}$ obtained by taking the VE term to zero.

The deviation as a function of the heavy star mass, M_1, for the Hebeler et al. parametrization is shown in Fig. 5.4. The negative values for δ mean that introducing a VE term lowers

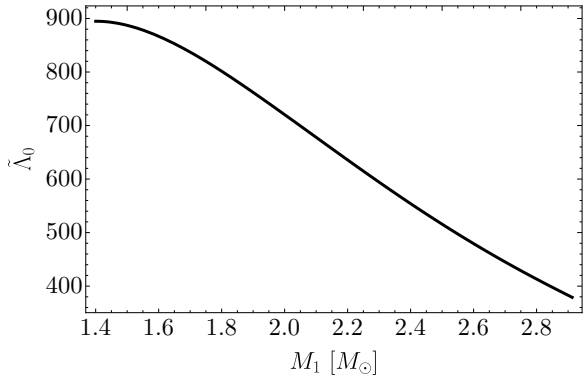

(a) $\mathcal{M} = 2^{-1/5}1.4M_\odot \approx 1.22M_\odot$

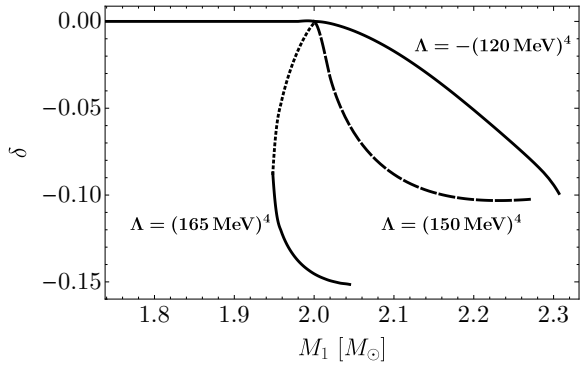

(b) $\mathcal{M} = 2^{-1/5}1.4M_\odot \approx 1.22M_\odot$

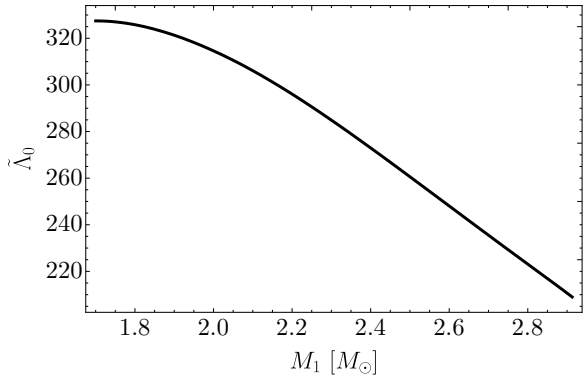

(c) $\mathcal{M} = 2^{-1/5}1.7M_\odot \approx 1.48M_\odot$

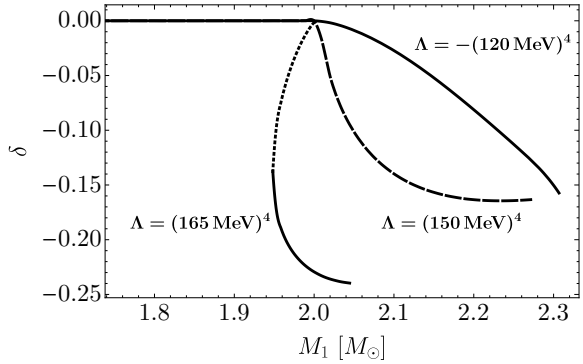

(d) $\mathcal{M} = 2^{-1/5}1.7M_\odot \approx 1.48M_\odot$

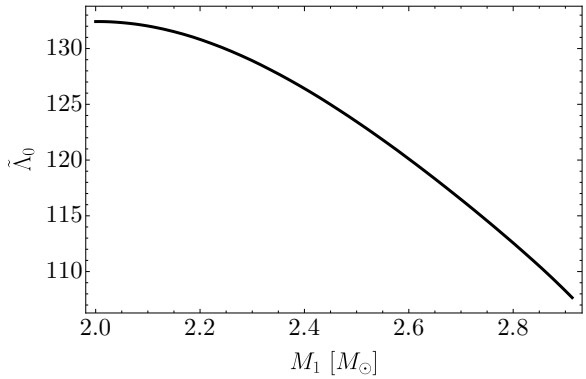

(e) $\mathcal{M} = 2^{-1/5}2.0M_\odot \approx 1.74M_\odot$

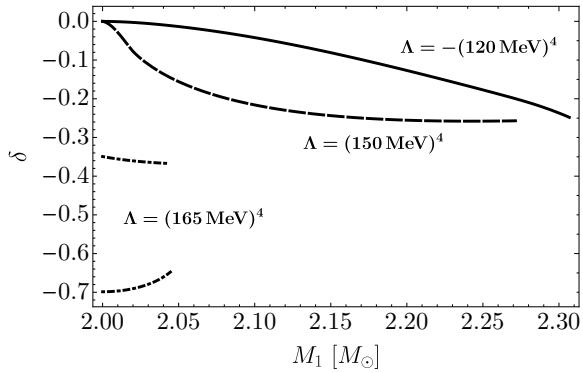

(f) $\mathcal{M} = 2^{-1/5}2.0M_\odot \approx 1.74M_\odot$

Figure 5.4: Plots on the right show the relative deviation of the combined dimensionless tidal deformability, $\tilde{\Lambda}$, as a function of the heaviest star mass for the Hebeler et al. parametrization with $\alpha = 3$ for various values of the chirp mass. Plots on the left show $\tilde{\Lambda}$ for vanishing VE for the same chirp masses. Dotted parts of the curves correspond to unstable configurations. The disconnected branches associated with two stable NS configurations allow for the largest deviations.

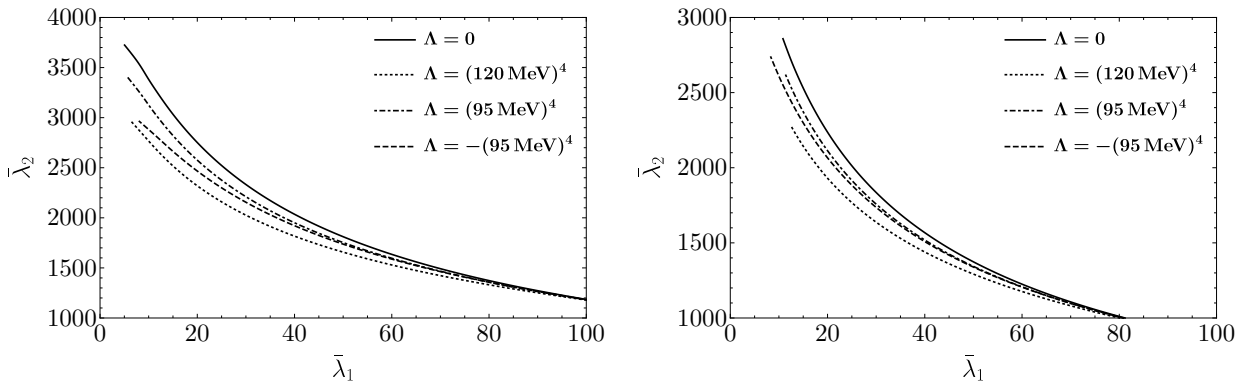

(a) SLy EoS

(b) AP4 EoS

Figure 5.5: Tidal deformability curves for a neutron star binary with SLy and AP4 EoS's. The chirp mass is taken to be $\mathcal{M} = 1.188 M_\odot$, which is the same value as in GW170817. $\bar{\lambda}_1$ and $\bar{\lambda}_2$ correspond to the dimensionless tidal deformability parameters for the heavy and light stars, respectively. Each curve is obtained by varying the heavy star mass while holding the chirp mass fixed. The α-parameter of (5.2.14) is chosen to be $\alpha = 3$.

the value of $\tilde{\Lambda}$. In order to isolate as much as possible the effects that a nonzero value of Λ has on the internal structure of the stars, we are comparing each point in a given curve with the corresponding event on the $\Lambda = 0$ curve that has the same neutron star masses. Therefore, any deviation in the value of $\tilde{\Lambda}$ comes entirely from the change in the tidal deformabilities, $\bar{\lambda}_i$.

Even with the more conservative SLy and AP4 models one still finds large deviations in $\tilde{\Lambda}$ for events with larger chirp masses. The case of the (smaller) chirp mass corresponding to GW170817 is displayed in Fig. 5.5, and the deviations in deformability are small. This is because the combined deformability is typically dominated by the contribution from the less massive star, which does not contain a core in the new phase where VE plays a role. However for higher chirp masses the effect of vacuum energy can be sizable even for the SLy and AP4 EoS's, as shown in Figs. 5.6 and 5.7. As the chirp mass increases more of the star contains the new phase, and eventually both stars typically contain cores in the new phase, yielding the increased sensitivity to VE. The high chirp mass we have chosen for these figures corresponds, if the stars are of equal mass, to individual masses of $1.9 M_\odot$, approaching that

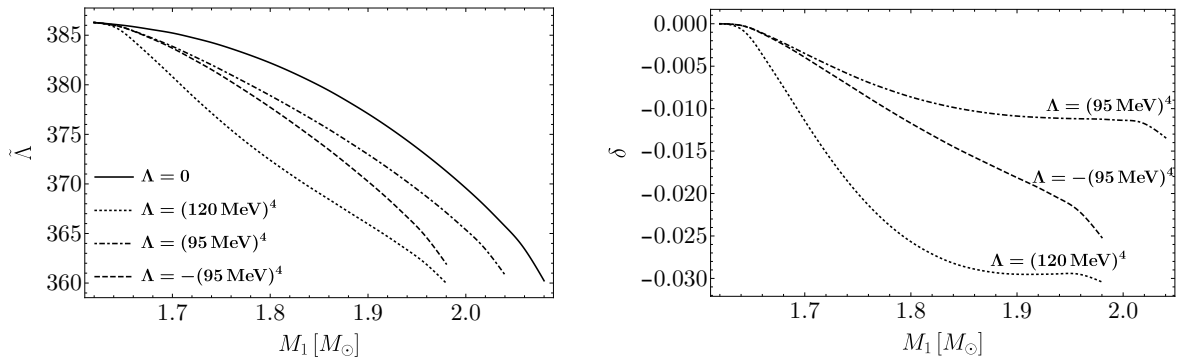

(a) $\mathcal{M} = 1.188 M_\odot$

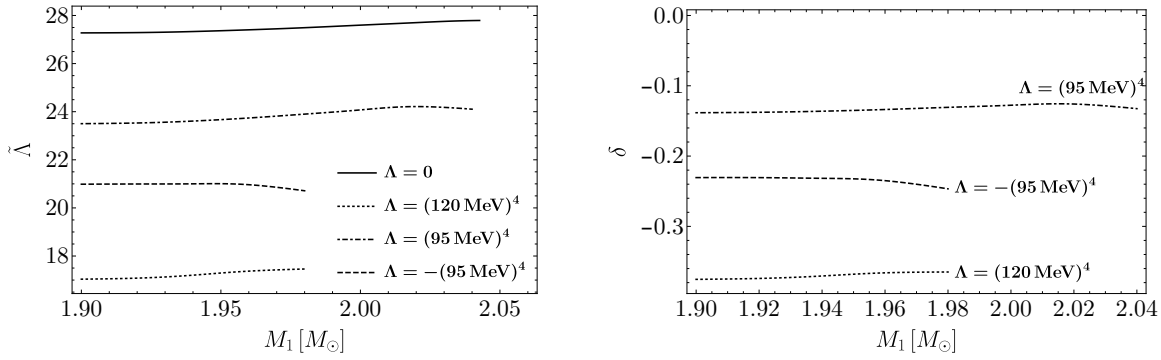

(b) $\mathcal{M} = 1.65 M_\odot$

Figure 5.6: Plot of the deviation of the combined dimensionless tidal deformability as a function of the heavy star mass for the SLy EoS with different values for the chirp mass. $\mathcal{M} = 1.188 M_\odot$ is the same as the one of GW170817, while $\mathcal{M} = 1.65 M_\odot$ corresponds to a chirp mass where if the two NS masses are equal they have a mass of $1.9 M_\odot$. For the smaller chirp mass the effect is rather small, however for a higher chirp mass the effect can be as large as 38%. The α-parameter of (5.2.14) is again chosen to be $\alpha = 3$.

of the most massive NS observed to date. One can see that for this case the deviation can be as large as 37%, even for these more conservative equations of state.

Since the chirp mass is the most accurately measured property of the NS merger, it is worthwhile to examine the dependence of δ (characterizing the sensitivity to VE) on the chirp mass. In Figs. 5.8 (Hebeler) and 5.9 (AP4 and SLy) we plot $\tilde{\Lambda}_0^{\max}$ and $\delta^{\max}$ as a function of the chirp mass. The superscript expresses the fact that, when evaluating the quantities in Eqs. (5.4.5) and (5.4.6), the mass of the heavy star is kept fixed at the maximal value allowed by the corresponding fixed value of Λ. Fixing one of the stars to have maximal mass

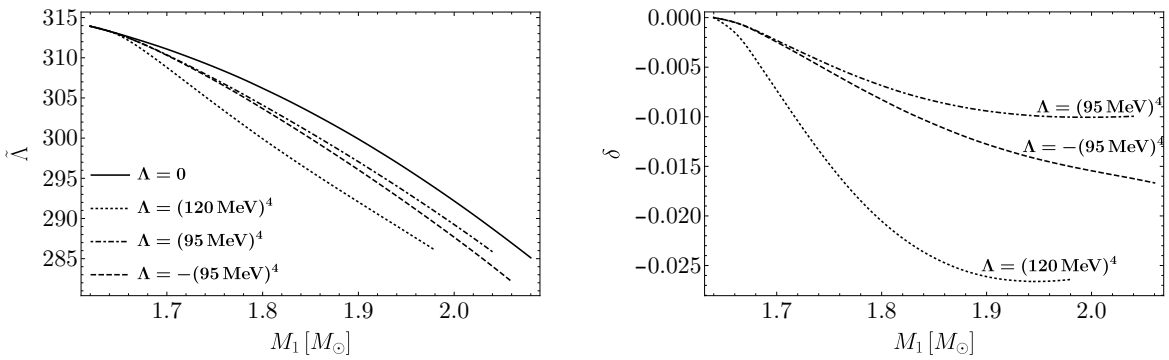

(a) $\mathcal{M} = 1.188 M_\odot$

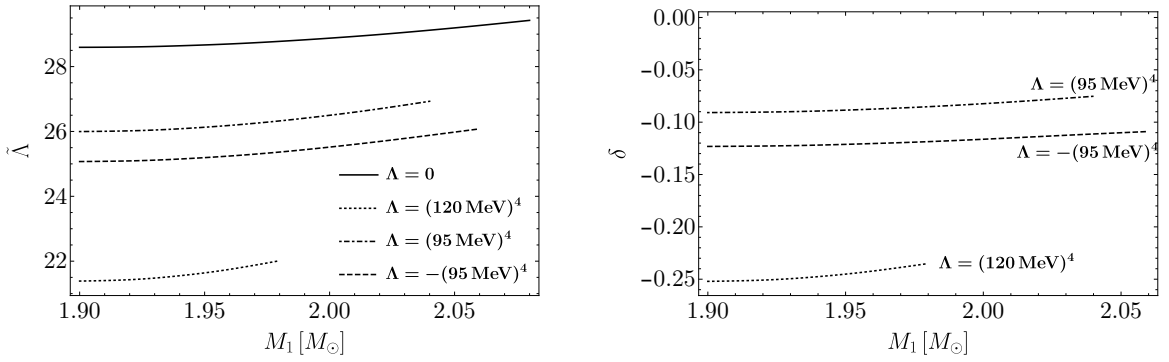

(b) $\mathcal{M} = 1.65 M_\odot$

Figure 5.7: Plot of the deviation of the combined dimensionless tidal deformability as a function of the heavy star mass for the AP4 EoS with different values for the chirp mass. Plots on the left show the value of $\tilde{\Lambda}$, while plots on the right show the fractional deviation, δ. The chirp mass $\mathcal{M} = 1.188 M_\odot$ is the same as the one of GW170817, while $\mathcal{M} = 1.65 M_\odot$ corresponds to a chirp mass where if the two NS masses are equal they have a mass of $1.9 M_\odot$. For the smaller chirp mass the effect is rather small, however for a higher chirp mass the effect can be as large as 25%. Again the α-parameter of (5.2.14) is chosen to be $\alpha = 3$.

will generically (though not always) give the largest VE effect on $\tilde{\Lambda}$. The important result of the plots is that the deviation increases substantially above a certain chirp mass denoted by the vertical gray line in the plots. This threshold corresponds to the chirp mass for which the lighter star mass also reaches the critical mass for the phase transition. Therefore, the large deviation can be understood from the fact that both stars are in the new phase.

In our final plot in Fig. 5.10, we display the limits that GW170817 places on VE assuming the Hebeler et al. parametrization. In particular, we note that including a VE term significantly

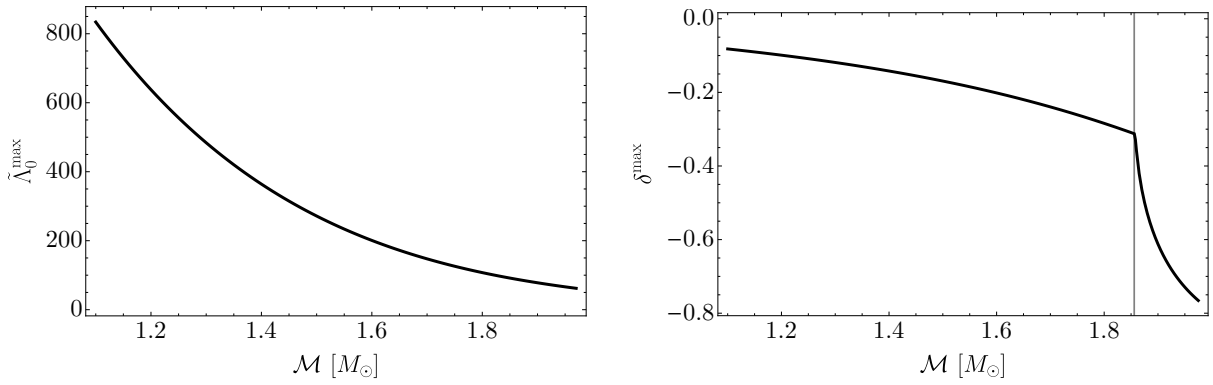

Figure 5.8: Dependence on the chirp mass in the Hebeler et al. parametrization, keeping the heaviest star mass fixed at $M_1 = 2.27 M_\odot$ (the maximum value for the $\Lambda = (150\,\mathrm{MeV})^4$ curve). The left plot shows the corresponding value of the combined tidal deformability for the $\Lambda = 0$ curve. The right plot represents the relative deviation of the combined tidal deformability by turning on $\Lambda = (150\,\mathrm{MeV})^4$ and is a measure of how the effect of VE potentially increases with the chirp mass.

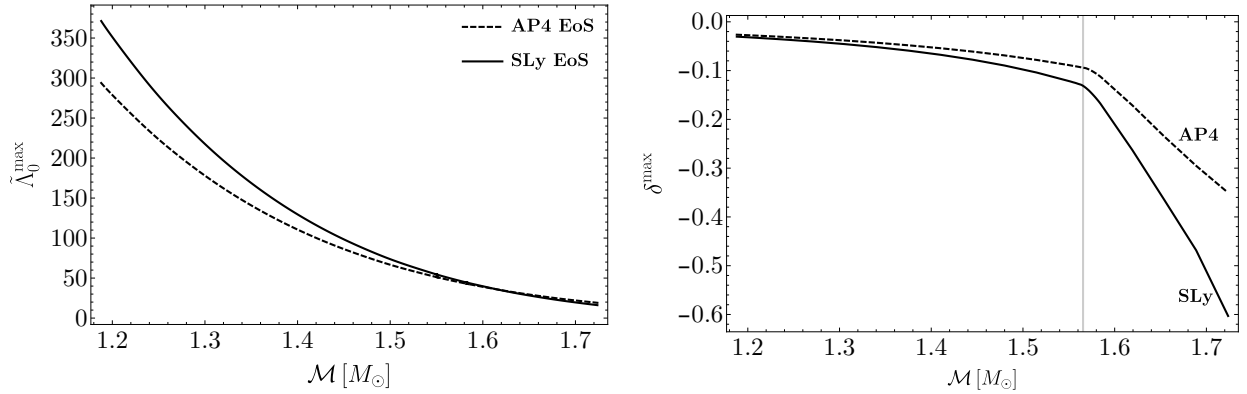

Figure 5.9: Dependence on the chirp mass in the AP4 and SLy parametrizations, keeping the heaviest star mass fixed at $M_1 = 1.98 M_\odot$ (the maximum value for the $\Lambda = (120\,\mathrm{MeV})^4$ curve). The chirp mass range is from $\mathcal{M} = 1.188 M_\odot$ to $\mathcal{M} \approx 1.72 M_\odot$, where the latter corresponds to the case when both stars have masses $M_{1,2} = 1.98 M_\odot$. The left plot shows the corresponding value of the combined tidal deformability for the $\Lambda = 0$ curves. The right plot represents the relative deviation of the combined tidal deformability and is a measure of how the effect of VE potentially increases with the chirp mass. The vertical gray line denotes the chirp mass at which the light star mass reaches the critical mass for the phase transition.

changes the allowed range of the individual masses for the high-spin assumption. The effect is less pronounced for the SLy and AP4 models. As more data on NS mergers are collected with some of those corresponding to mergers of more massive stars, strong limits could be placed on the EoS of dense nuclear matter. This will especially be true once the sensitivities

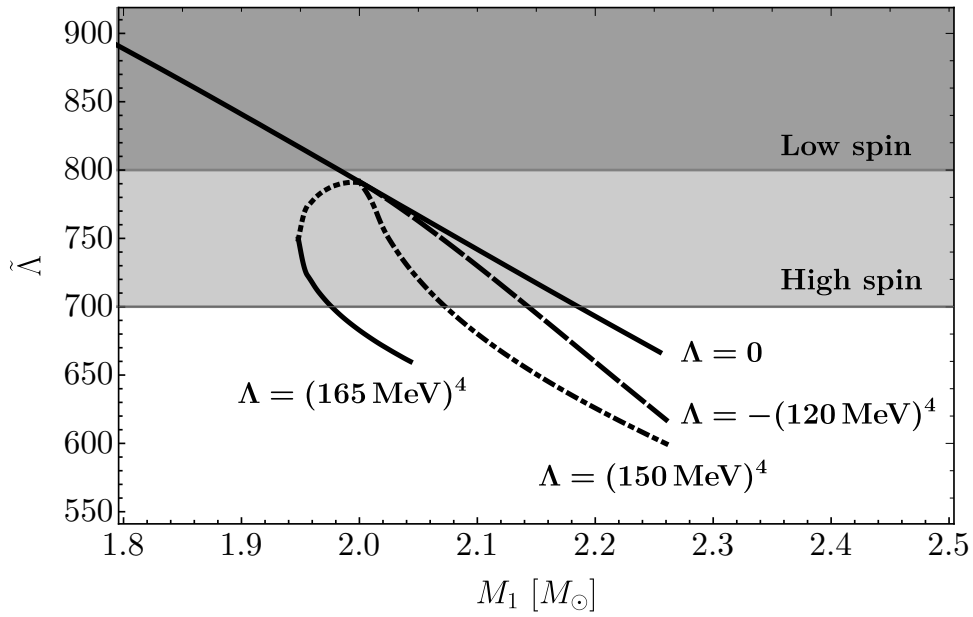

Figure 5.10: Combined tidal deformability $\tilde{\Lambda}$ as a function of the heavy star mass M_1 for the Hebeler et al. parametrization with $\alpha = 3$. The chirp mass is the same as in the event GW170817. The figure shows the upper bounds set by the LIGO/Virgo analysis and demonstrates how a nonzero value of Λ can affect the allowed mass range.

for probing the tidal contributions to the gravitational wave phase further improve.

The future outlook is difficult to extrapolate, but promising. At present, due to the sensitivity of the experiments, the limited statistics, and the number of parameters involved in the simulations, it is not possible to precisely and unambiguously determine from NS measurements the vacuum energy contribution to the QCD equation of state. However, the constraints that are placed in the coming years will depend strongly on currently uncertain characteristics of NS binaries or NS-black hole mergers that will be captured by upcoming data-taking runs at LIGO and other GW observatories [177]. Constraints will depend upon masses, spins, and branch populations in cases where there are multiple configurations with the same mass. In addition, the sensitivities of the experiments will evolve, and may be able to better capture higher order contributions to the waveforms. This will help single out the

different contributions to the observable quantities, for example distinguish the effects of vacuum energy from the rest of the EoS parameters, once the uncertainties on masses, radii and tidal deformabilities are reduced. Finally, utilization of neutron stars as laboratories to study very high density physics and VE depends crucially on a precise theoretical calculation of the QCD equation of state at high densities [178]. Such a calculation is certainly very difficult, mainly due to technical challenges rather than conceptual ones. Taking an optimistic viewpoint on these issues leads us to the conclusion that neutron star mergers can tell us about the interface of gravity and quantum field theory in a regime never before tested.

5.5 Conclusions

In this paper, we have argued that neutron star mergers can be a valuable tool for testing new phases of QCD at large densities, in particular for finding the contribution of a VE term in exotic high density phases. To study the effects of such a new phase on neutron star observables, we have started with the conventional 7-layer parametrization of the EoS, then assumed a nonzero value for the VE in the innermost layer leading to a jump in the energy density. For the three benchmark models we have chosen, we have calculated the $M(R)$ curves and tidal Love numbers for different values of the VE. By using those results, we have obtained individual tidal deformabilities and calculated the combined dimensionless tidal deformability parameter which can be constrained by neutron star mergers observed in gravitational wave observatories. We have found that for larger chirp masses, the nonzero VE at the innermost core can have an $\mathcal{O}(1)$ effect on the combined dimensionless tidal deformability parameter, hence future observations of neutron star merger chirps can place strong limits on the EoS of

dense nuclear matter. We have also shown that for some parameters, introducing a nonzero VE can create a disconnected branch of stable neutron star solutions allowing the possibility of having two neutron stars of the same mass with significantly different radii. This possibility is unique to EoS's which have a phase transition at the core, hence it is a smoking gun for new phases of QCD.

Bibliography

[1] G. Aad et al. (ATLAS), "Observation of a new particle in the search for the Standard Model Higgs boson with the ATLAS detector at the LHC", *Phys. Lett. B* **716**, 10.1016/j.physletb.2012.08.020 (2012) [arXiv:1207.7214 [hep-ex]].

[2] S. Chatrchyan et al. (CMS), "Observation of a New Boson at a Mass of 125 GeV with the CMS Experiment at the LHC", *Phys. Lett. B* **716**, 10.1016/j.physletb.2012.08.021 (2012) [arXiv:1207.7235 [hep-ex]].

[3] F. Englert, R. Brout, "Broken Symmetry and the Mass of Gauge Vector Mesons", *Phys. Rev. Lett.* **13**, edited by J. C. Taylor, 10.1103/PhysRevLett.13.321 (1964).

[4] P. W. Higgs, "Broken Symmetries and the Masses of Gauge Bosons", *Phys. Rev. Lett.* **13**, edited by J. C. Taylor, 10.1103/PhysRevLett.13.508 (1964).

[5] G. S. Guralnik, C. R. Hagen, T. W. B. Kibble, "Global Conservation Laws and Massless Particles", *Phys. Rev. Lett.* **13**, edited by J. C. Taylor, 10.1103/PhysRevLett.13.585 (1964).

[6] J. Terning, "Modern supersymmetry: Dynamics and duality" (2006).

[7] R. Contino, "The Higgs as a Composite Nambu-Goldstone Boson", in Theoretical Advanced Study Institute in Elementary Particle Physics: Physics of the Large and the Small (May 2010) [arXiv:1005.4269 [hep-ph]].

[8] B. Bellazzini, C. Csáki, J. Serra, "Composite Higgses", *Eur. Phys. J. C* **74**, 10.1140/epjc/s10052-014-2766-x (2014) [arXiv:1401.2457 [hep-ph]].

[9] G. Panico, A. Wulzer, "The Composite Nambu-Goldstone Higgs", Vol. 913 (Springer, 2016) [arXiv:1506.01961 [hep-ph]].

[10] C. Csaki, "TASI lectures on extra dimensions and branes", in Theoretical Advanced Study Institute in Elementary Particle Physics (TASI 2002): Particle Physics and Cosmology: The Quest for Physics Beyond the Standard Model(s) (Apr. 2004) [arXiv:hep-ph/0404096].

[11] C. Csaki, J. Hubisz, P. Meade, "TASI lectures on electroweak symmetry breaking from extra dimensions", in Theoretical Advanced Study Institute in Elementary Particle Physics: Physics in D $\geqq$ 4 (Oct. 2005) [arXiv:hep-ph/0510275].

[12] C. Csáki, S. Lombardo, O. Telem, "TASI Lectures on Non-supersymmetric BSM Models", in *Proceedings, Theoretical Advanced Study Institute in Elementary Particle Physics : Anticipating the Next Discoveries in Particle Physics (TASI 2016): Boulder, CO, USA, June 6-July 1, 2016*, edited by R. Essig, I. Low (WSP, 2018) [arXiv:1811.04279 [hep-ph]].

[13] V. Agrawal, S. M. Barr, J. F. Donoghue, D. Seckel, "Viable range of the mass scale of the standard model", *Phys. Rev. D* **57**, 10.1103/PhysRevD.57.5480 (1998) [arXiv:hep-ph/9707380].

[14] P. W. Graham, D. E. Kaplan, S. Rajendran, "Cosmological Relaxation of the Electroweak Scale", *Phys. Rev. Lett.* **115**, 10.1103/PhysRevLett.115.221801 (2015) [arXiv:1504.07551 [hep-ph]].

[15] N. Aghanim et al. (Planck), "Planck 2018 results. VI. Cosmological parameters", *Astron. Astrophys.* **641**, 10.1051/0004-6361/201833910 (2020) [arXiv:1807.06209 [astro-ph.CO]].

[16] S. Weinberg, "Anthropic Bound on the Cosmological Constant", *Phys. Rev. Lett.* **59**, 10.1103/PhysRevLett.59.2607 (1987).

[17] J. A. Harvey, "TASI 2003 lectures on anomalies", in (Sept. 2005) [arXiv:hep-th/0509097].

[18] G. F. Giudice, "Naturally Speaking: The Naturalness Criterion and Physics at the LHC", edited by G. Kane, A. Pierce, 10.1142/9789812779762_0010 (2008) [arXiv:0801.2562 [hep-ph]].

[19] P. Bak, C. Tang, K. Wiesenfeld, "Self-organized criticality", *Phys. Rev. A* **38**, 10.1103/PhysRevA.38.364 (1988).

[20] P. Bak, C. Tang, K. Wiesenfeld, "Self-organized criticality: An Explanation of 1/f noise", *Phys. Rev. Lett.* **59**, 10.1103/PhysRevLett.59.381 (1987).

[21] N. W. Watkins, G. Pruessner, S. C. Chapman, N. B. Crosby, H. J. Jensen, "25 years of self-organized criticality: concepts and controversies", *Space Science Reviews* **198**, 10.1007/s11214-015-0155-x (2015).

[22] M. J. Aschwanden et al., "25 Years of Self-Organized Criticality: Solar and Astrophysics", *Space Sci. Rev.* **198**, 10.1007/s11214-014-0054-6 (2016) [arXiv:1403.6528 [astro-ph.IM]].

[23] D. Sornette, "Discrete scale invariance and complex dimensions", *Phys. Rept.* **297**, 10.1016/S0370-1573(97)00076-8 (1998) [arXiv:cond-mat/9707012].

[24] P. Breitenlohner, D. Z. Freedman, "Stability in Gauged Extended Supergravity", *Annals Phys.* **144**, 10.1016/0003-4916(82)90116-6 (1982).

[25] D. B. Kaplan, J.-W. Lee, D. T. Son, M. A. Stephanov, "Conformality Lost", *Phys. Rev. D* **80**, 10.1103/PhysRevD.80.125005 (2009) [arXiv:0905.4752 [hep-th]].

[26] J. M. Maldacena, "The Large N limit of superconformal field theories and supergravity", *Adv. Theor. Math. Phys.* **2**, 10.1023/A:1026654312961 (1998) [arXiv:hep-th/9711200].

[27] S. R. Coleman, E. J. Weinberg, "Radiative Corrections as the Origin of Spontaneous Symmetry Breaking", *Phys. Rev. D* **7**, 10.1103/PhysRevD.7.1888 (1973).

[28] L. E. Ibanez, G. G. Ross, "SU(2)-L x U(1) Symmetry Breaking as a Radiative Effect of Supersymmetry Breaking in Guts", *Phys. Lett. B* **110**, 10.1016/0370-2693(82)91239-4 (1982).

[29] J. R. Ellis, J. S. Hagelin, D. V. Nanopoulos, K. Tamvakis, "Weak Symmetry Breaking by Radiative Corrections in Broken Supergravity", *Phys. Lett. B* **125**, 10.1016/0370-2693(83)91283-2 (1983).

[30] L. Alvarez-Gaume, J. Polchinski, M. B. Wise, "Minimal Low-Energy Supergravity", *Nucl. Phys. B* **221**, 10.1016/0550-3213(83)90591-6 (1983).

[31] H. Georgi, "Physics Fun with Discrete Scale Invariance", (2016) [arXiv:1606.03405 [hep-ph]].

[32] N. Arkani-Hamed, S. Dubovsky, A. Nicolis, G. Villadoro, "Quantum Horizons of the Standard Model Landscape", *JHEP* **06**, 10.1088/1126-6708/2007/06/078 (2007) [arXiv:hep-th/0703067].

[33] L. Randall, R. Sundrum, "A Large mass hierarchy from a small extra dimension", *Phys. Rev. Lett.* **83**, 10.1103/PhysRevLett.83.3370 (1999) [arXiv:hep-ph/9905221].

[34] R. Rattazzi, A. Zaffaroni, "Comments on the holographic picture of the Randall-Sundrum model", *JHEP* **04**, 10.1088/1126-6708/2001/04/021 (2001) [arXiv:hep-th/0012248].

[35] N. Arkani-Hamed, M. Porrati, L. Randall, "Holography and phenomenology", *JHEP* **08**, 10.1088/1126-6708/2001/08/017 (2001) [arXiv:hep-th/0012148].

[36] M. A. Luty, J. Polchinski, R. Rattazzi, "The a-theorem and the Asymptotics of 4D Quantum Field Theory", *JHEP* **01**, 10.1007/JHEP01(2013)152 (2013) [arXiv:1204.5221 [hep-th]].

[37] V. Emery, S. Kivelson, "Frustrated electronic phase separation and high-temperature superconductors", *Physica C: Superconductivity* **209**, https://doi.org/10.1016/0921-4534(93)90581-A (1993).

[38] A. Shapere, F. Wilczek, "Classical Time Crystals", *Phys. Rev. Lett.* **109**, 10.1103/PhysRevLett.109.160402 (2012) [arXiv:1202.2537 [cond-mat.other]].

[39] F. Wilczek, "Quantum Time Crystals", *Phys. Rev. Lett.* **109**, 10.1103/PhysRevLett.109.160401 (2012) [arXiv:1202.2539 [quant-ph]].

[40] S. A. Hartnoll, A. Lucas, S. Sachdev, "Holographic quantum matter", (2016) [arXiv:1612.07324 [hep-th]].

[41] J. S. Bains, M. P. Hertzberg, F. Wilczek, "Oscillatory Attractors: A New Cosmological Phase", *JCAP* **05**, 10.1088/1475-7516/2017/05/011 (2017) [arXiv:1512.02304 [hep-th]].

[42] D. A. Easson, T. Manton, "Stable Cosmic Time Crystals", *Phys. Rev. D* **99**, 10.1103/PhysRevD.99.043507 (2019) [arXiv:1802.03693 [hep-th]].

[43] D. Bunk, J. Hubisz, B. Jain, "A Perturbative RS I Cosmological Phase Transition", *Eur. Phys. J. C* **78**, 10.1140/epjc/s10052-018-5529-2 (2018) [arXiv:1705.00001 [hep-ph]].

[44] L. Vecchi, "A Natural Hierarchy and a low New Physics scale from a Bulk Higgs", *JHEP* **11**, 10.1007/JHEP11(2011)102 (2011) [arXiv:1012.3742 [hep-ph]].

[45] M. Geller, S. Bar-Shalom, A. Soni, "Higgs-radion unification: Radius stabilization by an SU(2) bulk doublet and the 126 GeV scalar", *Phys. Rev. D* **89**, 10.1103/PhysRevD.89.095015 (2014) [arXiv:1312.3331 [hep-ph]].

[46] A. Pomarol, "Light scalars: from lattice to the lhc via holography", Talk at Planck 2017.

[47] B. Bellazzini, C. Csaki, J. Hubisz, J. Serra, J. Terning, "A Naturally Light Dilaton and a Small Cosmological Constant", *Eur. Phys. J. C* **74**, 10.1140/epjc/s10052-014-2790-x (2014) [arXiv:1305.3919 [hep-th]].

[48] I. R. Klebanov, E. Witten, "AdS / CFT correspondence and symmetry breaking", *Nucl. Phys. B* **556**, 10.1016/S0550-3213(99)00387-9 (1999) [arXiv:hep-th/9905104].

[49] S. S. Gubser, I. R. Klebanov, "A Universal result on central charges in the presence of double trace deformations", *Nucl. Phys. B* **656**, 10.1016/S0550-3213(03)00056-7 (2003) [arXiv:hep-th/0212138].

[50] C. Csaki, M. Graesser, L. Randall, J. Terning, "Cosmology of brane models with radion stabilization", *Phys. Rev. D* **62**, 10.1103/PhysRevD.62.045015 (2000) [arXiv:hep-ph/9911406].

[51] C. Csaki, M. L. Graesser, G. D. Kribs, "Radion dynamics and electroweak physics", *Phys. Rev. D* **63**, 10.1103/PhysRevD.63.065002 (2001) [arXiv:hep-th/0008151].

[52] W. D. Goldberger, M. B. Wise, "Modulus stabilization with bulk fields", *Phys. Rev. Lett.* **83**, 10.1103/PhysRevLett.83.4922 (1999) [arXiv:hep-ph/9907447].

[53] V. L. Berezinsky, "Destruction of long range order in one-dimensional and two-dimensional systems having a continuous symmetry group. I. Classical systems", *Sov. Phys. JETP* **32** (1971).

[54] J. M. Kosterlitz, D. J. Thouless, "Ordering, metastability and phase transitions in two-dimensional systems", *J. Phys. C* **6**, 10.1088/0022-3719/6/7/010 (1973).

[55] M. A. Amin, J. Fan, K. D. Lozanov, M. Reece, "Cosmological dynamics of Higgs potential fine tuning", *Phys. Rev. D* **99**, 10.1103/PhysRevD.99.035008 (2019) [arXiv:1802.00444 [hep-ph]].

[56] L. Kofman, A. D. Linde, X. Liu, A. Maloney, L. McAllister, E. Silverstein, "Beauty is attractive: Moduli trapping at enhanced symmetry points", *JHEP* **05**, 10.1088/1126-6708/2004/05/030 (2004) [arXiv:hep-th/0403001].

[57] W. D. Goldberger, M. B. Wise, "Phenomenology of a stabilized modulus", *Phys. Lett. B* **475**, 10.1016/S0370-2693(00)00099-X (2000) [arXiv:hep-ph/9911457].

[58] M. A. Amin, J. Fan, K. D. Lozanov, M. Reece, "Cosmological dynamics of Higgs potential fine tuning", *Phys. Rev. D* **99**, 10.1103/PhysRevD.99.035008 (2019) [arXiv:1802.00444 [hep-ph]].

[59] G. F. Giudice, R. Rattazzi, J. D. Wells, "Graviscalars from higher dimensional metrics and curvature Higgs mixing", *Nucl. Phys. B* **595**, 10.1016/S0550-3213(00)00686-6 (2001) [arXiv:hep-ph/0002178].

[60] C. Eröncel, J. Hubisz, G. Rigo, "Self-Organized Higgs Criticality", *JHEP* **03**, 10.1007/JHEP03(2019)046 (2019) [arXiv:1804.00004 [hep-ph]].

[61] O. DeWolfe, D. Z. Freedman, S. S. Gubser, A. Karch, "Modeling the fifth-dimension with scalars and gravity", *Phys. Rev. D* **62**, 10.1103/PhysRevD.62.046008 (2000) [arXiv:hep-th/9909134].

[62] B. von Harling, G. Servant, "QCD-induced Electroweak Phase Transition", *JHEP* **01**, 10.1007/JHEP01(2018)159 (2018) [arXiv:1711.11554 [hep-ph]].

[63] S. Bruggisser, B. Von Harling, O. Matsedonskyi, G. Servant, "Baryon Asymmetry from a Composite Higgs Boson", *Phys. Rev. Lett.* **121**, 10.1103/PhysRevLett.121.131801 (2018) [arXiv:1803.08546 [hep-ph]].

[64] S. Bruggisser, B. Von Harling, O. Matsedonskyi, G. Servant, "Electroweak Phase Transition and Baryogenesis in Composite Higgs Models", *JHEP* **12**, 10.1007/JHEP12(2018)099 (2018) [arXiv:1804.07314 [hep-ph]].

[65] A. Pomarol, O. Pujolas, L. Salas, "Holographic conformal transition and light scalars", *JHEP* **10**, 10.1007/JHEP10(2019)202 (2019) [arXiv:1905.02653 [hep-th]].

[66] C. Cheung, P. Saraswat, "Mass Hierarchy and Vacuum Energy", (2018) [arXiv:1811.12390 [hep-ph]].

[67] J. M. Lizana, M. Olechowski, S. Pokorski, "A new way of calculating the effective potential for a light radion", *JHEP* **09**, 10.1007/JHEP09(2020)092 (2020) [arXiv:1911.11124 [hep-ph]].

[68] F. Abu-Ajamieh, J. S. Lee, J. Terning, "The Light Radion Window", *JHEP* **10**, 10.1007/JHEP10(2018)050 (2018) [arXiv:1711.02697 [hep-ph]].

[69] E. Witten, "Anti-de Sitter space and holography", *Adv. Theor. Math. Phys.* **2**, 10.4310/ATMP.1998.v2.n2.a2 (1998) [arXiv:hep-th/9802150].

[70] S. Fubini, "A New Approach to Conformal Invariant Field Theories", *Nuovo Cim. A* **34**, 10.1007/BF02785664 (1976).

[71] F. Coradeschi, P. Lodone, D. Pappadopulo, R. Rattazzi, L. Vitale, "A naturally light dilaton", *JHEP* **11**, 10.1007/JHEP11(2013)057 (2013) [arXiv:1306.4601 [hep-th]].

[72] V. Gorbenko, S. Rychkov, B. Zan, "Walking, Weak first-order transitions, and Complex CFTs", *JHEP* **10**, 10.1007/JHEP10(2018)108 (2018) [arXiv:1807.11512 [hep-th]].

[73] S. L. Adler, "Axial vector vertex in spinor electrodynamics", *Phys. Rev.* **177**, 10.1103/PhysRev.177.2426 (1969).

[74] J. S. Bell, R. Jackiw, "A PCAC puzzle: $\pi^0 \to \gamma\gamma$ in the σ model", *Nuovo Cim. A* **60**, 10.1007/BF02823296 (1969).

[75] S. L. Adler, W. A. Bardeen, "Absence of higher order corrections in the anomalous axial vector divergence equation", *Phys. Rev.* **182**, 10.1103/PhysRev.182.1517 (1969).

[76] S. L. Adler, "Anomalies to all orders", in *50 years of Yang-Mills theory*, edited by G. 't Hooft (2005) [arXiv:hep-th/0405040].

[77] G. 't Hooft, C. Itzykson, A. Jaffe, H. Lehmann, P. K. Mitter, I. M. Singer, R. Stora, eds., *Recent Developments in Gauge Theories. Proceedings, Nato Advanced Study Institute, Cargese, France, August 26 - September 8, 1979*, Vol. 59 (1980).

[78] N. Seiberg, "Electric - magnetic duality in supersymmetric nonAbelian gauge theories", *Nucl. Phys. B* **435**, 10.1016/0550-3213(94)00023-8 (1995) [arXiv:hep-th/9411149].

[79] K. A. Intriligator, N. Seiberg, "Lectures on supersymmetric gauge theories and electric-magnetic duality", *Nucl. Phys. B Proc. Suppl.* **45BC**, edited by A. Zichichi, 10.1016/0920-5632(95)00626-5 (1996) [arXiv:hep-th/9509066].

[80] M. E. Peskin, "Duality in supersymmetric Yang-Mills theory", in Theoretical Advanced Study Institute in Elementary Particle Physics (TASI 96): Fields, Strings, and Duality (Feb. 1997) [arXiv:hep-th/9702094].

[81] J. Wess, B. Zumino, "Consequences of anomalous Ward identities", *Phys. Lett. B* **37**, 10.1016/0370-2693(71)90582-X (1971).

[82] E. Witten, "Global Aspects of Current Algebra", *Nucl. Phys. B* **223**, 10.1016/0550-3213(83)90063-9 (1983).

[83] M. B. Green, J. H. Schwarz, "Anomaly Cancellation in Supersymmetric D=10 Gauge Theory and Superstring Theory", *Phys. Lett. B* **149**, 10.1016/0370-2693(84)91565-X (1984).

[84] A. Adams, O. DeWolfe, W. Taylor, "String universality in ten dimensions", *Phys. Rev. Lett.* **105**, 10.1103/PhysRevLett.105.071601 (2010) [arXiv:1006.1352 [hep-th]].

[85] B. Zumino, Y.-S. Wu, A. Zee, "Chiral Anomalies, Higher Dimensions, and Differential Geometry", *Nucl. Phys. B* **239**, 10.1016/0550-3213(84)90259-1 (1984).

[86] J. Manes, R. Stora, B. Zumino, "Algebraic Study of Chiral Anomalies", *Commun. Math. Phys.* **102**, 10.1007/BF01208825 (1985).

[87] R. Jackiw, "Topological Investigations of Quantized Gauge Theories", *Conf. Proc. C* **8306271**, edited by B. S. DeWitt, R. Stora (1983).

[88] B. Zumino, "Chiral Anomalies and Differential Geometry: Lectures Given at Les Houches, August 1983", in Les Houches Summer School on Theoretical Physics: Relativity, Groups and Topology (Oct. 1983).

[89] R. Stora, "Algebraic Structure and Topological Origin of Anomalies", edited by G. 't Hooft, A. Jaffe, H. Lehmann, P. K. Mitter, I. M. Singer, R. Stora (1983).

[90] S. Weinberg, "The quantum theory of fields. Vol. 2: Modern applications" (Cambridge University Press, Aug. 2013).

[91] C. G. Callan Jr., J. A. Harvey, "Anomalies and Fermion Zero Modes on Strings and Domain Walls", *Nucl. Phys. B* **250**, 10.1016/0550-3213(85)90489-4 (1985).

[92] E. Witten, "Fermion Path Integrals And Topological Phases", *Rev. Mod. Phys.* **88**, 10.1103/RevModPhys.88.035001 (2016) [arXiv:1508.04715 [cond-mat.mes-hall]].

[93] E. Witten, "The "Parity" Anomaly On An Unorientable Manifold", *Phys. Rev. B* **94**, 10.1103/PhysRevB.94.195150 (2016) [arXiv:1605.02391 [hep-th]].

[94] E. Witten, K. Yonekura, "Anomaly Inflow and the η-Invariant", in The Shoucheng Zhang Memorial Workshop (Sept. 2019) [arXiv:1909.08775 [hep-th]].

[95] K. Yonekura, "Dai-Freed theorem and topological phases of matter", *JHEP* **09**, 10.1007/JHEP09(2016)022 (2016) [arXiv:1607.01873 [hep-th]].

[96] D. J. Thouless, M. Kohmoto, M. P. Nightingale, M. den Nijs, "Quantized Hall Conductance in a Two-Dimensional Periodic Potential", *Phys. Rev. Lett.* **49**, 10.1103/PhysRevLett.49.405 (1982).

[97] E. Witten, "Three lectures on topological phases of matter", *Riv. Nuovo Cim.* **39**, 10.1393/ncr/i2016-10125-3 (2016) [arXiv:1510.07698 [cond-mat.mes-hall]].

[98] P. Horava, E. Witten, "Heterotic and type I string dynamics from eleven-dimensions", *Nucl. Phys. B* **460**, 10.1016/0550-3213(95)00621-4 (1996) [arXiv:hep-th/9510209].

[99] P. Horava, E. Witten, "Eleven-dimensional supergravity on a manifold with boundary", *Nucl. Phys. B* **475**, 10.1016/0550-3213(96)00308-2 (1996) [arXiv:hep-th/9603142].

[100] N. Arkani-Hamed, A. G. Cohen, H. Georgi, "Anomalies on orbifolds", *Phys. Lett. B* **516**, 10.1016/S0370-2693(01)00946-7 (2001) [arXiv:hep-th/0103135].

[101] C. A. Scrucca, M. Serone, L. Silvestrini, F. Zwirner, "Anomalies in orbifold field theories", *Phys. Lett. B* **525**, 10.1016/S0370-2693(01)01430-7 (2002) [arXiv:hep-th/0110073].

[102] G. von Gersdorff, M. Quiros, "Localized anomalies in orbifold gauge theories", *Phys. Rev. D* **68**, 10.1103/PhysRevD.68.105002 (2003) [arXiv:hep-th/0305024].

[103] C. A. Scrucca, M. Serone, "Anomalies in field theories with extra dimensions", *Int. J. Mod. Phys. A* **19**, 10.1142/S0217751X04018518 (2004) [arXiv:hep-th/0403163].

[104] R. Barbieri, R. Contino, P. Creminelli, R. Rattazzi, C. A. Scrucca, "Anomalies, Fayet-Iliopoulos terms and the consistency of orbifold field theories", *Phys. Rev. D* **66**, 10.1103/PhysRevD.66.024025 (2002) [arXiv:hep-th/0203039].

[105] L. Pilo, A. Riotto, "On anomalies in orbifold theories", *Phys. Lett. B* **546**, 10.1016/S0370-2693(02)02631-X (2002) [arXiv:hep-th/0202144].

[106] B. Gripaios, S. M. West, "Anomaly holography", *Nucl. Phys. B* **789**, 10.1016/j.nuclphysb.2007.08.008 (2008) [arXiv:0704.3981 [hep-ph]].

[107] X.-z. Dai, D. S. Freed, "η-Invariants and Determinant Lines", *J. Math. Phys.* **35**, [Erratum: J.Math.Phys. 42, 2343–2344 (2001)], 10.1063/1.530747 (1994) [arXiv:hep-th/9405012].

[108] D. Gaiotto, A. Kapustin, N. Seiberg, B. Willett, "Generalized Global Symmetries", *JHEP* **02**, 10.1007/JHEP02(2015)172 (2015) [arXiv:1412.5148 [hep-th]].

[109] D. Z. Freedman, S. D. Mathur, A. Matusis, L. Rastelli, "Correlation functions in the CFT(d) / AdS(d+1) correspondence", *Nucl. Phys. B* **546**, 10.1016/S0550-3213(99)00053-X (1999) [arXiv:hep-th/9804058].

[110] M. Henningson, K. Skenderis, "The Holographic Weyl anomaly", *JHEP* **07**, 10.1088/1126-6708/1998/07/023 (1998) [arXiv:hep-th/9806087].

[111] O. Aharony, J. Pawelczyk, S. Theisen, S. Yankielowicz, "A Note on anomalies in the AdS / CFT correspondence", *Phys. Rev. D* **60**, 10.1103/PhysRevD.60.066001 (1999) [arXiv:hep-th/9901134].

[112] M. Blau, K. S. Narain, E. Gava, "On subleading contributions to the AdS / CFT trace anomaly", *JHEP* **09**, 10.1088/1126-6708/1999/09/018 (1999) [arXiv:hep-th/9904179].

[113] S. Nojiri, S. D. Odintsov, "On the conformal anomaly from higher derivative gravity in AdS / CFT correspondence", *Int. J. Mod. Phys. A* **15**, 10.1142/S0217751X00000197 (2000) [arXiv:hep-th/9903033].

[114] A. Bilal, C.-S. Chu, "A Note on the chiral anomaly in the AdS / CFT correspondence and 1 / N**2 correction", *Nucl. Phys. B* **562**, 10.1016/S0550-3213(99)00553-2 (1999) [arXiv:hep-th/9907106].

[115] G. Panico, A. Wulzer, "Effective action and holography in 5D gauge theories", *JHEP* **05**, 10.1088/1126-6708/2007/05/060 (2007) [arXiv:hep-th/0703287].

[116] B. Gripaios, "Anomaly Holography, the Wess-Zumino-Witten Term, and Electroweak Symmetry Breaking", *Phys. Lett. B* **663**, 10.1016/j.physletb.2008.04.046 (2008) [arXiv:0803.0497 [hep-ph]].

[117] K. Agashe, P. Du, S. Hong, R. Sundrum, "Flavor Universal Resonances and Warped Gravity", *JHEP* **01**, 10.1007/JHEP01(2017)016 (2017) [arXiv:1608.00526 [hep-ph]].

[118] M. F. Atiyah, V. K. Patodi, I. M. Singer, "Spectral asymmetry and Riemannian Geometry 1", *Math. Proc. Cambridge Phil. Soc.* **77**, 10.1017/S0305004100049410 (1975).

[119] A. N. Redlich, "Gauge Noninvariance and Parity Violation of Three-Dimensional Fermions", *Phys. Rev. Lett.* **52**, edited by J. C. Taylor, 10.1103/PhysRevLett.52.18 (1984).

[120] A. N. Redlich, "Parity Violation and Gauge Noninvariance of the Effective Gauge Field Action in Three-Dimensions", *Phys. Rev. D* **29**, edited by F. Wilczek, 10.1103/PhysRevD.29.2366 (1984).

[121] G. V. Dunne, "Aspects of Chern-Simons theory", in Les Houches Summer School in Theoretical Physics, Session 69: Topological Aspects of Low-dimensional Systems (July 1998) [arXiv:hep-th/9902115].

[122] S. Hong, "In preparation",

[123] M. F. Atiyah, I. M. Singer, "The Index of elliptic operators. 1", *Annals Math.* **87**, 10.2307/1970715 (1968).

[124] L. Alvarez-Gaume, P. H. Ginsparg, "The Structure of Gauge and Gravitational Anomalies", *Annals Phys.* **161**, edited by A. Salam, E. Sezgin, [Erratum: Annals Phys. 171, 233 (1986)], 10.1016/0003-4916(85)90087-9 (1985).

[125] L. Alvarez-Gaume, S. Della Pietra, G. W. Moore, "Anomalies and Odd Dimensions", *Annals Phys.* **163**, 10.1016/0003-4916(85)90383-5 (1985).

[126] J. Hirn, V. Sanz, "Interpolating between low and high energy QCD via a 5-D Yang-Mills model", *JHEP* **12**, 10.1088/1126-6708/2005/12/030 (2005) [arXiv:hep-ph/0507049].

[127] J. Preskill, "Gauge anomalies in an effective field theory", *Annals Phys.* **210**, 10.1016/0003-4916(91)90046-B (1991).

[128] E. D'Hoker, S. Weinberg, "General effective actions", *Phys. Rev. D* **50**, 10.1103/PhysRevD.50.R6050 (1994) [arXiv:hep-ph/9409402].

[129] Y. Bai, G. Burdman, C. T. Hill, "Topological Interactions in Warped Extra Dimensions", *JHEP* **02**, 10.1007/JHEP02(2010)049 (2010) [arXiv:0911.1358 [hep-ph]].

[130] W. A. Bardeen, "Anomalous Ward identities in spinor field theories", *Phys. Rev.* **184**, 10.1103/PhysRev.184.1848 (1969).

[131] C.-S. Chu, P.-M. Ho, B. Zumino, "NonAbelian anomalies and effective actions for a homogeneous space G/H", *Nucl. Phys. B* **475**, 10.1016/0550-3213(96)00322-7 (1996) [arXiv:hep-th/9602093].

[132] C. T. Hill, "Anomalies, Chern-Simons terms and chiral delocalization in extra dimensions", *Phys. Rev. D* **73**, 10.1103/PhysRevD.73.085001 (2006) [arXiv:hep-th/0601154].

[133] S. Weinberg, "Implications of Dynamical Symmetry Breaking", *Phys. Rev. D* **13**, [Addendum: Phys.Rev.D 19, 1277–1280 (1979)], 10.1103/PhysRevD.19.1277 (1976).

[134] B. P. Abbott et al. (LIGO Scientific, Virgo), "GW170817: Observation of Gravitational Waves from a Binary Neutron Star Inspiral", *Phys. Rev. Lett.* **119**, 10.1103/PhysRevLett.119.161101 (2017) [arXiv:1710.05832 [gr-qc]].

[135] M. Baryakhtar, J. Bramante, S. W. Li, T. Linden, N. Raj, "Dark Kinetic Heating of Neutron Stars and An Infrared Window On WIMPs, SIMPs, and Pure Higgsinos", *Phys. Rev. Lett.* **119**, 10.1103/PhysRevLett.119.131801 (2017) [arXiv:1704.01577 [hep-ph]].

[136] D. Croon, A. E. Nelson, C. Sun, D. G. E. Walker, Z.-Z. Xianyu, "Hidden-Sector Spectroscopy with Gravitational Waves from Binary Neutron Stars", *Astrophys. J. Lett.* **858**, 10.3847/2041-8213/aabe76 (2018) [arXiv:1711.02096 [hep-ph]].

[137] J. Ellis, A. Hektor, G. Hütsi, K. Kannike, L. Marzola, M. Raidal, V. Vaskonen, "Search for Dark Matter Effects on Gravitational Signals from Neutron Star Mergers",

Phys. Lett. B **781**, 10.1016/j.physletb.2018.04.048 (2018) [arXiv:1710.05540 [astro-ph.CO]].

[138] B. Bellazzini, C. Csaki, J. Hubisz, J. Serra, J. Terning, "Cosmological and Astrophysical Probes of Vacuum Energy", *JHEP* **06**, 10.1007/JHEP06(2016)104 (2016) [arXiv:1502.04702 [astro-ph.CO]].

[139] D. D. Ivanenko, D. F. Kurdgelaidze, "Hypothesis concerning quark stars", *Astrophysics* **1**, 10.1007/BF01042830 (1965).

[140] J. R. Ellis, J. I. Kapusta, K. A. Olive, "Phase transition in dense nuclear matter with quark and gluon condensates", *Phys. Lett. B* **273**, 10.1016/0370-2693(91)90564-7 (1991).

[141] S. Bogdanov et al., "Neutron Star Dense Matter Equation of State Constraints with NICER", in Aas/high energy astrophysics division #16, Vol. 16, AAS/High Energy Astrophysics Division (Aug. 2017).

[142] E. E. Flanagan, T. Hinderer, "Constraining neutron star tidal Love numbers with gravitational wave detectors", *Phys. Rev. D* **77**, 10.1103/PhysRevD.77.021502 (2008) [arXiv:0709.1915 [astro-ph]].

[143] T. Hinderer, "Tidal Love numbers of neutron stars", *Astrophys. J.* **677**, 10.1086/533487 (2008) [arXiv:0711.2420 [astro-ph]].

[144] T. Hinderer, B. D. Lackey, R. N. Lang, J. S. Read, "Tidal deformability of neutron stars with realistic equations of state and their gravitational wave signatures in binary inspiral", *Phys. Rev. D* **81**, 10.1103/PhysRevD.81.123016 (2010) [arXiv:0911.3535 [astro-ph.HE]].

[145] S. Postnikov, M. Prakash, J. M. Lattimer, "Tidal Love Numbers of Neutron and Self-Bound Quark Stars", *Phys. Rev. D* **82**, 10.1103/PhysRevD.82.024016 (2010) [arXiv:1004.5098 [astro-ph.SR]].

[146] B. D. Lackey, L. Wade, "Reconstructing the neutron-star equation of state with gravitational-wave detectors from a realistic population of inspiralling binary neutron stars", *Phys. Rev. D* **91**, 10.1103/PhysRevD.91.043002 (2015) [arXiv:1410.8866 [gr-qc]].

[147] B. Margalit, B. D. Metzger, "Constraining the Maximum Mass of Neutron Stars From Multi-Messenger Observations of GW170817", *Astrophys. J. Lett.* **850**, 10.3847/2041-8213/aa991c (2017) [arXiv:1710.05938 [astro-ph.HE]].

[148] A. Bauswein, O. Just, H.-T. Janka, N. Stergioulas, "Neutron-star radius constraints from GW170817 and future detections", *Astrophys. J. Lett.* **850**, 10.3847/2041-8213/aa9994 (2017) [arXiv:1710.06843 [astro-ph.HE]].

[149] E. Zhou, A. Tsokaros, L. Rezzolla, R. Xu, K. Uryū, "Uniformly rotating, axisymmetric and triaxial quark stars in general relativity", *Phys. Rev. D* **97**, 10.1103/PhysRevD.97.023013 (2018) [arXiv:1711.00198 [astro-ph.HE]].

[150] L. Rezzolla, E. R. Most, L. R. Weih, "Using gravitational-wave observations and quasi-universal relations to constrain the maximum mass of neutron stars", *Astrophys. J. Lett.* **852**, 10.3847/2041-8213/aaa401 (2018) [arXiv:1711.00314 [astro-ph.HE]].

[151] E. Annala, T. Gorda, A. Kurkela, A. Vuorinen, "Gravitational-wave constraints on the neutron-star-matter Equation of State", *Phys. Rev. Lett.* **120**, 10.1103/PhysRevLett.120.172703 (2018) [arXiv:1711.02644 [astro-ph.HE]].

[152] J. M. Lattimer, M. Prakash, "Neutron star structure and the equation of state", *Astrophys. J.* **550**, 10.1086/319702 (2001) [arXiv:astro-ph/0002232].

[153] F. Douchin, P. Haensel, "A unified equation of state of dense matter and neutron star structure", *Astron. Astrophys.* **380**, 10.1051/0004-6361:20011402 (2001) [arXiv:astro-ph/0111092].

[154] J. S. Read, B. D. Lackey, B. J. Owen, J. L. Friedman, "Constraints on a phenomenologically parameterized neutron-star equation of state", *Phys. Rev. D* **79**, 10.1103/PhysRevD.79.124032 (2009) [arXiv:0812.2163 [astro-ph]].

[155] K. Hebeler, J. M. Lattimer, C. J. Pethick, A. Schwenk, "Equation of state and neutron star properties constrained by nuclear physics and observation", *Astrophys. J.* **773**, 10.1088/0004-637X/773/1/11 (2013) [arXiv:1303.4662 [astro-ph.SR]].

[156] H. Mueller, B. D. Serot, "Relativistic mean field theory and the high density nuclear equation of state", *Nucl. Phys. A* **606**, 10.1016/0375-9474(96)00187-X (1996) [arXiv:nucl-th/9603037].

[157] M. G. Alford, A. Schmitt, K. Rajagopal, T. Schäfer, "Color superconductivity in dense quark matter", *Rev. Mod. Phys.* **80**, 10.1103/RevModPhys.80.1455 (2008) [arXiv:0709.4635 [hep-ph]].

[158] M. Bejger, D. Blaschke, P. Haensel, J. L. Zdunik, M. Fortin, "Consequences of a strong phase transition in the dense matter equation of state for the rotational evolution of neutron stars", *Astron. Astrophys.* **600**, 10.1051/0004-6361/201629580 (2017) [arXiv:1608.07049 [astro-ph.HE]].

[159] D. E. Alvarez-Castillo, D. B. Blaschke, "High-mass twin stars with a multipolytrope equation of state", *Phys. Rev. C* **96**, 10.1103/PhysRevC.96.045809 (2017) [arXiv:1703.02681 [nucl-th]].

[160] M. G. Alford, A. Sedrakian, "Compact stars with sequential QCD phase transitions", *Phys. Rev. Lett.* **119**, 10.1103/PhysRevLett.119.161104 (2017) [arXiv:1706.01592 [astro-ph.HE]].

[161] M. G. Alford, S. Han, M. Prakash, "Generic conditions for stable hybrid stars", *Phys. Rev. D* **88**, 10.1103/PhysRevD.88.083013 (2013) [arXiv:1302.4732 [astro-ph.SR]].

[162] B. K. Agrawal, "Equations of state and stability of color-superconducting quark matter cores in hybrid stars", *Phys. Rev. D* **81**, 10.1103/PhysRevD.81.023009 (2010) [arXiv:1001.1584 [astro-ph.HE]].

[163] Z. F. Seidov, "The Stability of a Star with a Phase Change in General Relativity Theory", *Sov. Astronom.* **15** (1971).

[164] R. Schaeffer, L. Zdunik, P. Haensel, "Phase transitions in stellar cores. I - Equilibrium configurations", *Astron. Astrophys.* **126** (1983).

[165] W. Israel, "Singular hypersurfaces and thin shells in general relativity", *Nuovo Cim. B* **44S10**, [Erratum: Nuovo Cim.B 48, 463 (1967)], 10.1007/BF02710419 (1966).

[166] J. R. Oppenheimer, G. M. Volkoff, "On Massive neutron cores", *Phys. Rev.* **55**, 10.1103/PhysRev.55.374 (1939).

[167] A. E. H. Love, "Some Problems of Geodynamics" (1911).

[168] T. Damour, A. Nagar, "Relativistic tidal properties of neutron stars", *Phys. Rev. D* **80**, 10.1103/PhysRevD.80.084035 (2009) [arXiv:0906.0096 [gr-qc]].

[169] A. Akmal, V. R. Pandharipande, D. G. Ravenhall, "The Equation of state of nucleon matter and neutron star structure", *Phys. Rev. C* **58**, 10.1103/PhysRevC.58.1804 (1998) [arXiv:nucl-th/9804027].

[170] G. Baym, C. Pethick, P. Sutherland, "The Ground state of matter at high densities: Equation of state and stellar models", *Astrophys. J.* **170**, 10.1086/151216 (1971).

[171] J. M. Bardeen, K. S. Thorne, D. W. Meltzer, "A Catalogue of Methods for Studying the Normal Modes of Radial Pulsation of General-Relativistic Stellar Models", *Astrophys. J.* **145**, 10.1086/148791 (1966).

[172] N. K. Glendenning, C. Kettner, "Nonidentical neutron star twins", *Astron. Astrophys.* **353** (2000) [arXiv:astro-ph/9807155].

[173] P. Demorest, T. Pennucci, S. Ransom, M. Roberts, J. Hessels, "Shapiro Delay Measurement of A Two Solar Mass Neutron Star", *Nature* **467**, 10.1038/nature09466 (2010) [arXiv:1010.5788 [astro-ph.HE]].

[174] H. Heiselberg, M. Hjorth-Jensen, "Phase transitions in neutron stars and maximum masses", *Astrophys. J. Lett.* **525**, 10.1086/312321 (1999) [arXiv:astro-ph/9904214].

[175] C. Cutler, E. E. Flanagan, "Gravitational waves from merging compact binaries: How accurately can one extract the binary's parameters from the inspiral wave form?", *Phys. Rev. D* **49**, 10.1103/PhysRevD.49.2658 (1994) [arXiv:gr-qc/9402014].

[176] T. Dietrich, S. Bernuzzi, W. Tichy, "Closed-form tidal approximants for binary neutron star gravitational waveforms constructed from high-resolution numerical relativity simulations", *Phys. Rev. D* **96**, 10.1103/PhysRevD.96.121501 (2017) [arXiv:1706.02969 [gr-qc]].

[177] P. Kumar, M. Pürrer, H. P. Pfeiffer, "Measuring neutron star tidal deformability with Advanced LIGO: a Bayesian analysis of neutron star - black hole binary observations", *Phys. Rev. D* **95**, 10.1103/PhysRevD.95.044039 (2017) [arXiv:1610.06155 [gr-qc]].

[178] L. Rezzolla, K. Takami, "Gravitational-wave signal from binary neutron stars: a systematic analysis of the spectral properties", *Phys. Rev. D* **93**, 10.1103/PhysRevD.93.124051 (2016) [arXiv:1604.00246 [gr-qc]].

[179] L. D. Landau, E. M. Lifshitz, "Course of Theoretical Physics Volume I: Mechanics" (Butterworth-Heinemann, 1976).

[180] R. C. Tolman, "Static solutions of Einstein's field equations for spheres of fluid", *Phys. Rev.* **55**, 10.1103/PhysRev.55.364 (1939).

[181] N. Itoh, "Hydrostatic Equilibrium of Hypothetical Quark Stars", *Prog. Theor. Phys.* **44**, 10.1143/PTP.44.291 (1970).

[182] F. Ozel, D. Psaltis, Z. Arzoumanian, S. Morsink, M. Baubock, "Measuring Neutron Star Radii via Pulse Profile Modeling with NICER", *Astrophys. J.* **832**, 10.3847/0004-637X/832/1/92 (2016) [arXiv:1512.03067 [astro-ph.HE]].

[183] J. M. Lattimer, "The nuclear equation of state and neutron star masses", *Ann. Rev. Nucl. Part. Sci.* **62**, 10.1146/annurev-nucl-102711-095018 (2012) [arXiv:1305.3510 [nucl-th]].

[184] E. S. Fraga, R. D. Pisarski, J. Schaffner-Bielich, "Small, dense quark stars from perturbative QCD", *Phys. Rev. D* **63**, 10.1103/PhysRevD.63.121702 (2001) [arXiv:hep-ph/0101143].

[185] H. Heiselberg, "Neutron star masses, radii and equation of state", (2002) [arXiv:astro-ph/0201465].

[186] S. Banik, D. Bandyopadhyay, "Color superconducting quark matter core in the third family of compact stars", *Phys. Rev. D* **67**, 10.1103/PhysRevD.67.123003 (2003) [arXiv:astro-ph/0212340].

[187] J. L. Zdunik, P. Haensel, "Maximum mass of neutron stars and strange neutron-star cores", *Astron. Astrophys.* **551**, 10.1051/0004-6361/201220697 (2013) [arXiv:1211.1231 [astro-ph.SR]].

[188] R. Anglani, R. Casalbuoni, M. Ciminale, N. Ippolito, R. Gatto, M. Mannarelli, M. Ruggieri, "Crystalline color superconductors", *Rev. Mod. Phys.* **86**, 10.1103/RevModPhys.86.509 (2014) [arXiv:1302.4264 [hep-ph]].

[189] E. S. Fraga, A. Kurkela, A. Vuorinen, "Interacting quark matter equation of state for compact stars", *Astrophys. J. Lett.* **781**, 10.1088/2041-8205/781/2/L25 (2014) [arXiv:1311.5154 [nucl-th]].

[190] M. A. R. Kaltenborn, N.-U. F. Bastian, D. B. Blaschke, "Quark-nuclear hybrid star equation of state with excluded volume effects", *Phys. Rev. D* **96**, 10.1103/PhysRevD.96.056024 (2017) [arXiv:1701.04400 [astro-ph.HE]].

[191] J.-E. Christian, A. Zacchi, J. Schaffner-Bielich, "Classifications of Twin Star Solutions for a Constant Speed of Sound Parameterized Equation of State", *Eur. Phys. J. A* **54**, 10.1140/epja/i2018-12472-y (2018) [arXiv:1707.07524 [astro-ph.HE]].

[192] L. Lindblom, "Phase transitions and the mass radius curves of relativistic stars", *Phys. Rev. D* **58**, 10.1103/PhysRevD.58.024008 (1998) [arXiv:gr-qc/9802072].

[193] T. Binnington, E. Poisson, "Relativistic theory of tidal Love numbers", *Phys. Rev. D* **80**, 10.1103/PhysRevD.80.084018 (2009) [arXiv:0906.1366 [gr-qc]].

[194] J. W. Negele, D. Vautherin, "Neutron star matter at subnuclear densities", *Nucl. Phys. A* **207**, 10.1016/0375-9474(73)90349-7 (1973).

[195] K. Schertler, C. Greiner, J. Schaffner-Bielich, M. H. Thoma, "Quark phases in neutron stars and a 'third family' of compact stars as a signature for phase transitions", *Nucl. Phys. A* **677**, 10.1016/S0375-9474(00)00305-5 (2000) [arXiv:astro-ph/0001467].

[196] P. Haensel, "Equation of state of dense matter and maximum mass of neutron stars", *EAS Publ. Ser.* **7**, 10.1051/eas:2003043 (2003) [arXiv:astro-ph/0301073].

[197] F. PACINI, "High-energy astrophysics and a possible sub-nuclear energy source", *Nature* **209**, 10.1038/209389a0 (1966).

[198] D. Boccaletti, V. Sabbata, C. Gualdi, "The red- or violet-shift of quasars without any source motion", *Nuovo Cimento A Serie* **45**, 10.1007/BF02856399 (1966).

[199] K. Gendreau, Z. Arzoumanian, "Searching for a pulse", *Nature Astronomy* **1**, 10.1038/s41550-017-0301-3 (2017).

[200] K. Hebeler, J. M. Lattimer, C. J. Pethick, A. Schwenk, "Constraints on neutron star radii based on chiral effective field theory interactions", *Phys. Rev. Lett.* **105**, 10.1103/PhysRevLett.105.161102 (2010) [arXiv:1007.1746 [nucl-th]].

[201] P. Haensel, A. Y. Potekhin, D. G. Yakovlev, "Neutron Stars 1 : Equation of State and Structure", Vol. 326 (2007).

[202] M. G. Alford, S. Han, "Generic Conditions for Stable Hybrid Stars", *EPJ Web Conf.* **80**, edited by G. E. Bruno, G. Chiodini, P. Colangelo, C. Corianò, D. Creanza, F. De Fazio, E. Nappi, 10.1051/epjconf/20148000038 (2014).

[203] M. G. Alford, G. F. Burgio, S. Han, G. Taranto, D. Zappalà, "Constraining and applying a generic high-density equation of state", *Phys. Rev. D* **92**, 10.1103/PhysRevD.92.083002 (2015) [arXiv:1501.07902 [nucl-th]].

[204] T. Damour, A. Nagar, "Effective One Body description of tidal effects in inspiralling compact binaries", *Phys. Rev. D* **81**, 10.1103/PhysRevD.81.084016 (2010) [arXiv:0911.5041 [gr-qc]].

Gabriele Rigo

Curriculum Vitæ

CONTACT INFORMATION

Department of Physics, Syracuse University
Syracuse, NY 13244, USA
garigo@syr.edu

ACADEMIC APPOINTMENTS

2021–Present **Université Paris Saclay**, Gif-sur-Yvette, France
Postdoctoral Fellow

EDUCATION

2015–2021 **Syracuse University**, Syracuse, NY
Ph.D., Physics
Advisor: Prof. Jay Hubisz
Thesis: "Beyond the Standard Models of Particle Physics and Cosmology"

2015–2017 **Syracuse University**, Syracuse, NY
Master of Science, Physics
Advisor: Prof. Jay Hubisz

2012–2015 **Università degli Studi di Trieste**, Trieste, Italy
Bachelor of Science, Physics, 110/110 cum laude
Advisor: Prof. Emidio Gabrielli
Thesis: "Effects of Ultra Light, Spin Zero Particles on the Propagation of Light in Electric and Magnetic Fields"

PUBLICATIONS

[1] C. Eröncel, J. Hubisz, S. J. Lee, G. Rigo, B. Sambasivam, "Alternative Approach to a Holographic Phase Transition", In Preparation.

[2] C. Csáki, J. Hubisz, A. Ismail, G. Rigo, F. Sgarlata, "Dilaton Scattering and Positivity Bounds", In Preparation.

[3] S. Hong, G. Rigo, "Anomaly Inflow and Holography" [arXiv:2012.03964 [hep-th]].

[4] C. Eröncel, J. Hubisz, G. Rigo, "Radion-Activated Higgs Mechanism", *Phys. Rev. D* **101**, 055041 (2020) [arXiv:1912.11053 [hep-ph]].

[5] C. Eröncel, J. Hubisz, G. Rigo, "Self-Organized Higgs Criticality", *JHEP* **03**, 046 (2019) [arXiv:1804.00004 [hep-ph]].

[6] C. Csáki, C. Eröncel, J. Hubisz, G. Rigo, J. Terning, "Neutron Star Mergers Chirp About Vacuum Energy", *JHEP* **09**, 087 (2018) [arXiv:1802.04813 [astro-ph.HE]].

HONORS & AWARDS

2019	**Summer Dissertation Fellowship** *Syracuse University*
2018	**Travel Grant Award** *Syracuse University*
2018	**Phenomenology Symposium Travel Award** *Pittsburgh Particle Physics, Astrophysics, and Cosmology Center*
2012–2015	**Luciano Fonda Fellow** *Collegio Universitario Luciano Fonda Trieste*
2013	**Best Freshman in the Physics Department** *Università degli Studi di Trieste*

TALKS & CONFERENCES

January 2021	**CERN**, Geneva, Switzerland "Anomaly Inflow and Holography"
December 2019	**Carnegie Mellon University**, Pittsburgh, PA "Self-Organized Higgs Criticality"
December 2019	**University of Pittsburgh**, Pittsburgh, PA "Neutron Star Mergers Chirp About Vacuum Energy"

November 2019 **University of Maryland**, College Park, MD
"Neutron Star Mergers Chirp About Vacuum Energy"

November 2019 **Johns Hopkins University**, Baltimore, MD
"Neutron Star Mergers Chirp About Vacuum Energy"

July 2018 **Institut d'Etudes Scientifiques**, Cargèse, France
"Neutron Star Mergers Chirp About Vacuum Energy"

May 2018 **Phenomenology Symposium**, Pittsburgh, PA
"Neutron Star Mergers Chirp About Vacuum Energy"

May 2018 **Cornell University**, Ithaca, NY
"Neutron Star Mergers Chirp About Vacuum Energy"

March 2018 **Syracuse University**, Syracuse, NY
"Self-Organized Higgs Criticality"

March 2018 **Scuola Internazionale Superiore di Studi Avanzati**, Trieste, Italy
"Neutron Star Mergers Chirp About Vacuum Energy"

SCHOOLS & WORKSHOPS

October 2018 **Galileo Galilei Institute**, Firenze, Italy
"Beyond the Standard Model: Where Do We Go from Here?"
Johns Hopkins Workshop

July 2018 **Institut d'Etudes Scientifiques**, Cargèse, France
"Mass: From the Higgs to Cosmology"
International Summer School

January 2018 **Galileo Galilei Institute**, Firenze, Italy
Lectures on the Theory of Fundamental Interactions

July 2017 **Institute for Advanced Study**, Princeton, NJ
"Particle Physics at the LHC and Beyond"
Prospects in Theoretical Physics

June 2017 **International Centre for Theoretical Physics**, Trieste, Italy
Summer School on Particle Physics

TEACHING EXPERIENCE

Spring 2021	**PHY221** General Physics I Laboratory Teaching Assistant
Fall 2020	**PHY221** General Physics I Laboratory Teaching Assistant
Spring 2020	**PHY221** General Physics I Laboratory Teaching Assistant
Fall 2018	**PHY661** Quantum Mechanics I Grader
Fall 2018	**PHY621** Classical Mechanics Grader
Fall 2018	**PHY581** Methods of Theoretical Physics Grader
Spring 2018	**PHY102** Major Concepts of Physics II Teaching Assistant
Fall 2016	**PHY101** Major Concepts of Physics I Teaching Assistant
Spring 2016	**PHY102** Major Concepts of Physics II Teaching Assistant
Fall 2015	**PHY101** Major Concepts of Physics I Teaching Assistant

REFEREE ACTIVITY

European Physical Journal C